Technical Report Documentation Page

1. Report No.	2. Government Accession No.	3. Recipient's Catalog No.
FHWA/TX-87/474-1F		

4. Title and Subtitle	5. Report Date
Improved Asphalt Concrete Mixture Design Procedure	July 1988
	6. Performing Organization Code
7. Author(s)	8. Performing Organization Report No.
Kamyar Mahboub and Dallas N. Little	Research Report 474-1F
9. Performing Organization Name and Address	10. Work Unit No. (TRAIS)
Texas State Department of Highways and Public Transportation; Transportation Planning Division P.O. Box 5051 Austin, Texas 78763	11. Contract or Grant No. Study No. 2-9-85-474
	13. Type of Report and Period Covered Final September, 1984 August, 1987
12. Sponsoring Agency Name and Address	14. Sponsoring Agency Code
Texas Transportation Institute The Texas A&M University System College Station, Texas 77843	

15. Supplementary Notes

Research performed in cooperation with DOT, FHWA.
Research Study Title: Improved Asphalt Concrete Mixture Design Procedure

16. Abstract

An extension to the current Texas mixture design procedure was evaluated. The extended mixture design/analysis procedures addresses: 1) the potential of hot mix asphalt concrete (HMAC) mixture to permanently deform, 2) flexural fatigue cracking potential, 3) subgrade protection, and 4) thermal cracking potential.

The methodology is presented in an "easy-to-use" tabular and design chart format which can be incorporated into a mixture design/analysis sequence. The tests used to characterize mixture material properties are relatively simple and do not necessarily require sophisticated testing equipment. the properties required by the extended procedure include: compressive creep compliance, diametral resilient modulus and indirect tensile strength.

The criteria by which the material properties are evaluated are based on the climatic region within which the pavement using the HMAC exists or will be placed and the category of the pavement structure.

The compressive creep test proved to be a sensitive indicator of deformation potential. The creep test is used in the extended procedure as part of a new analysis procedure which accounts for viscoelastic nonlinearity of the asphalt concrete mixture as well as temperature sensitivity.

17. Key Words	18. Distribution Statement
Asphalt, asphalt mixture, fracture, fatigue, rutting, mix design.	No restriction. This document is available to the public through the National Technical Information Service 5285 Port Royal Road Springfield, Virginia 22161

19. Security Classif. (of this report)	20. Security Classif. (of this page)	21. No. of Pages	22. Price
Unclassified	Unclassified	253	

IMPROVED ASPHALT CONCRETE MIXTURE DESIGN PROCEDURE

by

Kamyar Mahboub
Research Associate

and

Dallas N. Little
Research Engineer

Research Report 474-1F
Research Study 2-9-85-474

Sponsored by

Texas State Department of Highways and Public Transportation

in cooperation with

U.S. Department of Transportation
Federal Highway Administration

July, 1988

TEXAS TRANSPORTATION INSTITUTE
The Texas A&M University System
College Station, Texas

METRIC CONVERSION FACTORS

Approximate Conversions to Metric Measures

Symbol	When You Know	Multiply by	To Find	Symbol
		LENGTH		
in	inches	*2.5	centimeters	cm
ft	feet	30	centimeters	cm
yd	yards	0.9	meters	m
mi	miles	1.6	kilometers	km
		AREA		
in^2	square inches	6.5	square centimeters	cm^2
ft^2	square feet	0.09	square meters	m^2
yd^2	square yards	0.8	square meters	m^2
mi^2	square miles	2.6	square kilometers	km^2
	acres	0.4	hectares	ha
		MASS (weight)		
oz	ounces	28	grams	g
lb	pounds	0.45	kilograms	kg
	short tons (2000 lb)	0.9	tonnes	t
		VOLUME		
tsp	teaspoons	5	milliliters	ml
Tbsp	tablespoons	15	milliliters	ml
fl oz	fluid ounces	30	milliliters	ml
c	cups	0.24	liters	l
pt	pints	0.47	liters	l
qt	quarts	0.95	liters	l
gal	gallons	3.8	liters	l
ft^3	cubic feet	0.03	cubic meters	m^3
yd^3	cubic yards	0.76	cubic meters	m^3
		TEMPERATURE (exact)		
°F	Fahrenheit temperature	5/9 (after subtracting 32)	Celsius temperature	°C

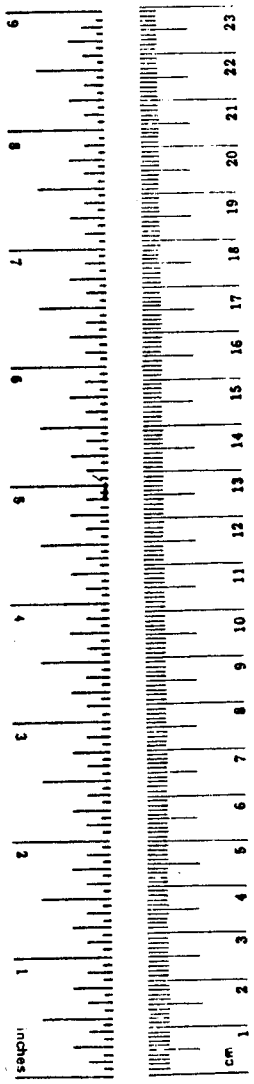

Approximate Conversions from Metric Measures

Symbol	When You Know	Multiply by	To Find	Symbol
		LENGTH		
mm	millimeters	0.04	inches	in
cm	centimeters	0.4	inches	in
m	meters	3.3	feet	ft
m	meters	1.1	yards	yd
km	kilometers	0.6	miles	mi
		AREA		
cm^2	square centimeters	0.16	square inches	in^2
m^2	square meters	1.2	square yards	yd^2
km^2	square kilometers	0.4	square miles	mi^2
ha	hectares (10,000 m^2)	2.5	acres	
		MASS (weight)		
g	grams	0.035	ounces	oz
kg	kilograms	2.2	pounds	lb
t	tonnes (1000 kg)	1.1	short tons	
		VOLUME		
ml	milliliters	0.03	fluid ounces	fl oz
l	liters	2.1	pints	pt
l	liters	1.06	quarts	qt
l	liters	0.26	gallons	gal
m^3	cubic meters	35	cubic feet	ft^3
m^3	cubic meters	1.3	cubic yards	yd^3
		TEMPERATURE (exact)		
°C	Celsius temperature	9/5 (then add 32)	Fahrenheit temperature	°F

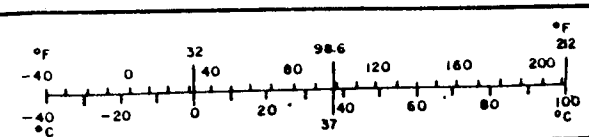

SUMMARY

This report summarizes the results of an asphalt concrete mixture design analysis study which incorporates material property tests which can be "rationally" linked to actual field performance. In this case, the term "rational" literally means that the material properties evaluated in the mixture analysis can be used together with a layered elastic pavement model and empirical formula which relate mechanistic parameters from the layered elastic analysis to observed performance. The procedures proposed in this study are to be used in conjunction with the current Texas State Department of Highways and Public Transportation (SDHPT) method of mix design in a complimentary fashion.

Three major modes of distress: 1) rutting, 2) flexural fatigue cracking, and 3) low temperature cracking, were addressed in this report through mixture characterization, pavement structural modeling and a series of failure criteria.

Analytical results indicate that structural arrangement of pavement layers and environmental factors have significant effects on the performance of the asphalt concrete mixture.

A significant contribution of this study was the development of a methodology by which to evaluate compression creep testing in the characterization of the deformation potential of hot mix asphalt concrete. Specifically, a simplified method was proposed by which to correct for the nonlinear stress dependency of asphalt concrete mixtures in compressive creep testing and analysis.

Field evaluation of the criteria developed in this study was conducted on a limited basis. This verification phase will be greatly enhanced through other TTI studies including Studies 1170 and 1121.

IMPLEMENTATION

In this report, a methodology is introduced which can be used to evaluate the performance potential of asphalt concrete paving mixtures. The methodology is not a replacement for the present Texas method of mixture design, but an extension of the present method.

At present, all findings do not warrant immediate implementation into the mix design/analysis procedure. This is because verification has not been completed. However, the research does demonstrate that:

a) A compressive creep and creep recovery test has been successfully developed to characterize hot mix asphalt concrete mixtures.
b) The methodology of analysis of compressive creep data and presentation of these data in a format which can be used to ascertain deformation potential has been developed.
c) The methodology of assessing the potential of asphalt concrete mixtures based on compressive creep testing and data analysis has been successfully accomplished and is ready for implementation on a limited basis. This limited implementation should be associated with data collection and the verification process.

This research has also identified areas where more research is required to fully develop parts of the mixture design/analysis procedure. These areas of additional research are:

a) Evaluation of a more fundamentally sound methodology to assess mixture stiffness to be used in evaluating thermal fracture potential.
b) Evaluation of permanent deformation potential based on the Mohr-Coulomb failure criteria.
c) Evaluation of a procedure by which to directly measure flexural fatigue potential in an efficient, effective manner in lieu of simply predicting fatigue based on an algorithm relating fatigue life to mixture stiffness and strain level within the pavement structure.

The findings in this research are positive and indicate that a substantially verified methodology by which to design/analyze asphalt concrete mixtures based on potential performance within a specified category of structural pavement is at hand.

The methodology by which to evaluate deformation within the asphalt concrete is now partially implementable as explained above. Implementation of procedures to evaluate flexural fatigue potential and low temperature cracking show great promise but must await additional research in Project 1170.

The potential savings which may result by extending the asphalt mixture design/analysis to a more complete and sensitive decision-making process are immense. The procedure presented in this report allows the engineer to evaluate, through a "rational" process, the influence of changes in mixture variables and the alteration of mixtures through the addition of asphalt modifiers.

DISCLAIMER

The contents of this report reflect the views of the authors who are responsible for the opinions, findings, and conclusions presented herein. The contents do not necessarily reflect the official view or policies of the Federal Highway Administration. This report does not constitute a standard, specification, or regulation.

There was no invention or discovery conceived or first actually reduced to practice in the course of or under this contract, including any art, method, process, machine, manufacture, design or composition of matter, or any new and useful improvement thereof, or any variety of plant which is or may be patentable under the patent laws of the United States of America or any foreign country.

ACKNOWLEDGEMENTS

The authors of this report acknowledge the guidance and leadership provided by Mr. Paul Krugler or the Materials and Testing Division of the Texas SDHPT. Appreciation is also extended to Mr. Henry Hardy of District 15, Mr. Blair Haynie of District 4, and Mr. Nick Turnham of District 17.

This study was conducted in cooperation with the U.S. Department of Transportation, Federal Highway Administration.

TABLE OF CONTENTS

TABLE OF CONTENTS - continued

LIST OF TABLES

LIST OF FIGURES

LIST OF FIGURES - continued

LIST OF FIGURES - continued

LIST OF FIGURES - continued

LIST OF FIGURES - continued

CHAPTER I

INTRODUCTION

Background

The design of hot mix asphalt concrete (HMAC) mixtures has been a trial and error process for a relatively long period of time. During the last four decades, two major methods of mix design have emerged as those most commonly used by asphalt paving technologists. The evolution of the Hveem (1) and Marshall (2) methods was based on empirical criteria associated with simple laboratory procedures.

There are many variations of these basic methods in use among highway agencies. Figure 1 illustrates the distribution of mix design methods used in the United States. The Texas State Department of Highways and Public Transportation (SDHPT) has its own unique method of mix design (3) which utilizes a modified Hveem Procedure.

According to the Asphalt Institute (4), all mix design procedures must provide the following:

a) Sufficient asphalt to ensure a durable pavement.
b) Sufficient mix stability to satisfy the demands of traffic without distortion or displacement.
c) Sufficient voids in the final compacted mix to allow for a slight amount of additional compaction due to traffic loading without flushing, bleeding and loss of stability, yet enough voids to keep out harmful air and moisture.
d) Sufficient workability to permit efficient placement of the mix without segregation or shoving.

Empirical methods of mix design currently in use have proven to be inadequate to address in-service performance problems associated with variations in the crude source and refining processes, use of additives (6), type of mix, and current trends toward heavier traffic loads and higher tire pressures (7). In these empirical procedures, mixture performance in the field is not related to fundamental engineering properties measured in the laboratory.

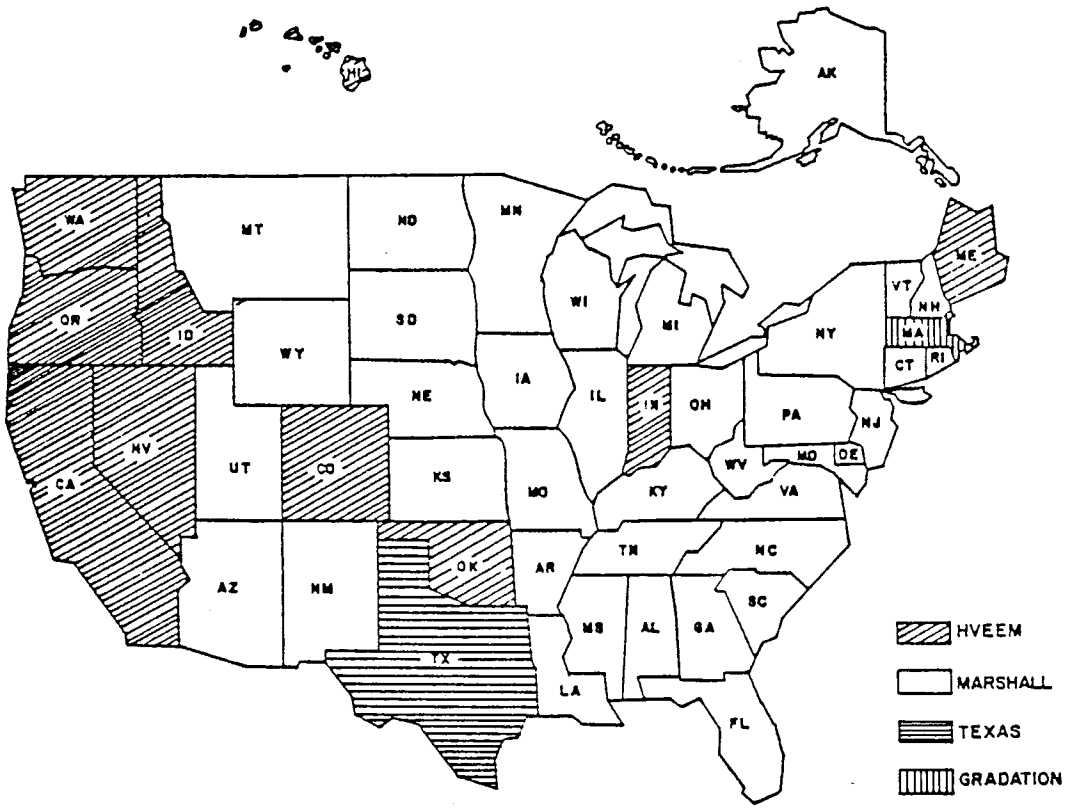

Figure 1. Distribution of mixture design methods used in the United States (after Reference 5).

During the past two decades, the problems associated with purely empirical methods have led researchers to develop methods based on mechanistic parameters.

The objective of this study has been to develop an integrated mix design and analysis procedure which addresses different modes of HMAC distress in terms of mechanistic parameters. Throughout this research, the main emphasis has been the permanent deformation or rutting characterization of HMAC.

Shell researchers (8, 9) pioneered the use of a simple static load creep test for predicting permanent deformation and rutting. The creep-recovery parameters explain the resistance of HMAC to deformation (i.e. stability) in terms of basic engineering parameters such as stiffness, stress, and strain.

In the last five years, interest has grown among researchers and state highway agencies in the use of the creep test for assessing rutting potential. The most notable of such agencies are the North Dakota Highway Department (10, 11), the Georgia Department of Transportation (12), and the Texas SDHPT (13, 14).

Another trend in recent years has been the development of a procedure which brings the mix design and structural design of pavements into an integrated system. This was the main theme of the 1985 Association of Asphalt Pavement Technologists (AAPT) mix design symposium (15) and also the 1986 American Society for Testing and Materials (ASTM) mix design conference (16).

Presently, Brent Rauhut Engineering (BRE) and Texas A&M researchers are working on a study which is funded by the National Cooperative Highway Research Program (NCHRP). This study, "Development of Asphalt-Aggregate Mixture Analysis System (AAMAS)," will provide guidelines for all aspects of HMAC mixture design (17).

Texas Mix Design Methodology

In the present Texas method of mix design (3), the basic philosophy is to produce a mix with adequate Hveem stability and a target air void content of three percent. The latter is supposed to represent the void content in the pavement after the second summer in service. Item 340 of the Texas SDHPT Construction Specifications (18) also requires that

aggregate used in hot mix asphalt concrete have adequate polish resistance, a minimum amount of crushed surfaces, and/or possess surface microtexture which reproduces itself upon wearing. An attempt to eliminate unstable and harsh, i.e., unworkable, mixes is made by introducing gradation specifications. In addition, a target window has been established for mid-sized aggregate (finer than the #10 sieve, but coarser than the #40 sieve) together with tight control over the mineral filler (minus #200 sieve portion) as a further attempt to guarantee optimum mixture workability and stability.

The Texas gyratory-shear method of compaction is used in specimen fabrication. This method closely simulates the kneading action of roller compactors and traffic and produces a laboratory mix density similar to what would be produced in the field following two summers of traffic. Traffic-induced densification has been investigated by the AAMAS research team (17). Researchers used the Texas gyratory-shear compaction device at different levels of compaction in an effort to simulate the compacted mix cored from the field. The ability of the gyratory compactor to produce the densification and material properties similar to those developed through field compaction, proved better than that of other traditionally-used laboratory compaction devices.

Durability of asphalt concrete is primarily a function of air voids content which is controlled by asphalt content, compactive effort, and aggregate gradation. Figure 2 shows, schematically, how the selection process of the optimum asphalt content is dependent on the judgement of the design engineer (19). The introduction of new binders, asphalt modifiers, and marginal aggregates further complicates the matrix and makes it even more difficult to rely on the old, purely empirical and judgmental design methods.

Recent computational advancements have made pavement structural analysis a routine task. Numerous analytical techniques have been used by researchers to investigate the effect of tire pressure (7), distribution of loads (20), etc., on pavement service life. Structural arrangement of pavement layers and bonding among layers has been shown to have a significant effect on the distribution of stresses within a pavement (21, 22). The magnitude and distribution of these stresses are responsible for the manifestation of different modes of pavement distress. Therefore, it

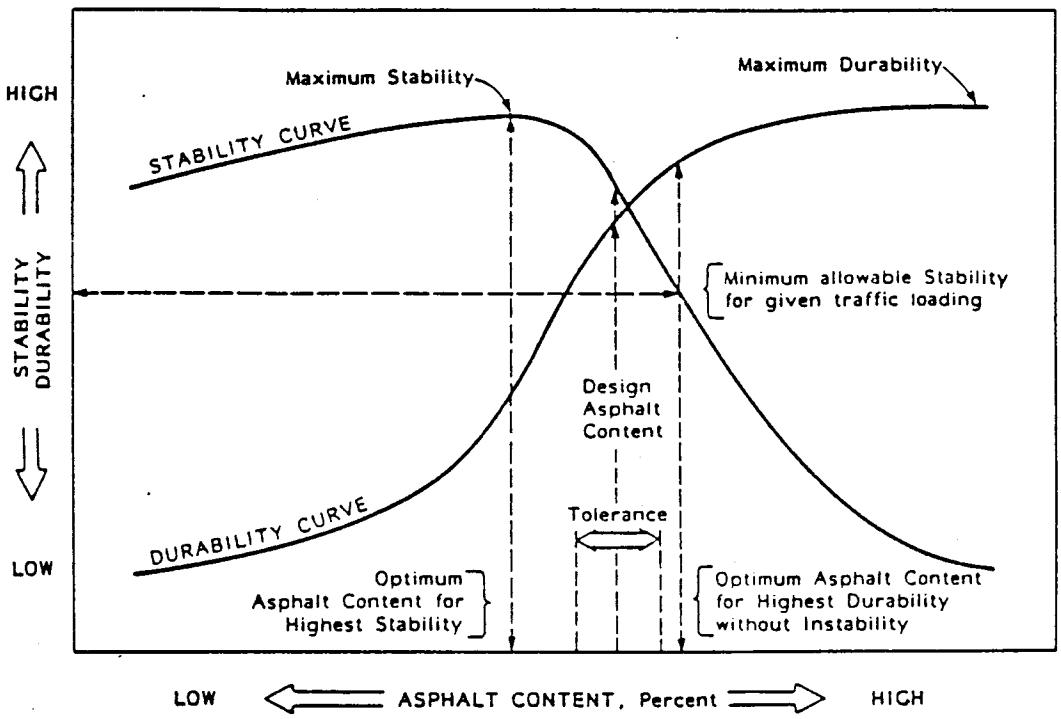

Figure 2. The trade-off between stability and durability (after Reference 19).

becomes clear that an improved mix design rationale should account for the structural pavement system within which the asphalt concrete layer is to be integrated.

For the first time, this research study introduces mix design guidelines tailored to specific structural configurations and environmental conditions commonly encountered in the State of Texas. These guidelines are assigned based on a set of acceptance criteria for three major modes of distress:

a) Rutting.
b) Load-related fatigue.
c) Low-temperature cracking.

The rutting criteria was given more attention than the others which were developed based on existing approaches found in the literature. In addition to these acceptance criteria, structural soundness of the pavement was based on its ability to protect the subgrade from excessive deformation.

Significance and Objective of Research

This research study describes the development of an extended and comprehensive asphalt concrete mixture design procedure, which is to be used as a supplement to the current Texas method (3). Once the density, air void content, stability, and optimum asphalt content are determined, the extended procedure allows the engineer to evaluate the mix with respect to a series of acceptance criteria: 1)subgrade protection; 2) fatigue cracking; 3)rutting potential; and, 4) thermal cracking.

This extended procedure is based upon fundamental engineering properties such as: creep-recovery behavior, resilient modulus, and tensile strength. Throughout this study, analyses were conducted using layered-elastic pavement models and the results evaluated in conjunction with realistic material properties and the most widely accepted failure criteria. This should insure a more fundamental link between laboratory measurements and field performance.

Research Approach

The philosophy of this extended procedure is to design a hot mix asphalt concrete (HMAC) that will provide a sufficient level of stiffness to protect the vulnerable subgrade by proper distribution of vertical compressive stresses. At the same time, however, there is a trade-off between the stiffness of HMAC and its flexibility. An adequate level of flexibility must be demonstrated by the HMAC for it to resist load-induced, flexural fatigue.

Once the stiffness/flexibility properties of HMAC are determined to be acceptable, the permanent deformation potential of HMAC can be assessed by means of a constant-stress creep analysis.

Finally, the low-temperature fracture potential is evaluated based on stiffness and tensile strength. The temperature sensitivity of the stiffness is characterized by variation of the diametral resilient modulus with temperature. The tensile strength is also evaluated diametrally (under monotonic loading) over a range of temperatures and at a slow rate of loading to simulate the diurnal thermal contraction process in the pavement.

The material properties which determine the success or failure of a pavement layer cannot be assessed without consideration of the pavement structure. A wide variety of pavement structures exist in the Texas SDHPT inventory. However, separation of pavement structures into representative categories is not only possible but appropriate. The approach used in this research was to identify four distinctive categories of pavement structures. The stress distributions within these pavement structures are typical and represent those that a Texas SDHPT engineer would encounter.

The four pavement structures listed below represent the four pavement types used in the development of acceptance criteria in this study. Asphalt concrete mixtures were evaluated based upon their performance within a selected category. This research verifies that assessments based on performance within the structures identified are conservative.

The structural categories and representative pavement cross-sections are:

a) Thick flexible pavements: 10 in. asphalt concrete, 12 in. crushed limestone base, subgrade (weak, moderate, or soft).

b) Thin flexible pavements: 3 in. asphalt concrete, 6 in. crushed limestone base, subgrade (weak, moderate, or soft).
c) Intermediate flexible pavements: 4 in. asphalt concrete, 12 in. crushed limestone base, subgrade (weak, moderate, or soft).
d) HMAC overlaying a portland cement concrete pavement (PCCP): 6 in. asphalt concrete, 8 in. PCCP, subgrade (weak, moderate, or soft).

The results of this study are presented as a series of charts and nomographs in a user-oriented package for the Texas SDHPT HMAC design engineers. The nomographic solutions allow the engineer to extend this methodology beyond the four pavement structures presented herein as representative of distincitive pavement categories in Texas to a specific pavement structure.

CHAPTER II

OVERVIEW OF METHODOLOGY

Background

This chapter presents a brief and general overview of the methodology incorporated in the proposed asphalt concrete mix design/analysis procedure. The methodology may be broken down into four phases:

a) Mixture design in accordance with Test Method TEX-204-F (3).
b) Stiffness characterization related to:
   1) threshold resilient modulus for subgrade protection, and
   2) stiffness/flexibility analysis for flexural fatigue evaluation.
c) Permanent deformation potential analysis.
d) Thermal cracking analysis.

A thorough explanation of Test Method TEX-204-F is given in Reference 3. The following sections introduce the methodology outlined above.

Stiffness Characterization

The main purposes of asphalt concrete surface layers are to: 1) prevent moisture from penetrating into underlying layers; 2) protect underlying materials (especially the subgrade) from being overstressed; and, after accomplishing 1 and 2, 3) provide an "acceptable" riding quality. The HMAC is normally the stiffest layer in the pavement structure and thus is the layer which contributes most effectively to distribution of vertical compressive stresses.

Proper distribution of vertical stresses is achieved through the use of stiffer HMAC layers. There is a life cycle cost penalty associated with this approach; that is, stiffer HMAC layers may exhibit shorter fatigue lives. Consequently, a trade-off situation exists with regard to

the mixture stiffness and service life which will be discussed in the following sections.

Threshold Resilient Modulus

The "acceptable" distribution of vertical compressive stresses within the pavement is achieved through a combination of layer moduli in which each layer is normally stiffer than the layer below. The general approach to insure that the HMAC layer provides adequate stiffness for subgrade protection is illustrated in Figure 3. Subsequent to applying Test Method TEX-204-F, the analysis for HMAC threshold modulus is initiated. The resilient modulus of the HMAC is evaluated over a range of temperatures to allow the engineer to select the moduli which corresponds to an applicable pavement temperature range in the field.

The methodology also accounts for the type of pavement structure in which the HMAC is to be placed. Figure 4 shows different pavement categories that are included in this study. Structural adequacy in terms of the threshold resilient modulus for vertical compressive stress distribution is checked with the aid of charts similar to Figure 5. These charts, which are presented in Chapter V, were developed for each structural pavement category, account for: a) traffic level in terms of the number of 18 kip equivalent single axle load (ESAL) standard axle passes; and b) the level of subgrade strength.

Flexural Fatigue

Once an adequate level of HMAC stiffness is achieved with respect to the subgrade protection criteria, the fatigue resistance of the mixture is analyzed in order to insure a proper stiffness/flexibility balance. Figure 6 depicts the methodology by which the load-induced fatigue life of the HMAC layer is evaluated.

The first step, which calls for the evaluation of the HMAC stiffness at the mean annual pavement temperature (MAPT), is illustrated in Figure 7. Based on this selected value of HMAC stiffness, measured in terms of resilient modulus, the induced tensile strain at the bottom of HMAC layer is evaluated. This repeated load-induced tensile strain, the primary cause of load-induced fatigue cracking, is evaluated from a series of charts developed for each category of pavement structure (Figure 8).

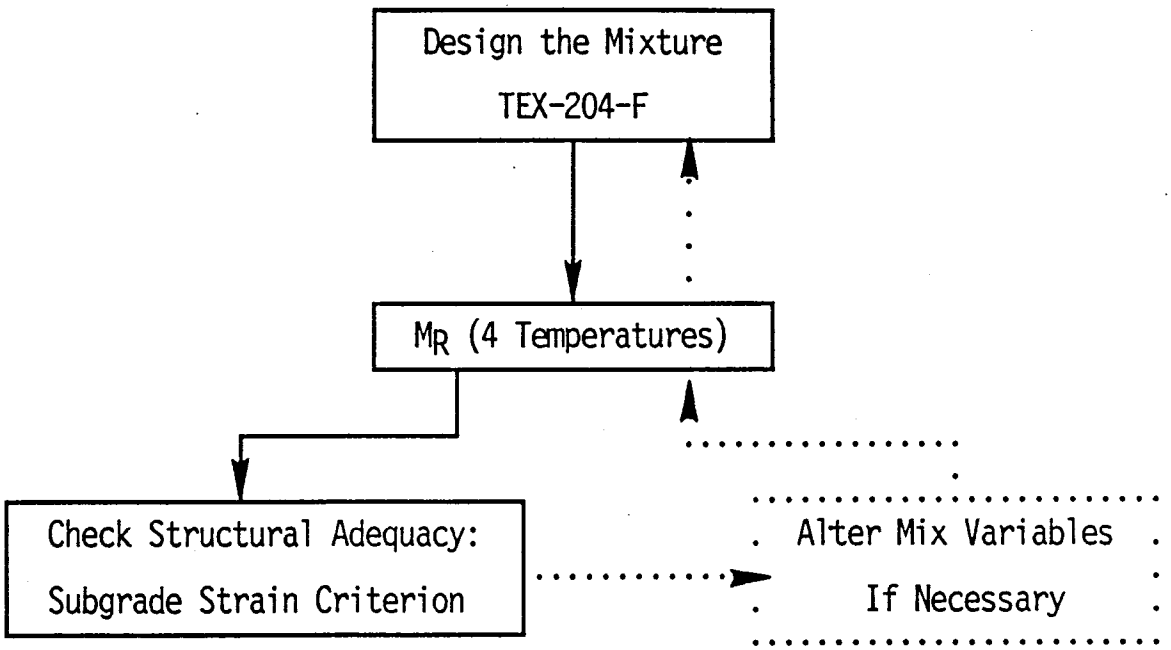

Figure 3. Flow chart for providing acceptable resilient modulus of HMAC in order to provide protection for weaker sublayers.

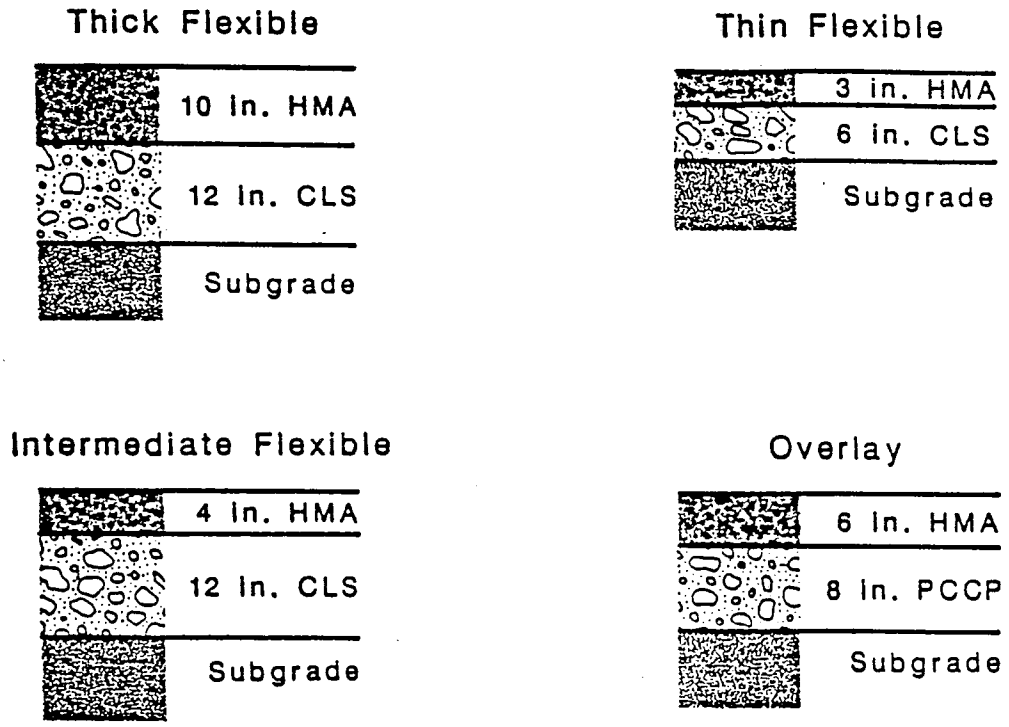

Figure 4. Illustration of pavement structural categories.

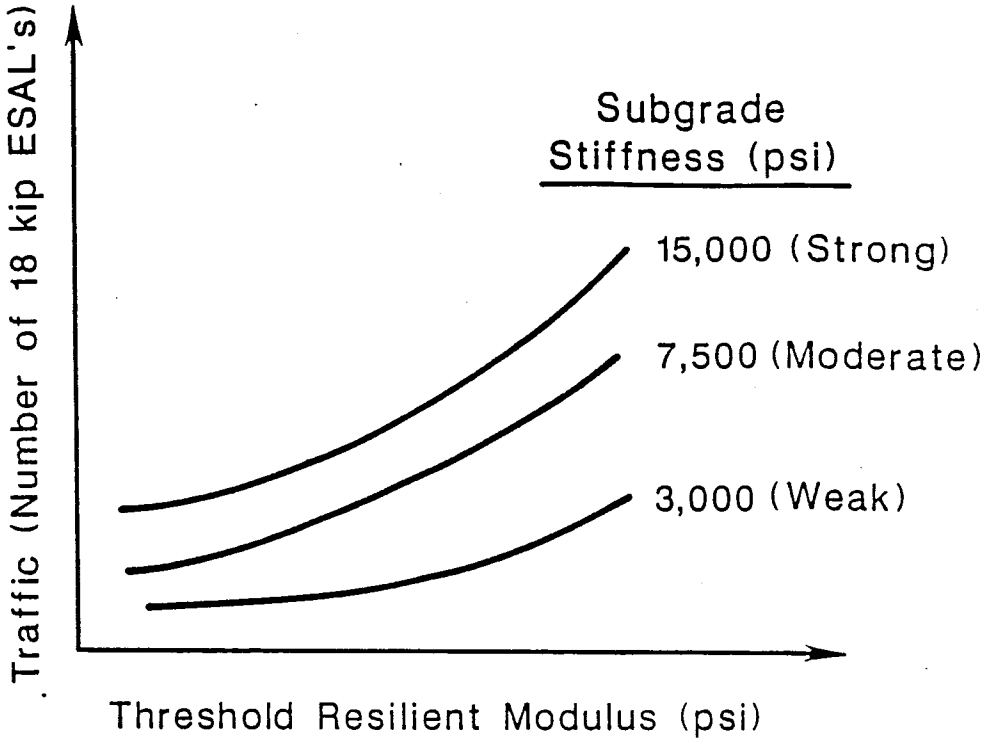

Figure 5. Selection of acceptable or threshold resilient modulus of the HMAC layer to insure subgrade protection based on subgrade stiffness and traffic level.

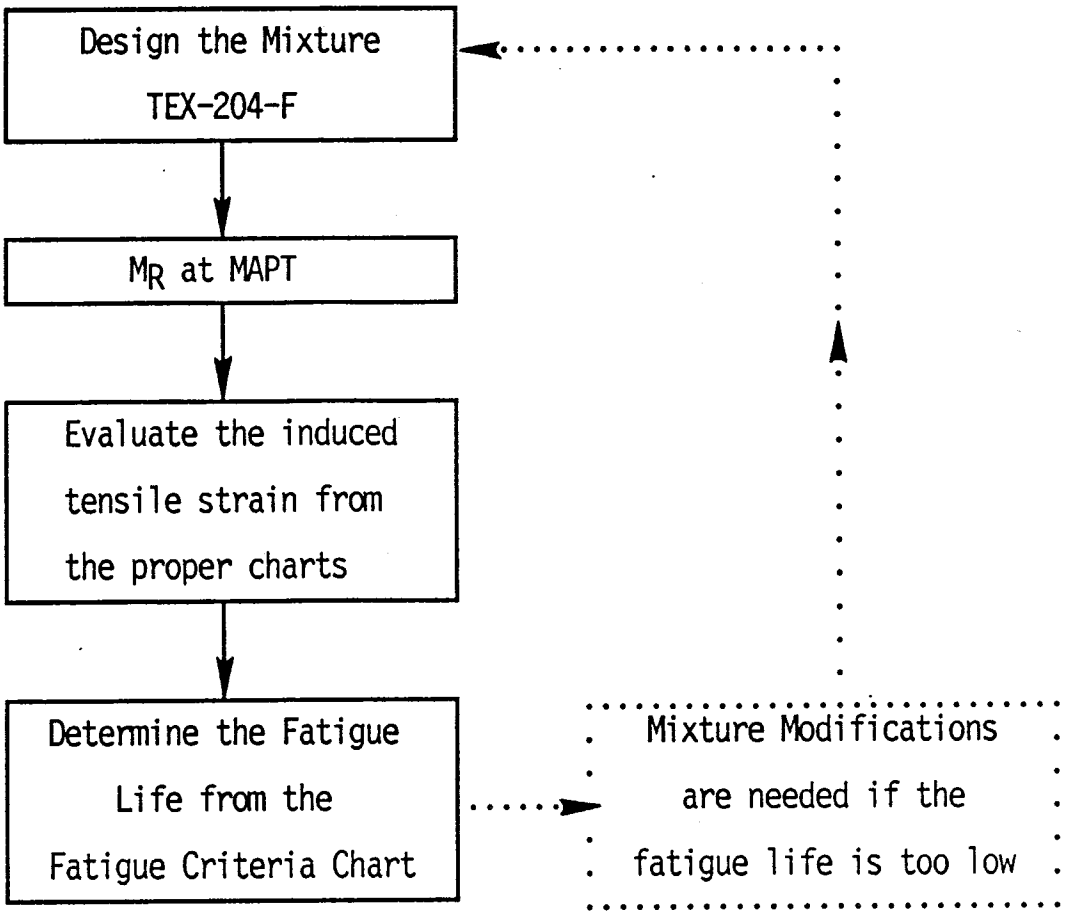

Figure 6. Flexure fatigue analysis flow chart

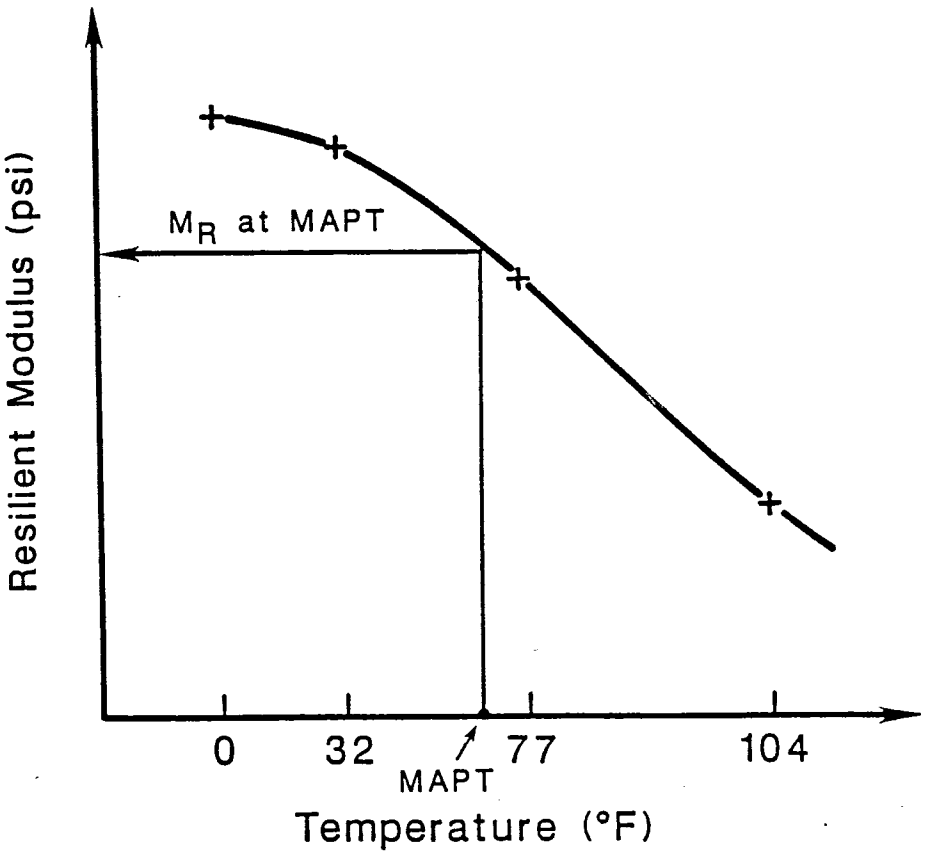

Figure 7. Selection of resilient modulus of the HMAC at the mean annual pavement temperature (MAPT).

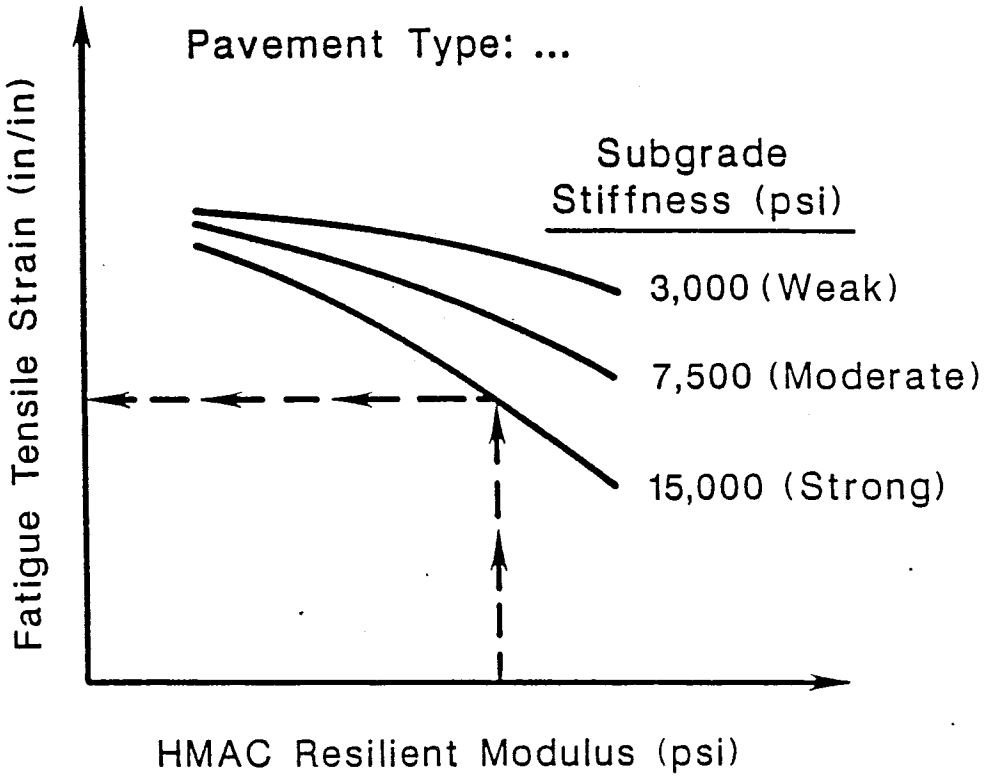

Figure 8. Selection of load-induced tensile strain in the HMAC layer for a given pavement structure.

These charts were developed using the results of over a hundred layered elastic computer runs. The final step in fatigue life evaluation is illustrated in Figure 9 employing flexural fatigue criteria which will be discussed in detail later.

Permanent Deformation

A flow chart summarizing the methodology incorporated in the permanent deformation evaluation is presented in Figure 10. As before, the first step is to generate the mix design in accordance with the existing Texas method of mix design, Test Method TEX-204-F (3).

The static creep and recovery tests are required to evaluate resistance to permanent deformation potential. The data from this simple test are collected in terms of deformations, both recoverable and irrecoverable, as a function of time. The irrecoverable portion of deformation is responsible for rutting; and by normalizing this viscoplastic deformation for laboratory stress conditions, a new parameter called viscoplastic stiffness is defined. Through the use of this parameter, rutting potential may be characterized by a series of charts on which actual creep/-recovery data are plotted. Depending upon the position of the data plots on the appropriate rutting criteria chart, one can adjust the potential of rutting from laboratory to field conditions. Figure 11 and 12 depict this process schematically. The mix under analysis is acceptable as its viscoplastic stiffness plot does not transgress into any regions representing areas of an unacceptable or questionable level of permanent deformation. Rutting criteria charts were developed for the four different classes of pavement structure with different levels of surface layer and subgrade stiffnesses addressed within.

Thermal Cracking

Low-temperature cracking of HMAC is evaluated in this procedure by the indirect tensile (IDT) failure envelope concept. Figure 13 illustrates the steps involved in the procedure. The conditions under which the failure envelope is developed simulate those that thermally activate pavement contractions. The laboratory measured failure envelope is plotted on the proper acceptance criteria chart and the acceptance or rejection decision is made based upon the position of the failure envelope

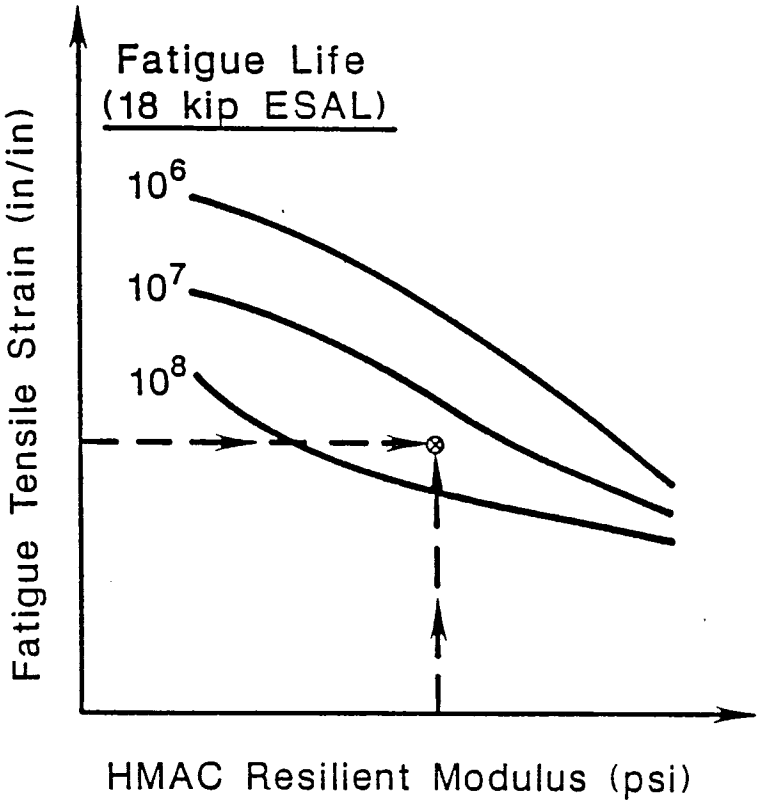

Figure 9. Approximation of fatigue life based on 18 kip ESAL's

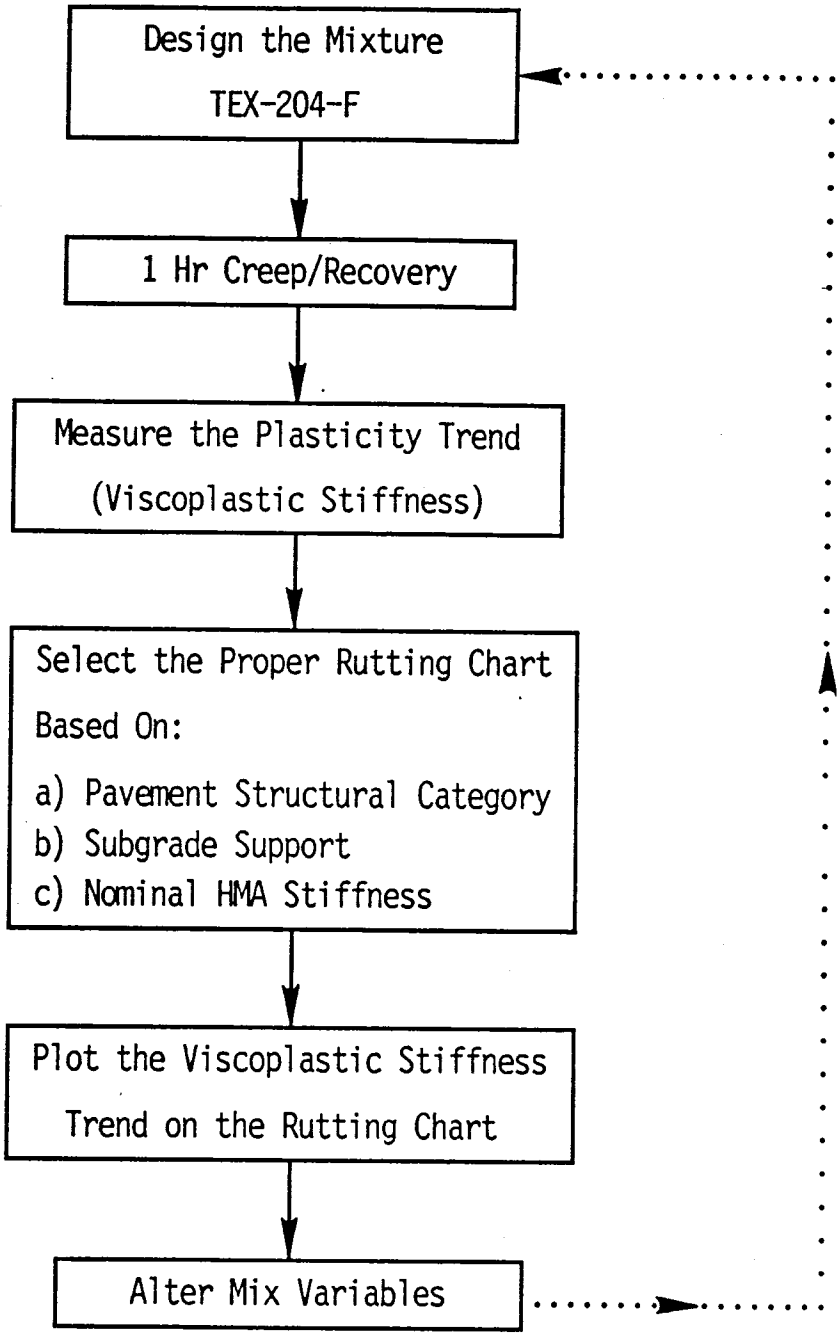

Figure 10. Flow chart for the evaluation of permanent deformation within the HMAC.

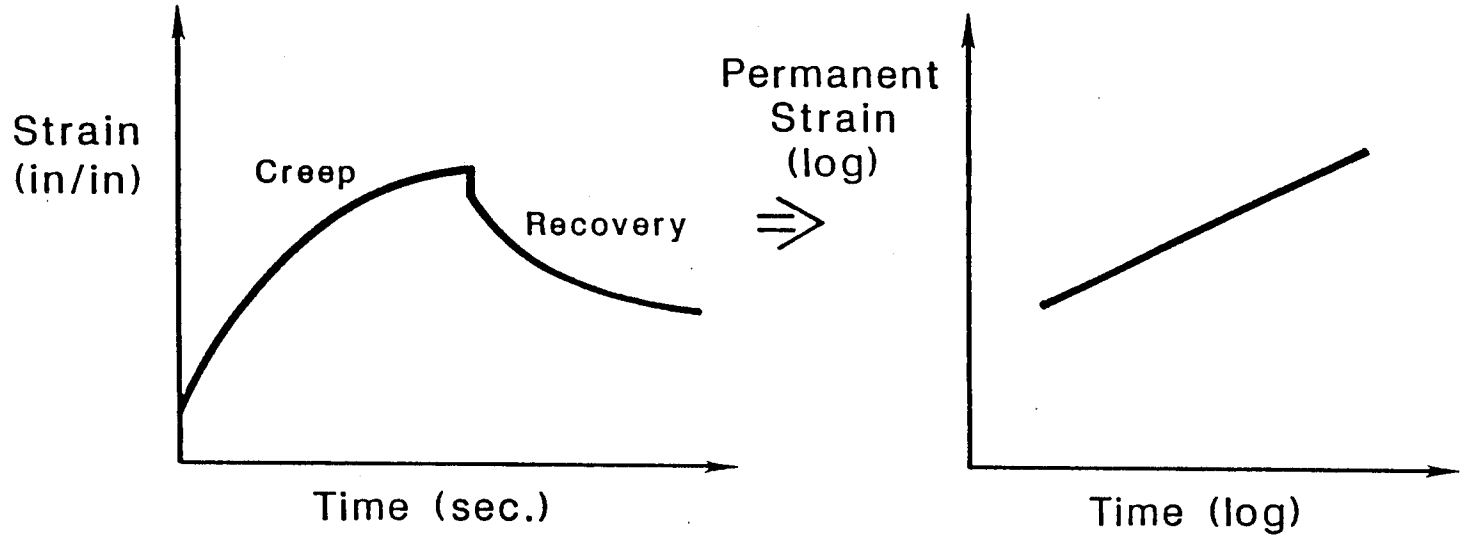

Figure 11. Permanent deformation versus time of loading developed from creep loading and creep recovery curves.

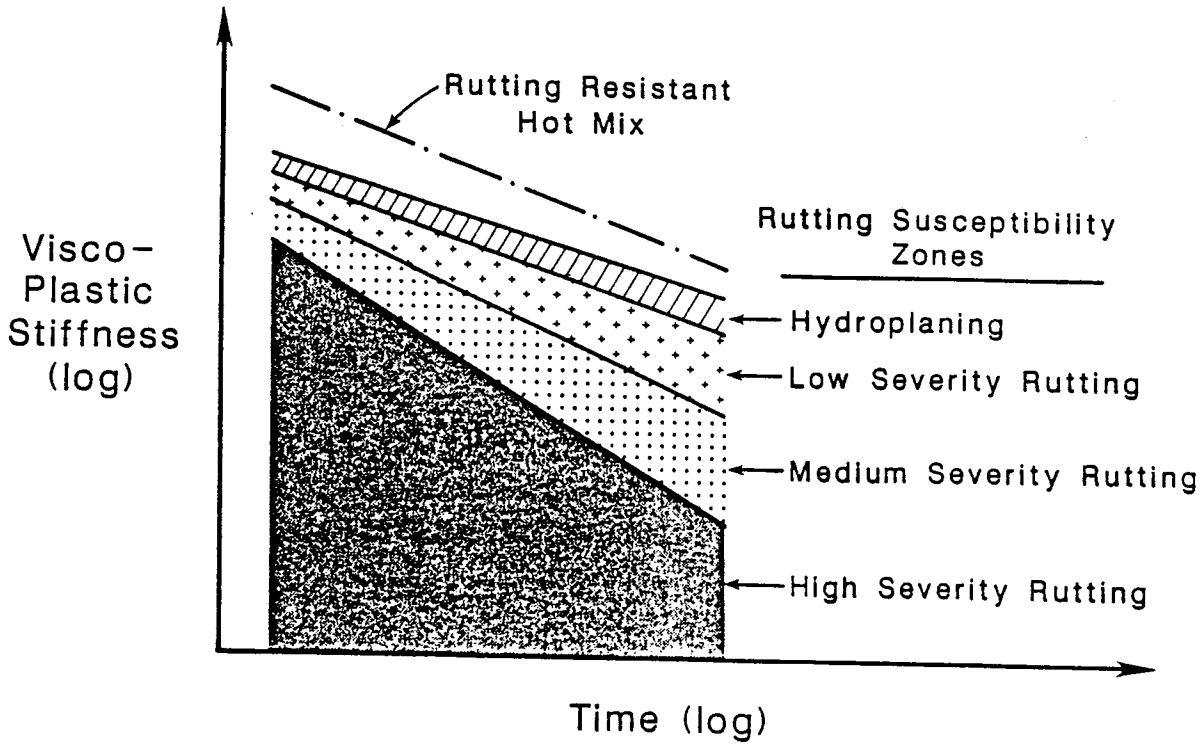

Figure 12. Evaluation of deformation or rutting potential based on viscoplastic stiffness as a function of time of loading.

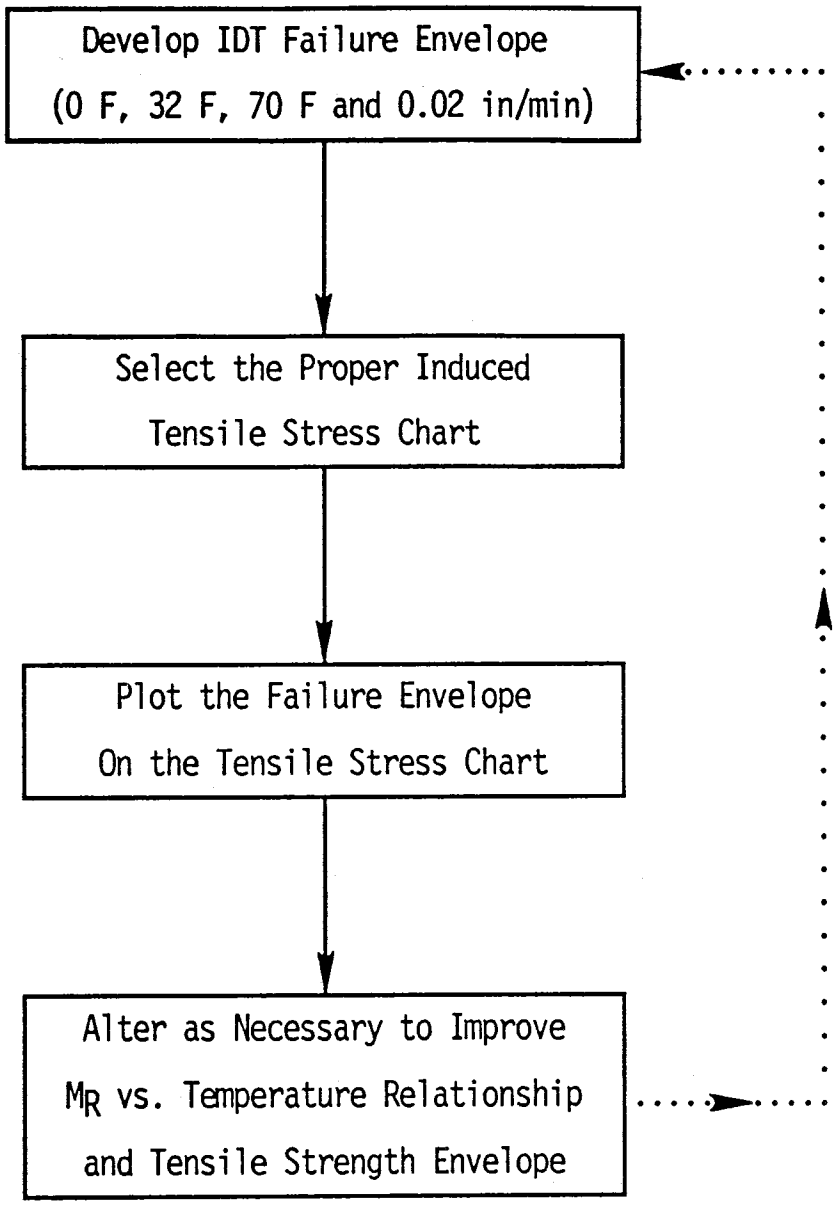

Figure 13. Flow chart illustrating evaluation of potential of thermal cracking in HMAC.

on the chart.

Thermal cracking criteria charts used to judge the IDT failure envelope are selected according to: a) the resilient modulus versus temperature relationship; and, b) the climatic regions of Texas in which the pavement will function. Utilizing the extensive body of existing resilient modulus versus temperature data, collected over the years at Texas A&M, different categories of response were established (Figure 14). A given mix will fall within one of the different regions based on its resilient modulus sensitivity to temperature. The proper, thermally-induced stress condition chart representing the climatic region of interest is selected next as a function of the modulus-temperature sensitivity region (Figure 15). Finally, the tensile strength failure envelope is superimposed on the proper low-temperature cracking chart (Figure 16), which is a function of modulus-temperature sensitivity (Figure 14) and climatic region.

In order to produce a mix more resistant to thermal cracking, it is necessary to achieve a balance between: a) tensile strength and b) resilient modulus. A softer mix at low temperature is more resistant to thermally-induced fracture than is a stiffer mix. Thus, an iterative process needs to be applied. If the stress envelope transgresses the selected boundary curve, mixture alterations are required to optimize the tensile strength versus resilient modulus relationship in order to promote resistance to thermal cracking.

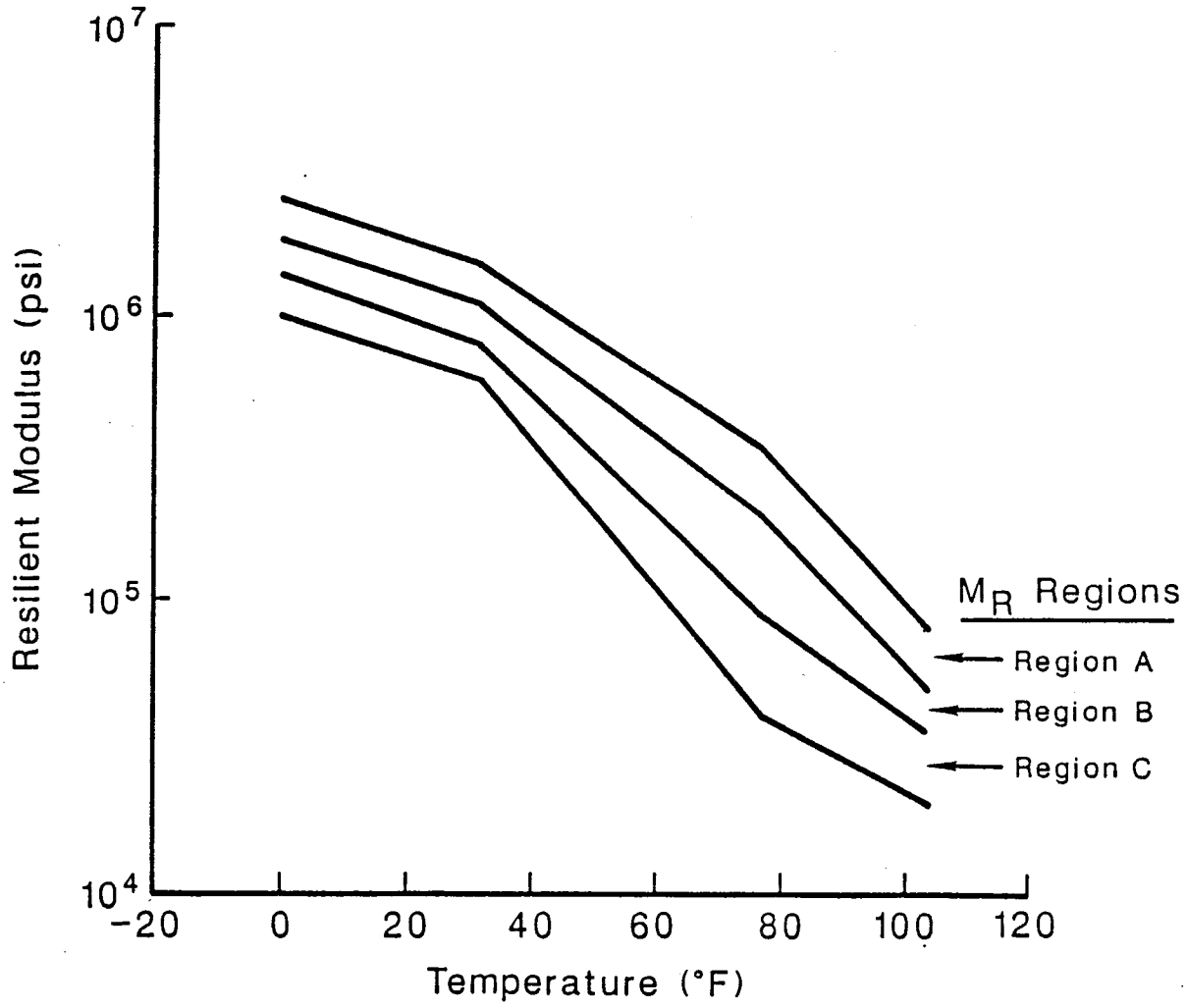

Figure 14. Resilient modulus versus temperature regions used in thermal fracture analysis.

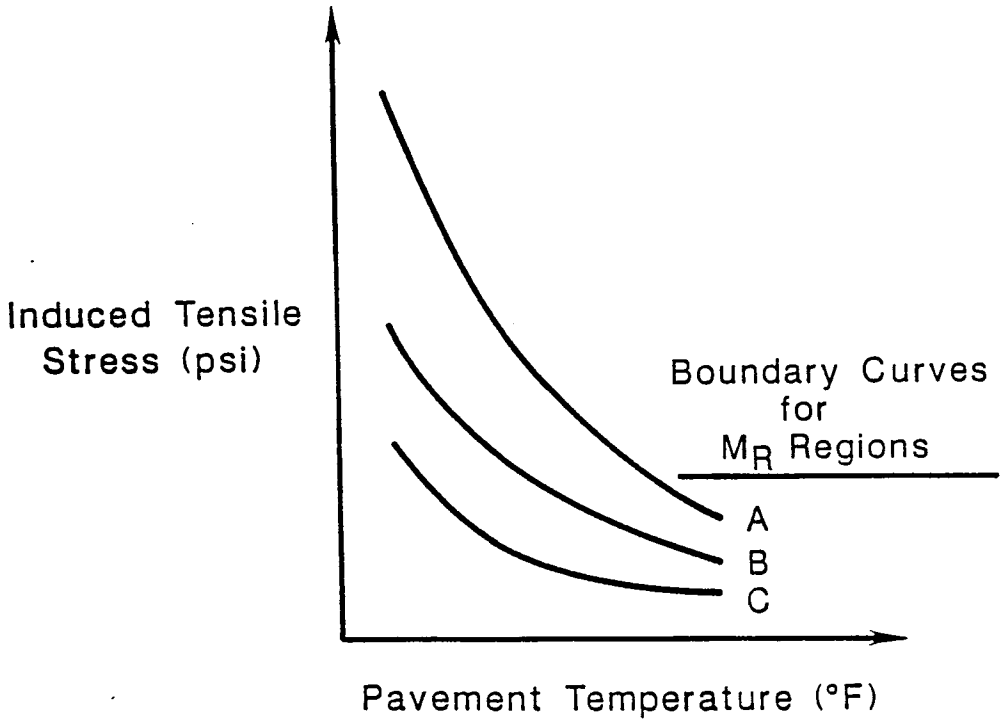

Figure 15. Induced stress versus pavement temperature as a function of resilient modulus versus temperature category.

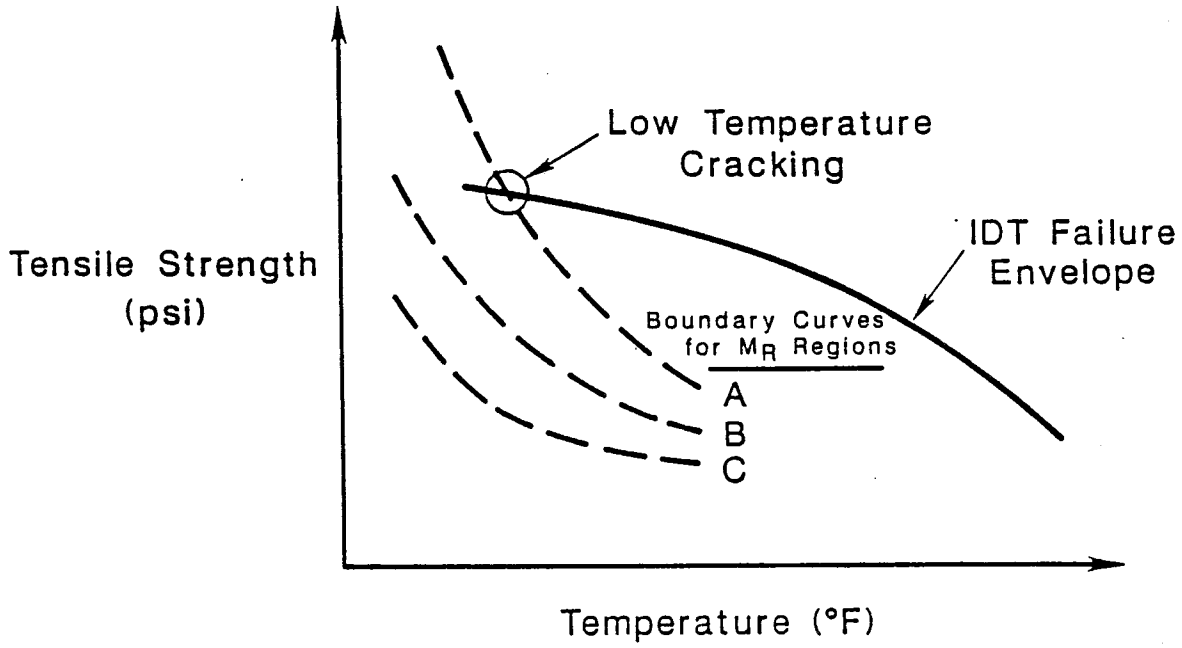

Figure 16. Illustration of method of evaluation of thermal fracture potential in HMAC using IDT failure envelope and proper regional boundary curve.

CHAPTER III

TEMPERATURE EFFECTS

Background

Mechanical behavior of asphaltic materials are highly dependent upon the temperature and the rate of loading. At higher temperatures, for a given loading rate, the HMAC is less stiff, hence it is less likely to adequately protect the base and the subgrade from being overstressed. Within the HMAC layer itself, resistance to permanent deformation drastically decreases at higher temperatures. At lower temperatures, HMAC is stiffer, and coupled with thermally-induced volume contractions, relatively high tensile stresses are mobilized which can lead to a greater potential for thermal cracking.

Texas Temperature Data

The climatic conditions across the State of Texas must be adequately accounted for in an extended analysis of a mix design procedure. Extensive temperature data are available from the State Climatologist (23). Examples of such data are illustrated in Figures 17, 18, and 19. This type of information was used as background in the development of temperature profiles within the actual pavement structures.

Researchers at Texas A&M University (24) have developed a regression model based on an extensive volume of weather data which predicts air temperature at any locality within Texas at any time during the year. The model then translates the predicted air temperature into pavement temperature profiles which are expressed as a function of depth for any category of pavement structure.

The regression model, which has been developed based on the 180 hottest days of an average year within the 30 years of the weather data studied, is divided into two important periods: one representing the daytime; another representing the nighttime. The representative R^2 values for these regression models for HMAC varying from 2 to 5 inches are all above 0.98. The general forms of the model are:

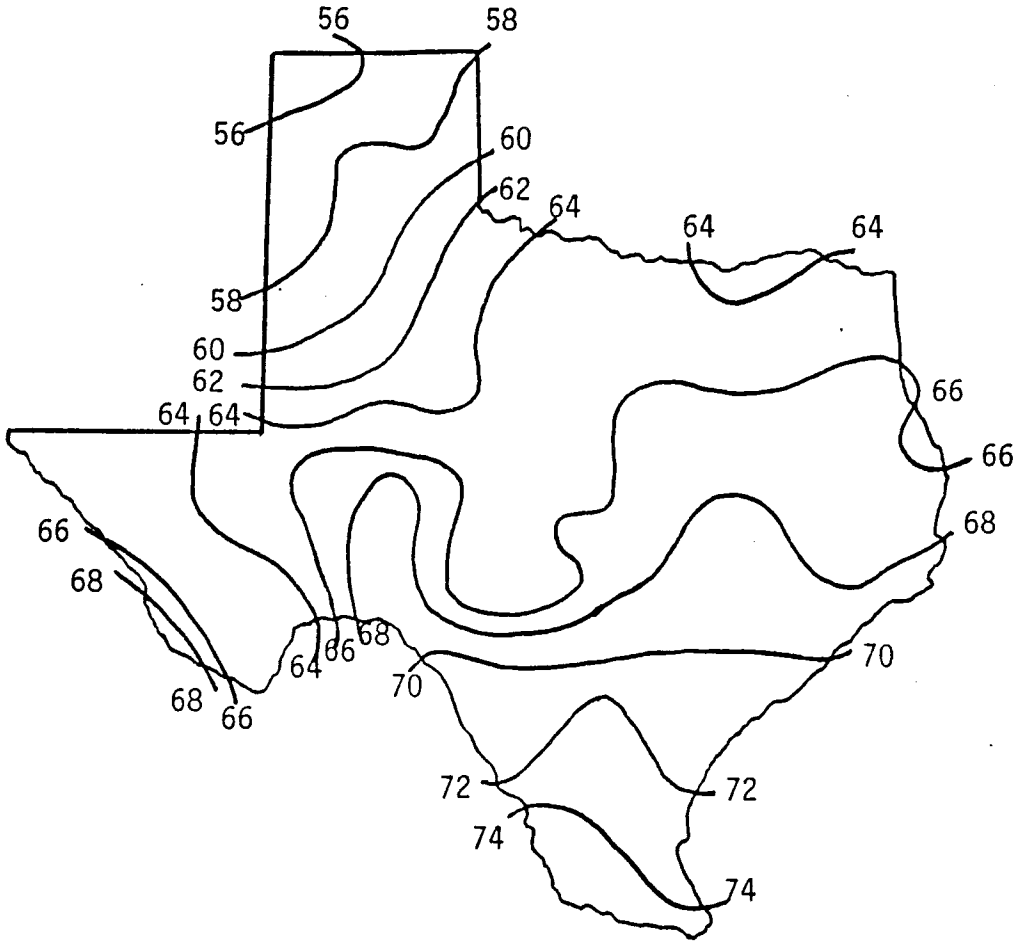

Figure 17. Texas weather data, mean annual air temperature in degrees Fahrenheit (after Reference 23).

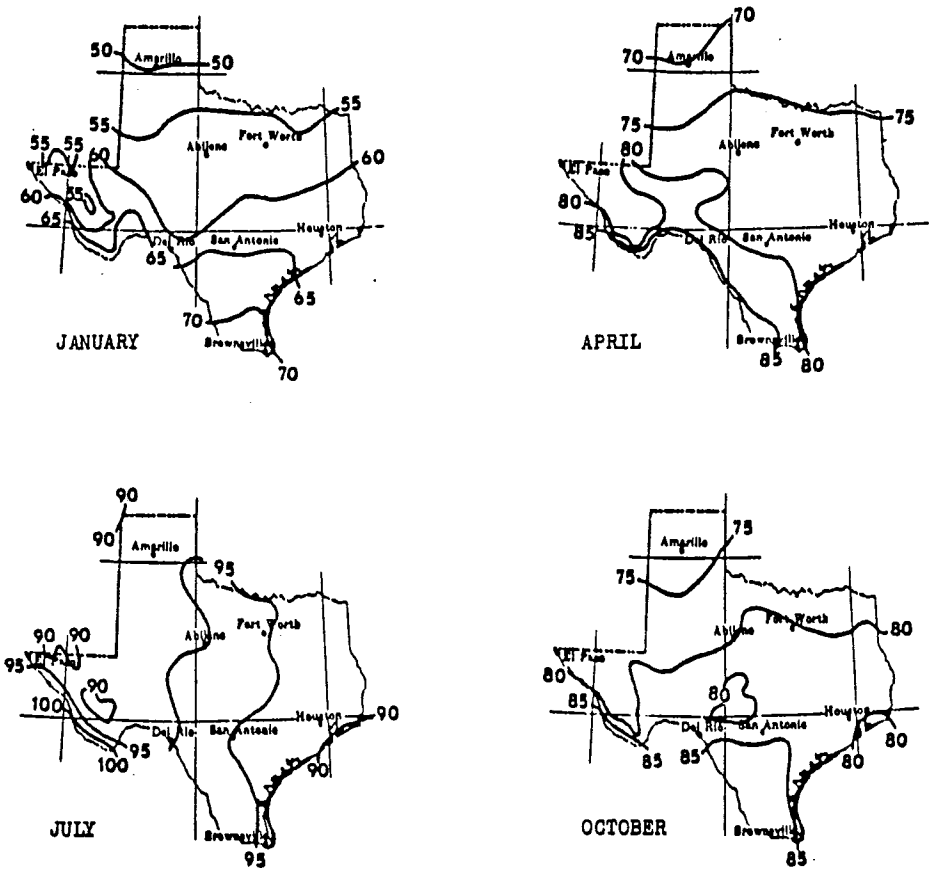

Figure 18. Texas weather data, normal daily maximum air temperature in degrees Fahrenheit (after Reference 23).

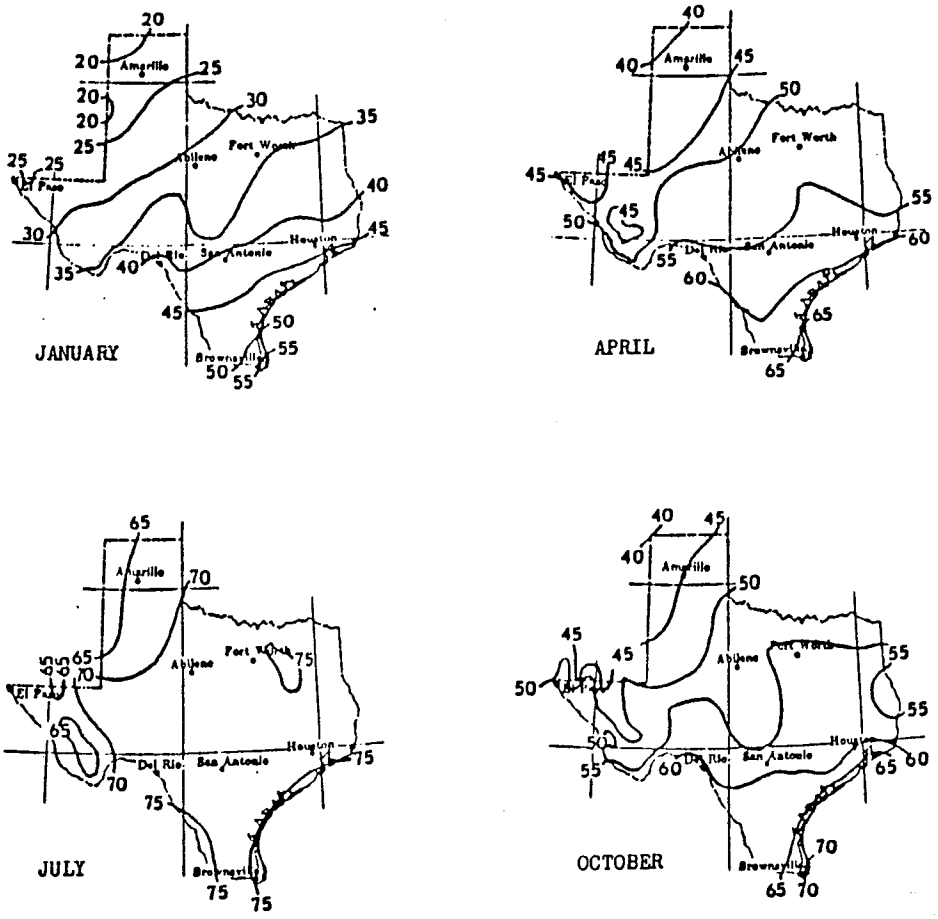

Figure 19. Texas weather data, normal daily minimum air temperature in degrees Fahrenheit (after Reference 23).

$$T = a_0 + a_1x + a_2y + a_3z + a_4yz + a_5x^2 + a_6y^2 + a_7y^2z + a_8y^3 \quad (1)$$

where: T = temperature at the center of each sub-layer,
x = period of year ($x = 1, 2, \ldots, 36$),
y = hour of the day ($y > 7$ and $y < 19$),
z = sublayer ($z = 1, 2, \ldots, n$), and
a's = regression constants,

and

$$T = b_0 + b_1x + b_2y + b_3z + b_4xz + b_5yx^2 + b_6y^3 + b_7y^4 \quad (2)$$

where: T = temperature at the center of each sub-layer,
x = period of year ($x = 1, 2, \ldots, 36$),
y = hour of the night ($y < 7$ and $y > 19$),
z = sublayer ($z = 1, 2, \ldots, n$), and
b's = regression constants.

These regression models offer the possibility of a comprehensive rutting prediction package in which one can superimpose the effect of traffic on the temperature. This can be done through an algorithm capable of performing a stepwise integration of traffic and temperature factors over the range of the common variable of time in a rutting model. A tentative procedure which was outlined by Li (24) offers the necessary tools for such an approach.

In the temperature analyses by climatic categories, the State of Texas was broken into four relatively distinct geographical regions (Figure 20). The study by Li (24) verifies that these four regions are statistically distinct for a mixture analysis of the type developed in this study. Temperature profiles for all four categories of pavement structure were generated for each climatic region within Texas. This was done using Texas weather data presented in Figures 17 through 19. Temperature profiles were generated using the methodology which was presented by Shell researchers (25).

For the rutting analysis, it was decided to select the hottest profile to represent the conservative case. The average condition of these hot profiles are summarized in Table 1. These average hot profiles are similar to those presented by Morris et al. (26), whose assumptions were assumed to be valid for this study:

Table 1. Design pavement temperatures for permanent deformation analysis derived from pavement temperature profile analysis.

Climatic Region	Pavement Structural Category			
	Thin Flexible	Intermediate	Thick Flexible	HMAC/PCCP Overlay
I	94*	95	90	92
II	110	106	102	104
III	107	105	100	102
IV	110	106	102	104

* Temperatures are in degrees Fahrenheit

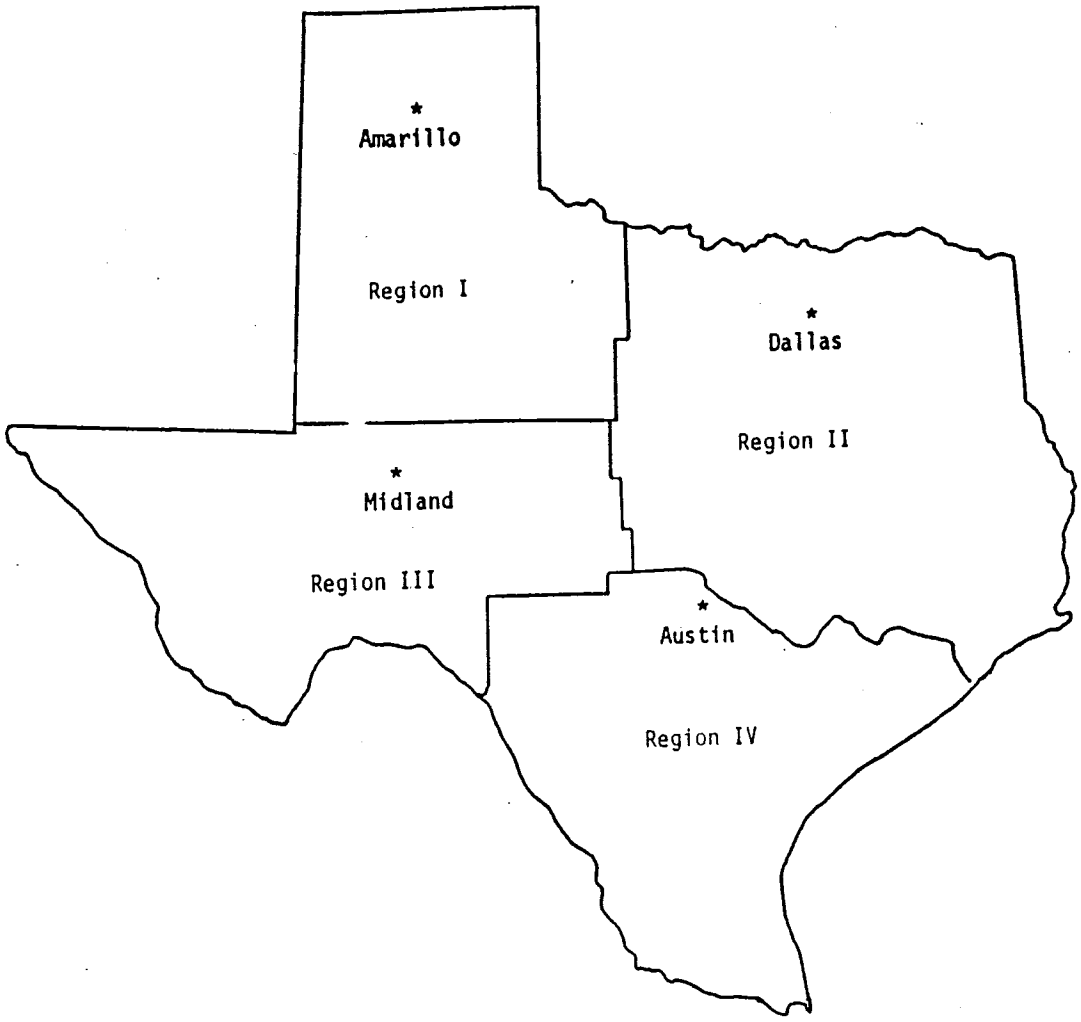

Figure 20. Temperature regions within Texas used in thermal analysis (after Reference 24).

a) Permanent deformation occurs daily over the time interval from 0730 to 1730 hours.

b) Permanent deformation occurs only in the period from April to October, inclusive.

c) Permanent deformation can be ignored at temperatures below 50°F.

CHAPTER IV

SPECIMEN FABRICATION TECHNIQUES

Background

The effect of specimen fabrication parameters on material characterization was investigated. A simple factorial study was conducted in order to consider mixing and compaction parameters such as: mixing temperature, compaction temperature, and method of compaction. The gyratory compactor is currently specified in Test Method TEX-204-F and unless clear justification is provided, it would be disruptive to change compaction procedures.

Furthermore, there is a growing consensus that the gyratory method of compaction more closely duplicates what actually occurs in the field during hot mix compaction (27, 28). In fact, the National Cooperative Highway Research Program (NCHRP), through the Asphalt Aggregate Mixture Analysis System (AAMAS) Project, is investigating the effects of various laboratory compaction methodologies such as Marshall impact, kneading, rolling wheel, and static compaction, on the void structure and engineering properties of asphalt mixtures. Based on the results of field-compacted and laboratory-compacted specimens, a decision will be made by AAMAS researchers as to which laboratory compaction method most closely simulates field compaction. Preliminary results from the AAMAS study indicate that the gyratory method of compaction is more consistent with actual field compaction based on air void content, density, and material properties of indirect tensile strength and resilient modulus (17). It was because of the breadth of the NCHRP study that an extensive comparison of compaction techniques was not included in this study.

Compaction Experiments

The objective of this phase of research was to select and recommend a "proper" method of compaction compatible with the new improved mix design procedure. Arrangements were made for either using the existing gyratory method or to propose a new method of compaction.

Laboratory specimens were fabricated using only two techniques: the Texas gyratory compaction, and mechanical Marshall impact compaction.

The gyratory compactor was selected because it is currently used for all Texas SDHPT mix design work. The mechanical Marshall impact compactor was selected because it is the most widely used among the bituminous community and it offers a different and simple alternative for comparison.

These experiments included two factors:

a) Method of compaction (two levels);
   1) Texas gyratory (Test Method TEX 204-F), and
   2) Marshall impact (ASTM 1559).
b) Compaction temperatures (three levels);
   1) 175°F,
   2) 250°F, and
   3) 300°F.

Each experimental cell contained three replicates so that statistically, it was possible to search for the compaction temperature at which the random variability in mechanical behavior of the HMAC, caused by non-uniform compaction, is minimized. The objective of this experiment was to select the method of compaction which would result in less random variability (noise) and therefore more uniform, laboratory-compacted specimens.

Mixing temperature was not included in this experimental matrix. Instead, the results of a recent study conducted at the University of Texas at Austin (UT) were used in this study (27, 28). Researchers at UT compared mixtures prepared in continuous dryer plants with batch plant mixes. They concluded that as long as the operating temperatures are within a "reasonable range," the mixing temperature does not significantly affect the engineering properties of HMAC - see Figures 21 through 24. The parameters which were investigated in the UT study included: density, Hveem stability, and tensile strength. None of these parameters were significantly affected by mixing temperatures ranging from 180°F to 320°F. Tahmoressi (27) concluded that the in-place field density had the most effect on engineering properties of hot mix.

Indirect tensile (IDT) tests were conducted on specimens manufactured by Marshall and Texas gyratory devices. The results are tabulated in Tables 2 and 3. Figures 25, 26, and 27 are graphical representations of

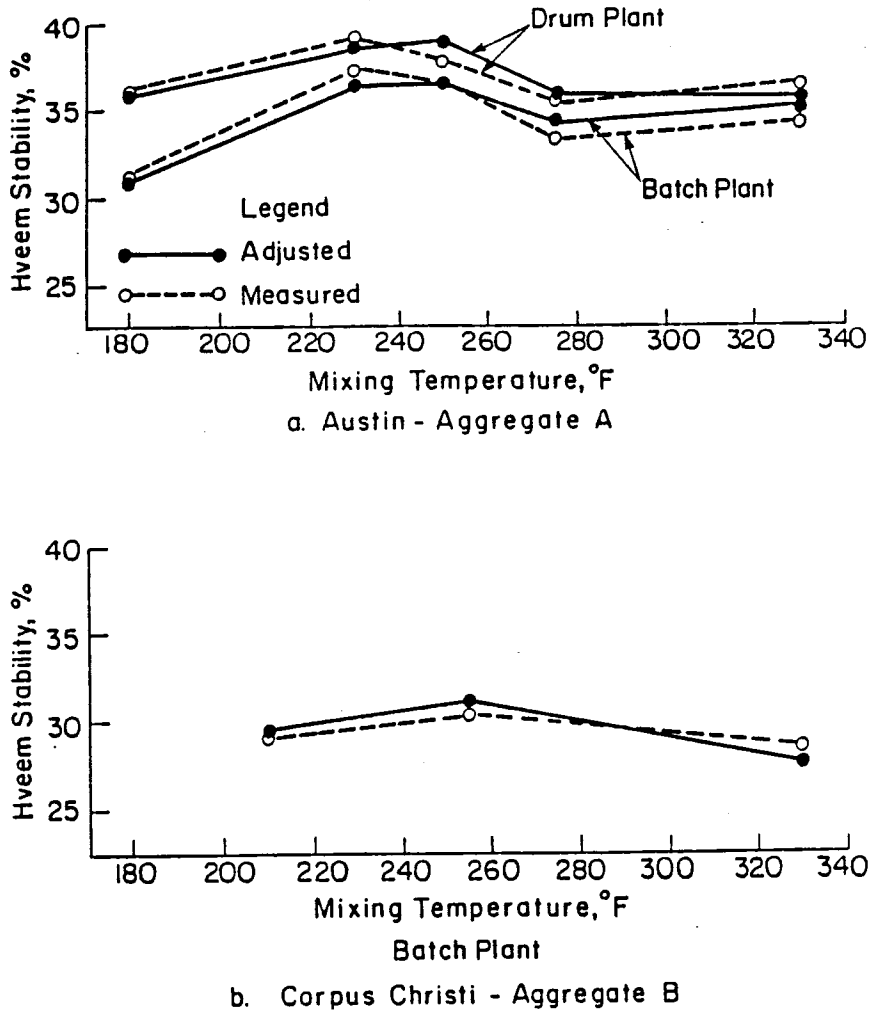

Figure 21. Relationship between mixing temperature and Hveem stability (after Reference 27).

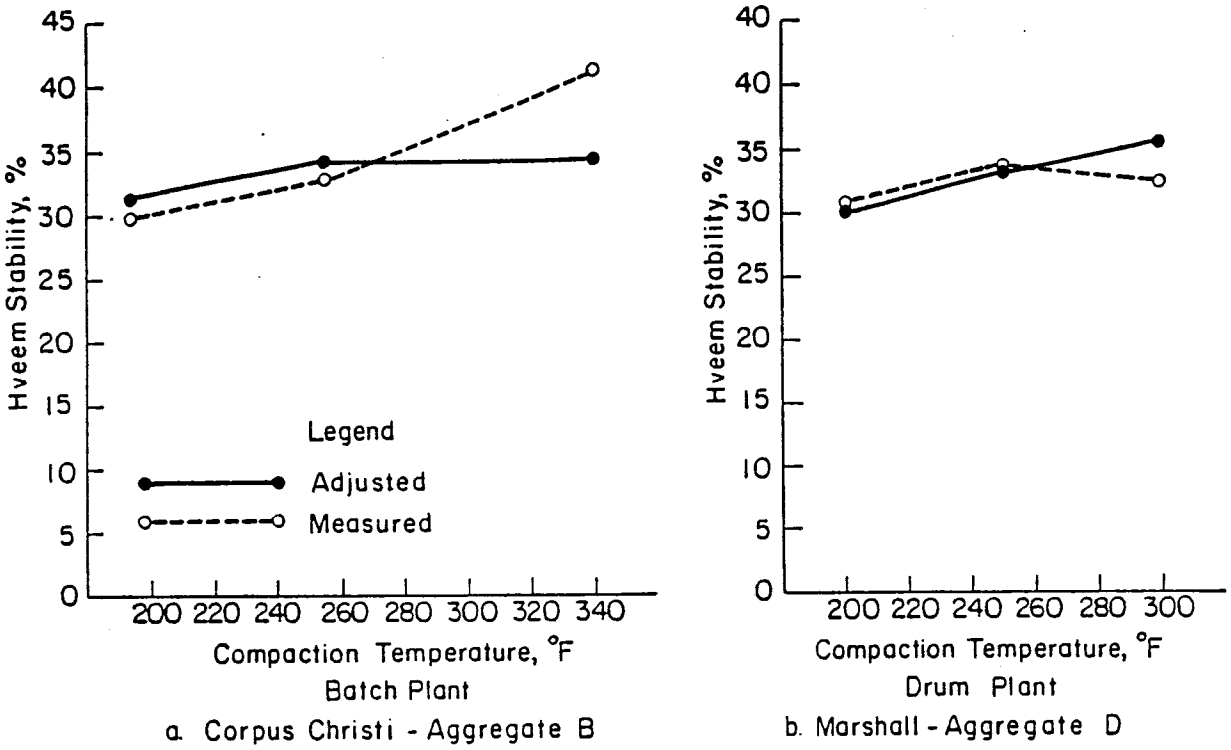

Figure 22. Relstionship between compaction temperature and Hveem stability (after Reference 27).

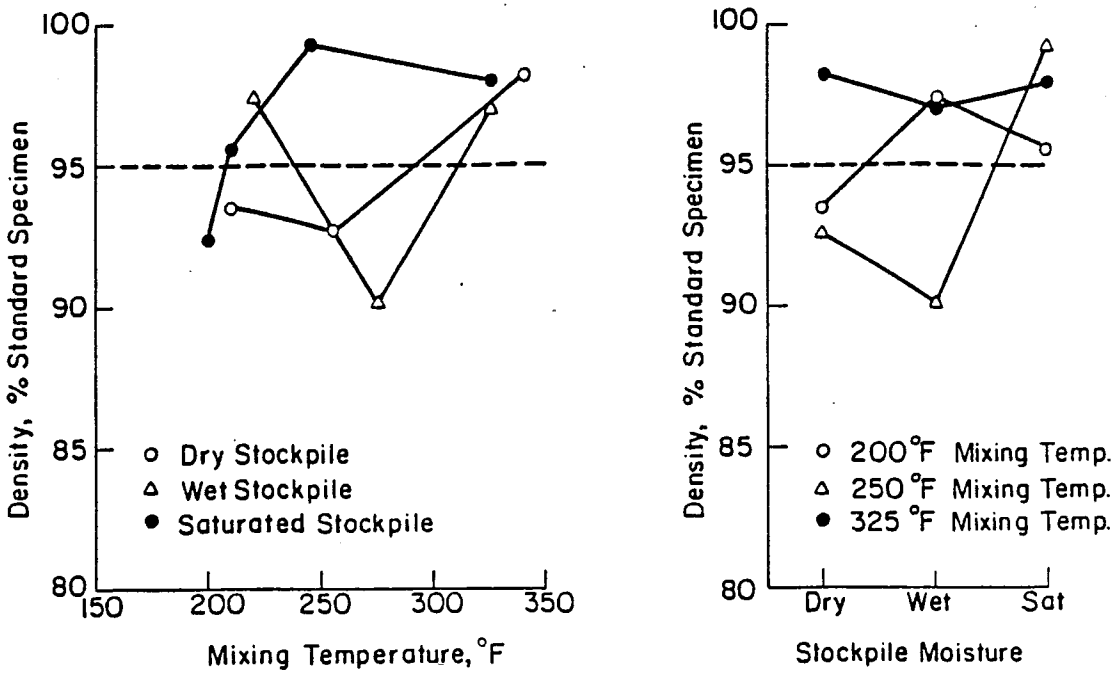

Figure 23. Relationship between measured core densities and mixing temperature and stockpile moisture (after Reference 27).

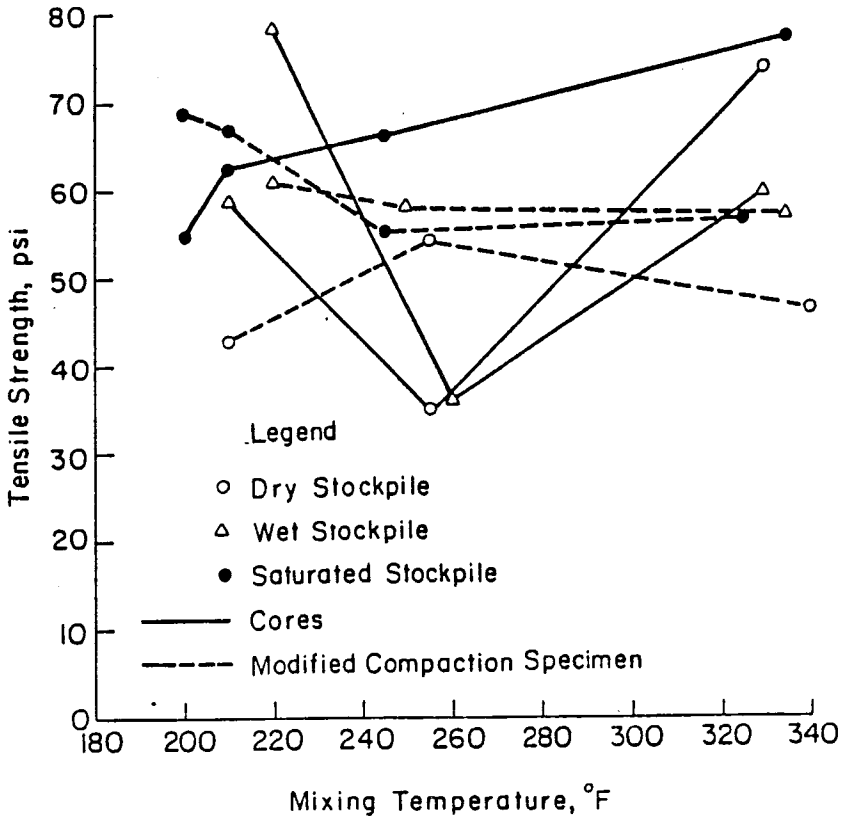

Figure 24. Comparison between tensile strength of cores and modified compaction specimens (after Reference 27).

Table 2. Indirect tensile results for specimens compacted according to the Marshall method.

Compaction Temperature, °F	Tensile Strength, psi	Strain at Failure, x 10^{-3} in/in	Average Percent Air Voids
175	75.47	4.67	
	76.62	3.75	7.74
	78.04	4.63	
250	106.59	3.69	
	115.76	3.56	5.14
	116.91	3.13	
300	140.57	3.13	
	137.17	3.13	3.44
	138.71	3.00	

Table 3. Indirect tensile results for specimens compacted according to the Texas gyratory method.

Compaction Temperature, °F	Tensile Strength, psi	Strain at Failure, x 10^{-3} in/in	Average Percent Air Voids
175	90.51	4.56	
	95.59	4.25	2.52
	91.59	4.00	
250	106.86	4.06	
	106.79	3.75	2.51
	109.76	3.75	
300	110.52	4.38	
	113.47	3.44	1.42
	121.73	3.44	

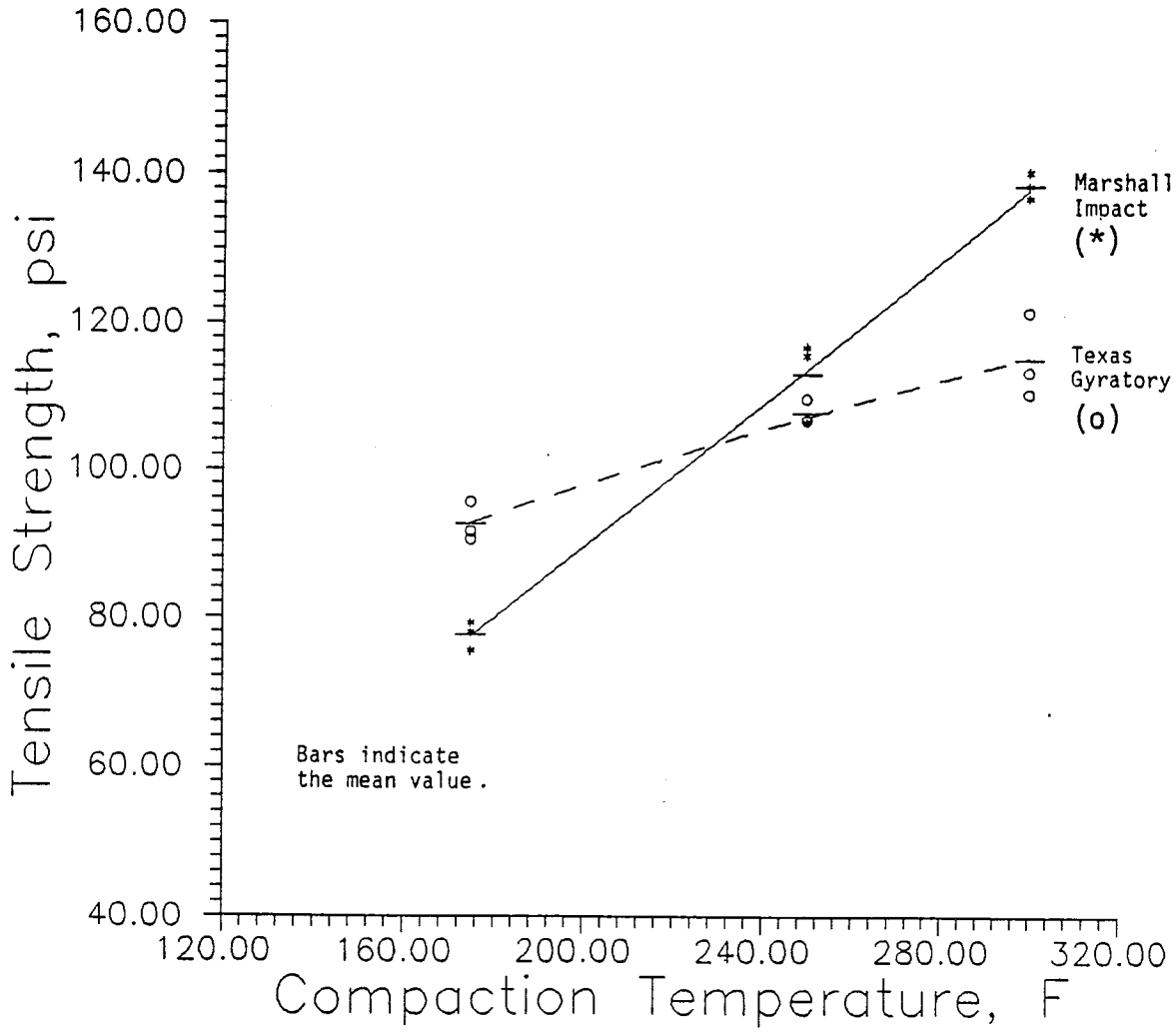

Figure 25. Tensile strength as a function of compaction temperature for two compaction methods.

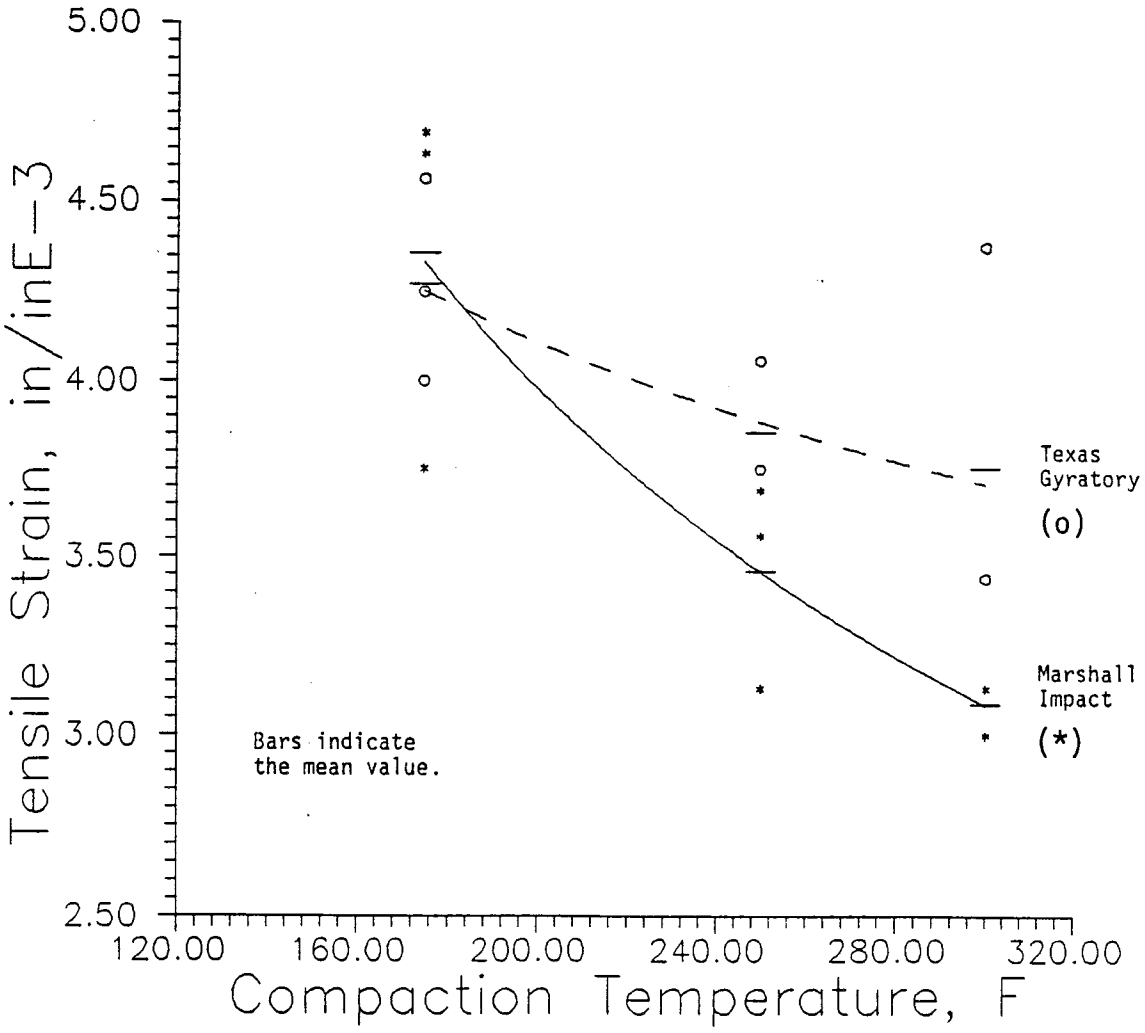

Figure 26. Tensile strain at failure as a function of compaction temperature for two compaction methods.

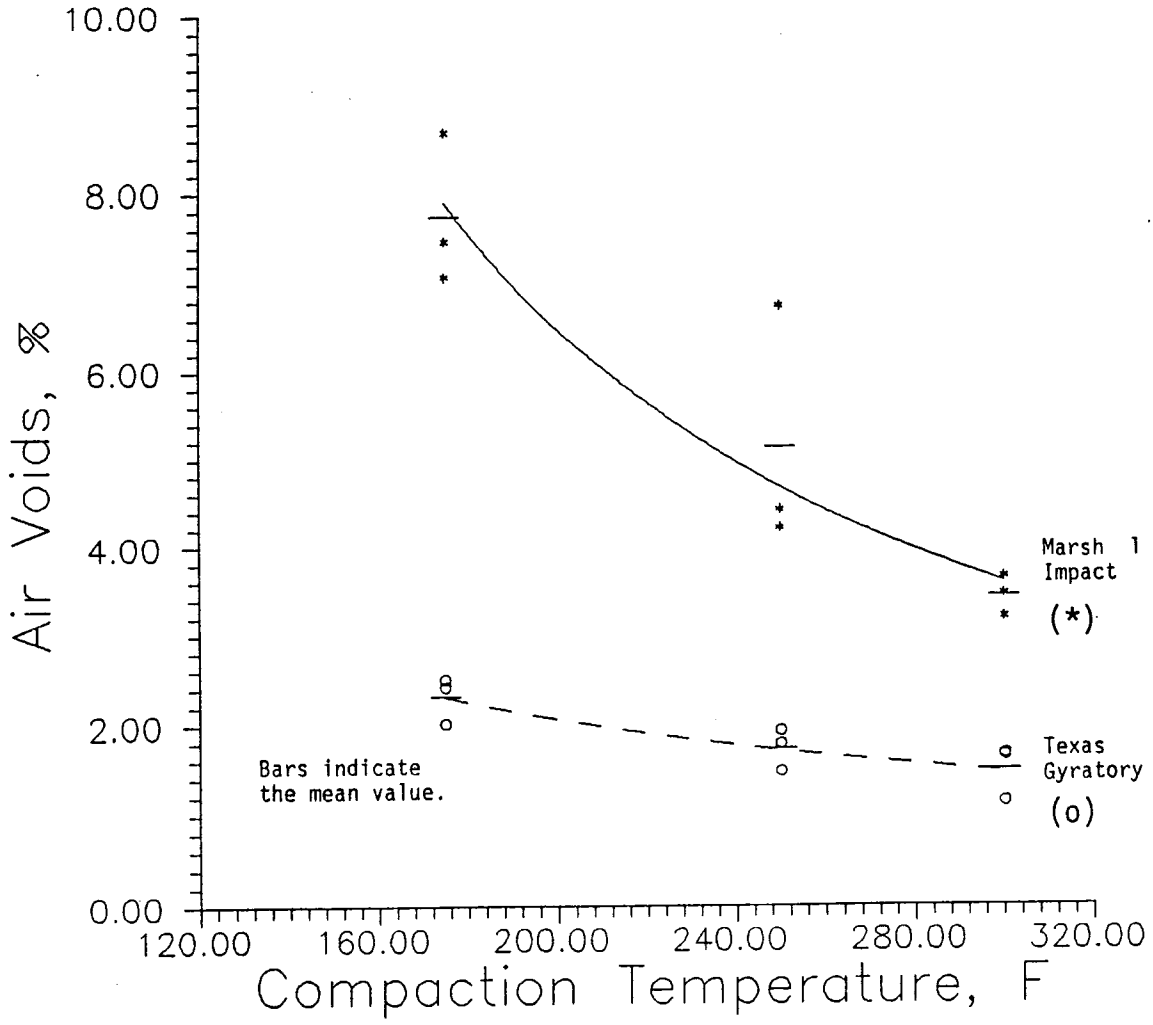

Figure 27. Air voids content as a function of compaction temperature for two compaction methods.

these data.

Statistical analyses were carried out to determine which method of compaction minimized variability in engineering properties of HMAC. The analyses were based on the stress at failure (tensile strength) and strain at failure. Tests for statistical significance were conductedusing the hypothesis of equality of variance between the two methods. The level of significance was set at 95% (α = 0.05). The statistical analyses led to the following conclusions:

a) Random variability (noise) in the tensile strength and strain at failure is unaffected by the method of compaction.
b) Variability in the air void content over the range of compaction temperatures was significantly lower for the gyratory compacted specimens. Therefore, it appears that the Texas gyratory method of compaction produces specimens that are more uniform.

As a result of these analyses, the Texas gyratory compaction device was selected for sample fabrications. This was also done with the added confidence that it realistically approximates field compaction and produces samples with acceptable variability when compared to one other widely-used compaction method.

During the course of this study, it was determined that laboratory-manufactured specimens should be compacted to different levels of air void content: a) 6-8% air void content representing conditions immediately after construction; and, b) 2-4% air void content representing in-service mixtures after two years of traffic-induced densification.

This rationale, which should be the topic of future research studies, could lead to a better characterization of premature failure of tender mixtures. In this regard, a Mohr-Coulomb-type failure envelope methodology can be utilized effectively. This is one topic of investigation of a follow-up study, TTI Project 1170.

CHAPTER V

MIXTURE STIFFNESS REQUIREMENTS

In a pavement system, the stiffness of an asphalt layer plays a critically important role in the distribution of stresses throughout the sublayers. Deformation characteristics of HMAC, both recoverable and irrecoverable, are greatly influenced by its stiffness. The irrecoverable portion of deformation, plastic and viscoplastic, in the asphalt layer is analyzed extensively in Chapter VI.

This chapter addresses the pseudo-elastic responses in the pavement structure which are heavily influenced by the HMAC, specifically, tensile strains within the HMAC layer, and vertical compressive stresses and strains at the top of the subgrade. These parameters are primarily controlled by layer thicknesses and layer moduli ratios for a given wheel load (i.e., 18 kip single-axle load). An iterative process is presented in this chapter for finding a threshold resilient modulus for the asphalt layer which will maximize subgrade protection and fatigue life.

Excessive Subgrade Deformation

The primary function of any pavement structure is the protection of the subgrade from high compressive stresses which induce permanent deformation within the subgrade, and in turn, pavement roughness.

Three categories of subgrades were included in this analysis: weak, moderate, and stiff. The approximate engineering properties of the three categories of subgrades are given in Table 4.

Table 4. Subgrade classification table.

	Engineering Properties		
Types of Subgrade	Resilient Modulus (psi)	CBR (%)	Texas Triaxial (class)
Weak	3,000	2	5.5
Moderate	7,500	5	4.5
Strong	15,000	10	3.5

Shell researchers state that the number of 18 kip axle passes which will produce a 3/4 inch rut depth in the wheel path can be approximated by the following relationship as reported by Monismith and Finn (29):

$$N_{18} = 6.15 \times 10^{-7} \epsilon_3^{-4} \quad (3)$$

where: N_{18} = number of 18 kip axle passes to cause a 3/4 inch subgrade deformation, and

ϵ_3 = vertical compressive strain at the top of the subgrade.

There are other subgrade rutting models similar to the Shell model. The comparisons of these are shown in Figure 28 (Reference 25). All of these models are empirical; however, they are performance-based. According to these models, a threshold or minimal resilient modulus of the HMAC layer is required to protect the softer, lower layers from being overstressed.

A series of charts was developed for determination of threshold resilient moduli for the four classes of pavement structures discussed earlier. The ensuing analytical evaluations were accomplished using a layered elastic computer model called CHEVPC (30). The results are presented in Figures 29 through 32. From these charts, one can select the minimum level of HMAC stiffness, measured in terms of its resilient modulus.

If the laboratory-measured resilient modulus is less than the required threshold value, some mixture alterations may be necessary. These alterations may include a change in asphalt cement (AC) grade and content, aggregate gradation modifications, or a combination of both.

Analyses of threshold resilient moduli are to be conducted at the mean annual pavement temperature. A simple chart is provided in Figure 33 which translates the air temperature into the pavement temperature. This chart accounts for the thickness of the HMAC layer and can lead to a reasonable estimate of HMAC temperature. This estimate can be made more accurate through the use of pavement temperature models which account for cloud cover, solar radiation, wind velocity, etc.. Models proposed by Corlew and Dickson (31), Dempsey (32), and Li (24) could improve the accuracy of pavement temperature predictions.

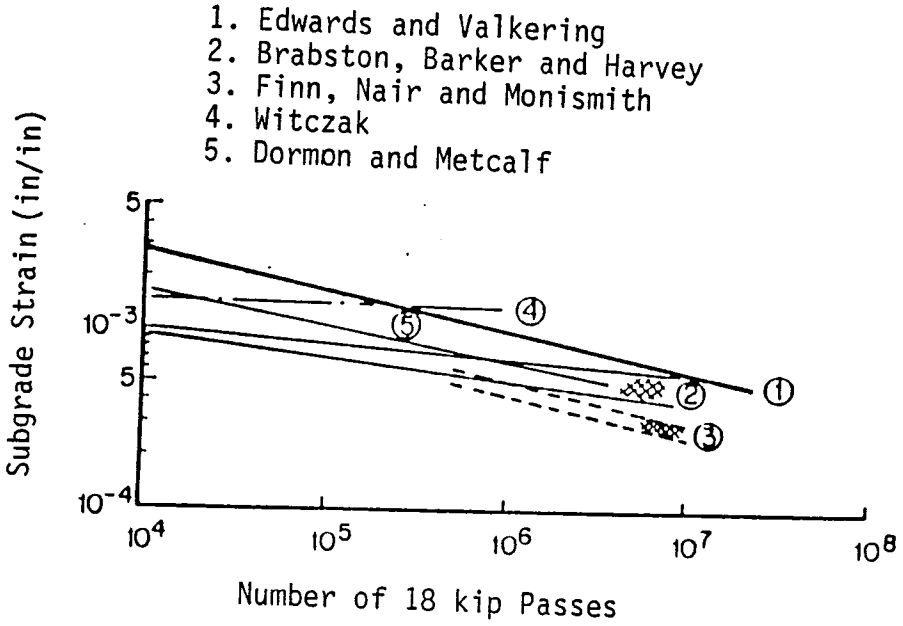

Figure 28. Excessive subgrade deformation criteria (after Reference 29).

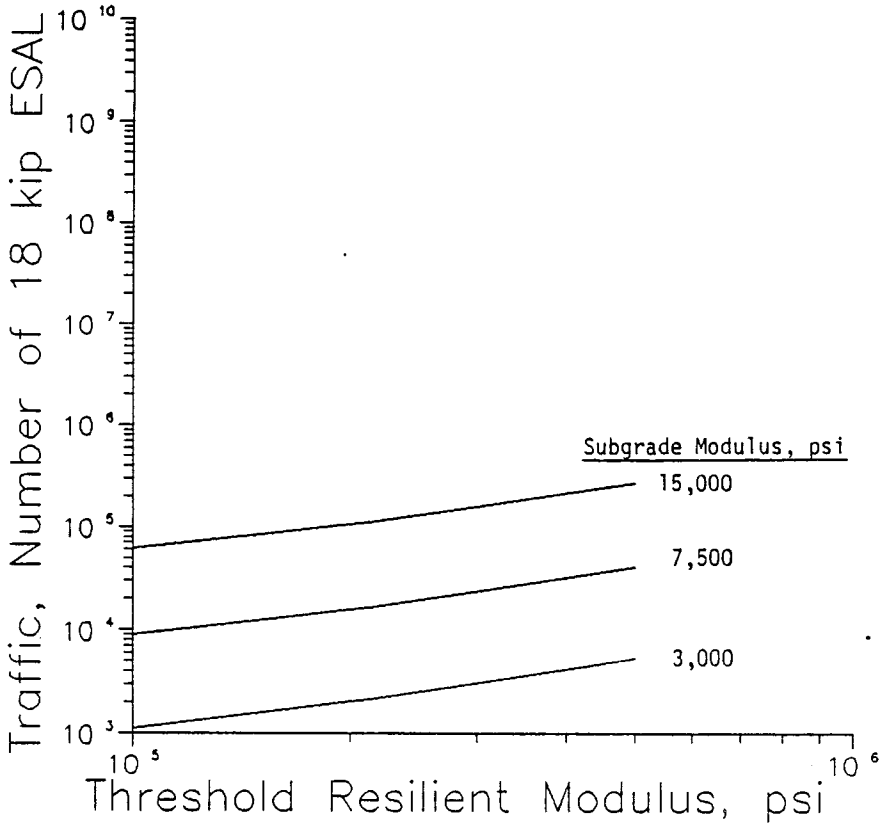

Figure 29. Threshold resilient modulus determination chart for a thin flexible pavement.

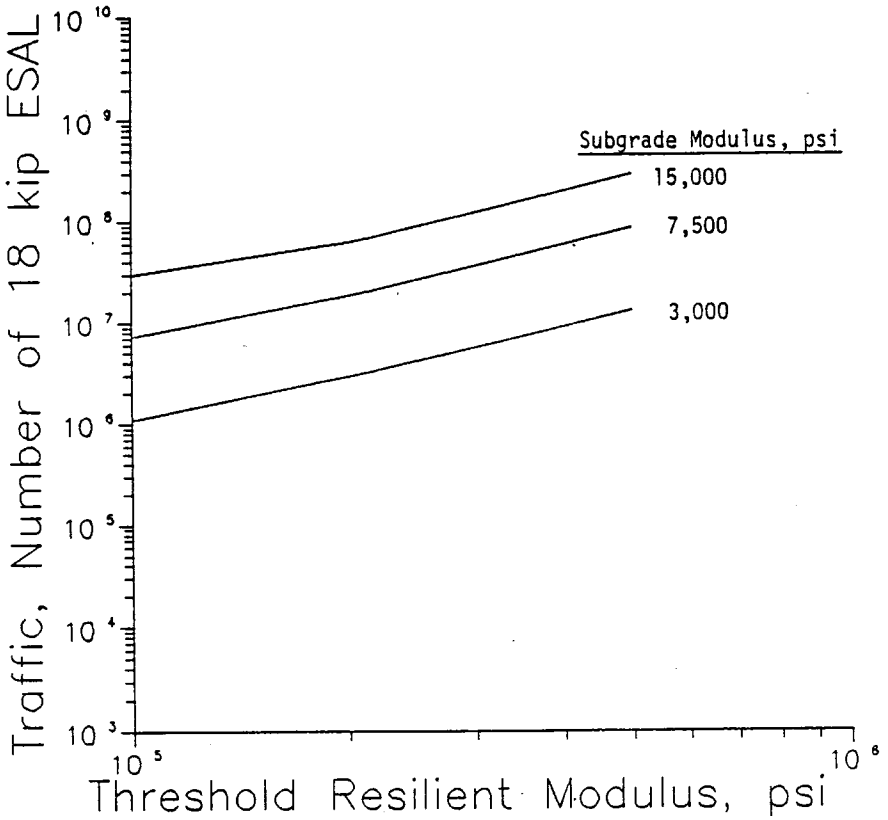

Figure 30. Threshold resilient modulus determination chart for a thick flexible pavement.

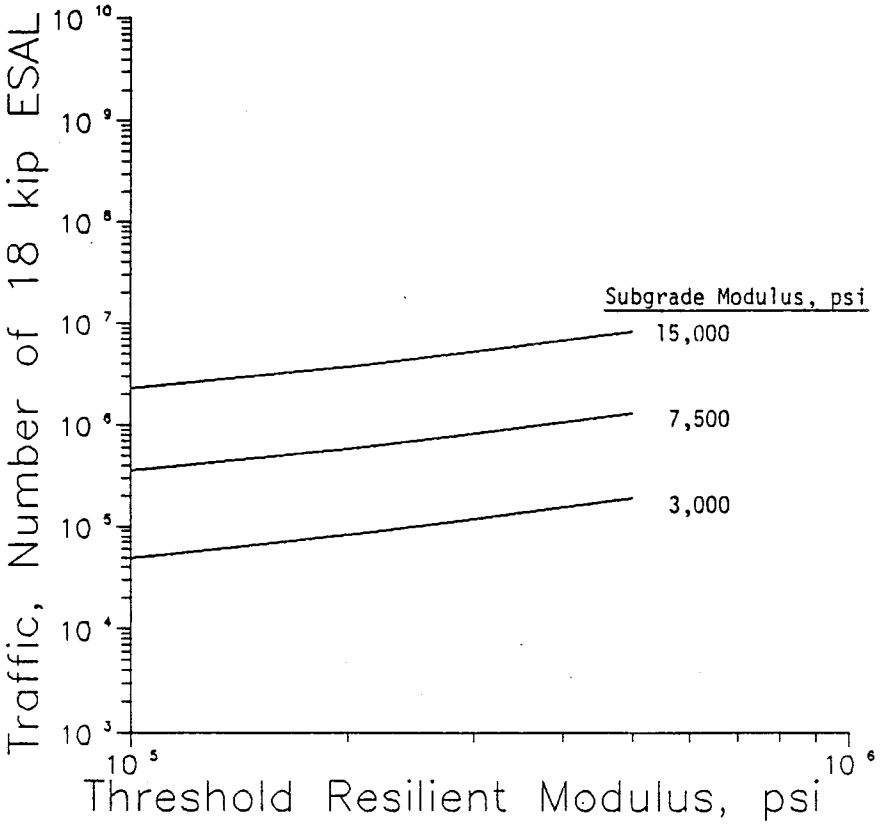

Figure 31. Threshold resilient modulus determination for an intermediately thick flexible pavement.

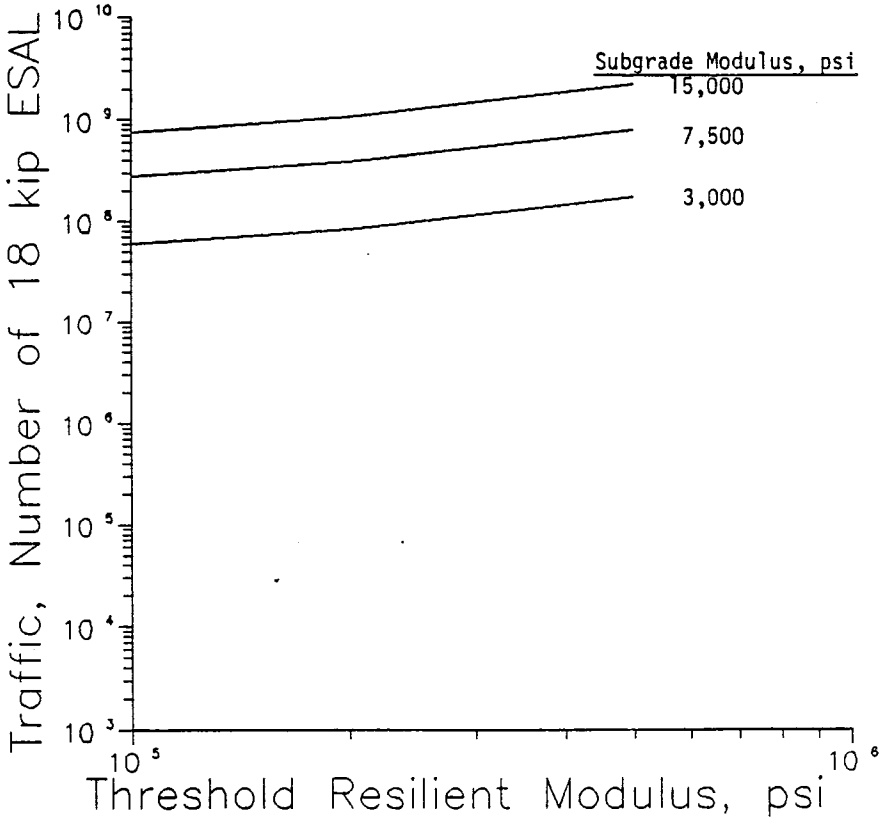

Figure 32. Threshold resilient modulus determination for an asphaltic concrete layer over a portland cement concrete pavement.

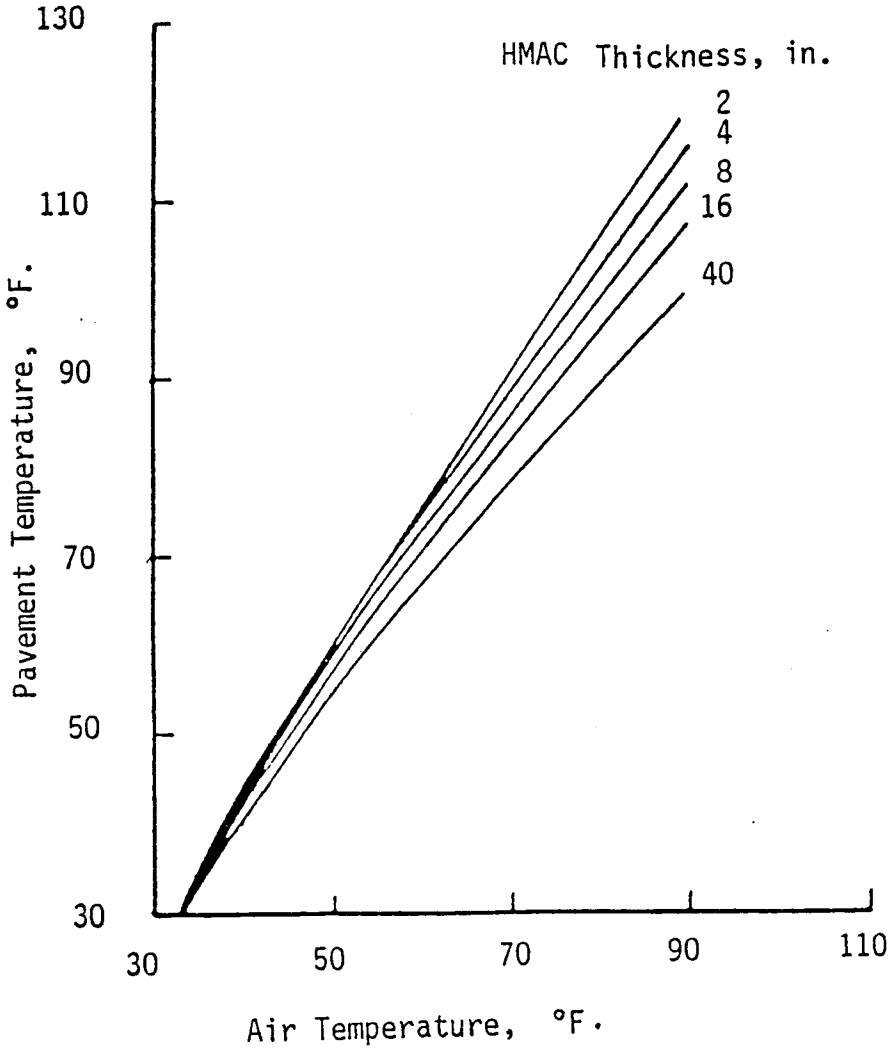

Figure 33. Air temperature to pavement temperature transformation chart (after Reference 25).

Load-Related Fatigue

The flexural fatigue mode of distress can be adversely affected by a relatively high level of stiffness in the HMAC surface layer. It is, therefore, crucial to establish a level of flexibility in the mixture compatible with the required stiffness as dictated by thestructural soundness requirements. The methodology by which the fatigue life of the mixture is established is discussed below.

Once the threshold resilient modulus for subgrade protection is established, the potential fatigue life is determined by means of a series of charts. These charts were developed based on a cumulative damage fatigue failure criterion. Fatigue is generally accepted to be a progressive process caused by traffic-induced repeated tensile strains at the bottom of the asphaltic layers (33). It has been shown, however, that the build-up of residual tensile stresses and strains on the upper portion of asphalt concrete layer can initiate fatigue cracks from the top (34). For the purposes of this study, it was assumed that the former, which is a more conventional approach, is a valid assessment.

The term "fatigue life" is defined in this study as: the magnitude of traffic, expressed in terms of the number of 18 kip equivalent axle passes, N_f, that a particular pavement structure can handle before a certain amount of distress, usually defined as about 10 percent cracking in the wheel path area, is observed.

Any improved mixture design/analysis procedure should account for the fatigue performance of the HMAC in light of the following variables:

a) Type of pavement (structural design).
b) Type of loading (traffic considerations).
c) Environmental effects (climatic regions).
d) Stress/strain state (material properties and mechanical response).

Finn et al. (35) developed a fatigue model based on laboratory and field data from the AASHTO Road Test (36) to predict up to 10 percent cracking in the wheel path area. This model states:

$$\log N_f = 15.947 - 3.291 \log (\epsilon_t) - 0.854 \log \left(\frac{E^*}{10^3}\right) \quad (4)$$

where: N_f = number of cycles to failure (18 kip ESAL),

ϵ_t = repeated tensile strain (in/in x 10^{-6}), and

E* = complex modulus of HMAC (psi), approximated by the resilient modulus in this study.

Monismith, Epps, and Finn stated that stiffness moduli detemined from the quotient of applied stress and recoverable strain (some investigators term this quotient the resilient modulus, M_R) should provide essentially the same moduli as determined from creep and sinusoidal loading (complex modulus) so long as the time of loading is the same and strains are comparatively small (37). Hence, the substitution of the resilient modulus for complex modulus in Equation 4 is assumed to be valid.

Equation 4 was obtained through laboratory testing followed by shifting laboratory data to match field observations of the AASHTO Road Test data. The resulting shift was about 1300 percent which suggests that the actual fatigue life of a pavement in the field is about 13 times greater than what is predicted based on laboratory measurements. One can offer the following explanations for this phenomenon:

a) Rest periods between traffic loadings, allowing viscoelastic relaxation and chemical rebounding of the asphalt.
b) Kneading action of tires.
c) Build-up of residual compressive stresses.
d) Environmental factors (high temperatures).

Tensile strains induced at the bottom of HMAC surface layer for the three classes of pavement structures are illustrated in Figures 34 through 36. Due to the peculiar nature of the HMAC/PCC overlay structure, flexural tensile strains are absent in this pavement type. As a result, only the three "flexible pavement" structures are incorporated in the flexural fatigue analyses. All of these analyses were conducted using the CHEVPC program which is a conventional layered-elastic computer model (30). The results which were obtained from these computerized solutions were entered into Finn's equation (Equation 4) and the fatigue lives for a large combination of pavement structures and layer moduli were calculated. The results were then compiled and summarized in Figure 37.

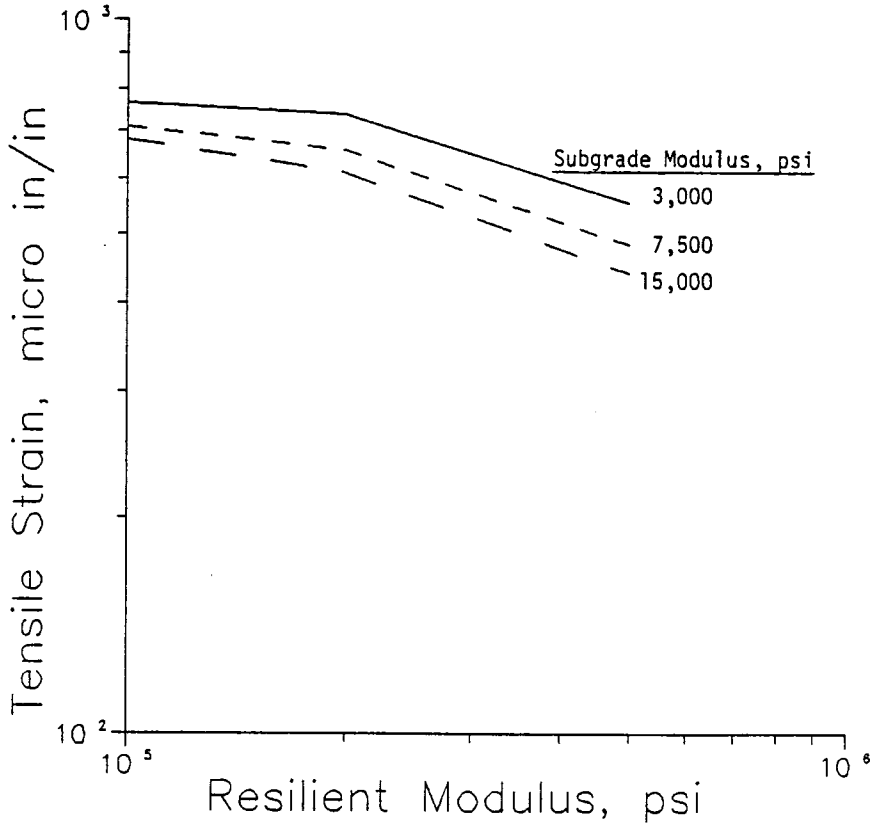

Figure 34. Load-induced tensile strains at the bottom of the asphalt surface layer in a thin flexible pavement.

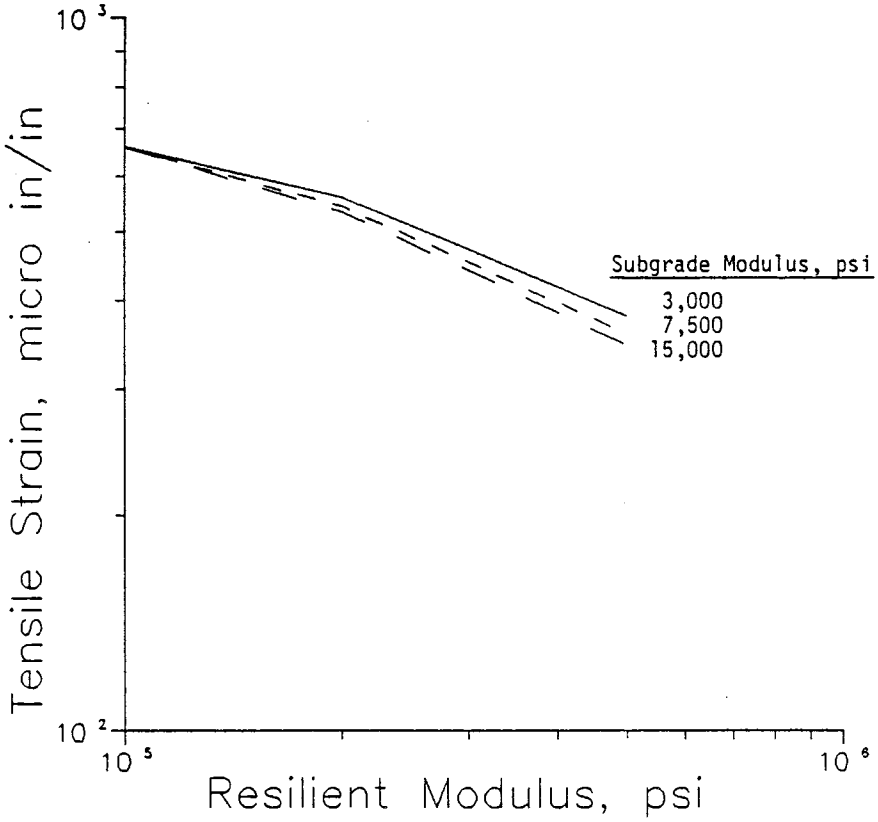

Figure 35. Load-induced tensile strains at the bottom of the asphalt surface layer in an intermediately thick flexible pavement.

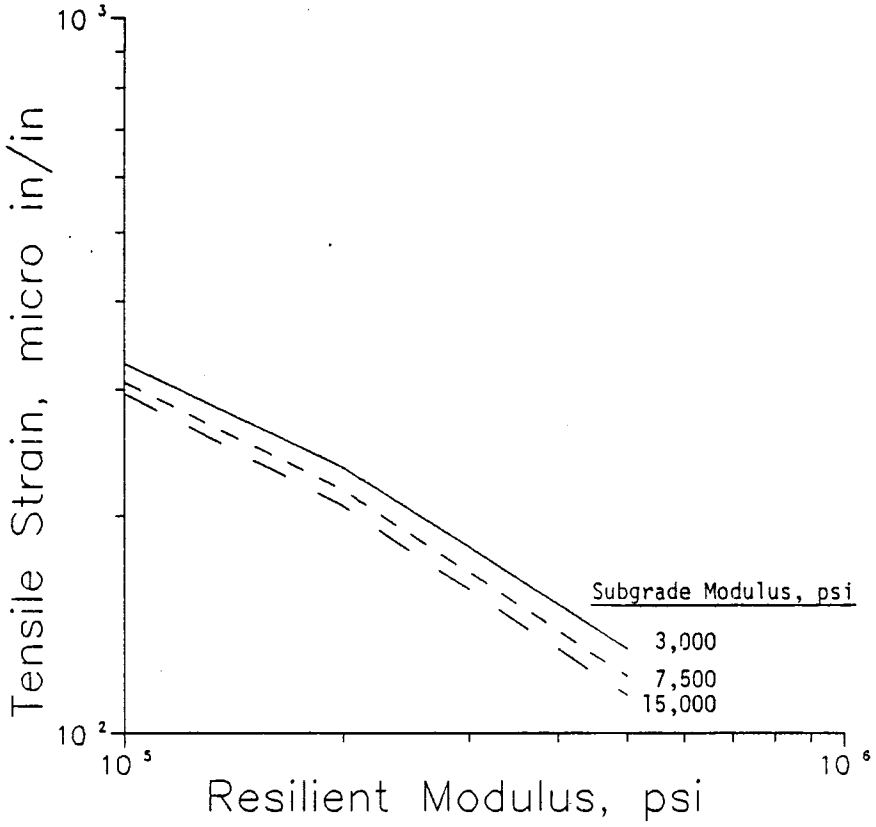

Figure 36. Load-induced tensile strains at the bottom of the asphalt surface layer in a thick flexible pavement.

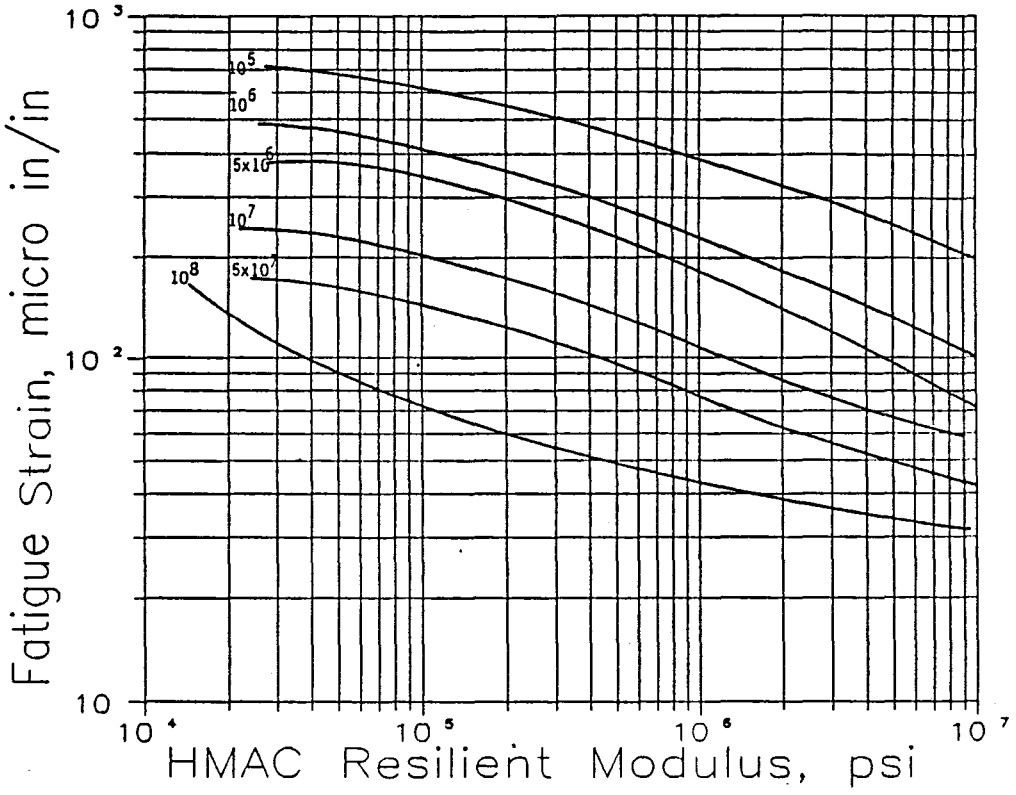

Figure 37. Fatigue criteria chart.

CHAPTER VI

PERMANENT DEFORMATION CHARACTERIZATION

Background

The compressive action of the tire on the pavement and the visco-elastoplastic, time and temperature dependent response of the asphalt concrete layer have been extensively investigated in this study.

Undoubtedly, the mechanical responses of the HMAC layer to various loading conditions are the result of a series of complex internal activities. For years, researchers have tried to relate these microscopic functions to the macroscopic rutting phenomenon. To date, no single universally accepted explanation of the mechanism(s) responsible for traffic-induced permanent deformation has emerged from the literature.

Some researchers have hypothesized that the relative movements of aggregate particles result in different arrangements of the particles in order to satisfy equilibrium conditions. It is further hypothesized that this process is not a reversible one, and upon the removal of the loads, equilibrium is achieved through a recovery process which involves some permanent deformations (38).

Others have taken the above theory one step further at the microscopic level and offered explanations of the mechanisms involved in particle reorientation and the collapse of the void network. They have suggested that the rheology of asphalt concrete and its "flow-like" behavior stem from viscous flow of the asphalt binder itself (9, 38). The flow of asphalt cement into the voids and reduction in the thickness of aggregate coating result in reduction in the relative distance between aggregate particles. Hence, a particle reorientation is caused by the flow of the bitumen into the voids (38).

In the field, the method by which the rutting is measured has a significant influence on the reported rutting values. Three types of rutting measurements are depicted in Figure 38. The application of a mechano-lattice methodology, a computer-simulated model developed by Yandell (40-45), revealed that the critical type of rutting is a function of different combinations of relative layer properties such as modular ratio, thickness ratio, and plasticity ratio. Figure 38 illustrates the

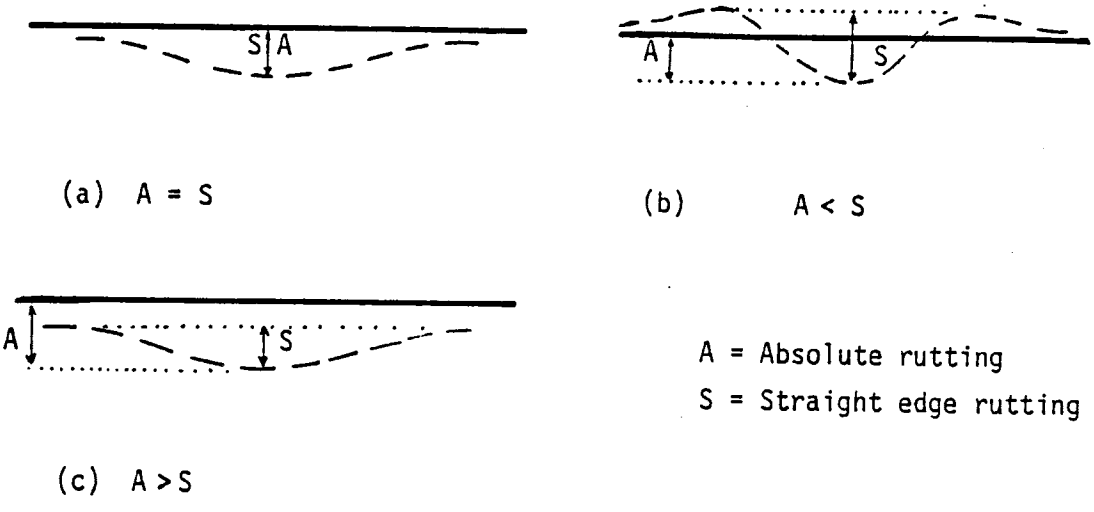

Figure 38. Three categories of rutting.

types or classes of rutting considered.

In this study, it was determined that the absolute rutting better represents the reduction in the HMAC layer thickness which occurs as a result of compressive stresses. This determination was made based on numerous mechano-lattice analyses conducted by Yandell. These runs included models of two different pavement sections which were included in the Pennsylvania State University Test Track (46). The analytical rutting results were obtained assuming both bound and unbound pavement layers. Rutting predictions in terms of absolute and straight edge rutting along with rutting trends predicted by the VESYS model (47) were compared to the actual field data. Results of Yandell's analyses are summarized in Figures 39 and 40. One can clearly observe from these two figures that for both bound and unbound cases, absolute rutting is the critical type of rutting under the actual field conditions.

The contribution to total pavement rutting and roughness made by non-asphaltic layers is considered to be outside the scope of this study. Attempts have been made, through the subgrade protection criteria, to insure adequate stiffness on the part of the HMAC layer for successful distribution of vertical compressive strains before they reach the softer lower layers.

Permanent Deformation and the Creep Test

After a careful review of existing rutting characterization methodologies, it was decided that the concepts introduced by Shell researchers (8, 9, 25, 38) offered the most promising direction to this research. Shell researchers have developed a pavement design system (25, 48) in which rutting potential of asphalt concrete is characterized by a simple creep test (49, 50). This has led to the establishment of an empirical link between the rheological properties of asphalt cement and the visco-elastoplastic behavior of asphalt concrete. Van der Poel's nomograph (51) is the system used by Shell which provides the stiffness of the bitumen at a given temperature, above or below the ring and ball softening point (AASHTO T53), and loading time. In development of the nomograph, bitumen stiffness values were measured by a series of dynamic and static tensile and bending tests. Van der Poel (51) indicated that static and dynamic

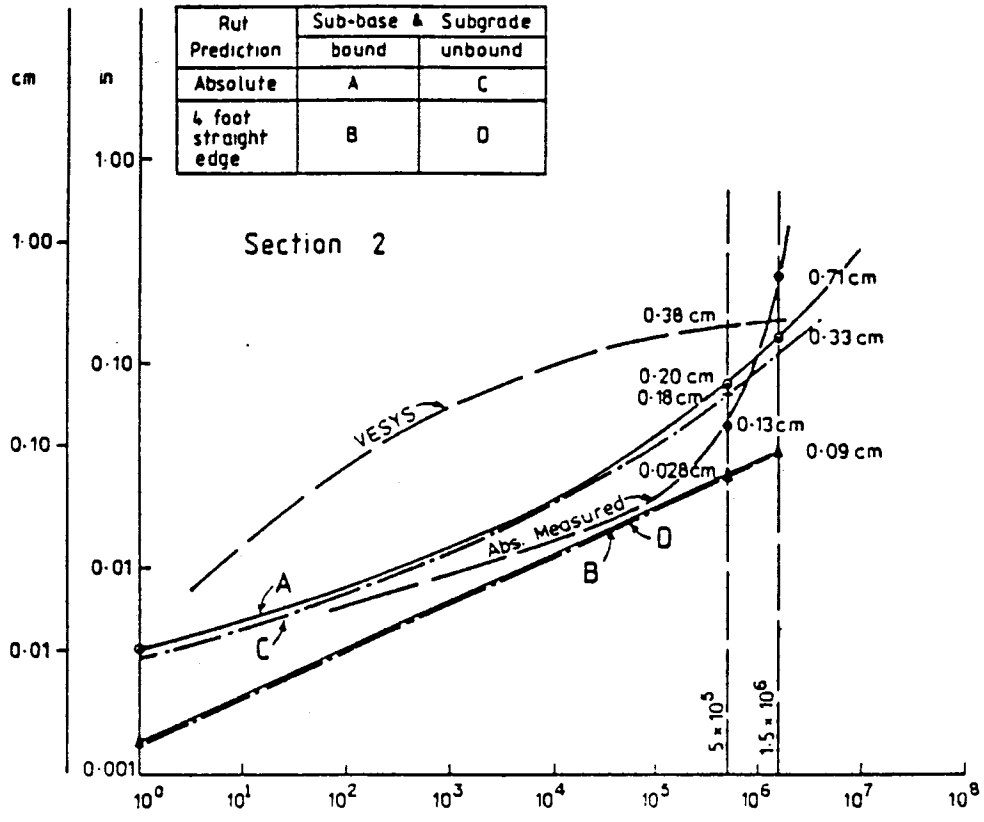

Figure 39. Comparison of VESYS and mechano-lattice predicted rutting with measured rutting for Section 2 of the Penn State Test Track (after Reference 41).

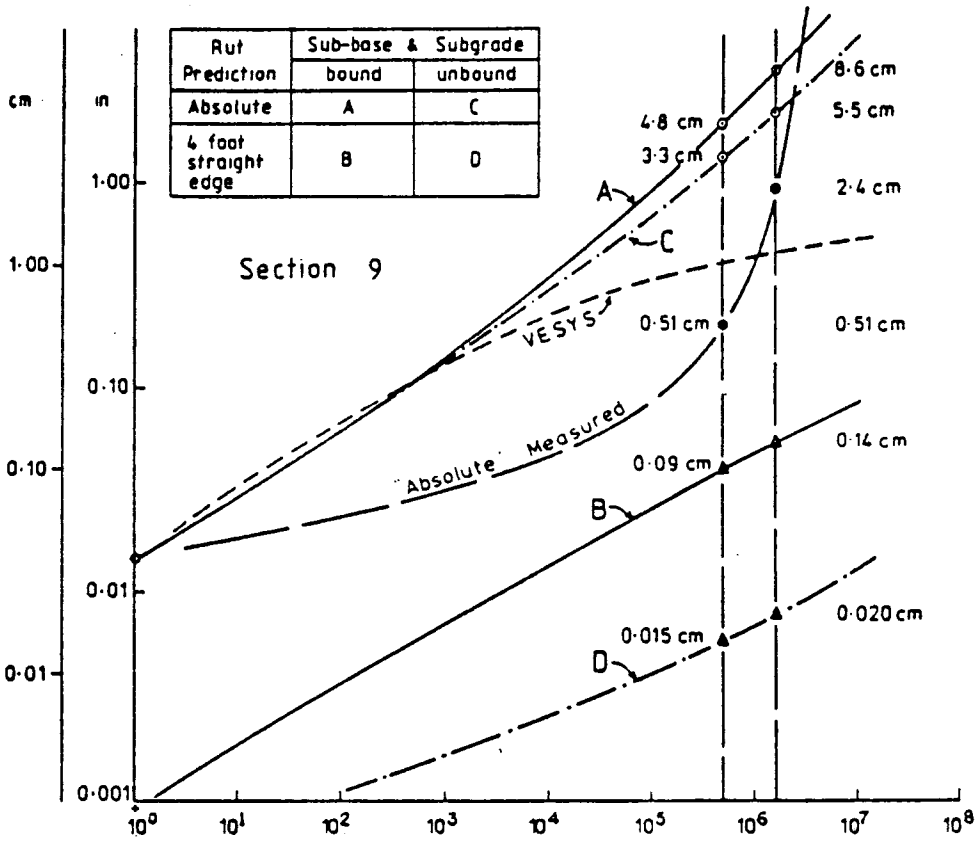

Figure 40. Comparison of VESYS and mechano-lattice predicted rutting with measured rutting for Section 9 of the Penn State Test Track (after Reference 41).

measurements provided similar stiffness trends, hence the static creep was viewed to be an adequate test.

The original Shell equation for rutting prediction was of the following form:

$$h = H \cdot C_m \cdot Z \cdot \frac{\sigma_{tire}}{S_{mix}} \qquad (5)$$

where:
- h = rut depth (inches),
- H = asphalt layer thickness (inches),
- C_m = correction factor accounting for dynamic loads in the field as opposed to the static creep test (see Table 5),
- Z = stress distribution factor (see References 24 and 47),
- σ_{tire} = tire inflation pressure (psi), and
- S_{mix} = total stiffness measured from the creep test (psi).

Table 5. Correction factor for dynamic effects, C_m (after Reference 9).

	Mix Type	C_m
Open	Sand sheet and lean sand mixes Lean open asphaltic concrete	1.6-2.0
	Lean bitumen macadam	1.5-1.8
	Asphaltic concrete Gravel sand asphalt Dense bitumen macadam	1.2-1.6
	Mastic types Gus-asphalt	1.0-1.3
Dense	Hot rolled asphalt	

There are major drawbacks associated with the original Shell equation:

a) The stiffness parameter, S_{mix}, is a pseudo-elastic parameter, and it is used in a Hooke's Law format:

$$\text{Strain} = \frac{\text{Stress } (Z\,\sigma_{tire})}{\text{Stiffness } (S_{mix})} . \qquad (6)$$

It is extremely important to remember that the above format only holds true for elastic (recoverable) deformations. As a result, using the total stiffness parameter, S_{mix}, which represents the combination of elastic, plastic, viscoelastic, and viscoplastic responses in a Hooke's Law format for rutting prediction is not valid.

b) The original Shell equation accounts for the field dynamic effects through the C_m factor. This factor magnifies the rutting predictions by 30 to 100 percent (Table 5). Normally in viscoelastic materials, dynamic loading causes less deformation than does static creep loading. This phenomenon was thoroughly explained by Kinder (52). Kinder's data suggest that static loads have a more deleterious effect on asphalt concrete than do dynamic and cyclic loads. According to these observations, the C_m factor should be a reduction factor (less than one) rather than its present form as reported by Shell researchers (ranging from 1.3 to 2.0) (Table 5). It is clear that Shell researchers have incorporated this factor into their rutting equation based on discrepancies that they had observed between their rutting predictions and the actual observed rutting in the field (8, 9). The source of these discrepancies lies in the fact that simple linear extrapolation of laboratory-measured deformation trends to field conditions is not adequate. This important point will be further explained in the following sections.

c) Another serious consequence of using a Hookian constitutive relationship for permanent deformation characterization is the assumption of linearity. Information in the literature (53) and Texas Transportation Institute's investigations (13) indicate that accumulation of permanent strains is not linearly proportional to stress level. In fact, the relationship between the independent variable (stress) and the dependent variable (permanent strain) is of a log-linear form. The slope of this log-linear relationship is approximately 1.61 as shown in Figure

41. The "intercepts" of this log-linear relationship is a function of mixture type. Softer mixescause a shift in the intercept while the slope remains almost constant. Similar results were reported by Perl, Uzan, and Sides (54) who suggest that log-linear slope in Figure 41 should be 1.45. This led to the conclusion that the logarithmic rate at which permanent strains are accumulated as a function of applied stress is relatively constant.

It is important to mention that the stress dependancy of permanent deformations, as defined in item c), was derived under conditions of equilibrium, i.e. accumulation of irrecoverable deformations become asymptotic, using a repeated-load compression test. It is, however, conceivable that under a large number of load repetitions, permanent deformations may accumulate at a faster rate which reflects beyond the equilibrium conditions. This may cause a "rebound" from the assumed asymptotic conditions.

Non-recoverable deformation of an asphaltic concrete layer in a pavement structure can be best characterized by the creep test. Although researchers agree on this point, they differ on the type of creep test that should be used. Shell researchers (8, 9), who pioneered the use of the static creep test, have developed their creep and rutting criteria based on the static compressive creep. Others have presented their rutting prediction models based on the repetitive load creep test. The VESYS model (47) and the Modified ILLIPAVE model (55) are two examples of predictive models which require repetitive load testing. Researchers at the Australian Road Research Board (ARRB) investigated both the static creep and the repetitive creep tests (52). They showed that although the magnitude of plastic deformation will be different depending on the type of the creep test, the irrecoverable deformation trends are similar. This conclusion is in agreement with the one made by Van der Poel (51) describing the dynamic and static responses of bitumens.

The above discussion suggests that perhaps no single method fully simulates field rutting behavior. Nevertheless, for qualitative comparisons, static creep data seem to be very effective, and can reasonably quantify deformation potential.

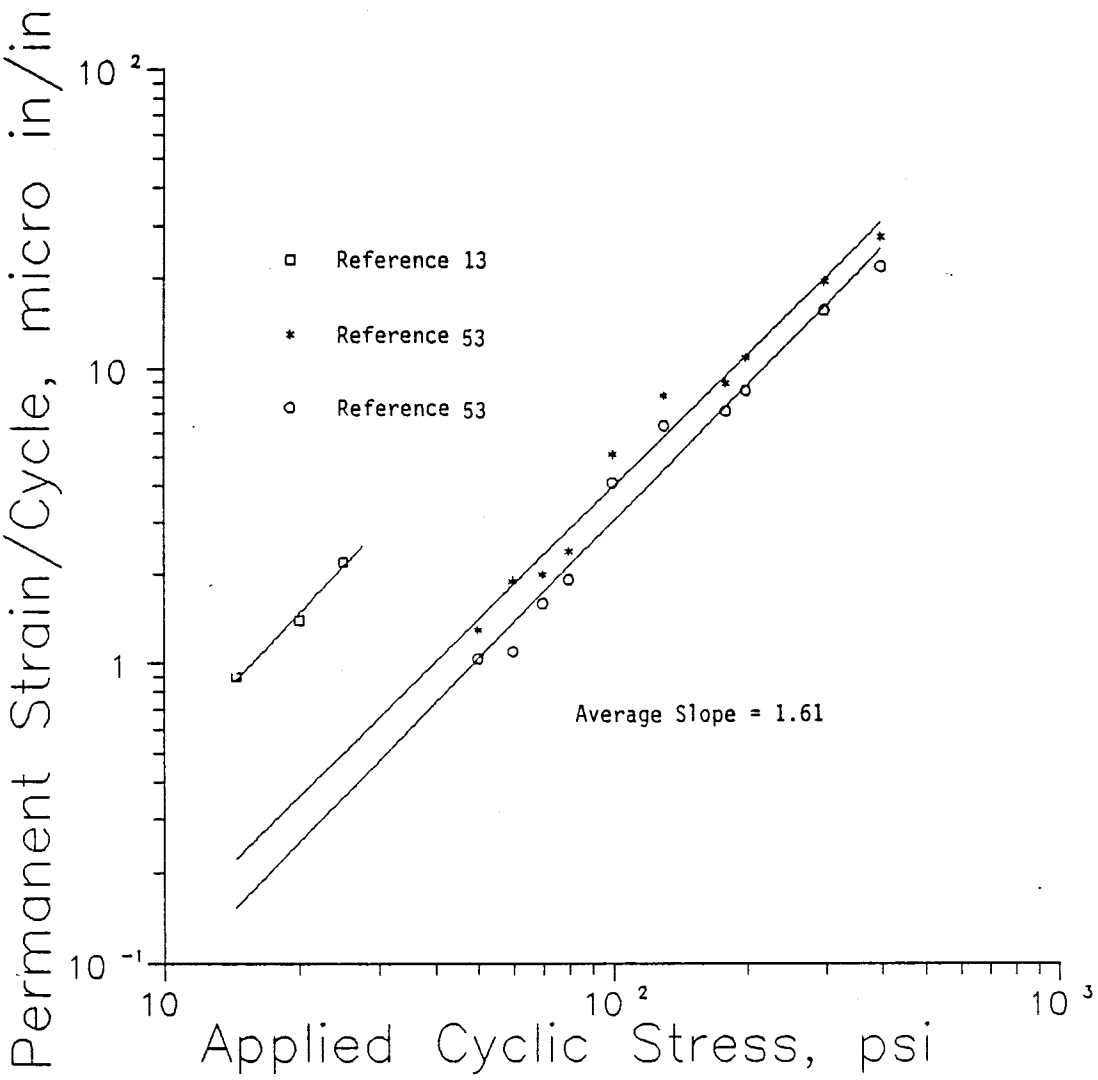

Figure 41. Log-linear relationship between the applied stress and the accumulated permanent deformation per cycle (averaged over the first 100 cycles of stable hysteresis.)

Modified Shell Equation

This section deals with the alterations that were made by this study to the original Shell equation. The analysis of any rutting prediction model requires an advanced knowledge of plasticity and viscoelasticity. The static creep test was the major material characterization tool in this study by which the viscous and plastic characteristics of asphaltic concrete mixtures were established for further use in the modified Shell equation. Procedural details for performing the static creep test are given in Appendix A.

The laboratory-measured viscoplastic characteristics are normalized in the modified Shell method to accommodate the stress levels at which they are developed. This allows transformation of laboratory-measured parameters to the field conditions where higher stresses are often encountered. As a result of this process, a parameter called the "viscoplastic component of mixture stiffness" was developed.

The original Shell method for rutting prediction (8, 9) assumes a linear relationship between the stress and the accumulated plastic strain. As previously discussed, the relationship is not linear. For example, doubling the stress level from σ to 2σ will lead to an increase in the accumulated viscoplastic strains from ϵ_{vp} to $3\epsilon_{vp}$; a three-fold increase as opposed to two. These observations led to the development of a refined version of the Shell rutting equation which does not depend on empirical correction factors. This modified Shell equation accounts for plasticity trends and nonlinearity of such deformations in the following format:

$$h = H \left[\frac{Z\sigma_{tire}}{\sigma_{lab}}\right]^{1.61} \epsilon_{vp}(t) \qquad (7)$$

where:
- h = calculated rut depth (inches),
- H = asphaltic layer thickness (inches),
- Z = vertical stress distribution factor (derived from layered elastic solutions, see Appendix C),
- σ_{tire} = average contact pressure (psi),
- σ_{lab} = stress level at which the creep test is conducted (psi), and

$\epsilon_{vp}(t)$ = viscoplastic trend of the mixture measured by the creep test (in/in).

In radial tires, the average contact pressure is the same as the tire inflation pressure. Due to the simplicity of the modified Shell equation, the assumption of radial tires was necessary. For bias-ply tires, studies indicate that the contact pressure is not uniform and peak values are often higher than the inflation pressure (7). Therefore, average of contact pressure should be used in the case of bias-ply tires.

The ratio of $Z\sigma_{tire}$ to σ_{lab} is raised to the 1.61 power in order to account for the non-linearities involved in the accumulation of viscoplastic deformations. This exponent was derived from Figure 41 and the justification is outlined below along with the constitutive plasticity law that was used in this study.

Most of the information in the literature suggests that the accumulation of permanent deformation as a function of time or number of load cycles (for static or cyclic creep, respectively) can be approximated by a simple power relationship (56). It is the form of the power law, however, which is the subject of dispute among researchers.

The VESYS model for permanent deformation (47) was developed based on the following form of power law which characterizes rutting as a strain hardening process (i.e. the exponent of the power relationship is less than one).

$$\epsilon_{vp} = at^b \tag{8}$$

where: ϵ_{vp} = viscoplastic strain;
t = time; and,
a,b = regression constants.

This basic concept has been employed by many analysts around the globe, particularly in Australia (41, 52).

Lai and Anderson (57) also suggest a power law format of a strain hardening nature with a stress dependent term, $a(\sigma)$:

$$\epsilon_{vp} = a(\sigma)t^b \tag{9}$$

where: ϵ_{vp} = viscoplastic strain,

t = time,

$a(\sigma)$ = $b_1\sigma + b_2\sigma^2$,

σ = creep stress, and

b, b_1, b_2 = regression constants.

Perl, Uzan, and Sides (54) have reported power relationships similar to Lai and Anderson's for both compressive and tensile modes of creep.

Studies show that the a-coefficient in a simple power law format is a function of creep stress and mixture stiffness (54, 57). The b-exponent, however, represents the rate at which permanent deformation is accumulated in a constant stress creep test as a function of time. For asphalt concrete, this exponenet appears to be relatively constant. Table 6 summarizes the results which have been reported by different researchers.

Table 6. Simple power law exponent as reported by different researchers

Reference	b-exponent
Kinder (51)	0.25
Perl, Uzan and Sides (53)	0.22
Lai and Anderson (56)	0.25
The author	0.17, 0.22, 0.25 (average: 0.21)

Tseng and Lytton (55) have proposed a 3-parameter power law for describing the permanent deformation under cyclic loading. Constants used in this model are generated from a nonlinear regression process. This model is of the following form:

$$\epsilon_a = \epsilon_o \cdot \text{EXP} - \left(\frac{\rho}{N}\right)^{\beta} \qquad (10)$$

where: ϵ_a = permanent strain,

N = load cycle, and

ϵ_o, β, ρ = regression constants.

The above model provides a better fit for the permanent deformation data and justifications for the form of the equation are based on activation energy concepts (58). Although this relationship provides a powerful tool

for permanent deformation data analysis, it requires repeated load testing rather than static creep testing, which has been selected for mixture design/analysis in this study because of its expedience. The three parameters in the Tseng-Lytton model, referred to as "material properties," are highly interdependent and are determined by nonlinear regression techniques. In the simple power law (Equation 8), the slope and intercept are treated as pseudo material properties.

This research study has produced a modified version of the Shell equation which:

a) Utilizes a simple power law constitutive relationship for permanent deformation characterization.
b) Accounts for the nonlinearity and stress dependency within the plasticity laws.

This was derived through the following steps based on a series of cyclic permanent deformation tests over a range of stresses, a power relationship was used to relate the plastic or irrecoverable strain to the stress magnitude as:

$$\epsilon_{vp}/N = a\sigma^{b} \quad (11)$$

where: ϵ_{vp}/N = accumulated, viscoplastic deformation per cycle,
σ = peak cyclic stress, and
a, b = regression parameters.

The parameter ϵ_{vp}/N was averaged over the last 10 cycles of about 100 cycles of the first stable hysteresis trend. Figure 41 (page 68) illustrates the data from two independent sources which suggest that asphalt mixtures of different stiffness have different "a-parameters." The "b-parameter," however, is relatively constant and is equal to 1.61. Consequently, one can rewrite Equation 11 for the two stress levels, one representing the field and the other representing the laboratory conditions:

$$(\epsilon_{vp}/N)_{field} = a_{field} \cdot [\sigma_{field}]^{1.61} \quad (12)$$

and likewise:

$$(\epsilon_{vp}/N)_{lab} = a_{lab} \cdot [\sigma_{lab}]^{1.61} \quad (13)$$

Therefore:

$$\frac{(\epsilon_{vp}/N)_{field}}{(\epsilon_{vp}/N)_{lab}} = \frac{a_{field}}{a_{lab}} \cdot \left[\frac{\sigma_{field}}{\sigma_{lab}}\right]^{1.61} \quad (14)$$

Assuming that the laboratory-manufactured specimen has identical properties to the field-constructed mix, one can assume a_{field} and a_{lab} to be equal. Equation 14 then becomes:

$$\frac{(\epsilon_{vp}/N)_{field}}{(\epsilon_{vp}/N)_{lab}} = \left[\frac{\sigma_{field}}{\sigma_{lab}}\right]^{1.61} \quad (15)$$

The above equation illustrates the nonlinear nature of permanent deformation accumulation. Any laboratory to field projection of rutting needs to be conducted using the above nonlinear equation. Indeed, rutting criteria charts that are included in this study were developed using the nonlinear analysis.

Development of Permanent Deformation Criteria

In the development of any rutting criteria, the question which must be addressed is: how much rutting is excessive rutting? Therefore, it is necessary to define some limiting values or levels of severity for rutting. In this study, the limiting values for rutting were obtained from the Federal Highway Administration, Highway Pavement Distress Identification Manual (59), which classifies rutting in severity levels of high, medium, and low. For safety considerations, a new class of rutting below the low severity level was developed to account for hydroplaning potential. The development of the limiting value for the hydroplaning class of rutting was based on:

a) A roadway cross-slope of one percent.
b) Vehicle speed of 55 miles per hour.
c) Average pavement surface texture depth of 0.04 inches.
d) Tire tread of 1/16 inches.

e) Accumulation of 0.08 inches of water in the wheel path.

The above conditions were considered to be representative of Texas roads (60, 61). Rutting limiting values are summarized in Table 7 from which a series of rutting criteria charts were developed.

Table 7. Rutting severity classification

Severity	Mean Rut Depth Criteria
Hydroplaning	0.20-0.25 in.
Low	>0.25-0.50 in.
Medium	>0.50-1.00 in.
High	>1.00 in.

These charts are used as acceptance or rejection guides in the improved mix design/analysis procedure. The process by which these charts were developed is summarized in the following paragraphs.

Researchers at the Australian Road Research Board (ARRB) (521) have indicated that viscoplastic strains, measured from a simple static creep test, when normalized for the stress level under which they are accumulated, exhibit the following form of relationship:

$$\epsilon_{vp}/\sigma = 0.47\ t^{0.25} \tag{16}$$

where: ϵ_{vp} = viscoplastic strain; and,
t = time.

The above expression is of the compliance form. In the inverted form, a parameter which will be referred to as viscoplastic stiffness is developed:

$$\sigma/\epsilon_{vp} = (1/0.47)\ t^{-0.25} \tag{17}$$

Equation 17 suggests that the viscoplastic stiffness is a decreasing function of time with the decay rate of -0.25 on a log-log scale. Perl, Uzan, and Sides studies suggest a decay rate of -0.22 for the viscoplastic stiffness parameter (54). These observations have been verified in this study by laboratory measurements which reflected decay rate values ranging

from -0.17 to -0.25 (Table 6). These findings have been incorporated into the development of rutting criteria charts.

The viscoplastic stiffness rate of decay as a function of time was utilized in the development of boundary curves. This was done by the following stepwise procedures:

a) The viscoplastic stiffness necessary to yield a certain level of rutting (e.g. low severity rutting) after one million passes of standard 18 kip axles was back-calculated. This would establish an end-point in the rutting criteria chart representing the final rutting stage in the HMAC layer.
b) Based on this back-calculated terminal value (the end-point) and the rate of viscoplastic stiffness decay (the slope), the trend of this parameter was established as a function of time.

The rutting criteria charts were developed accounting for the following variables:

a) Levels of subgrade strength (3 levels).
b) Types of pavement structures (4 types).
c) Range of HMAC layer moduli (3 moduli).

These charts are presented in Appendix B. Upon the completion of the rutting criteria charts, it was decided that it is necessary to be able to evaluate a wider range of the above variables (a through c) in order to better approximate the actual field conditions. It was, therefore, decided that an extended analysis procedure should be developed which addresses the following variables:

a) Broader range of layer moduli.
b) Traffic levels other than one million 18 kip axle load.
c) Variations in temperature profiles and traffic distributions.

This was accomplished through the extension of the same analytical procedures which were used in the development of rutting criteria charts. The results are presented in a series of nomographs in Appendix C. The nomographs provide ample flexibility for the specific needs of the bituminous design engineer.

Experimental Matrix

Laboratory verification of the creep/recovery procedures was conducted on a series of asphaltic mixtures. As a result of these investigations, viscoplastic deformation, which is the primary cause of rutting in the pavement, was evaluated for a wide range of asphalt mixtures, were evaluated.

This effort included two types of aggregates and three grades of Texaco asphalts. The aggregates were: a) rounded siliceous Brazos River gravel; and, b) crushed Brownwood limestone. Gradation information for these aggregates are given in Figures 42 and 43, Tables 8 and 9. The asphalt grades were: a) AC-5, b) AC-10, and c) AC-20. These aggregates and asphalts were considered to be "typical" for use in Texas asphaltic mixtures. Table 10 illustrates the experimental matrix. The results of this rutting characterization analysis will be discussed in the subsequent sections.

Rutting Design/Analysis Procedure

The primary objective of this procedure is to provide a relatively simple and user-oriented methodology by which the rutting potential of HMAC can be evaluated as part of a routine mixture design/analysis procedure. The methodology is general enough to account for a large array of variables as listed in earlier sections.

Mechanical properties of asphaltic layers are highly dependent upon the stiffness of the mixture. Stiffness of HMAC, however, is a function of two rheological variables, namely: temperature and loading rate. In a pavement structure, for analysis purposes, one can assume a fixed rate of loading corresponding to that induced by the predominant traffic. At this fixed loading rate, the temperature distribution profile within the cross-section of the HMAC layer has a profound effect on the elastic response of the asphalt layer. As a result, a "modulus profile" is produced within the HMAC layer. Therefore, it is imperative to investigate how substantially the distributions of vertical compressive stresses, assumed to be responsible for rutting, are altered due to the presence of a temperature profile. The effect of shear stresses on accumulation of permanent deformations is the subject of investigations in TTI Project 2452.

Morris et al. (26) have demonstrated that the distribution of

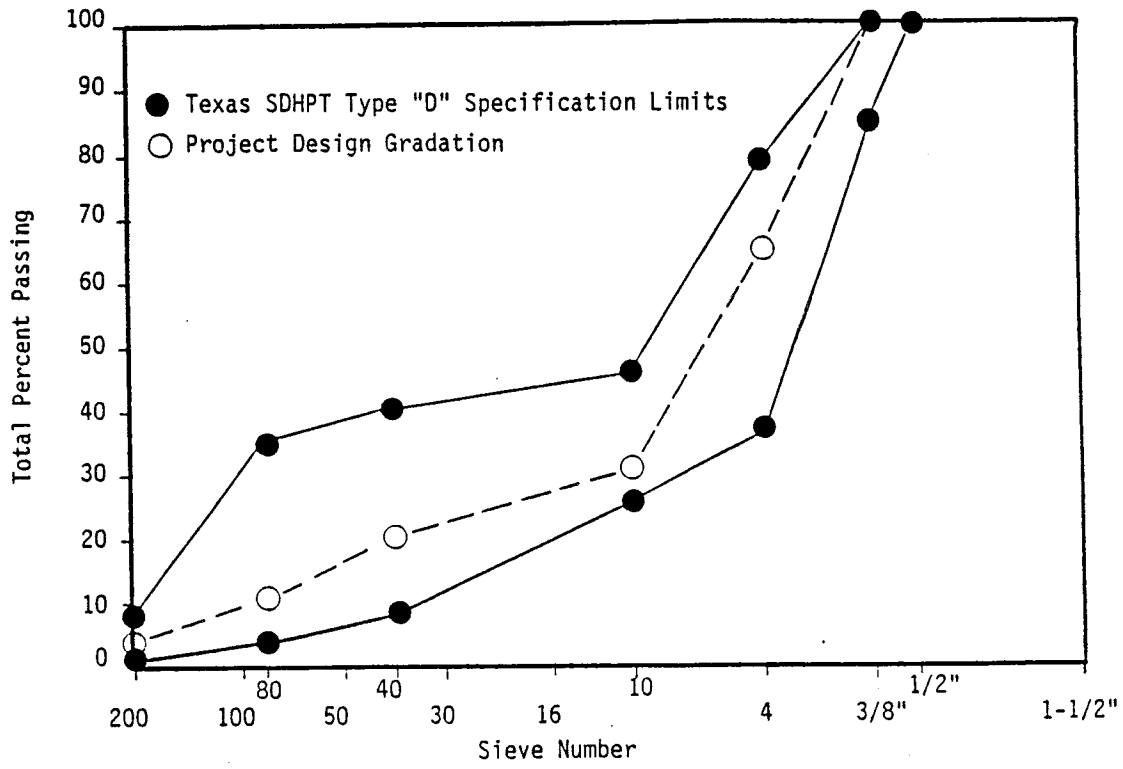

Figure 42. Gradation chart for siliceous gravel aggregates used in the sensitivity study of mixture variables on permanent deformation potential.

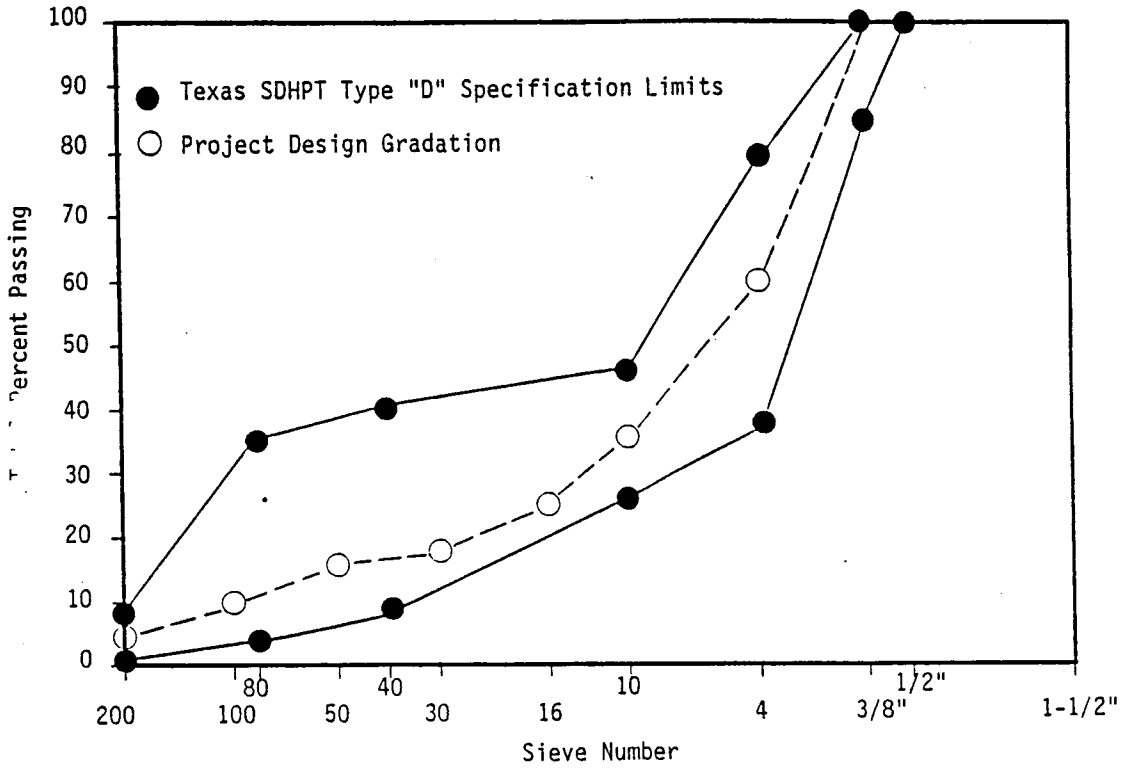

Figure 43. Gradation chart for crushed limestone aggregates used in the sensitivity study of mixture variables on permanent deformation potential.

Table 8. Compositional distribution of the Brazos River gravel aggregate

Aggregate	Job Mix Formula (%)
Pea gravel	50%
Washed sand	30%
Field sand	10%
Limestone crusher fines	10%

Table 9. Compositional distribution of the crushed limestone aggregate

Aggregate	Job Mix Formula (%)
Limestone rock (-3/8, + 1/4)	25%
Limestone rock (-1/4, 30)	35%
Limestone fines (+30)	20%
Limestone fines (-30)	12%
Field sand	8%

Table 10. Creep/recovery experiment matrix.

Aggregate	Crushed Limestone		Siliceous Brazos River Gravel		
Asphalt Grade	AC-5	AC-20	AC-5	AC-10	AC-20
Asphalt Content					
4%					
5%					
6%					

Replictes = 3

compressive stresses, within a pavement structure, does not change significantly as a result of incorporating the temperature profile into the stress analysis. One can verify this conclusion by dividing the HMAC layer into sublayers, each having a different layer modulus corresponding to the average temperature of that sublayer. Analytical investigations can then be conducted by means of layered elastic solutions. Indeed, this was done on a very limited basis in this study, and the results were almost identical to Morris' conclusions (26) (Figure 44). This suggests that analytical modeling of an asphaltic layer with a single modulus value representing the elastic behavior of the entire thickness of HMAC, as opposed to a multilayer analysis, is a valid one. Hence, in layered elastic analyses conducted in this study, individual layers of each pavement structure were assumed to have the following set of continuum properties:

a) Homogeneous.
b) Isotropic.
c) Isothermal.

With the help of the above assumptions, rutting potential of asphaltic mixtures can be estimated based on a series of rutting criteria charts which were discussed earlier. The steps involved in this procedure can be summarized as follows:

a) Once the stiffness requirements for structural soundness are satisfied, the viscoplastic deformation properties are studied by means of a creep test. Appendix A contains the procedural details of the static creep test employed in this study.
b) Time dependent viscoplastic strains are then normalized for the stress level at which they are measured in the laboratory. This produces a parameter called the viscoplastic component of stiffness. As a result, transformation of laboratory-measured parameters to account for the actual pavement conditions in the field is made possible through a nonlinear modified form of the Shell equation (Equation 7, page 69).
c) The normalized trend of viscoplastic deformations is then

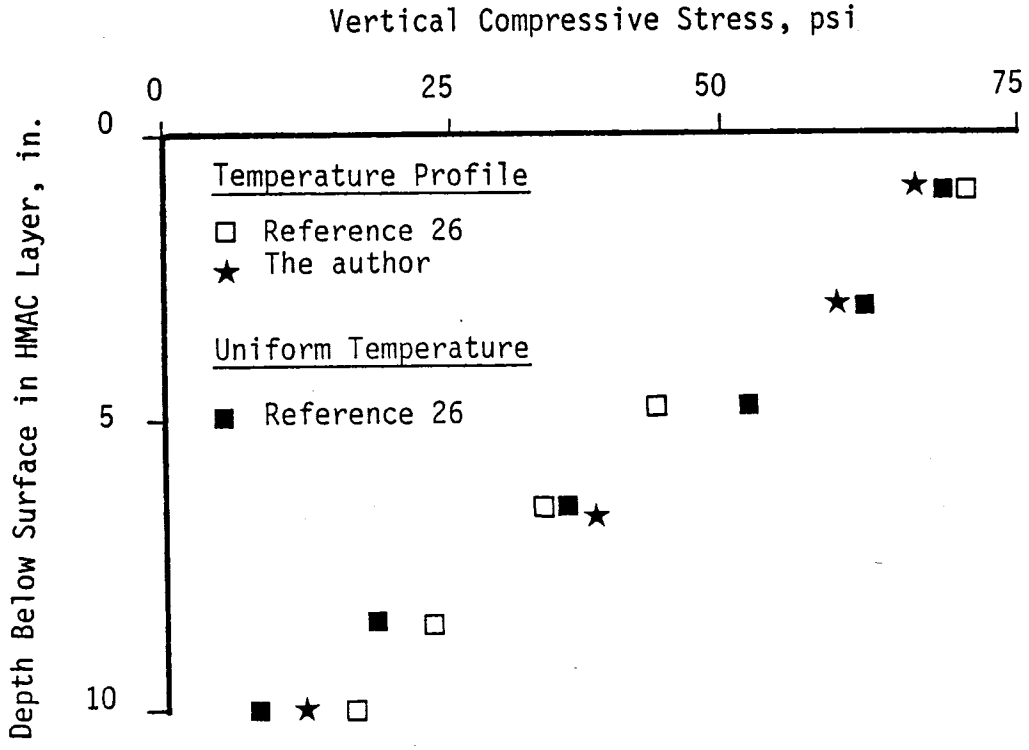

Figure 44. Effect of temperature profile on the distribution of vertical compressive stresses (after Reference 26).

plotted on a rutting criteria chart developed to account for the type of pavement structure, the annual critical stiffness of the asphalt layer corresponding to a critical temperature, and the levels of subgrade stiffness.

Depending on where the viscoplastic stiffness data plots on the rutting criteria charts, an acceptance or rejection decision is madewith respect to the asphaltic mixture under investigation. In case of rejection, modifications in the binder content and/or binder type can lead to a mixture which is less susceptible to rutting. Minor adjustments in the gradation of aggregate, adjustments to the percent of minus 200 sieve material, adjustments to void contents, and replacement of smooth, surface-textured, sand-size particles by crushed fine portions are other approaches which may yield success in reducing the rutting potential of the mix.

Experimental Results

In order to investigate the sensitivity of the proposed methodology for rutting potential evalution, an experimental matrix was developed. This section summarizes a series of creep/recovery tests conducted on the mixtures described in Table 11.

In general, the results from creep/recovery tests demonstrate the following:

a) Lower viscosity asphalts make the mixture less stiff and therefore more susceptible to irrecoverable deformations, i.e. rutting.
b) Higher asphalt cement contents producing lower air void contents increase rutting potential; and,
c) Dense crushed limestone aggregates produce mixtures less susceptible to rutting than mixtures made with siliceous river gravel only if air voids are kept below 7 percent.

The performance of high versus low air void contents was compared in the experimental matrix in order to demonstrate the sensitivity of the

Table 11. Detailed experimental matrix for the creep/recovery study.

Aggregate	Asphalt Cement	Percent Binder	Percent Air Voids	Texas Stability (%)
Crushed Limestone	AC-5	4	12.6	48
		5	9.6	47
		6	7.7	40
	AC-20	4	5.9 - 13.7*	52 - 47*
		5	6.4 - 11.7*	55 - 46*
		6	4.9 - 8.5*	40 - 38*
Siliceous Brazos River Gravel	AC-5	4	12.5	43
		5	6.5	40
		6	3.1	35
	AC-10	4	10.5	45
		5	6.0	42
		6	3.4	40
	AC-20	4	9.6	47
		5	7.1	40
		6	3.4	41

* These values represent mixtures which were compacted at a lower compactive effort in order to achieve higher air voids.

creep test to mixture densification. Analysis of the irrecoverable deformation trends of mixtures over the range of air voids indicated in Table 11 demonstrates that the creep test is greatly sensitive to this parameter. These conclusions were made from a series of permanent deformation trends derived from creep or recovery tests. The results of these tests are discussed in the following paragraphs.

Figure 45 demonstrates the influence of an increase in the asphalt content of a crushed limestone and AC-5 mixture on permanent deformation potential. The reduction in air voids as a result of an increase in the asphalt content of the mix indicates that the available asphalt cement is filling the void space. As a result of this process, the increase of asphalt content in this mixture is equivalent to introduction of lubricants between aggregate particles otherwise separated by a very tight network of air voids. This phenomenon causes the mixture with richer asphalt content to be more susceptible to permanent deformation induced by viscous flow of asphalt between aggregate particles.

Figure 46 illustrates permanent deformation trends for AC-20 and crushed limestone mixtures. The data presented in Figures 45 and 46 exhibit similar trends. The sensitivity of the static creep test results to different levels of air void content, which were induced by adjusting the compactive effort, is shown in Figure 46. Two mixtures of the same asphalt content may exhibit permanent deformation potentials that are substantially different from one another as a result of variations in their degree of densification (air void content). A high air void content, introduced by a low level of compaction, leads to susceptibility to permanent deformation induced by the collapse of a large number of small void pockets in the HMAC matrix. Whereas, at a higher asphalt content, a similar level of compaction may produce a tendency to increase the viscous flow in the matrix of HMAC leading to more rutting susceptibility.

In Figure 46, the mixture containing 4% asphalt cement and 5.9% air voids does not follow the previously described patterns and shall be viewed as a test anomaly. These anomalous results are often encountered in the cylindrical HMAC specimens that are compacted in three layers using the kneading compaction device. A detailed research study is required to investigate the cause of the permanent deformation patterns that do not

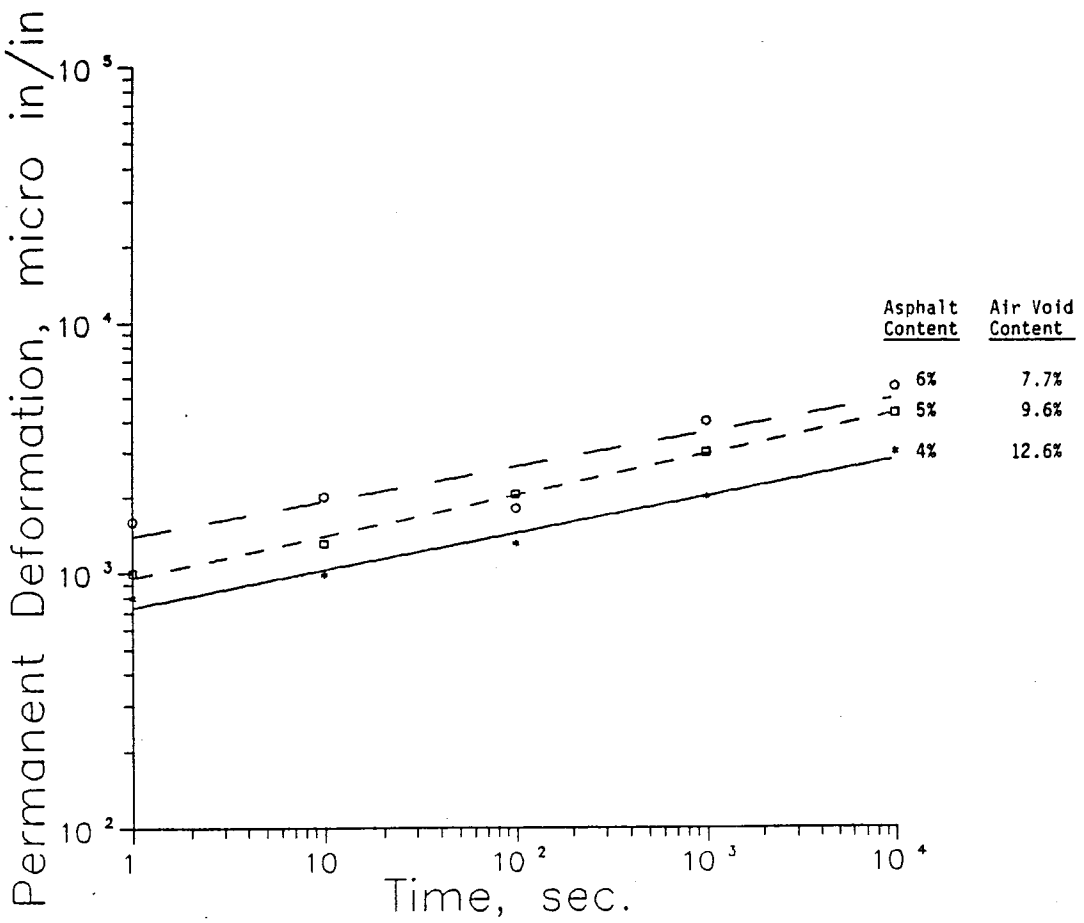

Figure 45. Permanent deformation trends for AC-5 and crushed limestone mixtures.

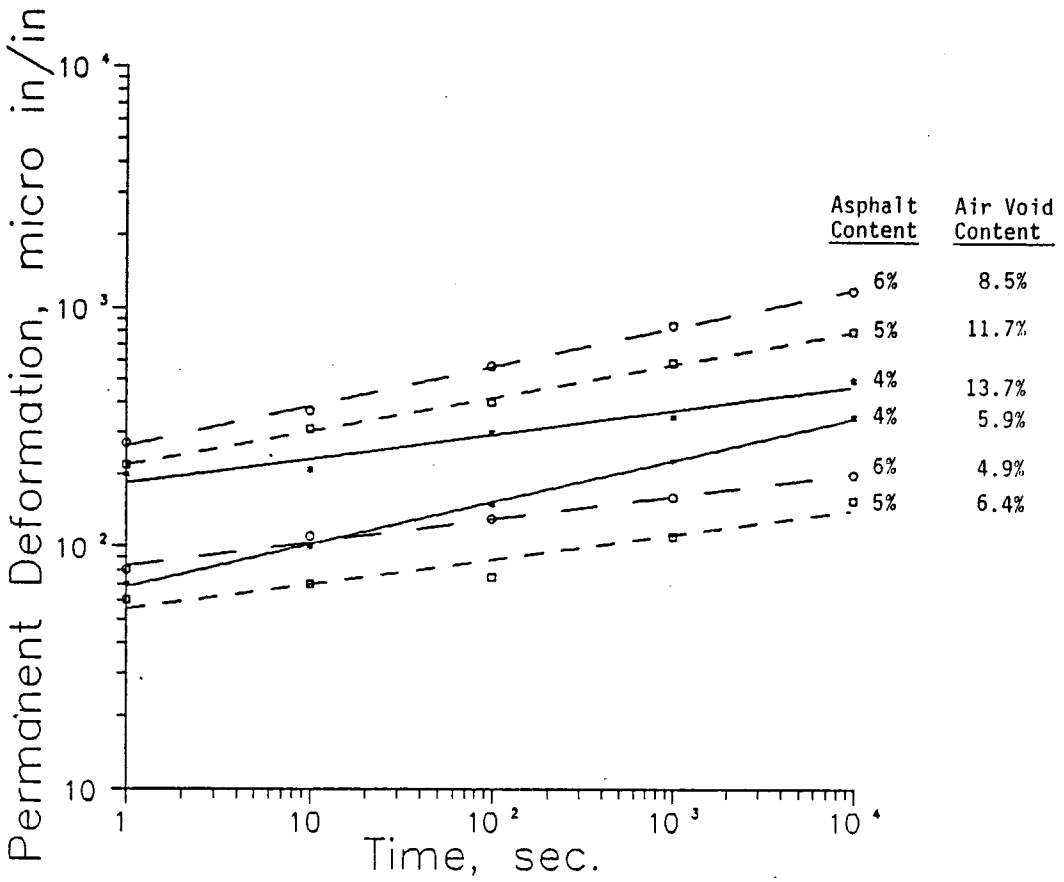

Figure 46. Permanent deformation trends for AC-20 and crushed limestone mixtures.

follow any defineable trends. This may offer explanations for some of the creep/recovery data that are thus far regarded as inconclusive in this study.

Figure 47 illustrates an example of the sensitivity of the creep test to the distribution of air voids in the HMAC. The patterns in Figure 47 do not follow any logical trend. These anomalous data prompted an investigation into the distribution of air voids content within the 4-inch diameter by 8-inch tall creep/recovery specimens. These specimens were compacted in 3 layers by a kneading compaction device. It was only during the verification phase (Chapter VIII), that 6-inch diameter by 8-inch tall Texas gyratory compacted specimens were used for the creep/recovery test.

Results of the air void analysis indicates that the kneading compaction of cylinders in three layers introduces an air void gradient. Visual observations during kneading compaction of cylinders suggest that tender mixes exhibit excessive shoving which may make the distribution of air voids even less uniform.

Figure 48 illustrates the distribution of air voids in three parts of the 4-inch by 8-inch cylinders of AC-5 and river gravel. The mid-section of these cylindrical specimens was poorly compacted, which may have been caused by shoving during compaction. It is hypothesized that the nonuniform distribution of voids in the mid-section of AC-5 and river gravel specimen may have caused stress concentrations along the interfaces with denser top and bottom portions. The development of those stress concentrations along the interface layers could potentially lead to localized failure. These potentially erratic deformations are recorded by the Linear Variable Transducers (LVDT's), which are positioned at the mid-section of the specimen and are reported as erroneous creep strains. The effect of the air void gradient on the engineering properties of HMAC is the subject of investigation in the AAMAS study (17). The hypothesized explanantion of anomalous permanent deformation behavior, which was depicted in Figures 46 and 47, needs to be verified in TTI Project 1170 as well as in the AAMAS study.

Figures 49 through 52 illustrate the distribution of air voids in the remainder of the experimental matrix mixtures. These data indicate that a variation of $\pm$1.5% in the air void content along the height of the 4-inch diameter by 8-inch tall, kneading-compacted cylinders should be expected.

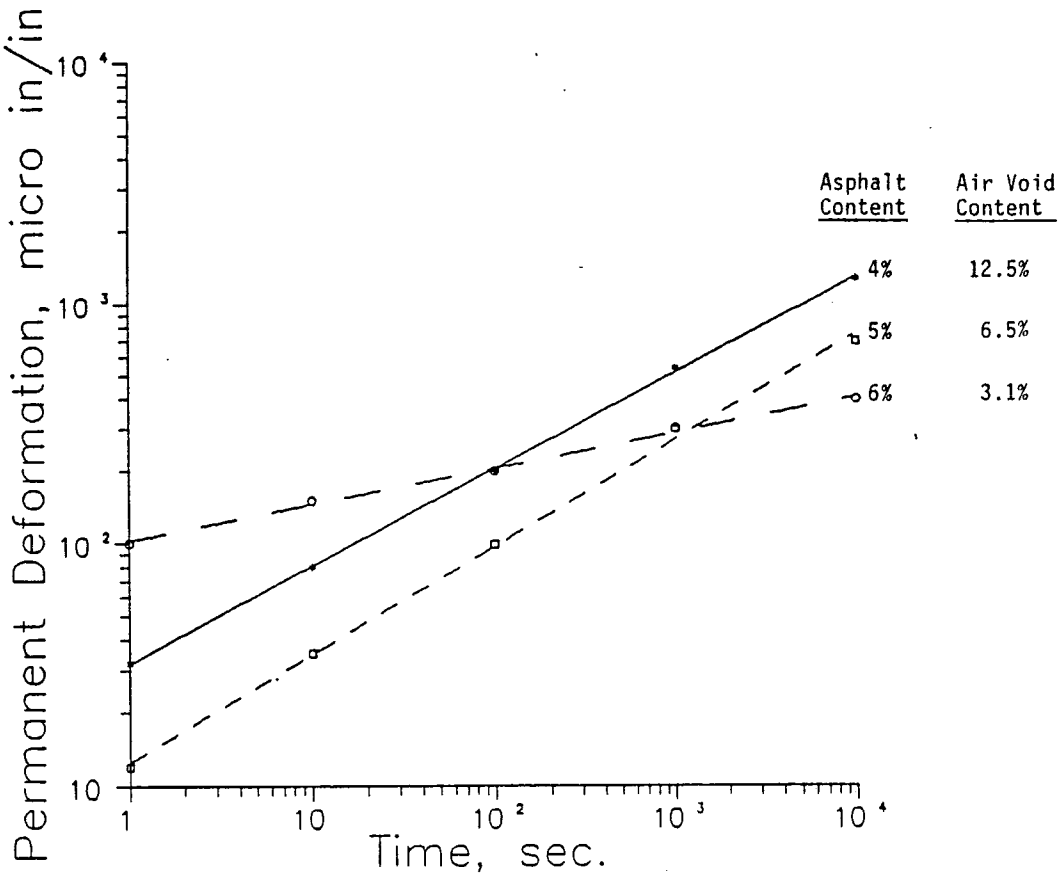

Figure 47. Permanent deformation trends for AC-5 and siliceous gravel mixtures.

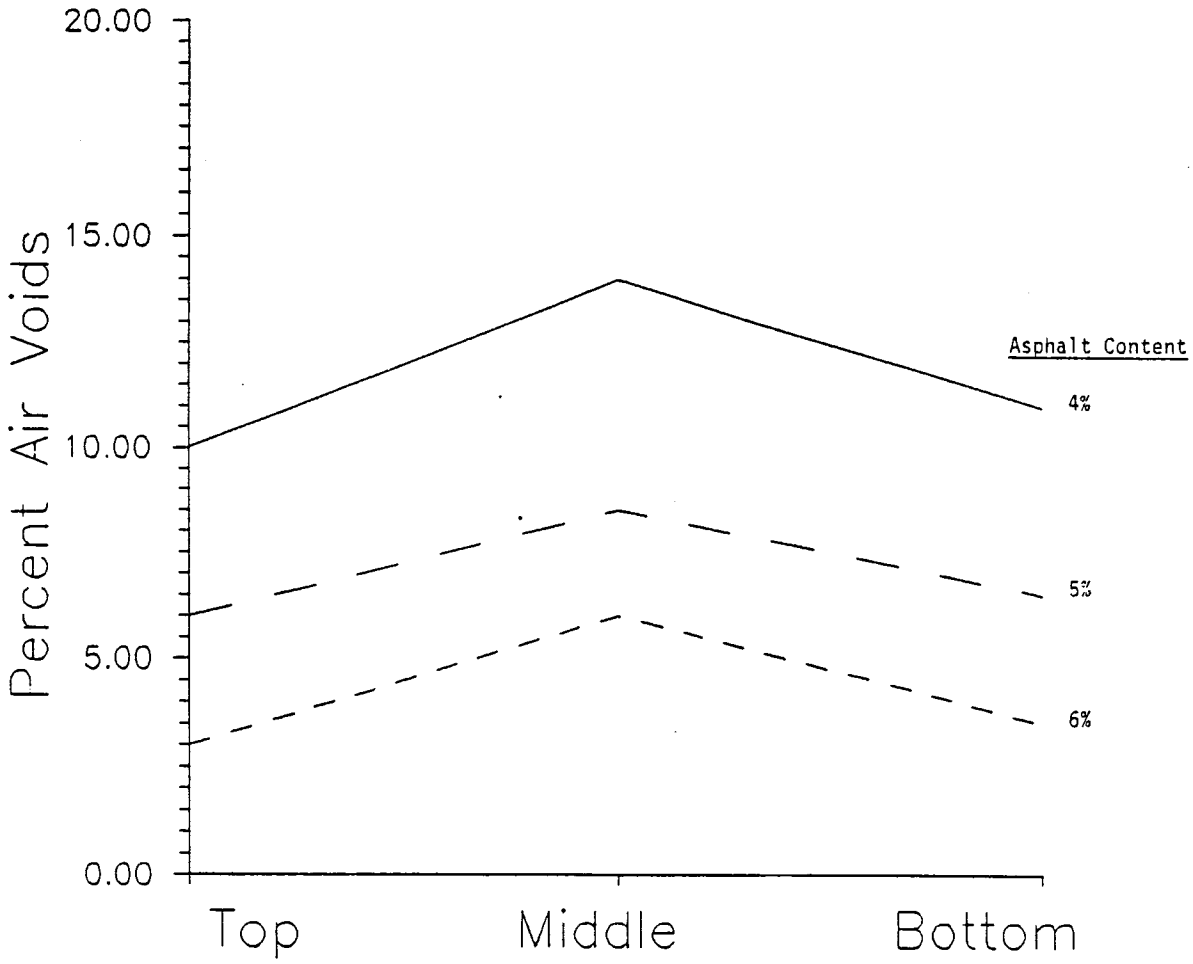

Figure 48. Distribution of air voids in 4-inch diameter by 8-inch tall, AC-5 and river gravel cylindrical HMAC specimen compacted in three layers using the kneading device.

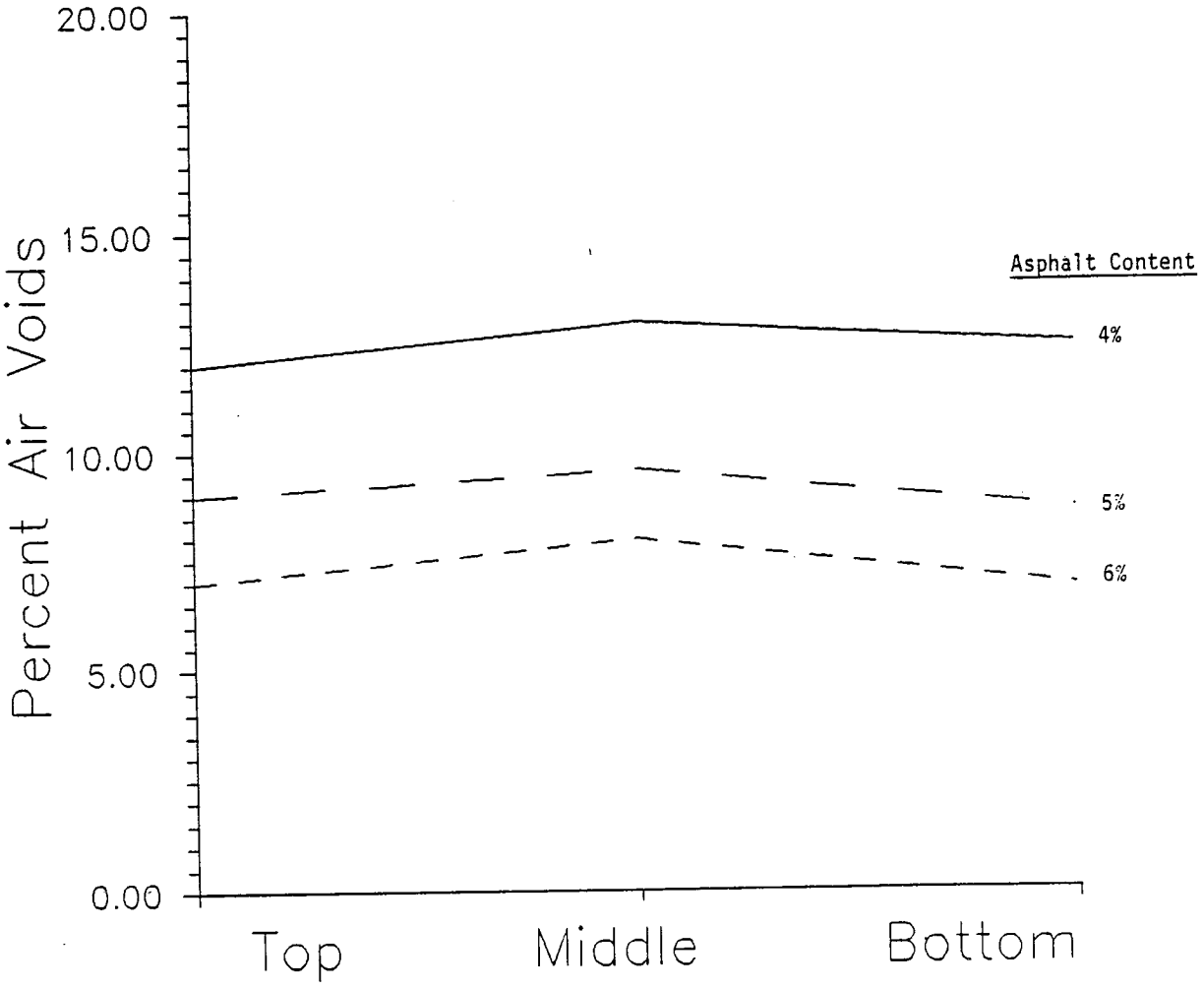

Figure 49. Distribution of air voids in 4-inch diameter by 8-inch tall AC-5 and crushed limestone cylindrical HMAC specimens compacted in three layers using the kneading device.

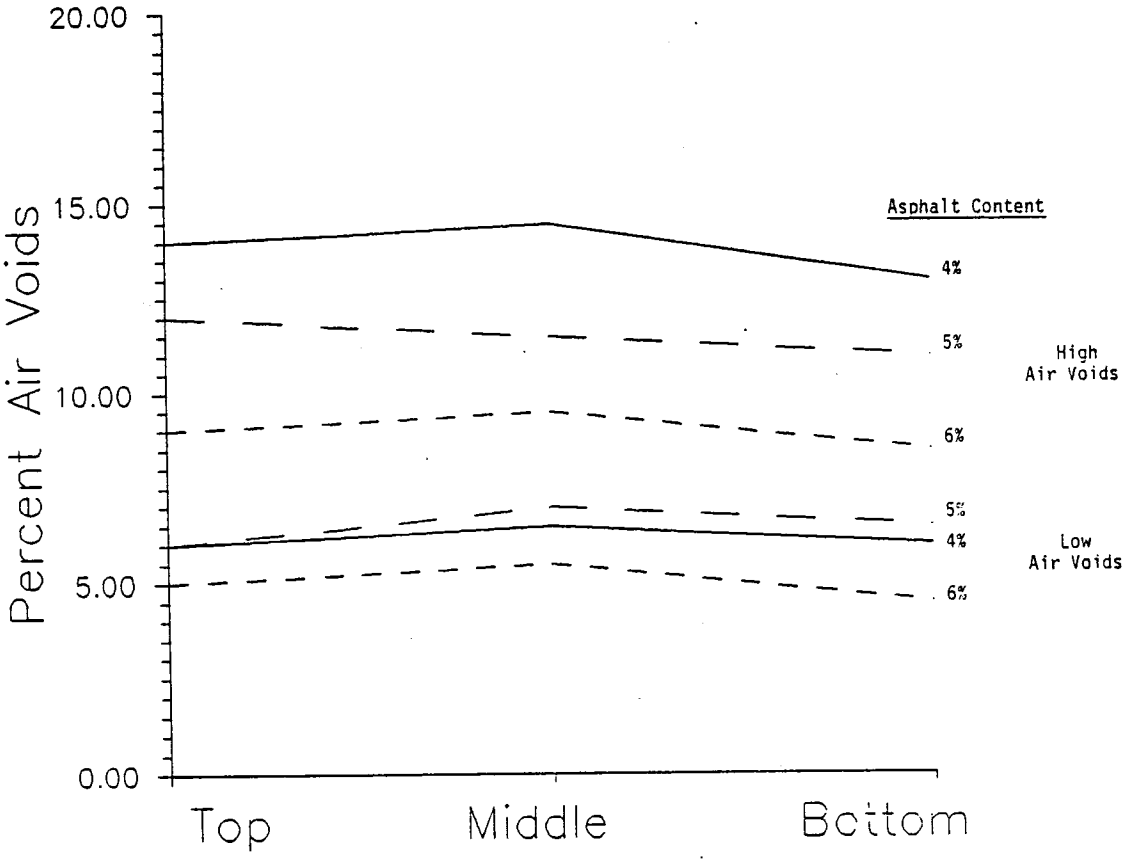

Figure 50. Distribution of air voids in 4-inch diameter by 8-inch tall AC-20 and crushed limestone cylindrical HMAC specimens compacted in three layers using the kneading device.

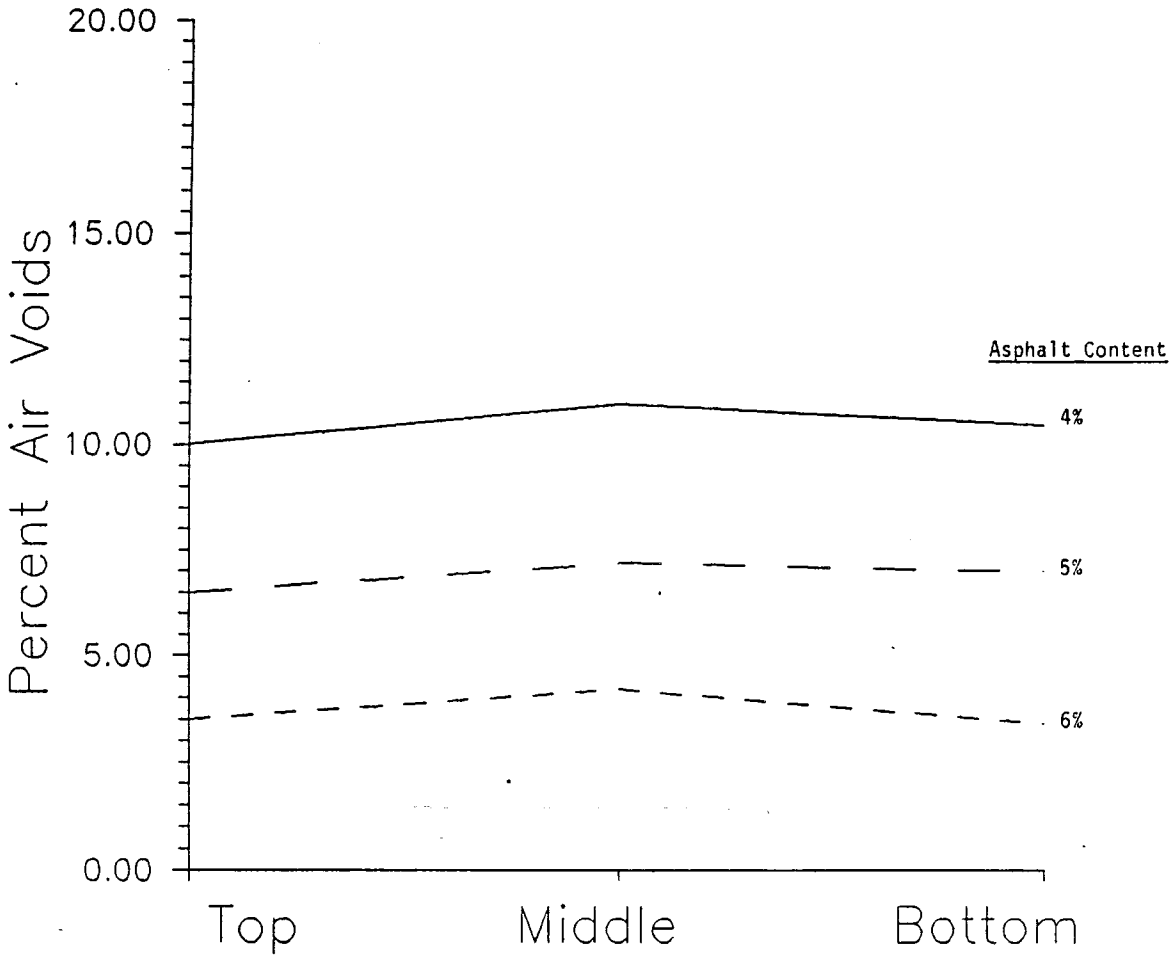

Figure 51. Distribution of air voids in 4-inch diameter by 8-inch tall AC-10 and river gravel cylindrical HMAC specimens compacted in three layers using the kneading device.

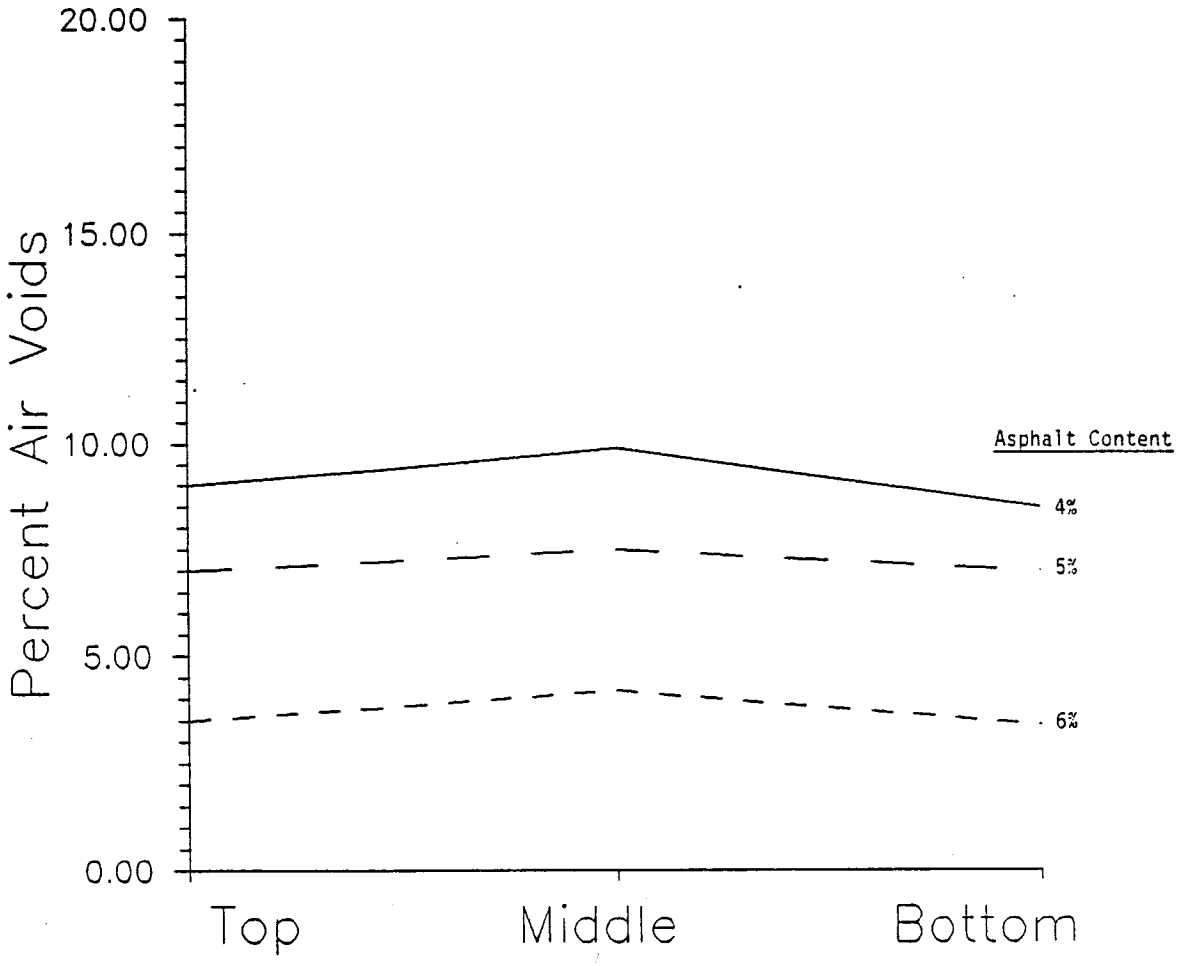

Figure 52. Distribution of air voids in 4-inch diameter by 8-inch tall AC-20 and river gravel cylindrical HMAC specimens compacted in three layers using the kneading device.

This problem was remedied by the Texas gyratory compaction method which produced a much more uniform distribution of air voids. Variations in air void contents are about ±0.5% along the 6-inch diameter by 8-inch tall cylindrical specimens that are compacted by the Texas gyratory device (Figure 53).

Figure 54 illustrates the permanent deformation potential of AC-10 and river gravel mixtures. The trends for mixtures containing 4% and 6% asphalt contents follow the normal pattern as described for Figure 45. The mixtures containing 5% asphalt cement exhibited tenderness during compaction causing an average air void content of 6%. The compactive effort was maintained constant throughout this portion of the study which makes the air void content a function of mixture response to compaction.

Figure 55 depicts the permanent deformation potential of AC-20 and river gravel mixtures. The increase in asphalt content induces a rather conventional trend as described for Figure 45. In general, the trends in Figure 55, when compared to the trends illustrated in Figure 46, indicate that permanent deformation potential is greater for mixtures of AC-20 with siliceous river gravel than with AC-20 with crushed limestone aggregate.

The optimum asphalt content should be determined based on preliminary evaluation of stability, density, and air voids content. This determination is then further evaluated based on creep/rutting criteria for specific environmental conditions and structural categories of the pavement.

It is extremely important to identify the type of pavement structure to which the mixture will be applied. In order to demonstrate the importance of the structural effects, the following example is provided. The mixtures shown in Table 12, were used in this investigation. Gradation charts for the Brazos River Gravel and Brownwood Limestone are provided in Figures 42 and 43. The creep specimens were compacted using the kneading device and Texas stability values, reported in Table 12, were measured according to Test Method TEX-204-F.

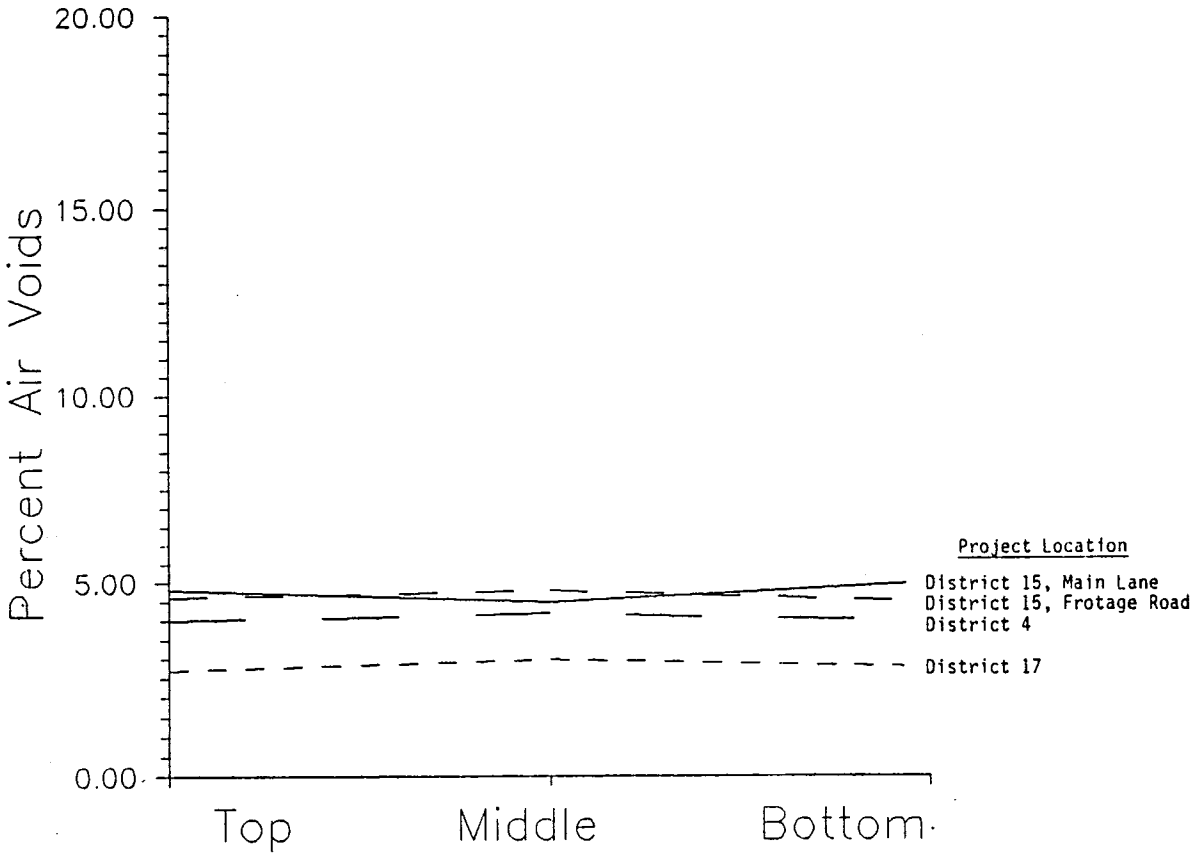

Figure 53. Distribution of air voids in 6-inch diameter by 8-inch tall cylindrical HMAC specimens compacted in one layer using the Texas gyratory device.

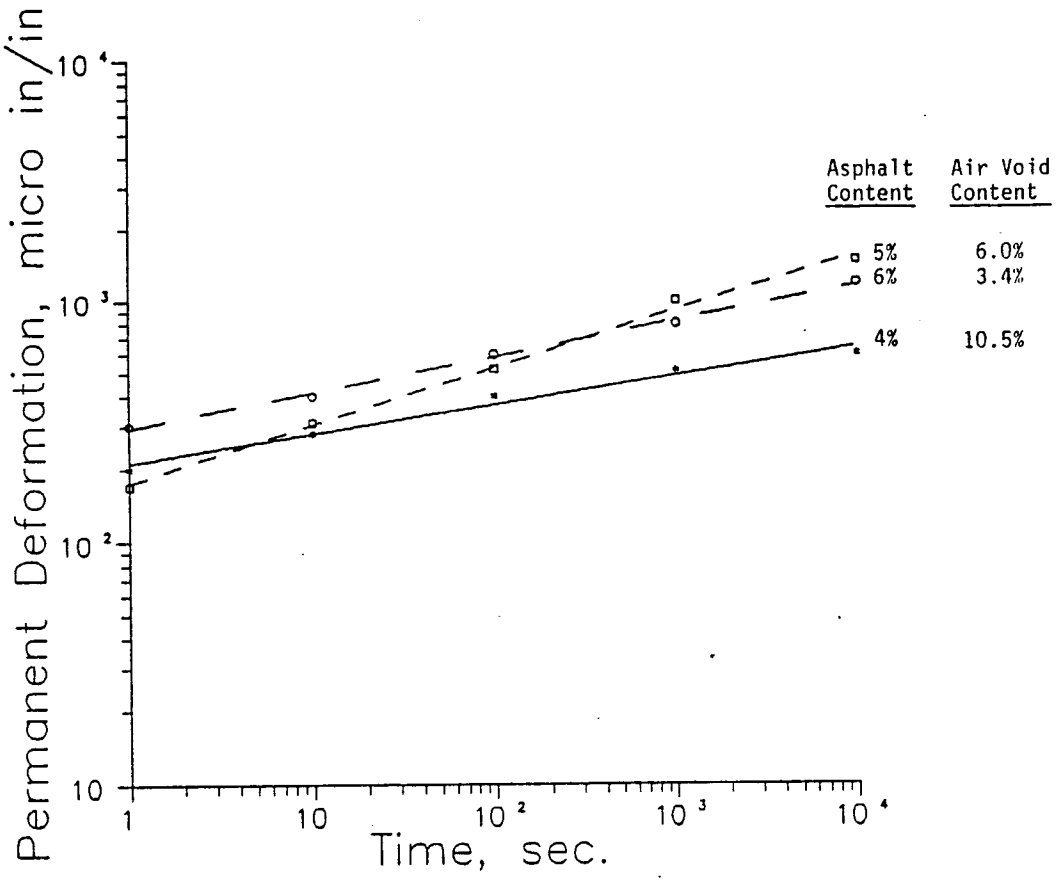

Figure 54. Permanent deformation trends for AC-10 and siliceous gravel mixtures.

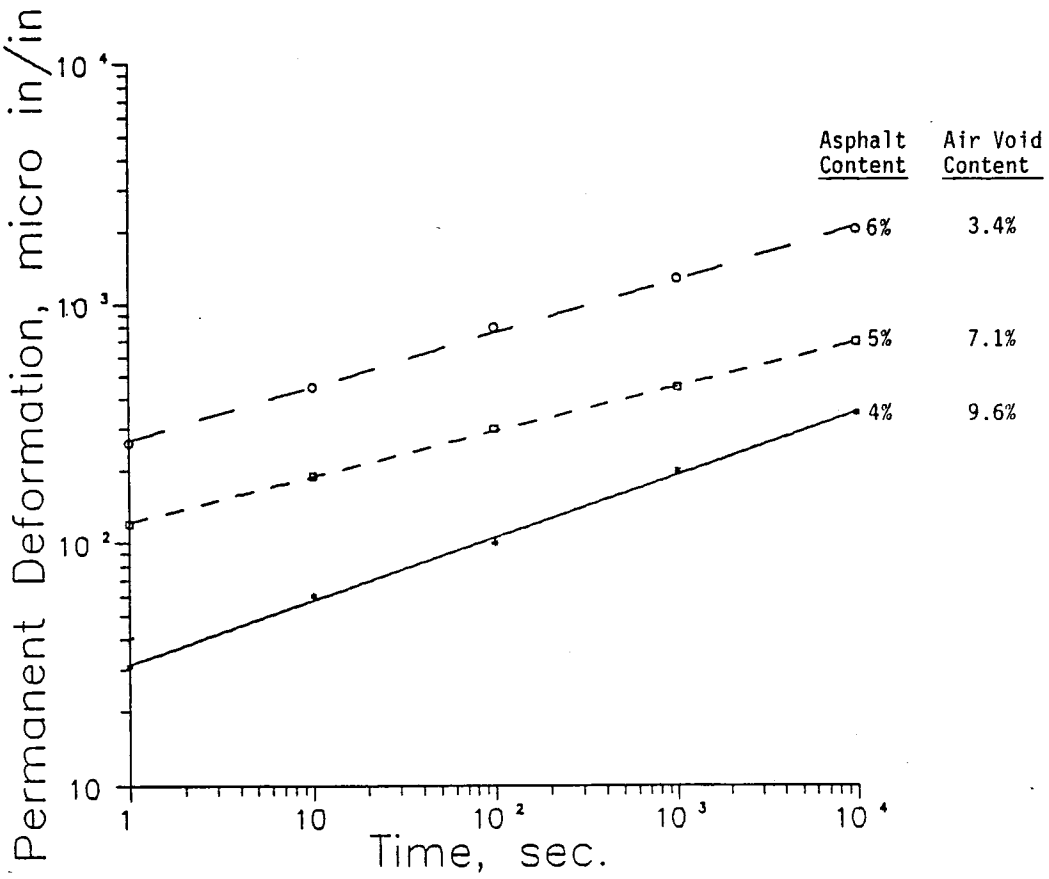

Figure 55. Permanent deformation trends for AC-20 and siliceous gravel mixtures.

Table 12. Identification of mixtures used to demonstrate sensitivity of procedure to pavement structural category.

Asphalt Cement	Aggregate	Air Voids (%)	Texas Stability (%)
AC-5 (5%)	Brazos River Gravel	7.0	43
AC-10 (4%, 5%)	Brazos River Gravel	7.0	43
AC-20 (4%)	Crushed Limestone	5.5	52

The results of this phase of rutting analysis are illustrated in Figures 56 through 59. In these figures, the viscoplastic stiffness is plotted versus time of creep loading. The viscoplastic stiffness trends are then plotted on rutting severity evaluation charts for all four categories of pavement structure that were included in this study. In conclusion, the type of pavement structure has a significant influence on the magnitude of compressive stresses in the asphalt layer. This could result in satisfactory or unsatisfactory rutting behavior purely due to the structural category within which the HMAC will be used. Figures 56 through 59 illustrate how the structural arrangements shift the rutting performance of a mixture from acceptable to marginal or even unacceptable zones.

Bitumen-Mixture Relationship

Historically, researchers who pioneered the use of a simple creep test for rutting characterization, have done so by incorporating the bitumen properties into their analyses (8, 9, 29, 38, 51, 62). This was done in order to establish an empirical link between the mixture stiffness and the bitumen stiffness derived from Van der Poel's nomograph (49-51). In recent years, there has been a resurgence of these basic ideas among the bitmuninous community. The American Society for Testing and Materials (ASTM) Symposium in December, 1985, is a good example (63).

In this study, an attempt was made to provide enough background information so that one can assess the mixture stiffness based upon bitumen properties. Such a task was accomplished through presenting charts in terms of bitumen stiffness, S_{bit}, and mixture stiffness, S_{mix}, parameters. This is illustrated in Figures 60 and 61. With the aid of these figures, one can estimate the mixture stiffness by knowing the basic

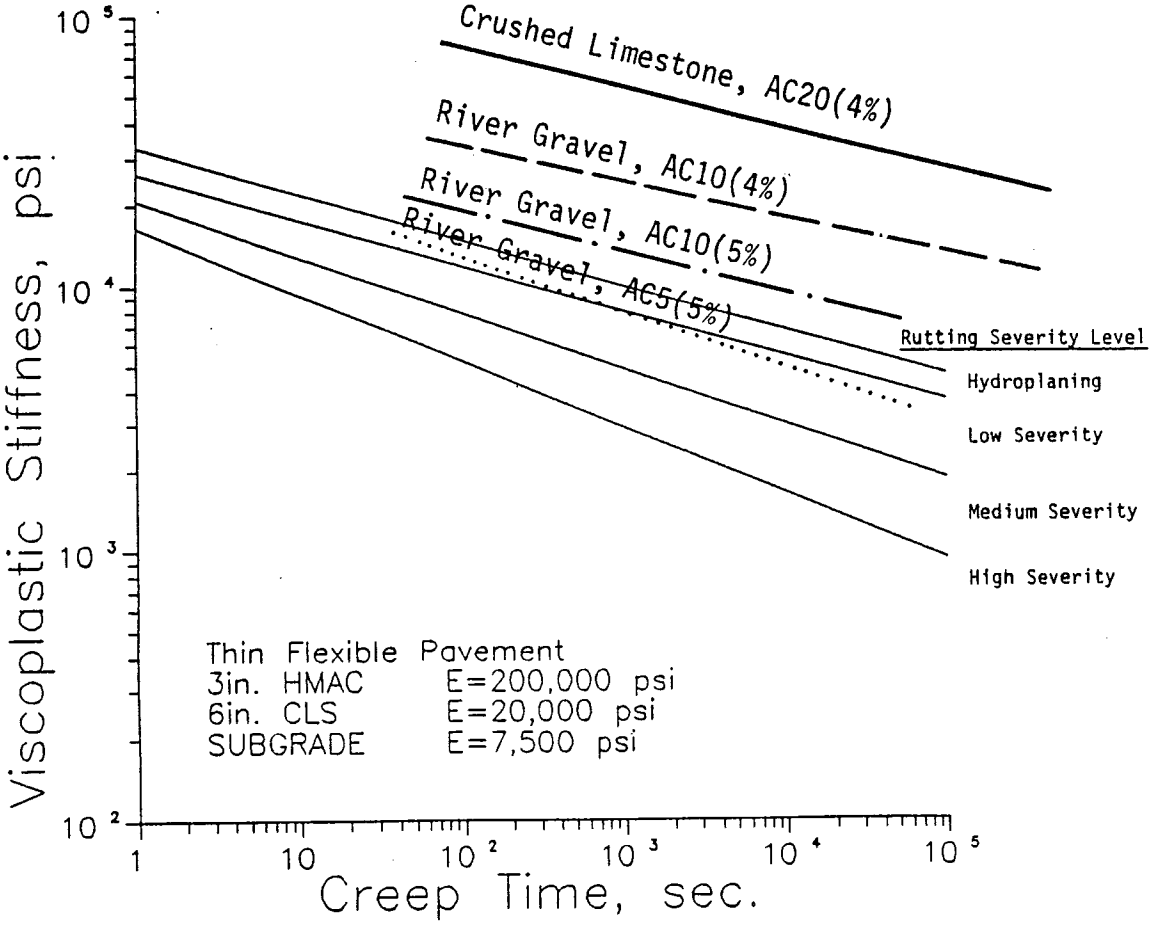

Figure 56. Rutting potential for mixtures identified in Table 12 in a thin flexible pavement.

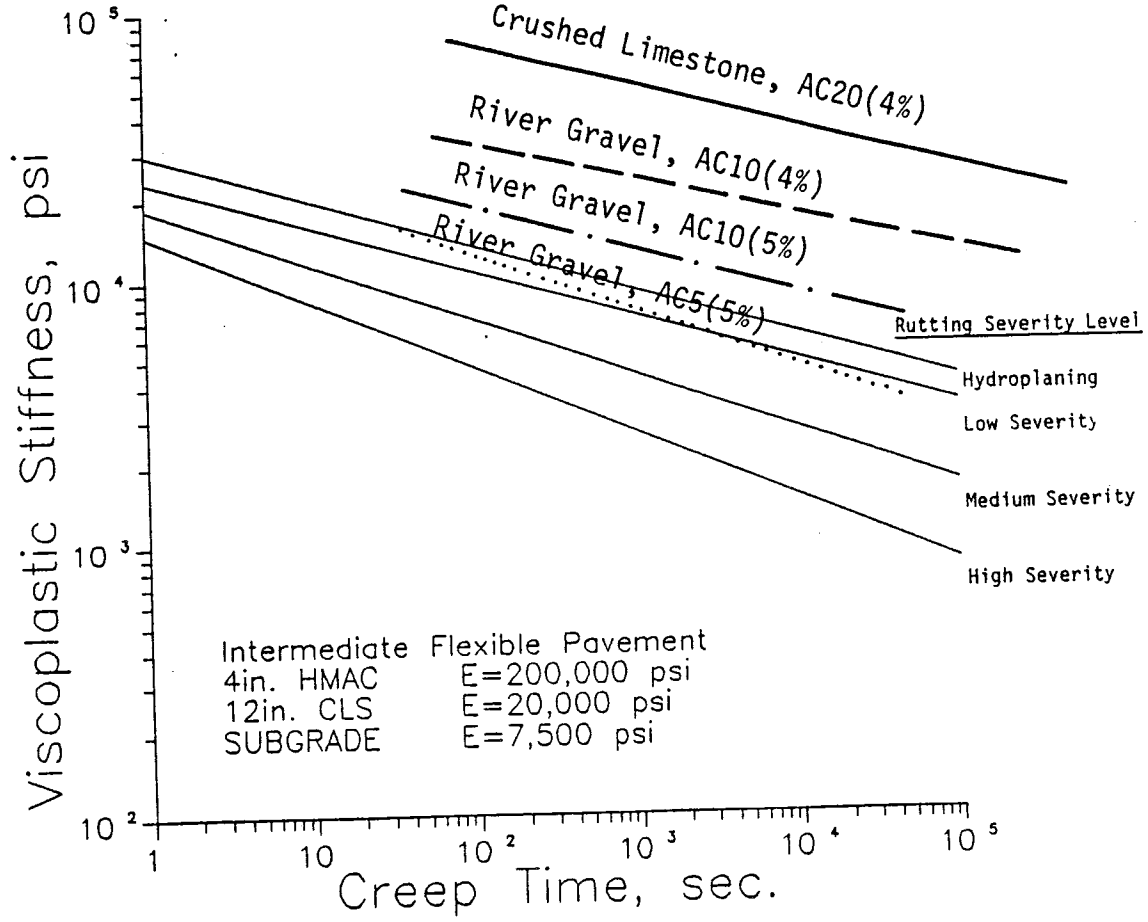

Figure 57. Rutting potential for mixtures identified in Table 12 in an intermediate flexible pavement.

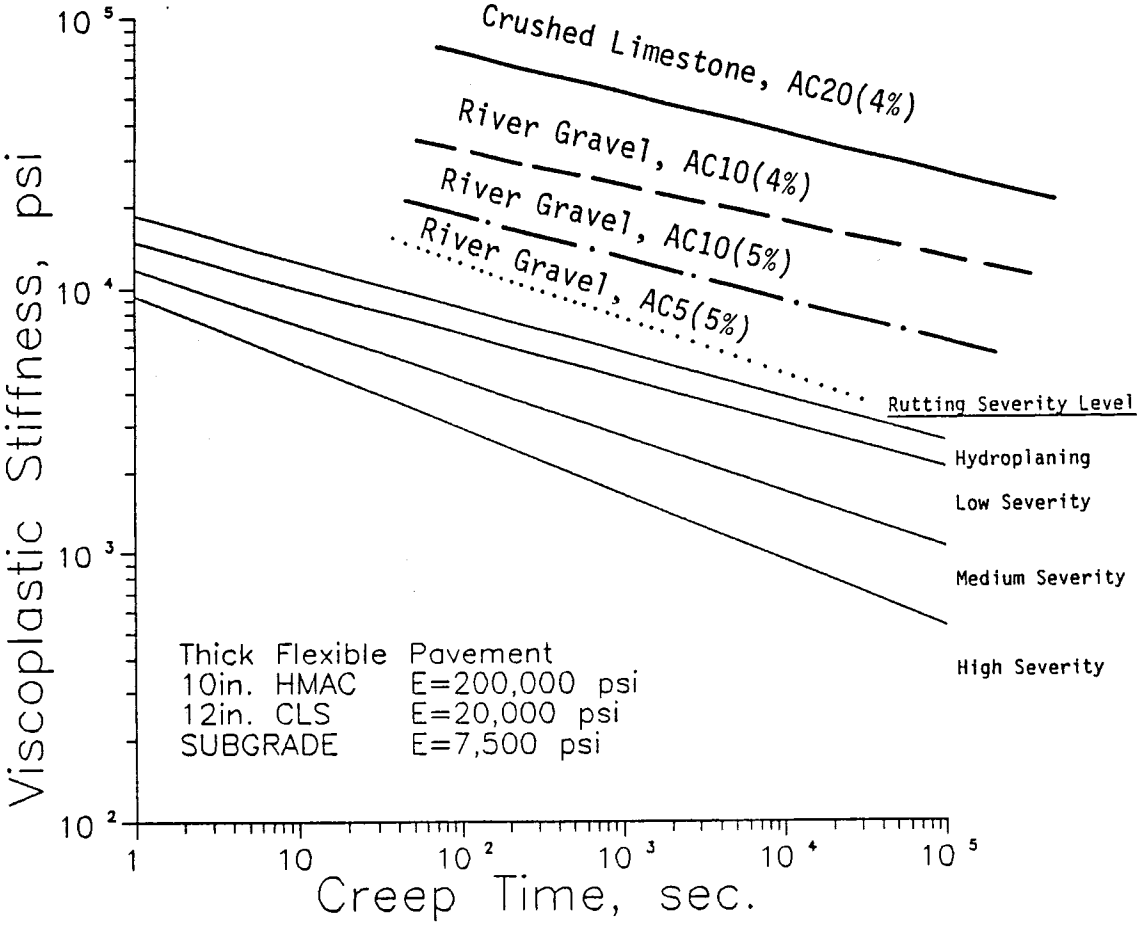

Figure 58. Rutting potential for mixtures identified in Table 12 in a thick flexible pavement.

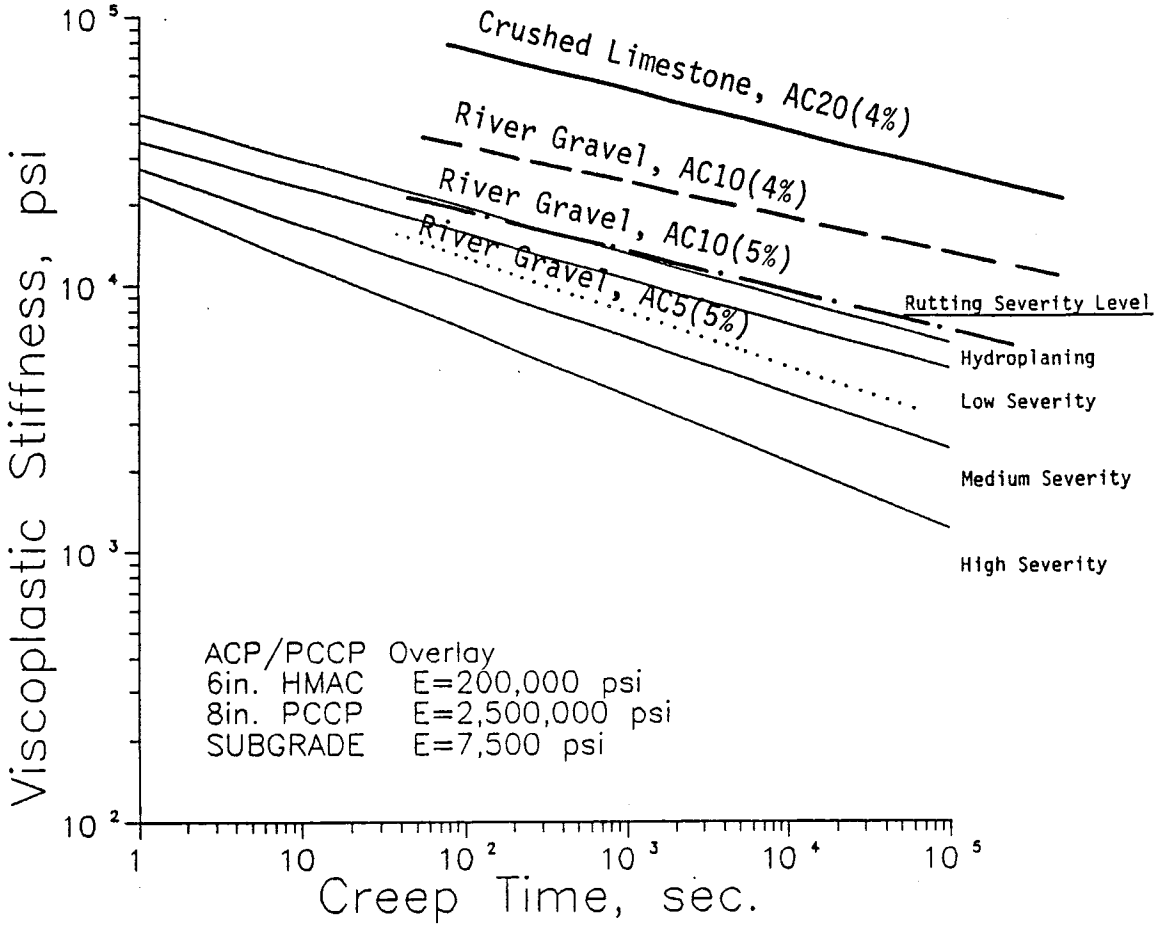

Figure 59. Rutting potential for mixtures identified in Table 12 in an overlay structure.

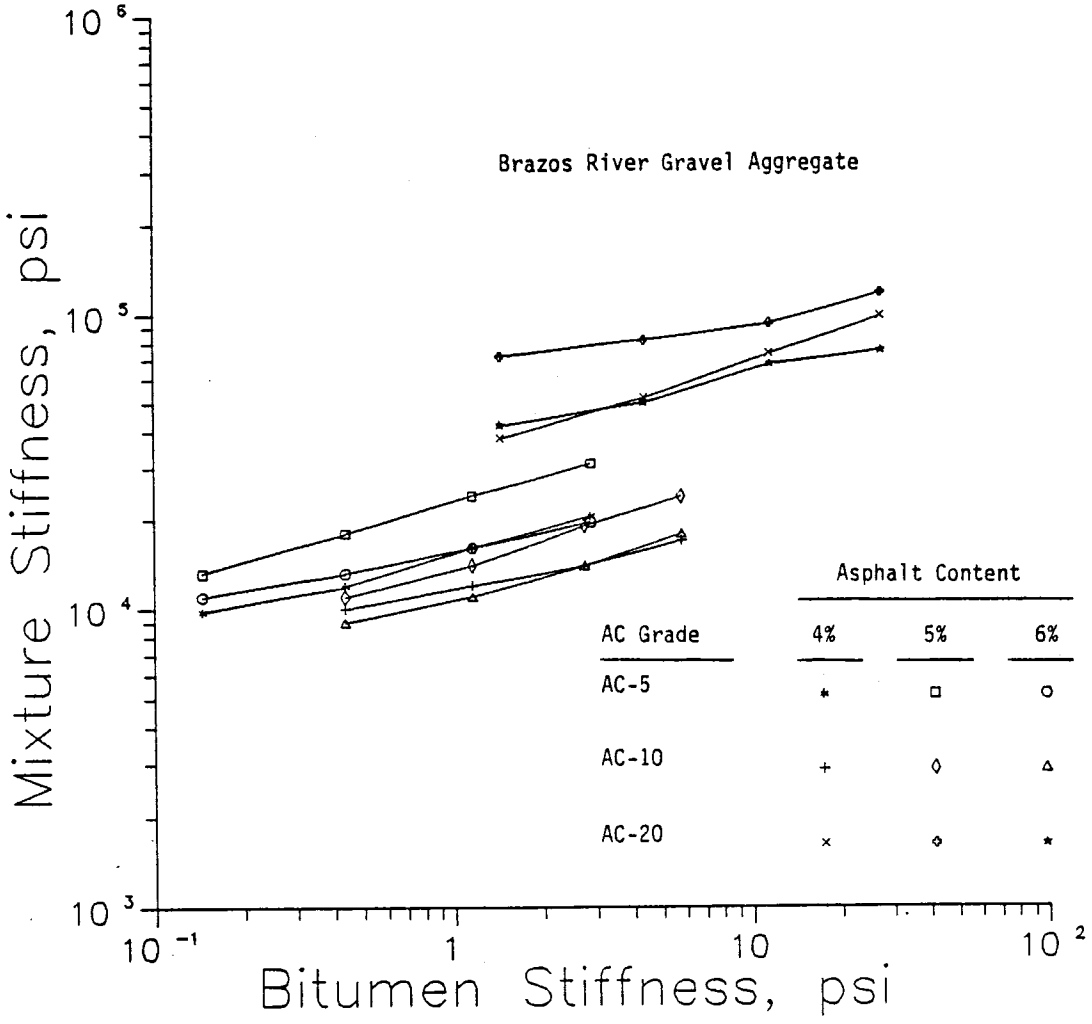

Figure 60. Relationship between mixture stiffness and bitumen stiffness for siliceous gravel mixes identified in Table 11.

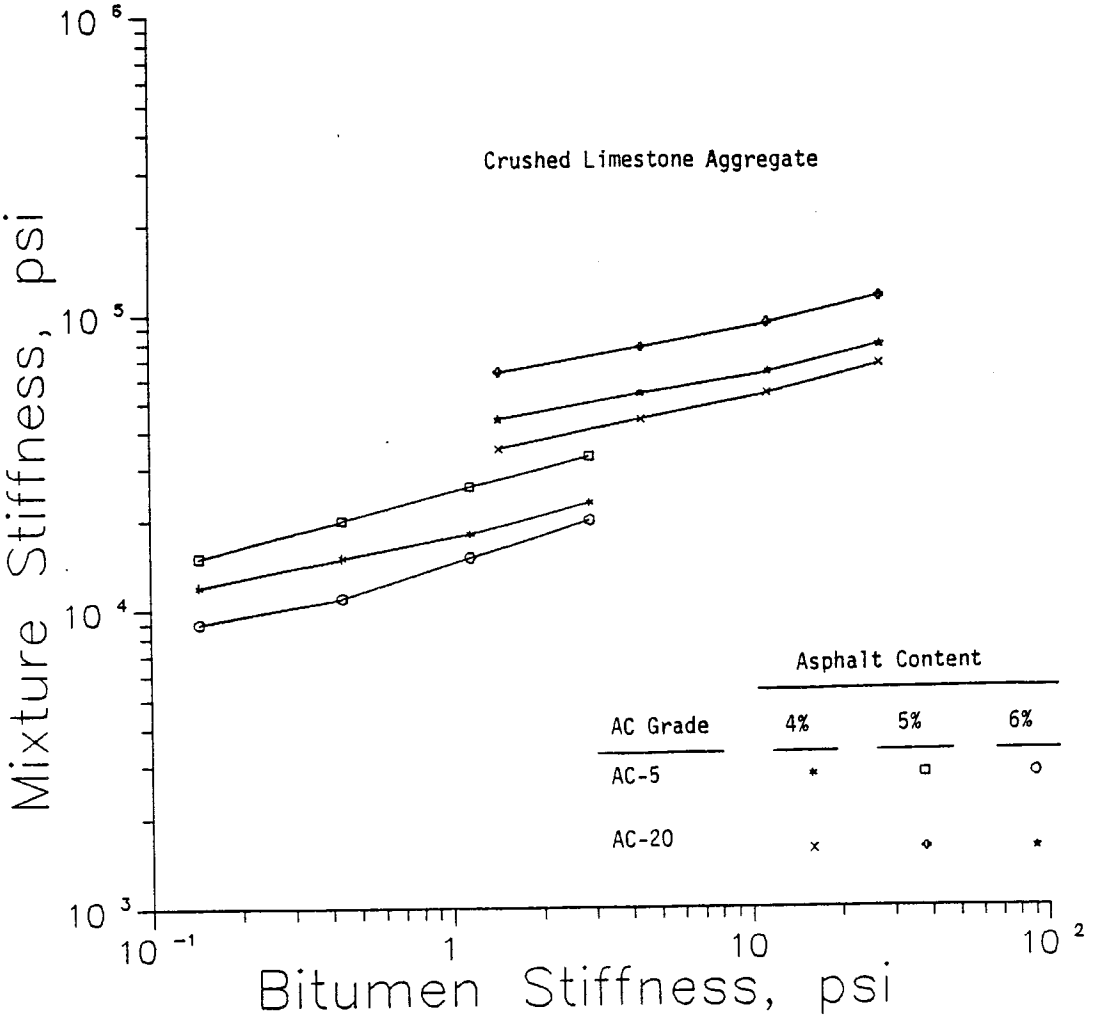

Figure 61. Relationship between mixture stiffness and bitumen stiffness for crushed limestone mixtures identified in Table 11.

bitumen properties such as: penetration, viscosity, and ring and ball temperature. In the absence of any creep or recovery data, this methodology offers reasonable estimates of HMAC stiffness.

The methodology uses a simple system of nomographs which was introduced by Van der Poel (51), and it was further refined by McLeod (64, 65). The refinements were necessary for waxy asphalts which exhibit somewhat of a "false softening point."

As a result of these investigations, a shift factor can be developed to account for the effect of temperatures encountered in the field which are different than the creep test temperature. In order to accomplish this task, the stiffness values of hypothetical bitumens having penetration indices ranging from +2 to -2 and temperature differences from the ring and ball temperature ranging from -60° to +40°F were evaluated using Van der Poel's nomograph (Figure 62). The viscous component of bitumen stiffness, which is viewed to be responsible for permanent deformation was derived for the above conditions. Figures 63 through 67 illustrate the result of this analytical work. Through empirical relationships, such as the one illustrated in Figure 68, the viscous component of mixture stiffness values for conditions depicted in Figures 63 through 67 were determined. This is presented in Figures 69 through 73.

The actual values for stiffness shift factors were derived from the viscous component of mixture/stiffness versus time plots which were evaluated over a range of temperatures. Principles of time-temperature superposition along with the assumption that HMAC can be regarded as thermo-rheologically simple, led to the shift factor relationship which is illustrated in Figure 74. The assumption of thermo-rheological simplicity of HMAC was shown to be a valid one by the Shell researchers (8, 9).

The availability of this mixture stiffness shift factor provides the opportunity for a "laboratory-to-field shift" in the permanent deformation data in order to approximate rutting at high temperatures. Viscoplastic stiffness data can be shifted to account for the actual field temperatures, which may be higher than the creep test temperature. The shifted trends are then plotted on the appropriate rutting criteria charts for performance prediction with respect to rutting. Appendices C and D contain examples of such laboratory-to-field shift.

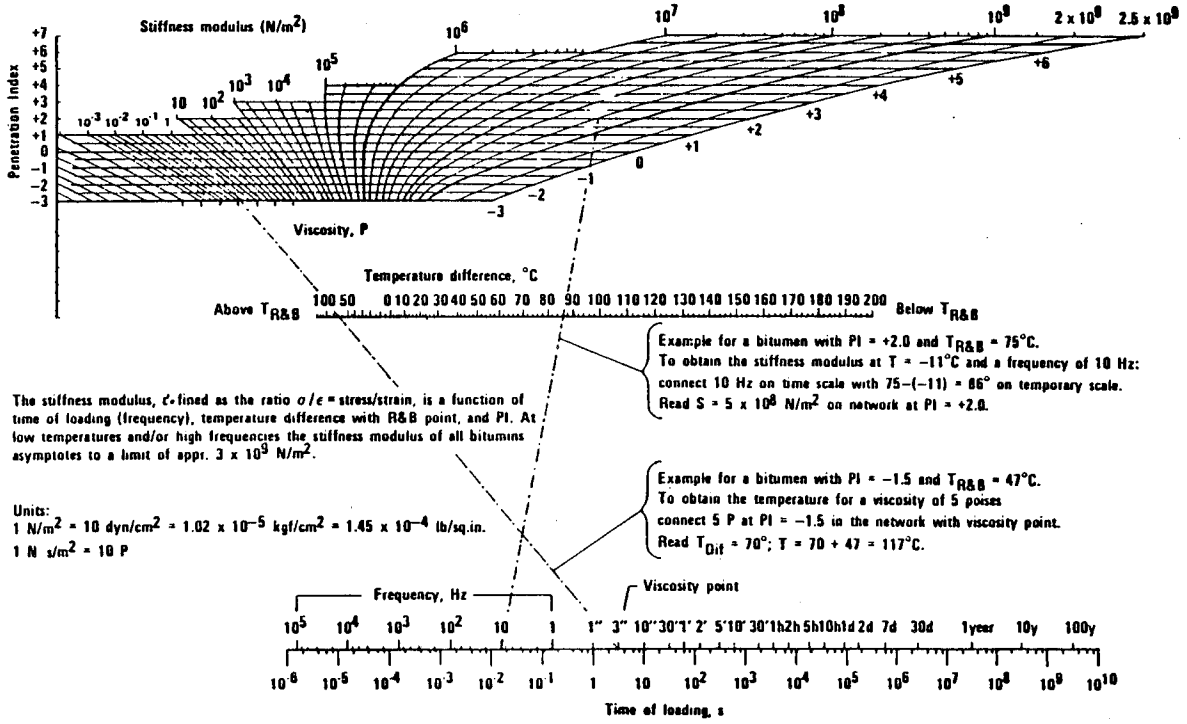

Figure 62. Van der Poel's nomograph (after Reference 51).

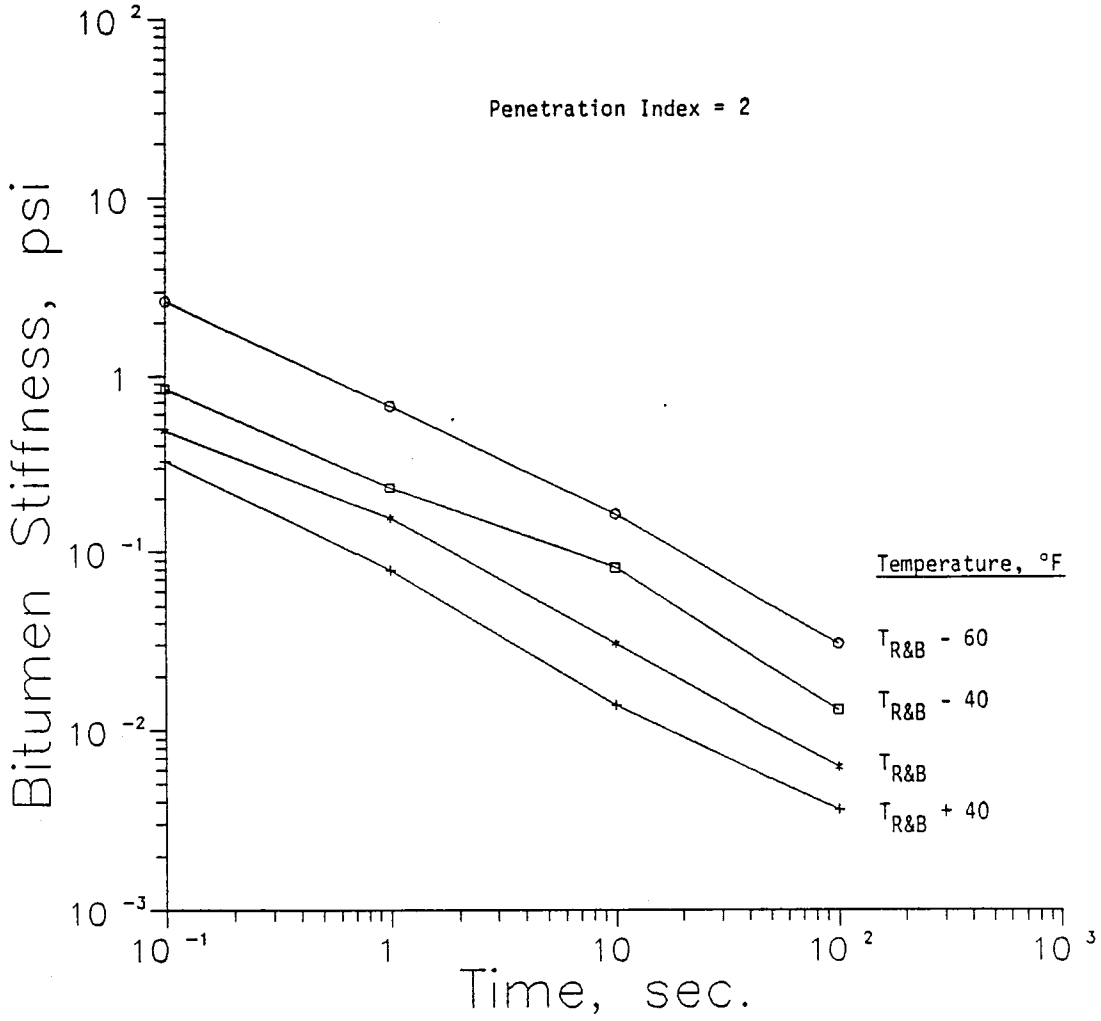

Figure 63. Viscous component of bitumen stiffness as a function of time expressed at different temperatures with respect to ring and ball softening point for a hypothetical bitumen with a penetration index of +2.0.

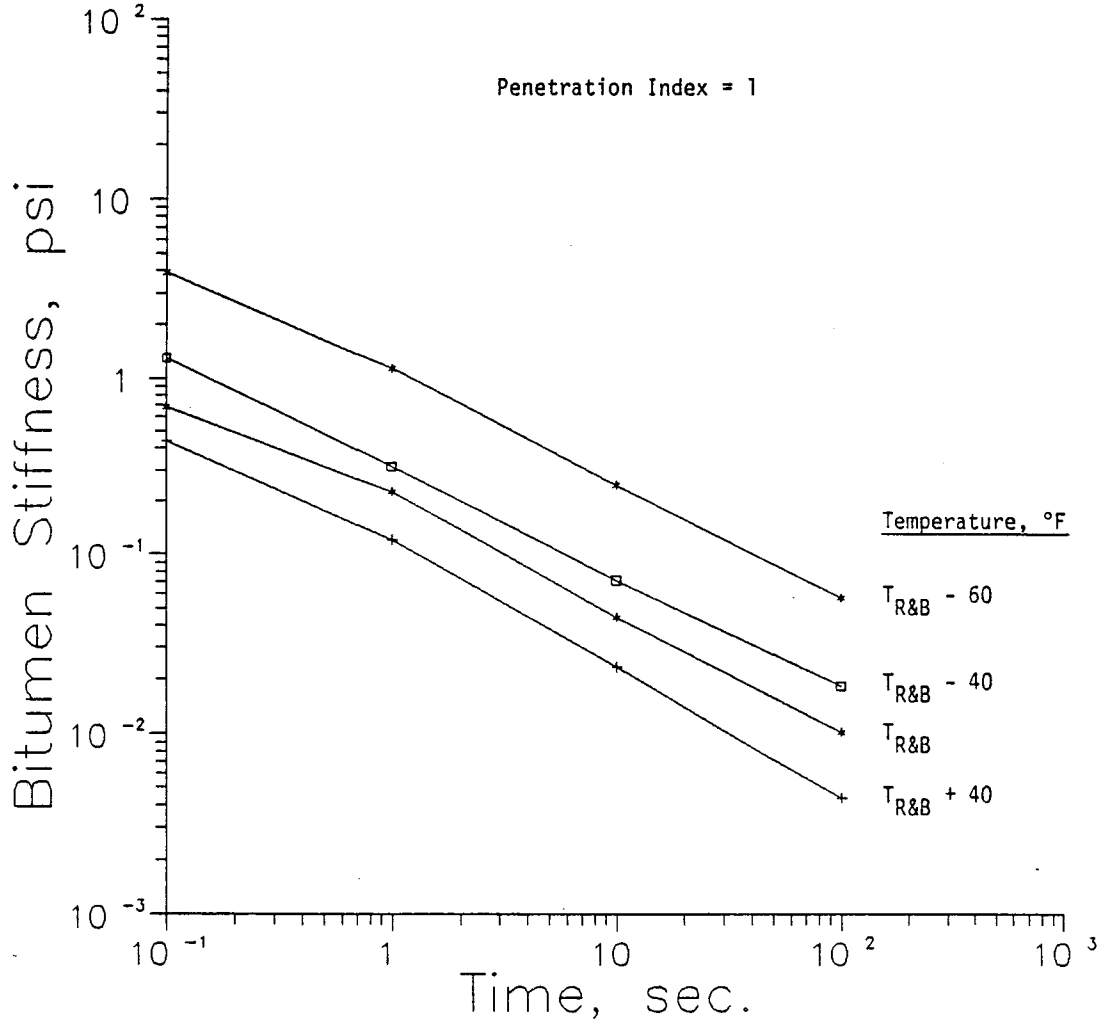

Figure 64. Viscous component of bitumen stiffness as a function of time expressed at different temperatures with respect to ring and ball softening point for a hypothetical bitumen with a penetration index of +1.0.

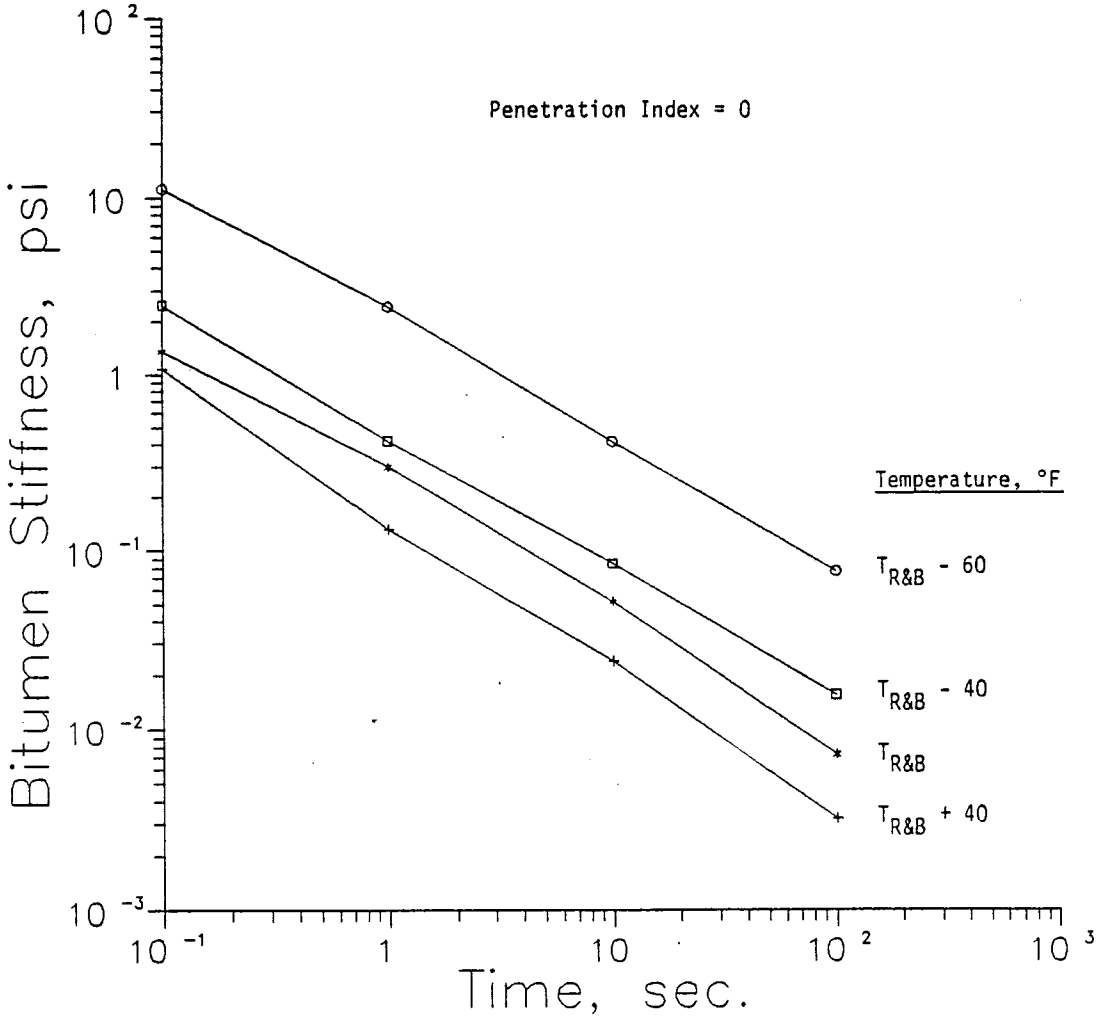

Figure 65. Viscous component of bitumen stiffness as a function of time expressed at different temperatures with respect to ring and ball softening point for a hypothetical bitumen with a penetration index of 0.0.

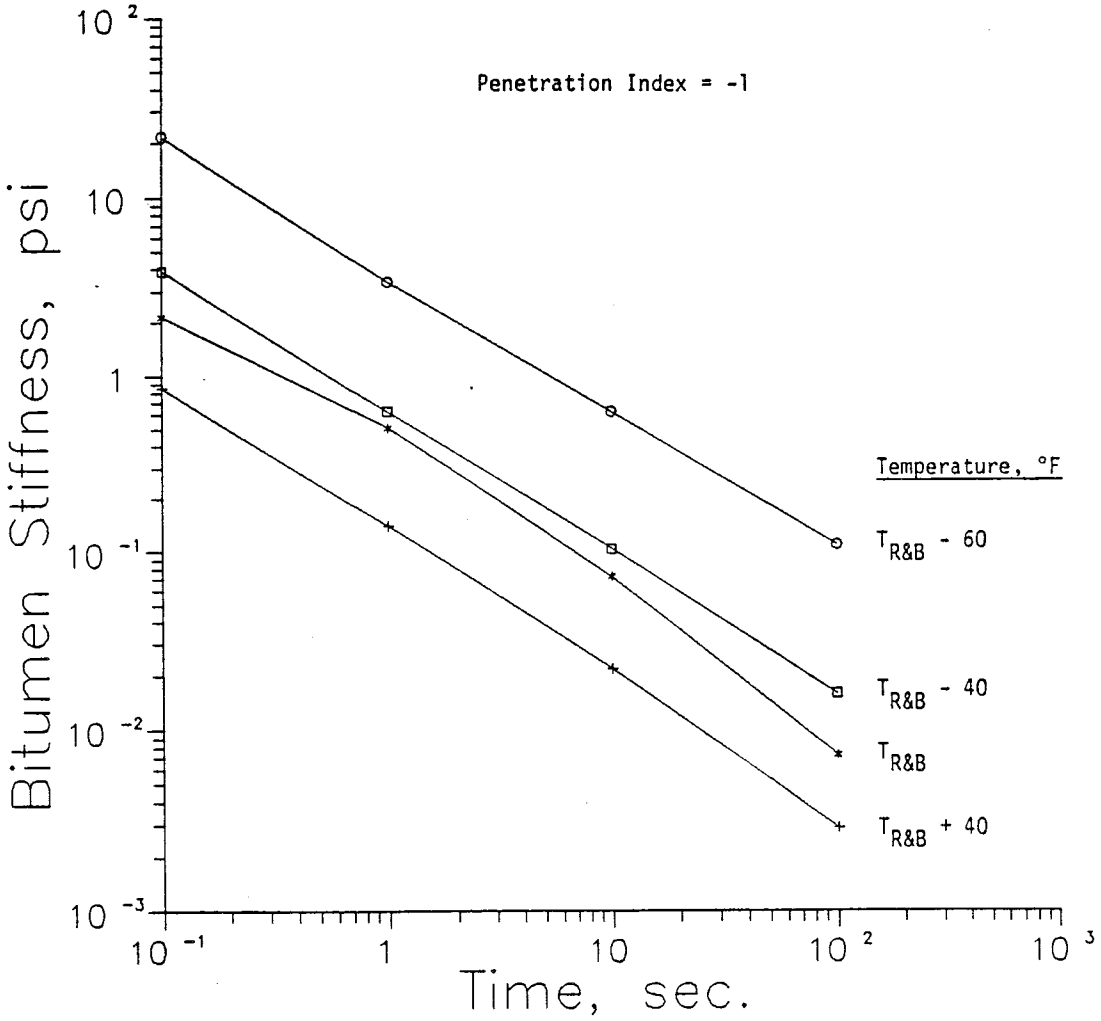

Figure 66. Viscous component of bitumen stiffness as a function of time expressed at different temperatures with respect to ring and ball softening point for a hypothetical bitumen with a penetration index of -1.0.

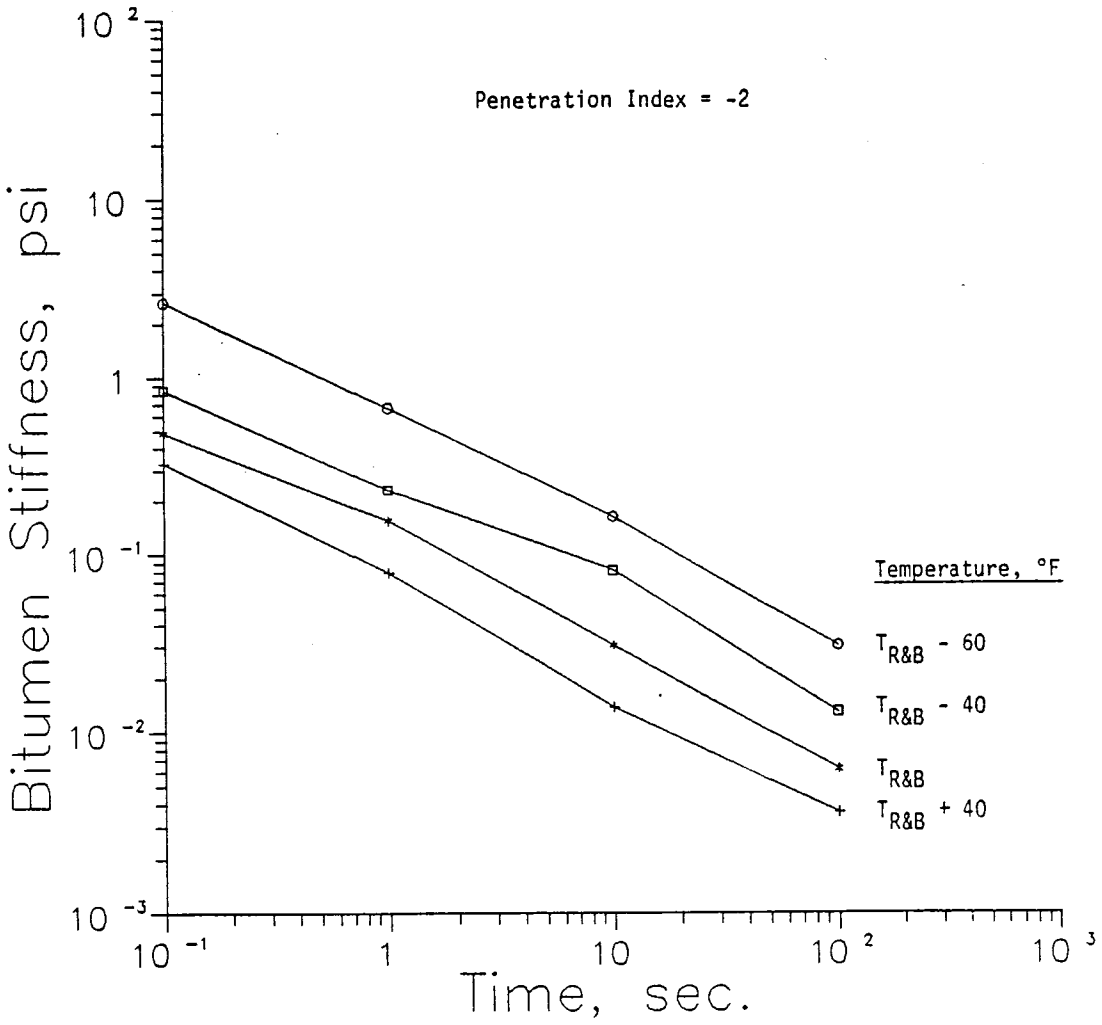

Figure 67. Viscous component of bitumen stiffness as a function of time expressed at different temperatures with respect to ring and ball softening point for a hypothetical bitumen with a penetration index of -2.0.

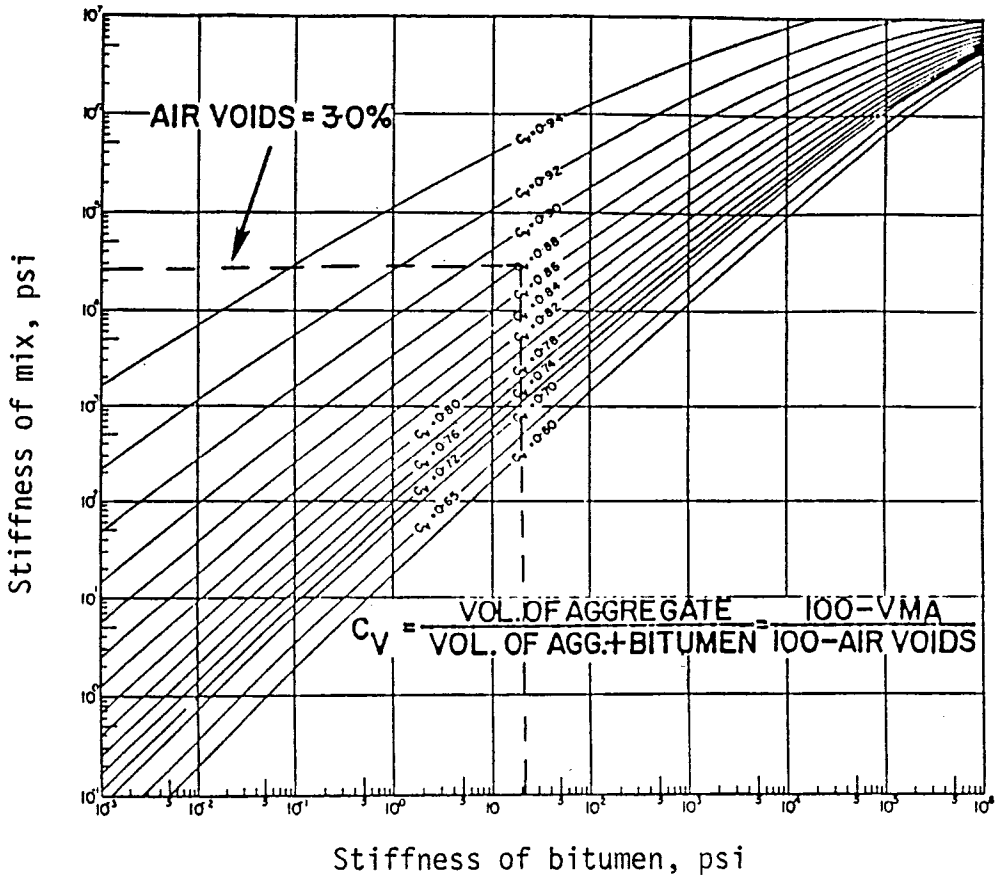

Figure 68. Relationship between stiffness of mix and stiffness of bitumen (after Reference 64).

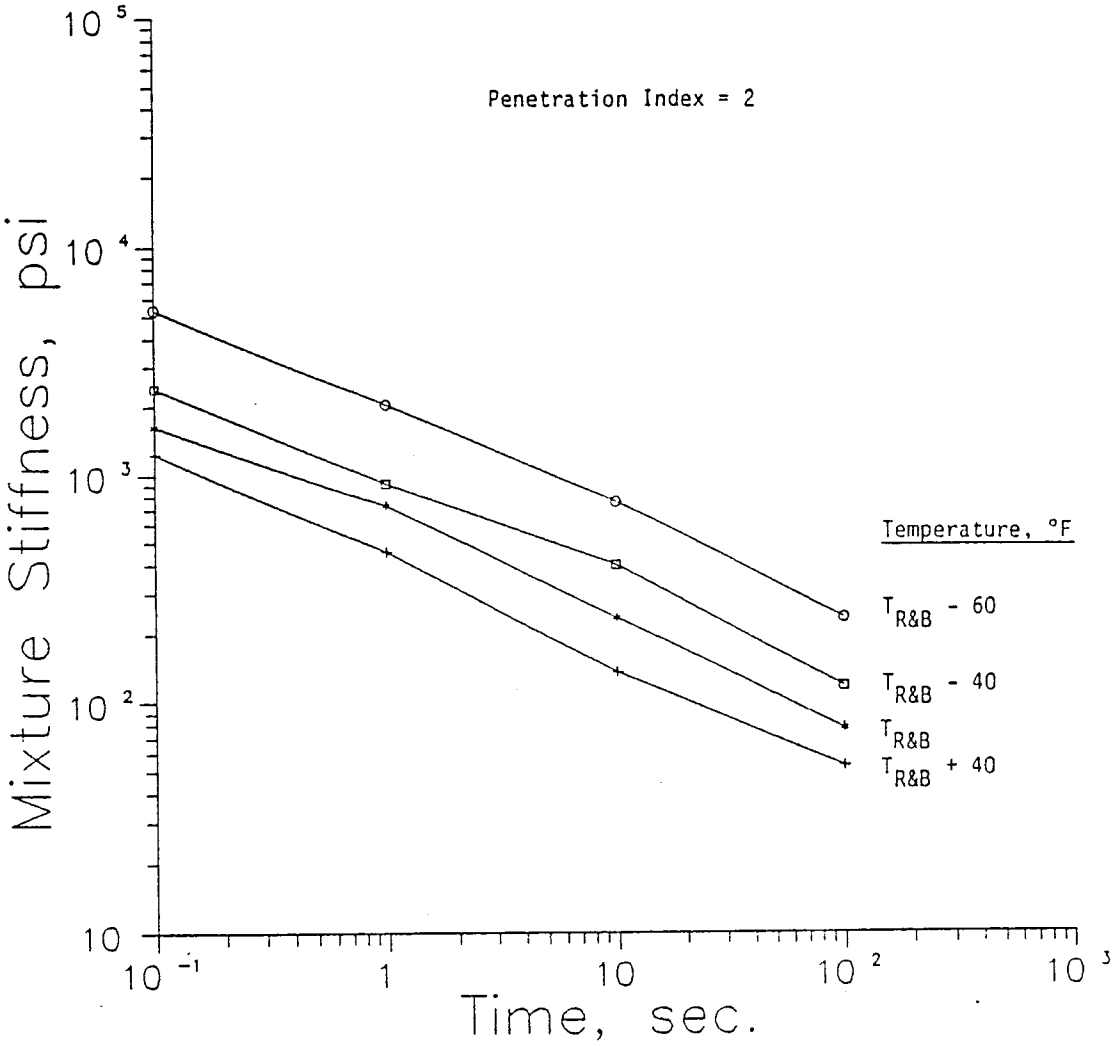

Figure 69. Viscoplastic component of mixture stiffness as a function of time expressed at different temperatures with respect to the ring and ball softening point for a hypothetical bitumen with a penetration index.of +2.0.

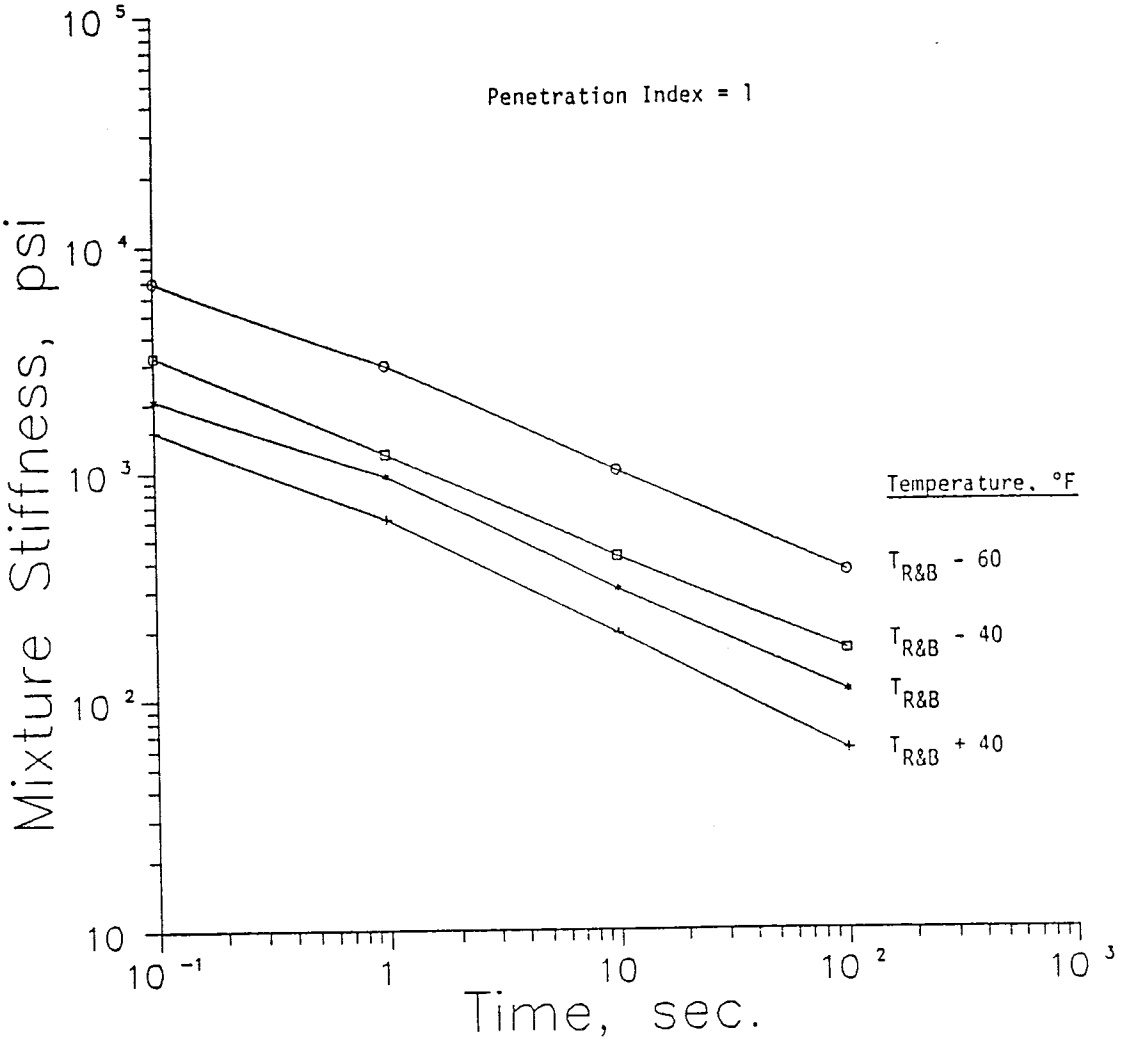

Figure 70. Viscoplastic component of mixture stiffness as a function of time expressed at different temperatures with respect to the ring and ball softening point for a hypothetical bitumen with a penetration index.of +1.0.

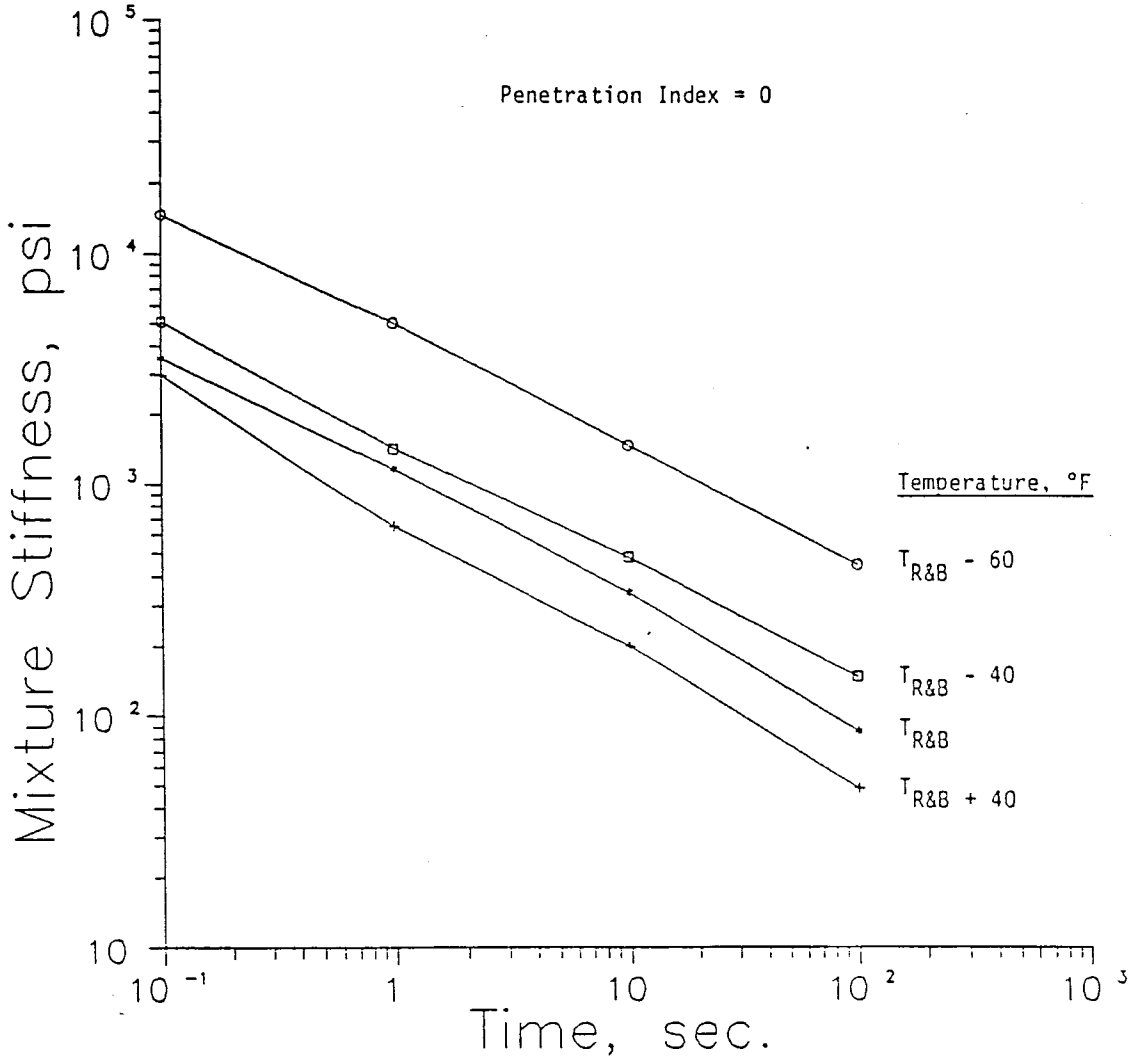

Figure 71. Viscoplastic component of mixture stiffness as a function of time expressed at different temperatures with respect to the ring and ball softening point for a hypothetical bitumen with a penetration index.of 0.0.

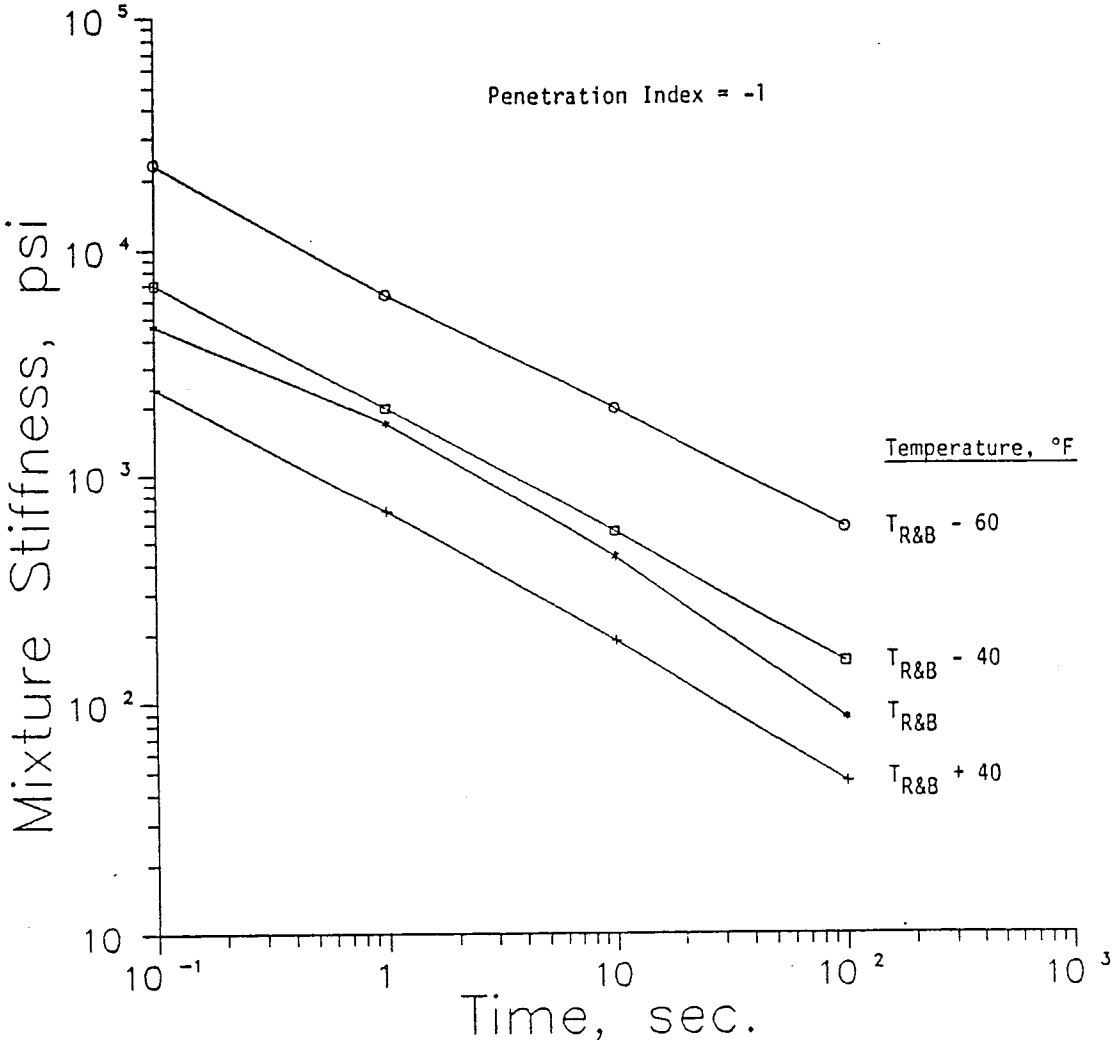

Figure 72. Viscoplastic component of mixture stiffness as a function of time expressed at different temperatures with respect to the ring and ball softening point for a hypothetical bitumen with a penetration index.of -1.0.

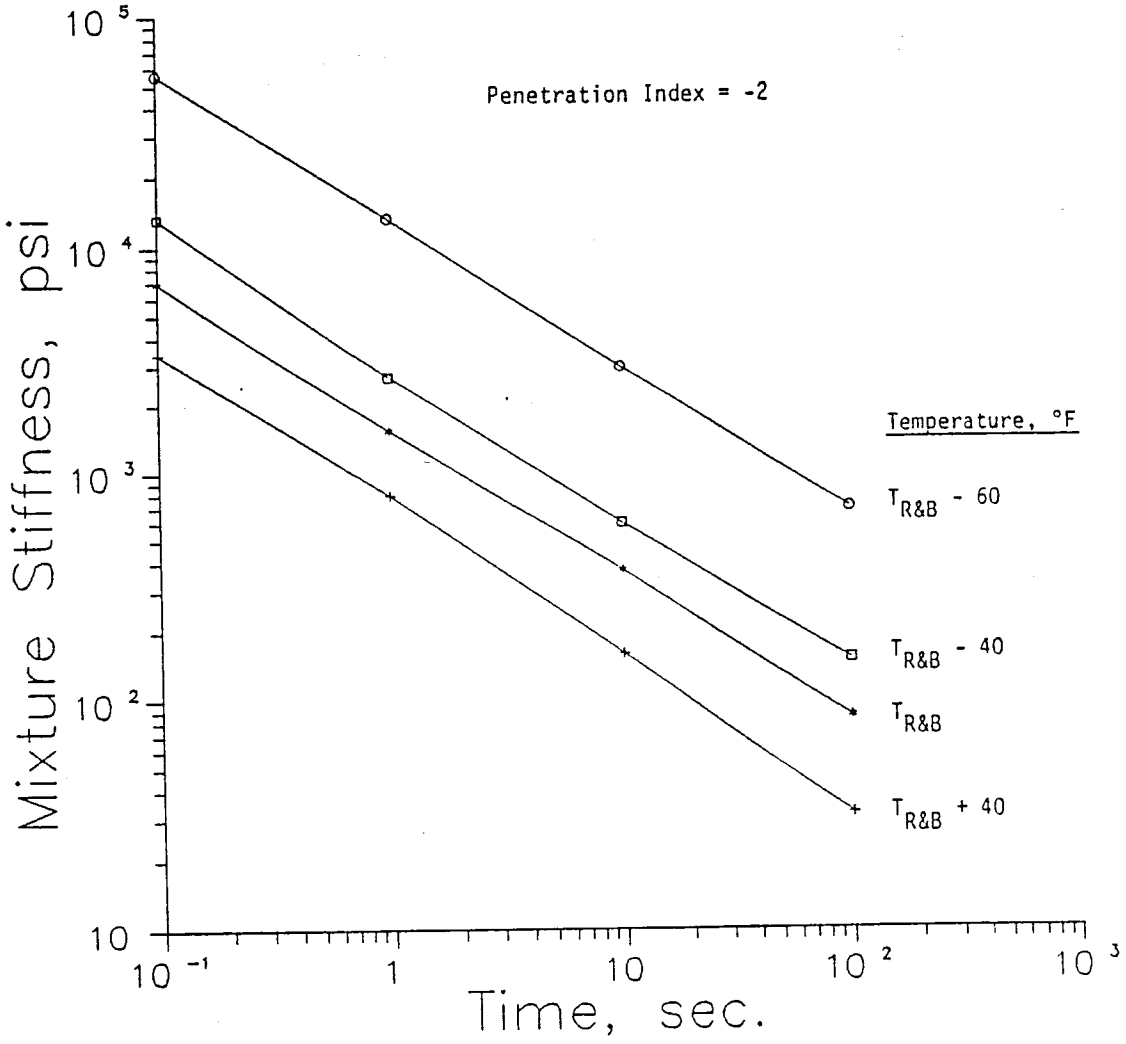

Figure 73. Viscoplastic component of mixture stiffness as a function of time expressed at different temperatures with respect to the ring and ball softening point for a hypothetical bitumen with a penetration index.of -2.0.

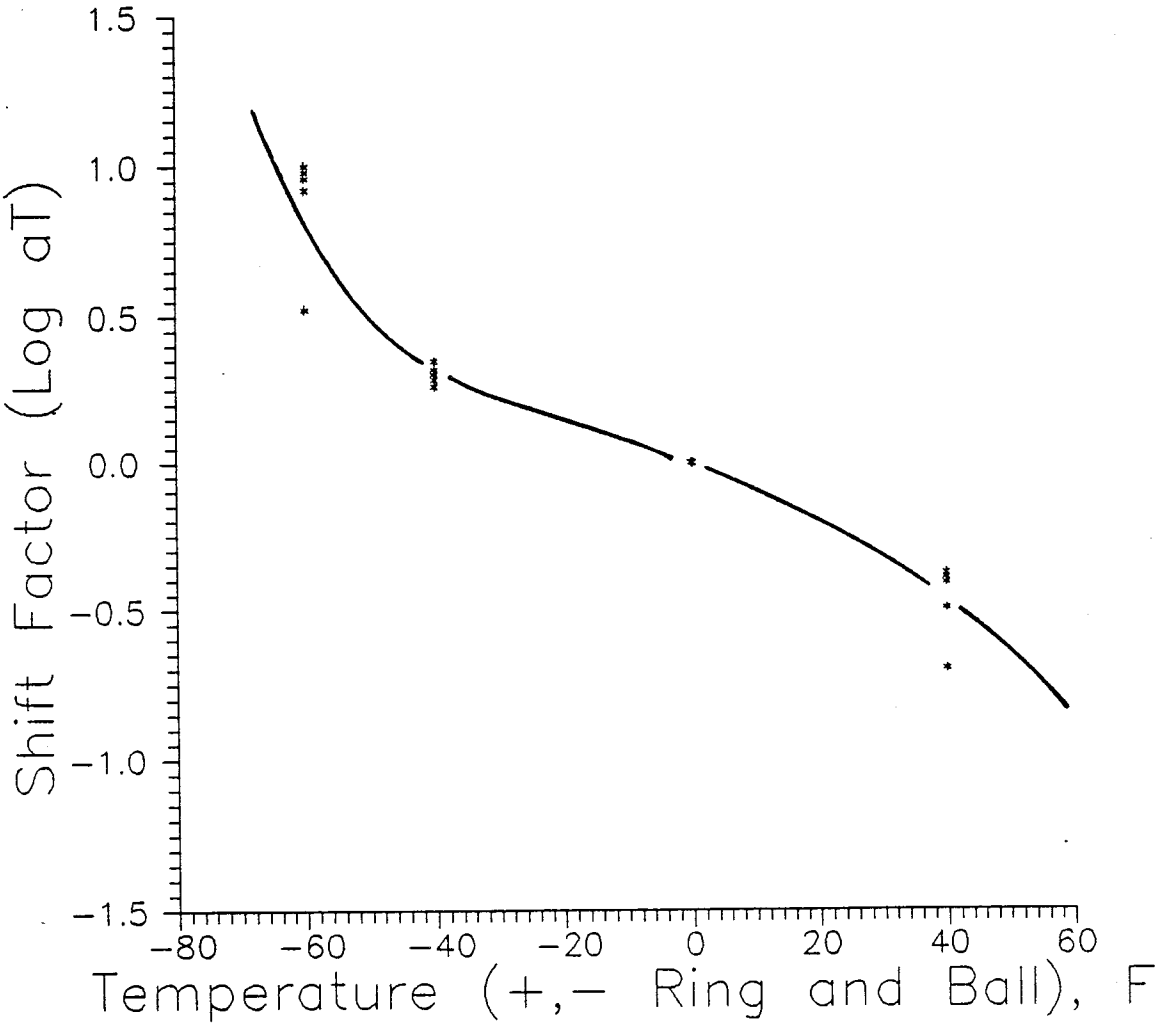

Figure 74. Shift factor for viscoplastic component of stiffness of mix expressed as a function of temperature above or below the ring and ball softening point.

CHAPTER VII

THERMAL CRACKING

Background

Low temperature cracking of flexible pavements is a very significant and often a costly mode of distress in many areas of Texas. This mode of pavement distress occurs as the result of thermal stresses developing in all pavement layers, including the subgrade. However, this phenomenon should be distinguished from block cracking which is caused by volume shrinkage of cement-stabilized layers or other sublayers which shrink. For the purposes of this study, the author has concentrated on thermal stresses induced in the asphaltic concrete layer which leads to transverse cracking.

Analytical Tools

Most methods for calculation of thermally-induced stresses are based on algorithms similar to those used in the computer program COLD (66). This program originally was developed by Christison (67) at the University of Alberta. Based on thermal properties of the pavement, solar radiation, and air temperature, the program COLD generates a series of temperature profiles through the use of a one dimensional finite element heat transfer routine. The temperature drop with time induces thermal stresses which could potentially exceed the tensile strength of HMAC and cause cracking.

Users of the COLD Program have the option of using either a pseudo-elastic beam or a pseudo-elastic slab analysis. The slab option was used in this study. Thermally induced stresses in the slab are calculated as:

$$\sigma_x(t) = \int_{t_0}^{t} S(\Delta t,T) \cdot \alpha \cdot dT(t) \qquad (18)$$

where:

	t	=	time;
	T	=	temperature;
	$\sigma_x(t)$	=	induced thermal stress;
	$S(\Delta t,T)$	=	mix stiffness, time and temperature dependent; and,
	α	=	coefficient of thermal expansion.

The stiffness parameter in the above equation plays an important role in the magnitude of calculated, induced thermal stresses. The current version of the COLD Program characterizes the HMAC stiffness in terms of resilient modulus input over a range of temperatures. The program then performs the integration in a stepwise fashion over small time intervals, each assigned a stiffness value from resilient modulus interpolations.

Researchers, however, have proposed that the mode of loading which induces thermal stresses, is of a slow or creep nature. Therefore, the application of diametral resilient modulus, which is evaluated at a dynamic rate of loading, may not be the best one to use in calculation of thermally induced stresses. Ruth et al. (68) suggested that one can arrive at this creep stiffness through the bitumen's properties which are later transformed into mixture stiffness by the Shell nomographic method (51,65). Khosla (69), however, showed that the stiffness measurements obtained from a compressive creep test and a diametral tensile creep test are consistent for the most part but diverge at longer loading times (greater than 1000 seconds).

For the purposes of this study, all analytical work for calculation of induced thermal stresses was done using resilient modulus values to characterize the HMAC stiffness. Some interim analyses were also conducted using creep stiffness, both tensile and compressive. The results are presented in the following sections.

Boundary Curves

Two sets of low temperature cracking boundary curves were developed for this study based on: a) average low temperature conditions in Texas, and b) extreme low temperature conditions in Texas. Each chart depicts the magnitude of critical, thermally-induced tensile stresses over the entire year as a function of average daily air temperature. These stresses are induced in the asphalt layer as the result of a temperature drop. Temperature drops used in this analysis are characteristic of the most severe thermal changes that occur within selected regions of Texas.

Analytical Method

The potential of HMAC to crack due to thermally-induced stresses is essentially a function of three mixture properties: a) mixture stiffness

at the low pavement temperature; b) the thermal coefficient of contraction; and, c) tensile strength at the low pavement temperatures. Of these material properties, the mix stiffness or resilient modulus and tensile strength are by far the most significant. Thus, the methodology to control thermal cracking is based on control of these two most important material properties: stiffness and tensile strength over the critical temperature range.

Based on the resilient modulus versus temperature relationship, the HMAC is classified as being within a certain response zone (Figure 75). These response zones were developed based on extensive Texas Transportation Institute research on typical resilient modulus versus temperature relationships for asphalt concrete used in Texas (70, 71).

Once the resilient modulus versus temperature region is specified, a chart of thermally-induced stresses as a function of pavement temperature is selected. These relationships were derived based on a conservative representation of the resilient modulus versus temperature relationship for the region in question. In addition to the modulus versus temperature relationship, the climatic region within which the HMAC will be used is required to select the proper criteria chart. These criteria charts are shown in Figures 76 and 77.

The tensile strength of the HMAC mixture is determined by indirect tensile testing. The tensile strength versus temperature failure envelope is then superimposed on the respective criteria chart. Thermal cracking is indicated by transgression of the failure envelope beyond the boundary criteria curve.

Figure 78 presents induced thermal stress versus temperature plots for stiffnesses determined by resilient modulus, creep stiffness-compressive, and creep stiffness-tensile. The great difference illustrates the need to select a more realistic measurement of stiffness which is representative of loading rates and loading configurations. This is one of the areas which will be addressed in Texas Transportation Institute's Project 1170 for the Texas State Department of Highways and Public Transportation.

Tensile Strength Characterization

In the evaluation of tensile strength of asphaltic mixtures, Anderson et al. (72, 73) used a nominal stroke rate of 0.06 inches per minute for

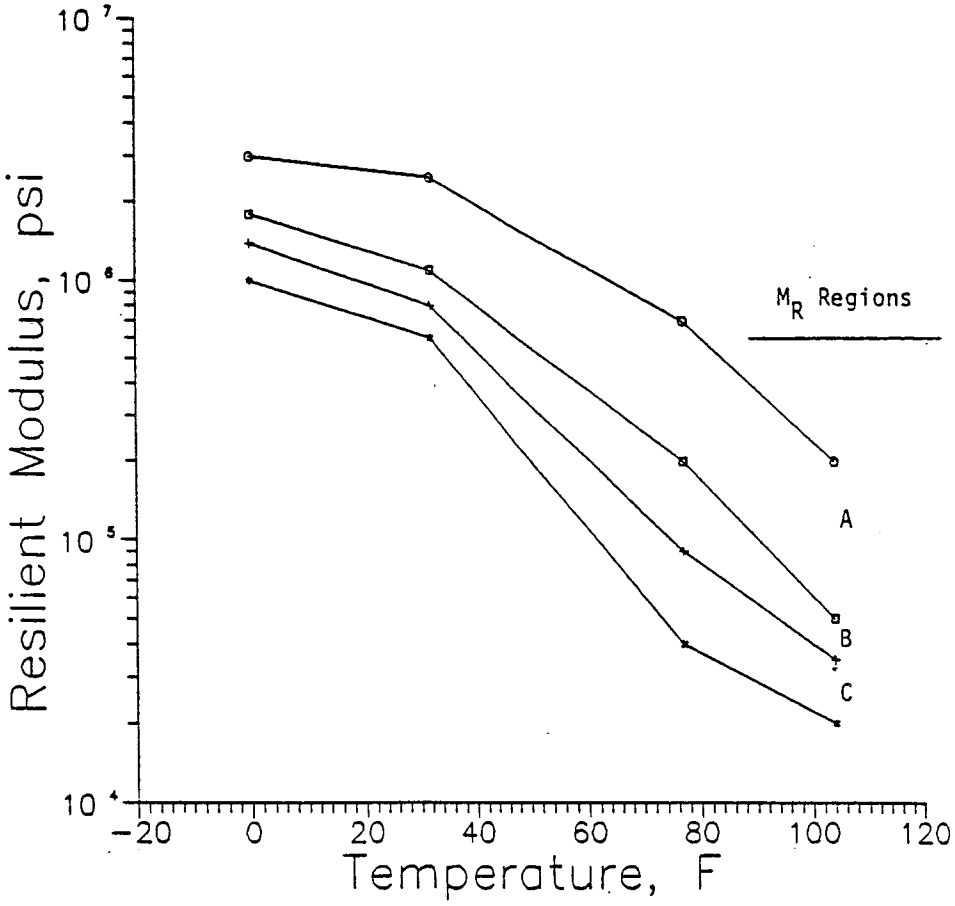

Figure 75. Resilient modulus versus temperature regions to be used in thermal fracture analysis.

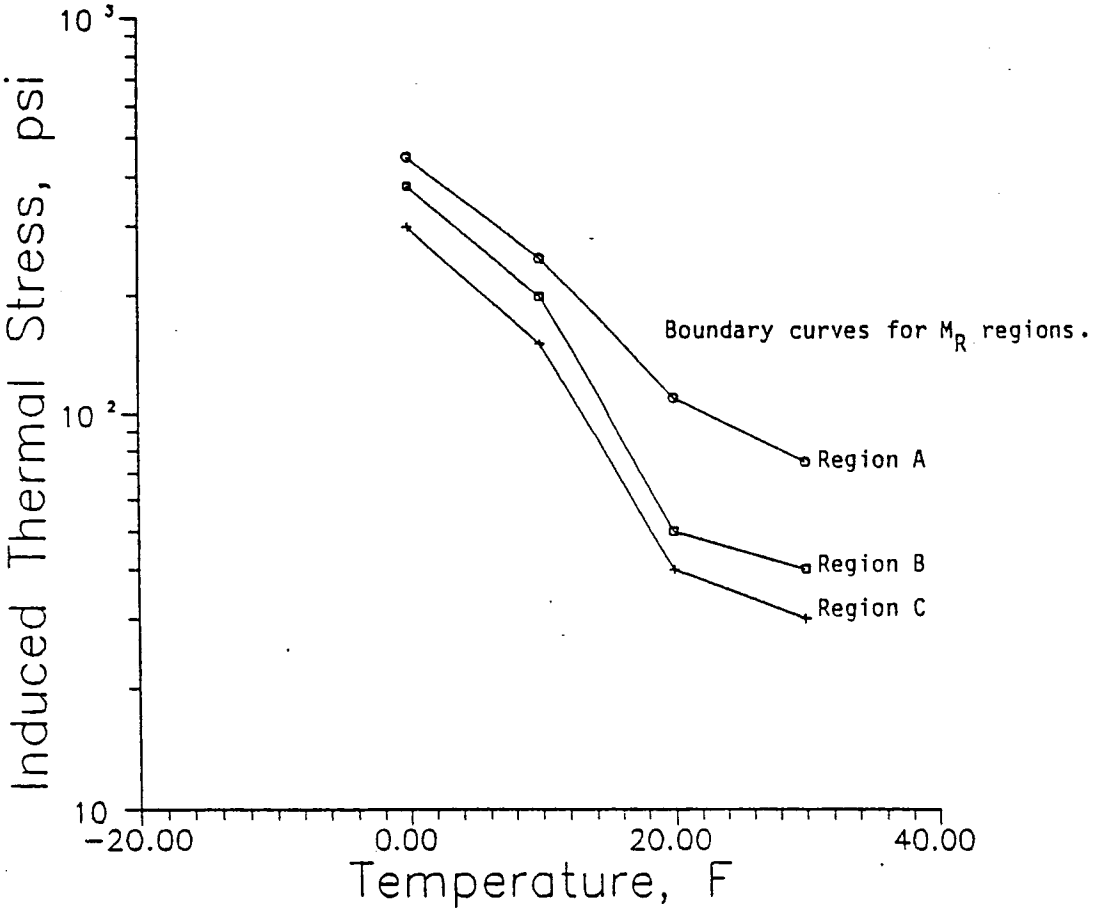

Figure 76. Induced thermal stress versus temperature relationship for climatic regions I and III as designated in Figure 20, page 37.

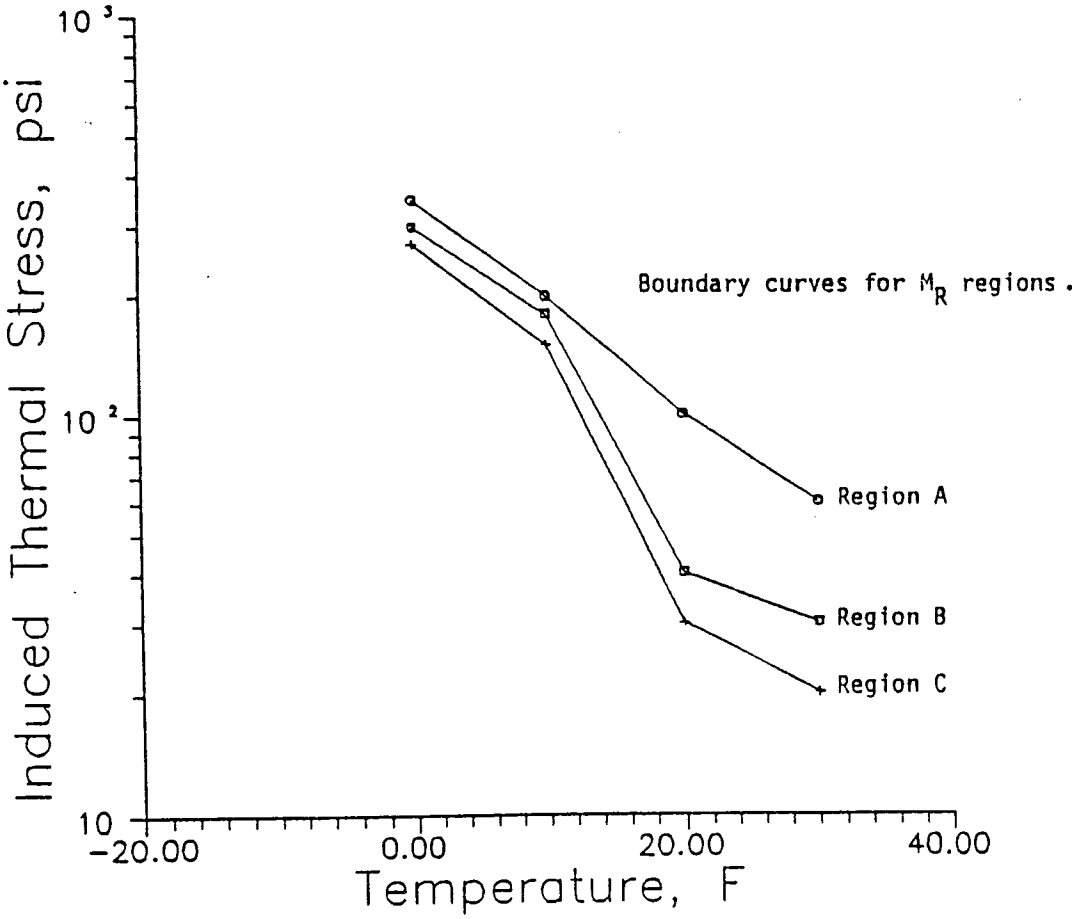

Figure 77. Induced thermal stress versus temperature relationship for climatic regions II and IV as designated in Figure 20, page 37.

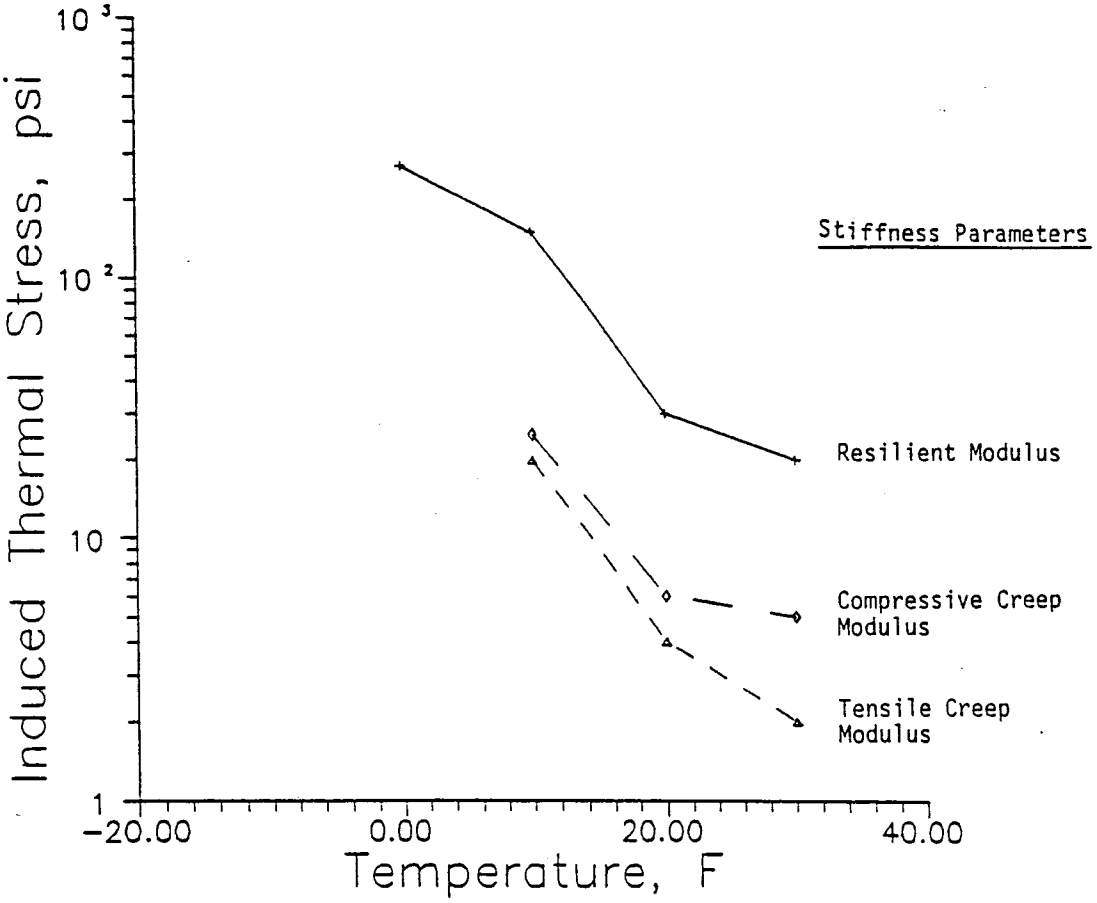

Figure 78. Induced thermal stress versus temperature relationship developed based on three types of mixture stiffness parameters.

their IDT tests. Anderson, in his evaluation of the IDT method (73), suggests that, generally, rate effects at low temperatures are minimal. Data presented by Tons and Krokosky (74) and Haas (75) are in agreement with Anderson's conclusions. This is because HMAC behaves predominantly elastically at low temperatures; hence it is less sensitive to variations in the loading rate.

The loading rate proposed in this study is 0.02 inches per minute at temperatures 0°F and 32°F. This seems to be representative of slow loading rates and low temperatures in the field. The results of IDT testing versus temperature are to be superimposed on the induced stress versus average air temperature evaluation charts. If the superimposed IDT strength envelope transgresses beyond the criteria boundary, then failure is predicted. This is developed in later sections dealing with a mix design example and verification of the methodology.

CHAPTER VIII

VERIFICATION PHASE

General

In order to verify and implement the findings of this study in actual field situations, a set of projects was selected for evaluation. These projects were selected by Texas Transportation Institute and Texas SDHPT officials to represent the diverse nature of climatic conditions, aggregate sources, asphalt grades, traffic, and construction practices within Texas. Post-construction performance of these new pavements and overlays was predicted according to the mix design and analysis criteria developed in this study. The actual performance of each pavement will eventually provide the basis by which the methodology and acceptance criteria developed in this study were evaluated.

This phase of the investigation requires long term pavement performance monitoring. This task could not be completed in this study. Hence, close coordination with TTI Project 1121, "Evaluation of Rutting in Flexible Pavements," sponsored by Texas SDHPT, will satisfy this need. During the summer of 1987, site selection, sample collection and other activities of Project 1121 were reviewed for use in this study. It is expected that these activities will be fully continued and enhanced over the duration of TTI Project 1170 which serves as an extension of this mix design study.

The following is a summary of specifics regarding the four selected field projects.

1. District 17: U.S. Highway 21, Burleson County:

   This project was selected primarily because of proximity to Texas A&M. It was also decided that siliceous Brazos River field sand, used in the aggregate blend, was worthy of inclusion in this study. Later, it was revealed that this project would be also included in the Strategic Highway Research Program (SHRP) which requires a thorough performance monitoring (76). The traffic level on Texas Highway 21 is on the moderate side with an appreciable amount of truck traffic. Among all modes of distress, rutting seems to be predominant in this district. Exxon AC-20 was used in the HMAC

for this project. Figure 79 shows the location of this project.

2. District 4: U.S. Highway 60, Carson/Gray Counties

This project was selected because of its location in the Texas panhandle area. Thermal cracking is a primary mode of distress in this region of Texas. Another interesting aspect of this project is the use of a crushed siliceous aggregate. The asphalt cement used was Shamrock AC-20. The traffic on U.S. Highway 60 is moderate. The mix was placed over an existing asphalt pavement. Figure 80 shows the project locations.

3. District 15: Loop 410 South, Main Lane, Bexar County

Initially, the mix design for this project employed a lightweight aggregate. However, the mixture demonstrated a severe tenderness to rolling in the field and compaction to the specified densities was impossible. As a result, the mix design underwent a significant change and large portions of the lightweight aggregates were replaced with crushed limestone. The asphalt cement was Exxon AC-20. Hot mix was placed over a composite structure of several overlays. Figure 81 shows the project location.

4. District 15: Loop 410 South, Frontage Road, Bexar County

The mix design for this project employed a crushed limestone aggregate and Exxon AC-40. This rather unconventional, "high stiffness" mix has been used in District 15 on a few projects and performance has been very satisfactory. The "high stiffness" mixture will be exposed to relatively high daytime temperatures accompanied by relatively high levels of low-speed traffic generated by Lackland Air Force Base which uses this frontage road as the main access thoroughfare. This HMAC layer was placed over a previously distressed flexible pavement. Figure 81 also shows the geographical location of this project.

The results of laboratory measurements and field performance predictions, in light of the previously discussed failure criteria, for the four selected projects, are summarized in Appendix E.

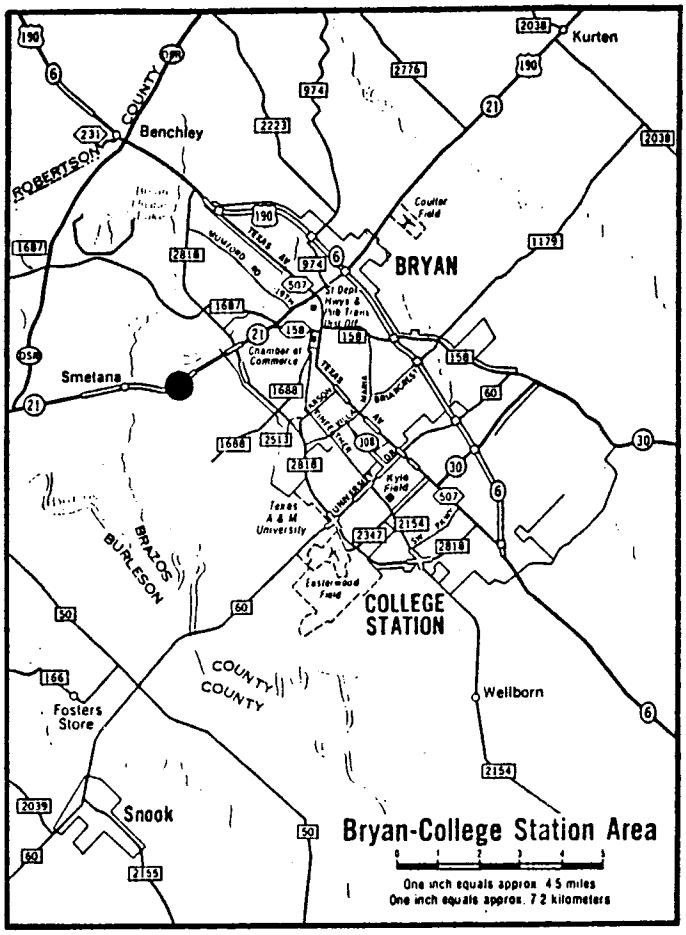

Figure 79. Location of District 17 verification project.

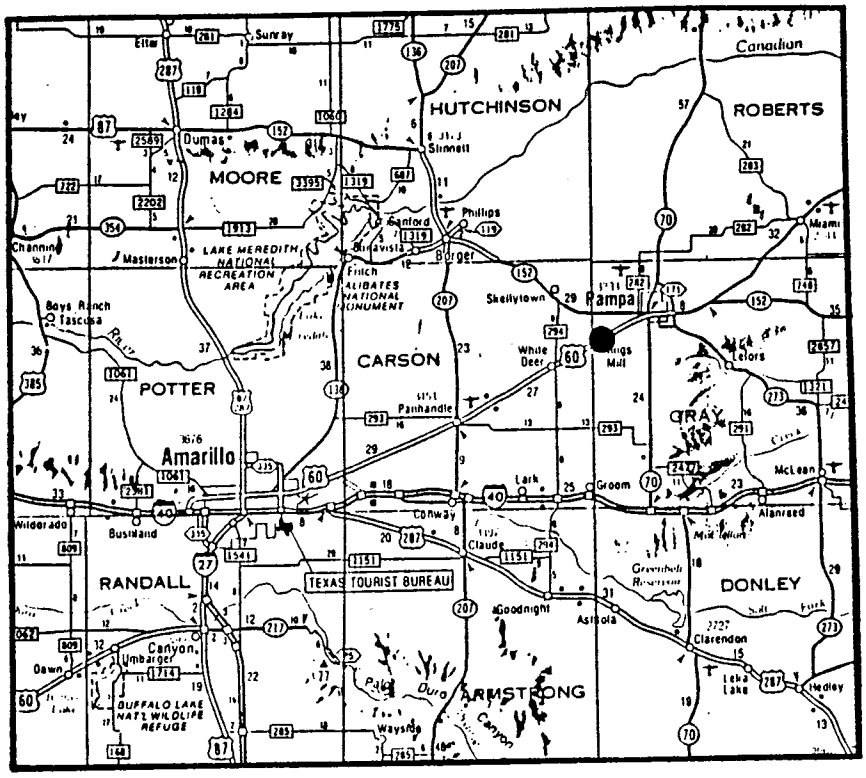

Figure 80. Location of District 4 verification project.

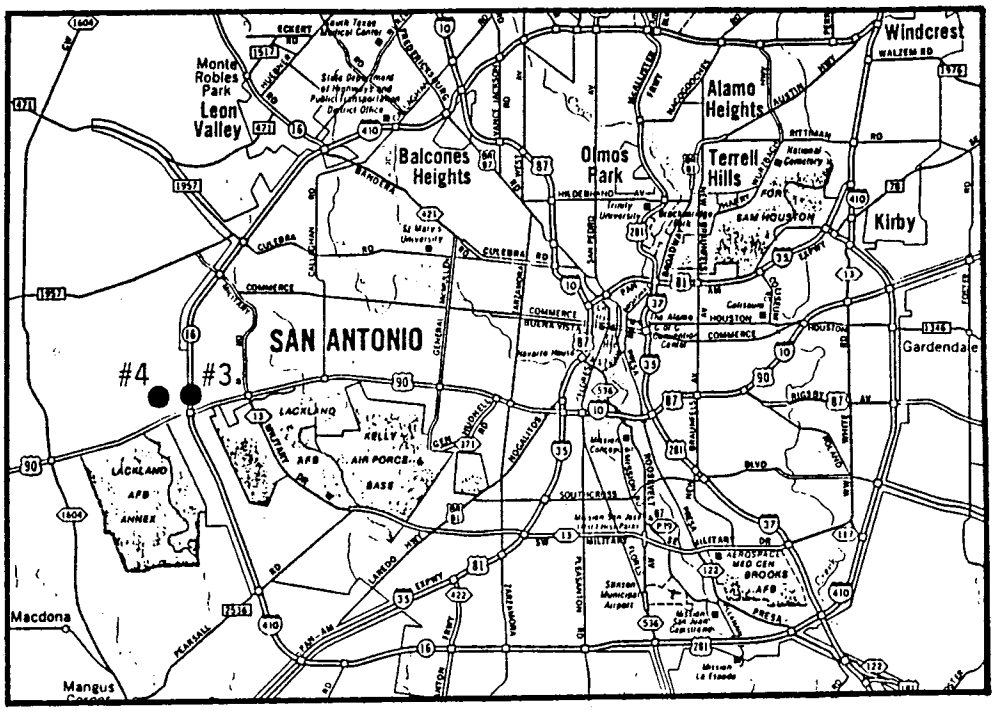

Figure 81. Location of District 15 verification project: #3 refers to the Loop 410 main lane project and #4 refers to the Loop 410 frontage road project.

CHAPTER IX

CONCLUSIONS AND RECOMMENDATIONS

It is possible to design and analyze HMAC using fundamental material properties rather than test properties. Different modes of distress in a variety of asphaltic pavement structures were investigated in order to make the proposed methodology a performance-based one. A series of failure criteria is developed based on fundamental engineering parameters which accounts for the following modes of distress:

a) Subgrade excessive deformation.
b) Load-induced fatigue cracking.
c) Permanent deformation.
d) Thermal cracking.

The criteria presented in this study are developed mechanistically while accounting for:

a) Pavement structural category.
b) Levels of subgrade strength.
c) Climatic regions in Texas.
d) Tire pressure.
e) Number of equivalent 18 kip passes.

The results of this study are presented in an "easy-to-use" and "user-oriented" chart and nomograph format.

One can offer the following set of recommendations for further investigation to improve the methodology developed in this study:

a) Evaluate which type of modulus of asphalt concrete (dynamic complex, resilient, etc.) (76) most accurately simulates field conditions for various types of loading and environmental conditions.
b) Develop an improved methodology by which climatic parameters,

traffic patterns, and mixture properties are integrated into one comprehensive rutting prediction model.

c) Evaluate the use of other mechanistic parameters such as: strain energy density, energy of distortion, and octahedral shear stress for use in predictive rutting algorithms. Hence, final rutting predictions can be checked and verified by several independent parameters.

d) Evaluate a methodology by which to more accurately evaluate mixture stiffness at low temperatures and slow loading rates, such as the indirect tensile creep test. This is crucial for a more accurate simulation of thermal cracking phenomenon.

e) Conduct all laboratory measurements on HMAC specimens at two levels of air voids: 1) air void which corresponds to the air void content immediately after construction (7-10%); and 2) air void which is achieved after sufficient traffic-induced densification (3-4%). This will provide a better material characterization both in terms of short-term behavior and long-term performance.

f) Design and construct a simple loading frame for the creep test. Such a device can be very similar to the soil consolidation frame.

g) Explore the feasibility of a quasi-dynamic permanent deformation test. Sides, Uzan,and Perl (54) utilized such a test over a wide range of dwell times (4-100 seconds) and load cycles (1-20 cycles). This methodology allows the characterization of both static and dynamic responses of HMAC with regard to permanent deformation.

h) Whenever possible, the creep/recovery test should be conducted at a temperature which is the same as the expected pavement temperature. In lieu of this, shift factors presented in Chapter VI are offered as an expedient tool.

REFERENCES

1. Test Methods No. 304, 305, 307, 308, 366, 367. In Materials Manual, Vol. 2. State of California, Department of Transportation, Sacramento, California, 1984.

2. Bituminous Pavement Standard Practice, TM5-822-8. Department of the Army, Washington, D.C., 1971.

3. Manual of Testing Procedures. 200-F Series. Texas State Department of Highways and Public Transportation, Austin, Texas 1985.

4. Mix Design Methods for Asphalt Concrete and Other Hot-Mix Methods for Asphalt Concrete And Other Hot-Mix Types, MS-2. The Asphalt Institute, College Park, Maryland, 1979.

5. P.S. Kandal and W.S. Koehler. Marshall Mix Design: Current Practices. AAPT, Vol. 54, 1985, pp. 285.

6. D.N. Little, J.W. Button, R.M. White, E.K. Ensley, Y. Kim, and S.J. Ahmed. Investigation of Asphalt Additives. Report No. DTFH-61-84-C-00066. Texas Transportation Institute, College Station, Texas, 1986.

7. F.L. Roberts, J.T. Tielking, D. Middleton, R.L. Lytton, and K.H. Tseng. Effects of Tire Pressure on Flexible Pavements. Report No. 372-1F. Texas Transportation Institute, College Station, Texas, 1986.

8. P.J. Van de Loo. Creep Testing: a Simple Tool to Judge Asphalt Mix Stability. AAPT, Vol. 43, 1974.

9. P.J. Van de Loo. The Creep Test, a Key Tool in Asphalt Mix Design and in the Prediction of Pavement Rutting. AAPT, Vol. 47, 1978.

10. M.G. Braver, R.T. Peterson, C. Larson, C., and O.E. Manz. An Evaluation of the Shell Creep Test Procedure to Predict Rutting in Asphalt Pavements. Final Report on Phase I, State Study (1)-80(8). North Dakota State Highway Department, Bismarck, North Dakota, June 1980.

11. M.G. Braver. An Evaluation of the Shell Creep Test Procedure to Predict Rutting in Asphalt Pavements. Final Report on Phase II, State Study (1)-80(8). North Dakota State Highway Department, Bismarck, North Dakota, January 1982.

12. J.S. Lai. Development of a Simplified Test Method to Predict Rutting Characteristics of Asphalt Mixes. Report No. GA DOT No. 8503. Georgia Institute of Technology, Atlanta, Georgia, July 1986.

13. K. Mahboub and D.N. Little. An Interim Report on the Methodology for Analysis and Design of Hot Mix Asphalt Concrete Mixtures. Study 2474. Texas Transportation Institute, College Station, Texas, July 1987.

14. J.W. Button. Investigation of Rutting in Asphalt Concrete Pavements. Study 2-8-87-1121. Texas Transportation Institute, College Station, Texas.

15. Symposium on Mix Design, Vol. 54. Association of Asphalt Paving Technologists, San Antonio, Texas, February 1985, pp. 238-431.

16. Symposium on Implementation of Aggregates in the Design, Construction, and Performance of Flexible Pavements. American Society for Testing and Materials, New Orleans, Louisiana, December 1986.

17. H.L. Von Quintas, J.A. Sherocman, C.S. Hughes, and T.W. Kennedy. Development of Asphalt-Aggregate Mixture Analysis System, Phase II, Interim Report, Submitted to National Cooperative Highway Research Program, Washington, D.C., December 1987.

18. Standard Specifications for Construction of Highways, Streets, and Bridges. Texas State Department of Highways and Public Transportation, Austin, Texas, 1982.

19. B.A. Vallerga and W.R. Lovering. Evaluation of the Hveem Stabilometer Method of Designing Asphalt Paving Mixtures. AAPT, Vol. 54, 1985, pp. 243-265.

20. K.M. Marshek, H.H. Chen, R.B. Connell, and C.L. Saraf. The Effect of Truck Tire Inflation Pressure and Axle Load on Flexible and Rigid Pavement Performance. Presented at 65th Meeting of Transportation Research Board, Washington, D.C., 1986.

21. S.H. Carpenter and T.J. Freeman. Characterizing Permanent Deformation in Asphalt Concrete Placed over Portland Cement Concrete Pavements. In Transportation Research Record 1070, TRB, National Research Council, Washington, D.C., 1986.

22. H.H. Chen, K.M. Marshek, and C.L. Saraf. The Effects of Truck Tire Contact Pressure Distribution on the Design of Flexible Pavements - A 3D Finite Element Approach. Presented at 65th Meeting of Transportation Research Board, Washington, D.C., 1986.

23. Weather Bureau Climatologist. Environmental Science Services Administration, Austin, Texas, 1963.

24. J. Li. Use of Climatic Data for the Prediction of Permanent Deformation in Flexible Pavements. Master of Engineering Report. Texas A&M University, College Station, Texas, August 1987.

25. A.I.M. Claessen, J.M. Edwards, P. Sommer, and P. Uge. Asphalt Pavement Design: the Shell Method. Proc., Fourth International Conference on Structural Design of Asphalt Pavements, The University of Michigan, Ann Arbor, Michigan, 1977.

26. J. Morris, R.C.G. Haas, P. Reilly, and E.T. Higrell. Permanent Deformation in Asphalt Pavements Can Be Predicted. AAPT, Vol. 43, 1974, pp. 41-76.

27. M. Tahmoressi. Detailed Analysis of the Effects of Mixing Temperature and Stockpile Moisture on Engineering Properties of Asphalt Mixtures. Master of Science Thesis. The University of Texas at Austin, Austin, Texas, 1985.

28. T.W. Kennedy and G.A. Huber. The Effects of Mixing Temperature and Stockpile Moisture on Asphalt Mixtures. Research Report 358-1. Center for Transportation Research, The University of Texas at Austin, Austin, Texas, August 1984.

29. C.L. Monismith and F.N. Finn. Flexible Pavement Design: State-of-the-Art. In ASCE Journal of Transportation Engineering, 1977, pp. 30.

30. An Introduction to Pavement Analysis Using Elastic Layered Theory and CHEVPC. The Washington State Transportation Center, Seattle, Washington, 1985.

31. J.S. Corlew and P.F. Dickson. Methods for Calculating Temperature Profiles of Hot-Mix Asphalt Concrete as Related to the Construction of Asphalt Concrete Pavements. AAPT, Vol. 37, 1968, pp. 101.

32. B.J. Dempsey. A Heat Transfer Model for Evaluating Frost Action and Temperature Related Effects in Multilayered Pavement Systems. Ph.D. Dissertation, University of Illinois, Urbana, Illinois, 1969.

33. E.J. Yoder and M.W. Witczak. Principles of Pavement Design, 2nd Edition. John Wiley and Sons, New York, New York, 1975.

34. W.O. Yandell and R.L. Lytton. Residual Stresses Due to Travelling Loads and Reflection Cracking. Report FHWATX79-207-6. Texas Transportation Institute and the Texas State Department of Highways and Public Transportation, College Station, Texas, June 1979.

35. F.N. Finn, C. Saraf, R. Kulkarni, K. Nair, W. Smith, and A. Abdullah. The Use of Distress Prediction Subsystems for the Design of Pavement Structures. Proc., Fourth International Conference on the Structural Design of Asphalt Pavements, Vol. I. The University of Michigan, Ann Arbor, Michigan, 1977, pp. 3-38.

36. The AASHTO Road Test. Special Report 73. Highway Research Board, National Research Council, Washington, D.C., 1962.

37. C.L. Monismith, J.A. Epps, and F.N. Finn. Improved Asphalt Mix Design. AAPT, Vol. 54, 1985, pp. 347-406.

38. J.F. Hills. The Creep of Asphalt Mixes. In Journal of the Institute of Petroleum, Vol. 59, No. 570, November 1973.

39. R.L. Davis. Relationship Between Rheological Properties of Asphalt and the Rheological Properties of Mixtures and Pavements. In ASTM, STP 941, 1987, pp. 28-50.

40. W.O. Yandell. New Method of Simulating Layered Systems of Unbound Granular Material. In Transportation Research Record 1022, TRB, National Research Council, Washington, D.C., 1985.

41. W.O. Yandell. The Prediction of the Behavior of Elastoplastic Roads During Repeated Rolling Using the Mechano-Lattice Analog. In Highway Research Record 374, HRB, National Research Council, Washington, D.C., 1971, pp. 29-41.

42. W.O. Yandell. Measurement and Prediction of Forward Movement and Rutting in Pavements under Repetitive Wheel Loads. In Transportation Research Record 888, TRB, National Research Council, Washington, D.C., 1982, pp. 77-84.

43. W.O. Yandell. Possible Effects of Relative Plastic Behavior on Pavement Life. In Transportation Research Record 930, TRB, National Research Council, Washington, D.C., 1983, pp. 86-90.

44. W.O. Yandell. The Use of the Mechano-Lattice Analysis to Investigate Relative Plastic Behavior. Proc., International Conference on Constitutive Laws for Engineering Materials, Tucson, Arizona, January 1983.

45. W.O. Yandell. Residual Stresses and Strains and Fatigue Cracking. In Journal of Transportation Engineering, ASCE, Vol. 108, No. TE1, January 1982, pp. 103-110.

46. M.G. Sharma, W.J. Kenis, T.D. Lawson, and W.L. Camling. Evaluation of Flexible Pavement Methodology Based Upon Field Observations at Pennsylvania State University test Track. Proc., Fourth International Conference on Structural Design of Asphalt Pavements, Vol. II, Ann Arbor, Michigan, 1977, pp. 158-174.

47. W.J. Kenis. Predictive Design Procedures, VESYS User's Manual. FHWA Report 77-154, Federal Highway Administration, Washington, D.C., 1978.

48. Shell Pavement Design Manual. Shell Petroleum Company, London, 1978.

49. H.A. Bolk. The Creep Test. Center for Road Construction, Arnhem, The Netherlands, February 1981.

50. E.O. Hilster, and P.J. Van de Loo. The Creep Test: Influence of Test Parameters. Shell Laboratories, Amsterdam, The Netherlands, 1977.

51. Van der Poel. A General System Describing the Viscoelastic Properties of Bitumens and Its Relation to Routine Test Data. In Journal of Applied Chemistry, Vol. 4, May 1954.

52. D.F. Kinder. A Study of Both the Viscoelastic and Permanent Deformation Properties of a New South Wales Asphalt. 13th Australian Road Research Board, New South Wales, Australia, 1986.

53. S.A. Khedr. Deformation Mechanism in Asphaltic Concrete. In Journal of Transportation, ASCE, Vol, 112, No. 1, 1986, pp. 29-45.

54. M. Perl, J. Uzan, and A. Sides. Visco-Elastic-Plastic Constitutive Law for Bituminous Mixtures Under Repeated Loading. In Transportation Research Record 911, TRB, National Research Council, Washington, D.C., 1984.

55. K.H. Tseng and R.L. Lytton. Prediction of Permanent Deformation in Flexible Pavement Materials. Presented at ASTM Symposium on Implication of Aggregates in the Design, Construction, and Performance of Flexible Pavements, New Orleans, Louisiana, December 1986.

56. W.N. Findley, J.S. Lai, and K. Onaran. Creep and Relaxation of Nonlinear Viscoelastic Materials. North-Holland Publishing Co., New York, 1976.

57. J.S. Lai, and D. Anderson. Irrecoverable and Recoverable Nonlinear Viscoelastic Properties of Asphalt Concrete. In Transportation Research Record 468, TRB, National Research Council, Washington, D.C., 1973.

58. R.L. Lytton. Personal Communication. Department of Civil Engineering, Texas A&M University, College Station, 1987.

59. Highway Pavement Distress Identification Manual for Highway Conditions and Quality of Highway Construction Survey. DOT-HFH-11-9175/NCHRP 1-19, Department of Transportation, Washington, D.C., March 1979.

60. B.M. Gallaway, and J.G. Rose. Macro-Texture, Friction, Cross Slope and Wheel Track Depression Measurements on 41 Typical Highway Pavements. Research Report 138-2. Texas Transportation Institute, College Station, Texas, June 1970.

61. D.F. Hays and A.L. Brown. The Physicals of Tire Traction, Theory and Experiment. General Motors Research Laboratories, Plenum Press, New York, 1974.

62. J.F. Hills. The Correlation of Rutting and Creep Tests on Asphalt Mixes. Paper IP74-001. In Journal of Institute of Petroleum, January 1974.

63. Asphalt Rheology: Relationship to Mixture. In ASTM, STP 941, Symposium on Roads and Paving Materials, 1987.

64. N.W. McLeod. Asphalt Cements: Pen-Vis Number and Its Application to Moduli of Stiffness. In Journal of Testing and Evaluation, Vol. 4, No. 4, July 1976, pp. 275-282.

65. N.W. McLeod. Using Paving Asphalt Rheology to Impair or Improve Asphalt Pavement Design and Performance. ASTM, STP 941, 1987, pp. 51-57.

66. F.N. Finn, C.L. Saraf, R. Kulkarni, K. Nair, W. Smith, and A. Abdullah. Development of Pavement Structural Subsystems. NCHRP 1-108. Final Report, Vol. 2, National Research Council, Washington, D.C., February 1977.

67. J.J. Christison and K.O. Anderson. The Response of Asphalt Pavements to Low Temperature Climatic Environments. Proc., Third International Conference on Structural Design of Asphalt Pavements, London, 1972, pp. 41-52.

68. B.E. Ruth, L.A. Bloy, and A.A. Avital. Prediction of Pavement Cracking at Low Temperatures. AAPT, Vol. 51, 1982, pp. 53-103.

69. N.P. Khosla. Effect of the Test Method for Characterization of Asphalt Mixtures on the Prediction of Pavement Performance. Proc., Canadian Technical Asphalt Association, Vol. 30, 1985.

70. D.N. Little. Structural Evaluation of Recycled Pavement Material. Ph.D. Dissertation, Texas A&M University, College Station, Texas, August 1979.

71. J.A. Epps, D.N. Little, R.J. Holmgreen, and R.L. Terrel. Guidelines for Recycling Pavement Materials. In Transportation Research Record 224, TRB, National Research Council, Washington, D.C., September 1980.

72. K.O. Anderson and W.P. Hahn. Design and Evaluation of Asphalt Concrete with Respect to Thermal Cracking. AAPT, Vol. 37, 1968, pp. 1-31.

73. R. Haas and K.O. Anderson. A Design Subsystem for the Response of Flexible Pavements at Low Temperatures. AAPT, Vol. 38, 1969, pp. 179-223.

74. E. Tons and E.M. Krokosky. Tensile Properties of Dense Graded Bituminous Concrete. AAPT, Vol. 32, 1963.

75. R. Haas and T.H. Topper. Thermal Fracture Phenomena in Bituminous Surfaces. In Highway Research Special Report 101, TRB, National Research Council, Washington, D.C., 1968.

76. Annual Report. Strategic Highway Research Program (SHRP), National Research Council, Washington, D.C., October 1987.

77. M.S. Mamlouk and R.T. Sarofim. The Modulus of Asphalt Mixtures - An Unresolved Dilemma. Submitted at the 67th Annual Meeting of the Transportation Research Board, Washington, D.C., October 1987.

78. J.B. Rauhut, J.C. O'Quin, and W.R. Hudson. Sensitivity Analysis of FHWA Structural Model VESYS II, Vol. 1, Prepatory and Related Studies. Report No. FHWA-RD-76-23, Federal Highway Administration, Washington, D.C., March 1976.

APPENDIX A

THE STATIC CREEP TEST

APPENDIX A

THE STATIC CREEP TEST

General

This test has been designed for the following purposes: a) measure the compressive stiffness/compliance properties of the mixture; and, b) establish plastic flow potential under various stress states in terms of viscoplastic strains.

Cylindrical samples are tested in compression and vertical displacements measured by means of LVDT's (Figure A1). This will allow a comprehensive characterization of visco-elastoplastic response of asphaltic mixtures.

Shell researchers (8-9) realized the "direct link" between the creep behavior of asphalt concrete and its rutting potential. Consequently, they have developed a system of pavement design procedures in which creep characterization is emphasized.

Although the Shell method was developed based on an extensive volume of laboratory and field data, it suffers from the basic fact that it is an empirical method. Therefore, the results cannot be extrapolated beyond the conditions for which Van der Poel's nomograph (51) was developed.

In this study, the creep test is an integral part of mixture design/-analysis procedure. A more direct link between the laboratory measured creep properties and rutting potential has been established. The procedure accounts for the direct measurement of viscous and plastic properties of HMAC. As a result, the rutting predictions for the actual pavement structure in the field can be made with a somewhat smaller margin of error.

Creep Specimen Manufacturing

At the outset of this research project, HMAC specimens were compacted in a cylindrical shape of 4 inches in diameter and 8 inches high. The compactive effort was delivered by a kneading compactor. Due to reasons explained in Chapter IV and Chapter VI, the Texas gyratory compaction device was proposed for sample fabrication. The creep specimens shall be compacted with the "large size" Texas gyratory machine which produces

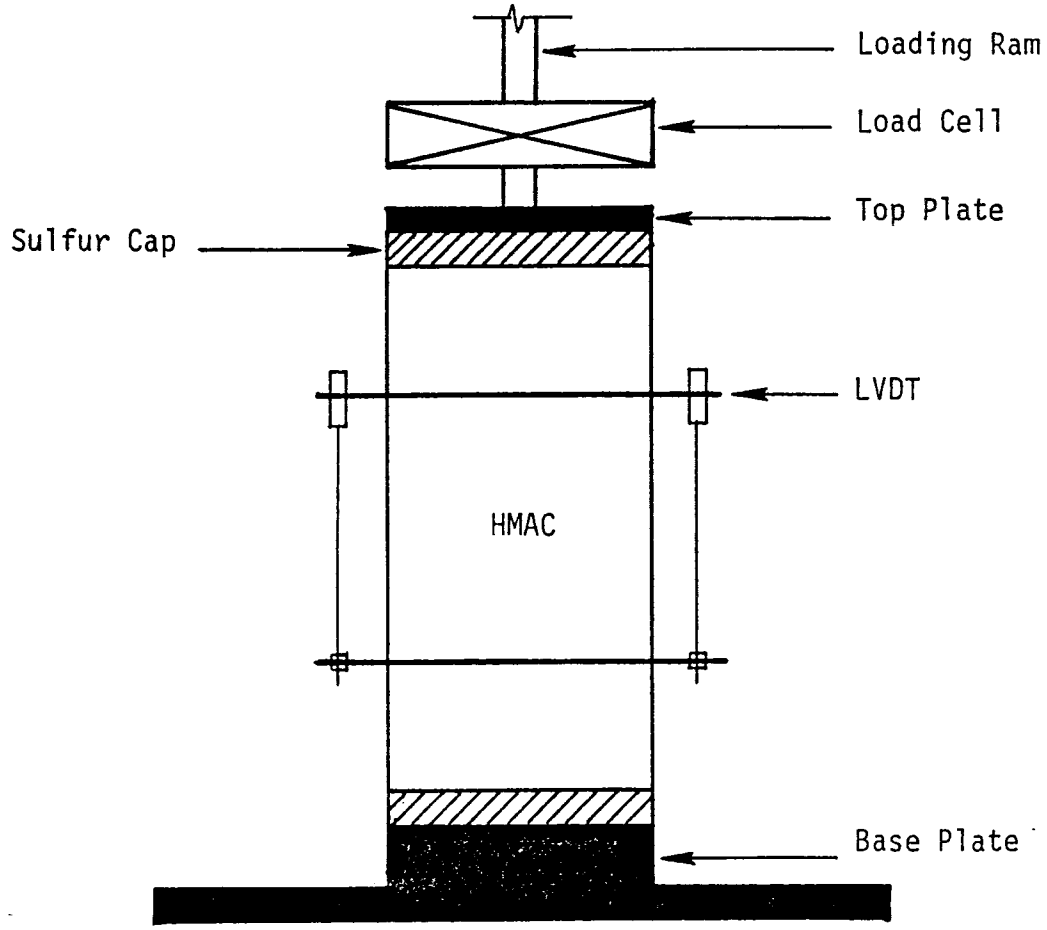

Figure A1: The creep test setup.

specimens that are 6 inches in diameter and normally 8 inches in height.

Specimen Conditioning

Traditionally, a pre-test loading, referred to as specimen conditioning, has been used in most creep tests. This is especially true in the case of the VESYS creep test (47) which calls for three 10 minute periods of constant load, at the same magnitude as the actual creep test, each followed by three 10 minute periods of recovery. VESYS investigators such as Rauhut, O'Quin, and Hudson (78) indicated that conditioning is an attempt to simulate the short-term, post-construction, traffic-induced loads. In this study, all 4-inch by 8-inch cylindrical specimens which were compacted by the kneading device were subjected to the above preconditioning procedure.

During the field verification phase of this research, it was decided that the Texas gyratory method of compaction can be effectively used in manufacturing 6-inch by 8-inch cylindrical specimens that closely match roller-compacted hot mix in the field. It was further decided that no preconditioning shall be applied to these specimens. The recommendation has been made, suggesting the fabrication of creep specimens at two different levels of air voids; one representing immediate post-construction conditions, and the other simulating traffic-densified HMAC.

Test Procedure

Once the cylindrical specimens of HMAC are fabricated, capped with sulfur, and cured for at least 48 hours, the creep test is conducted according to the following procedure.

The procedure calls for a loading frame capable of delivering and maintaining a stress step function (15-20 psi) for the period of one hour. During this period, the vertical displacements are measured at the following intervals: 1, 2, 4, 8, 15, 30 seconds, and 1, 2, 4, 8, 15, 30, 45, and 60 minutes. This data is collected by means of LVDT's and a Y-time chart recorder. Upon removal of the load, the recovery is also measured using the same time intervals.

For testing purposes, researchers at TTI have used a closed loop hydraulic system (MTS) which is similar to the unit recently acquired by

Texas SDHPT. With simple modifications, one can successfully adapt a soils consolidation machine for the purposes of the creep test.

The creep load, 14.5 psi at 70°F as suggested by Shell researchers, for a nondestructive creep-recovery test, shall be maintained for one hour, after which the load is removed instantaneously. During the loading and unloading processes, vertical displacements are monitored by two LVDT's on each side of the specimen. Figure A2 shows, schematically, the creep/recovery data.

Different components of vertical displacements or vertical strains are separated according to the following regression procedures:

$$\epsilon_{creep} = a_1 t^{b1} \quad \text{(A1)}$$

and,

$$\epsilon_{recovery} = a_2 t^{b2} \quad \text{(A1)}$$

where ϵ_{creep} = vertical strain recorded during the creep phase;

$\epsilon_{recovery}$ = vertical strain recorded during the recovery phase; and,

a_1, a_2, b_1, b_2 = regression constants.

Mixing

Aggregates and asphalt are mixed according to Texas SDHPT Test Method TEX-204-F. After proper mixing, the temperature of the HMAC material is raised up to 250-270°F for compaction.

Compaction

Upon interviews with Texas SDHPT officials, it was decided that the laboratory compaction should be performed using available agency equipment. It was further decided that the large size gyratory-shear compactor can be effectively used with 6 in. diameter and 8 in. high cylinders. This method of compaction appears to have three advantages: a) it best simulates field compaction; b) unlike the kneading method, cylinders of mixtures containing relatively large top-size (0.5-1.0 in.) aggregates can be manufactured; and, c) it is available in Texas SDHPT districts.

Once the HMAC material has reached the compaction temperature, the

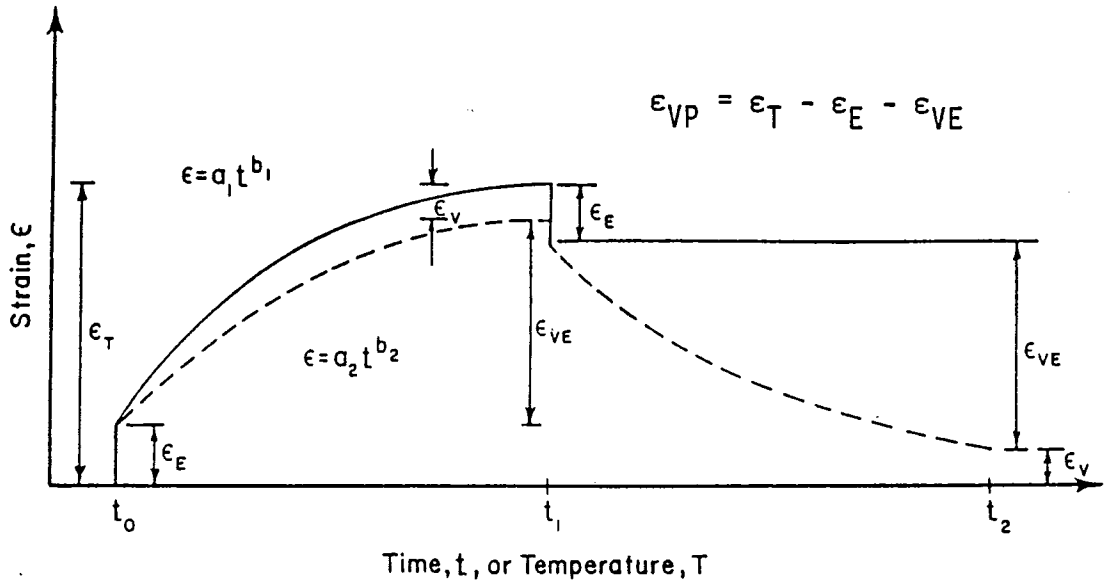

Figure A2. Displacements recorded in a creep/recovery test.

cylinder is molded in one layer. Compaction of molded cylinder is then conducted according to Test Method TEX-126-E with some minor adjustments. The following modified compaction procedure is needed to ensure the target air void value of 3-5%.

a) 1 minute gyration at 35 psi with the tilt on.
b) 1 minute gyration at 70 psi with the tilt on.
c) 3 revolutions at 35 psi without tilt.

It is worthy of note that for rough-textured blends of aggregates with relatively large top-size particles, the above compaction procedure may need further modification so that the target air void is satisfied. This may be achieved through a combination of adjustments including but not limited to the time of gyration and/or compactive pressure.

Data Analysis

Time dependent viscoplastic strain which is the source of rutting can be separated from other components of total strain as:

$$\epsilon_{vp} = \epsilon_{creep} - \epsilon_{recovery} = a_1 t^{b1} - a_2 t^{b2} \qquad (A3)$$

The viscoplastic component of stiffness is defined as $\sigma_{lab}/\epsilon_{vp}$ which is a time dependent function. It is this particular component of stiffness which is plotted on the rutting charts as a material property and will ultimately determine the rutting potential of the mixture under investigation.

It is most desirable to have the creep tests conducted at the critical temperature of the climatic region under study. For the purpose of this report, the average high monthly temperature is considered to be the critical temperature.

It is possible, however, to transform the stiffness data and its plastic component, measured at a given temperature, into a different temperature domain. This is accomplished by shift factors and the assumption is that the HMAC is thermo-rheologically simple. Figure 74 demonstrates the shift factors for one such transformation of data. In summary, time-temperature transformation of creep data according to the

following step-by-step procedure provides a more accurate measure of rutting potential.

a) Obtain the viscoplastic deformation trend of the mixture in question from the creep/recovery test.

b) Normalize this laboratory-measured deformation trend for laboratory stress conditions and obtain the viscoplastic component of stiffness versus creep time plot.

c) Select the critical rutting temperature according to:
   1) pavement structural category, and
   2) climatic region within which the pavement is placed.

d) Transform the laboratory-measured viscoplastic stiffness trend data for the expected field temperature using the shift factor.

e) Conduct the rutting analysis with the transformed viscoplastic stiffness data according to the mix design example (Appendix D).

APPENDIX B

RUTTING CRITERIA CHARTS

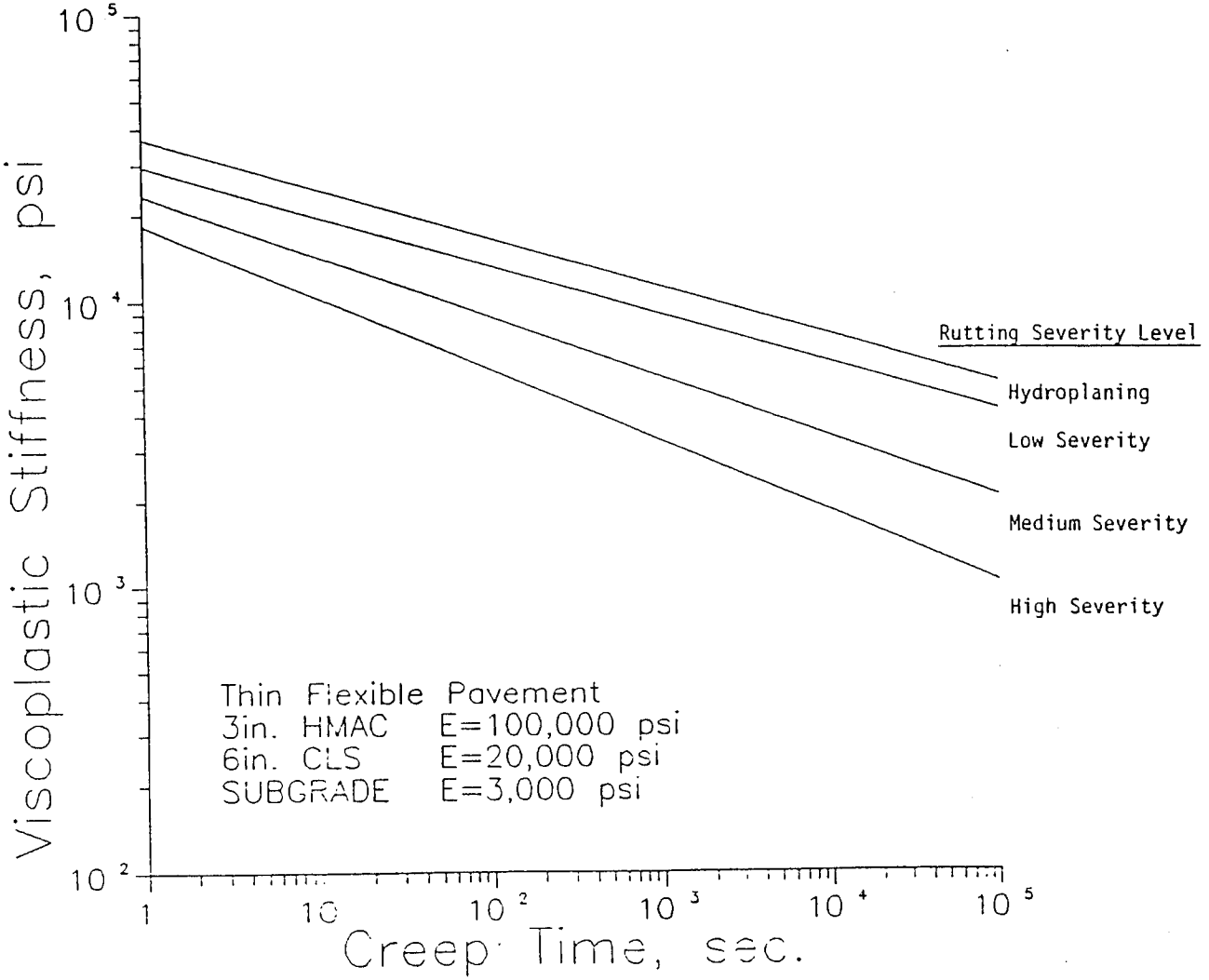
Viscoplastic Stiffness, psi
10 5
10 4
10 3
10 2
1
10
10 2
10 3
10 4
10 5
Creep Time, sec.
Rutting Severity Level
Hydroplaning
Low Severity
Medium Severity
High Severity
Thin Flexible Pavement
3in. HMAC E=100,000 psi
6in. CLS E=20,000 psi
SUBGRADE E=3,000 psi

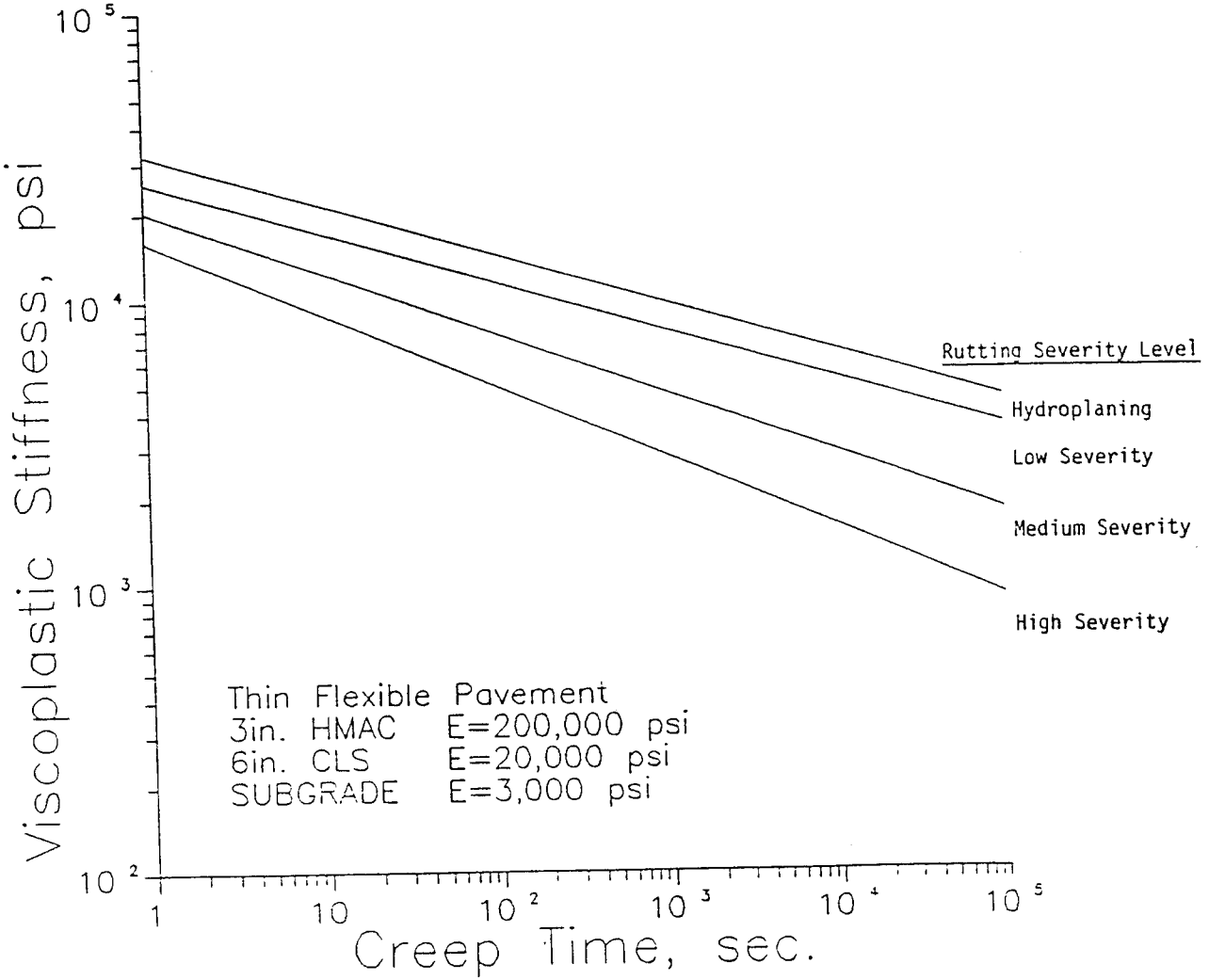
Viscoplastic Stiffness, psi
10^5
10^4
10^3
10^2
1
10
10^2
10^3
10^4
10^5
Creep Time, sec.
Rutting Severity Level
Hydroplaning
Low Severity
Medium Severity
High Severity
Thin Flexible Pavement
3in. HMAC E=200,000 psi
6in. CLS E=20,000 psi
SUBGRADE E=3,000 psi

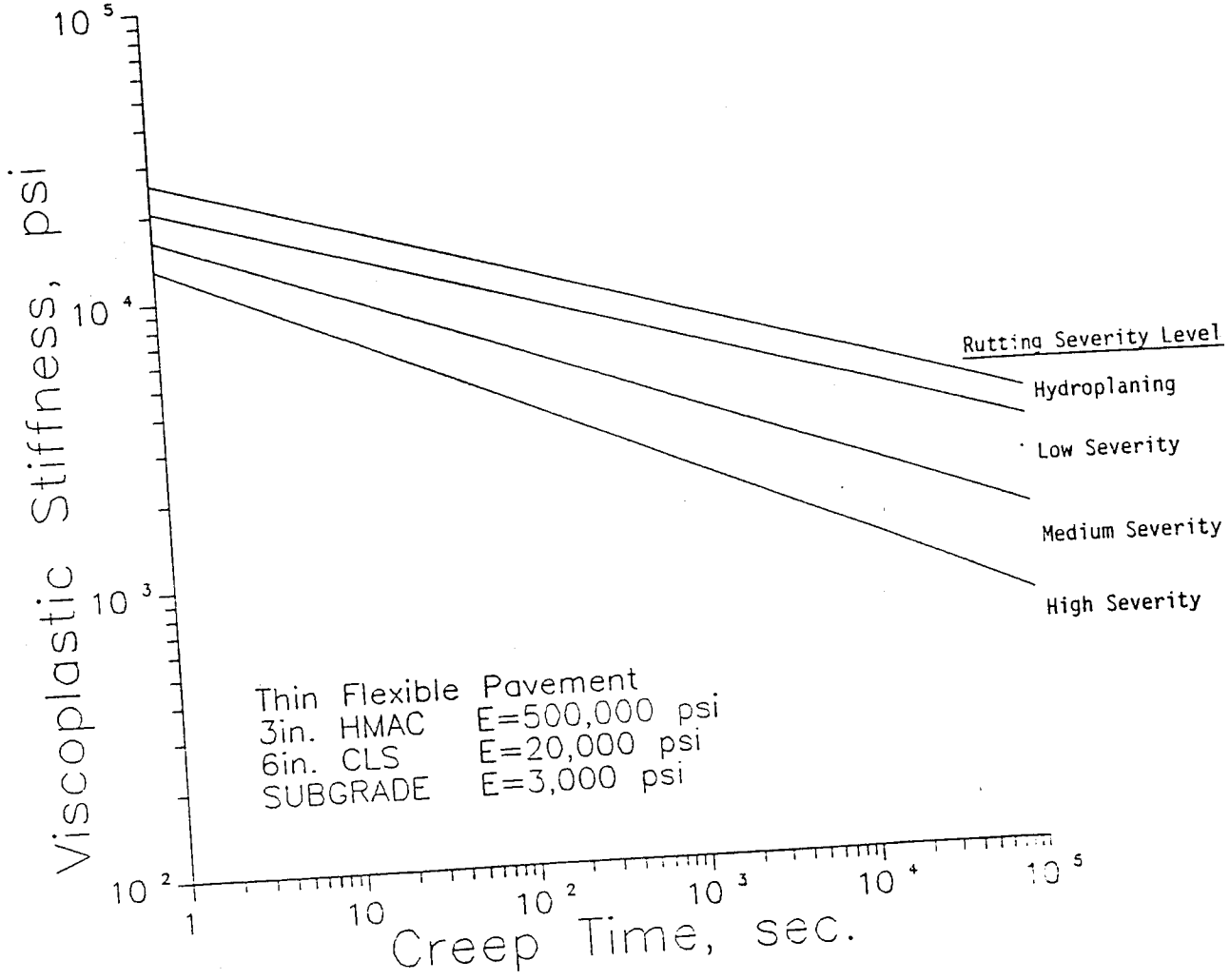
Viscoplastic Stiffness, psi
10^5
10^4
10^3
10^2
Creep Time, sec.
1
10
10^2
10^3
10^4
10^5
Rutting Severity Level
Hydroplaning
Low Severity
Medium Severity
High Severity
Thin Flexible Pavement
3in. HMAC E=500,000 psi
6in. CLS E=20,000 psi
SUBGRADE E=3,000 psi

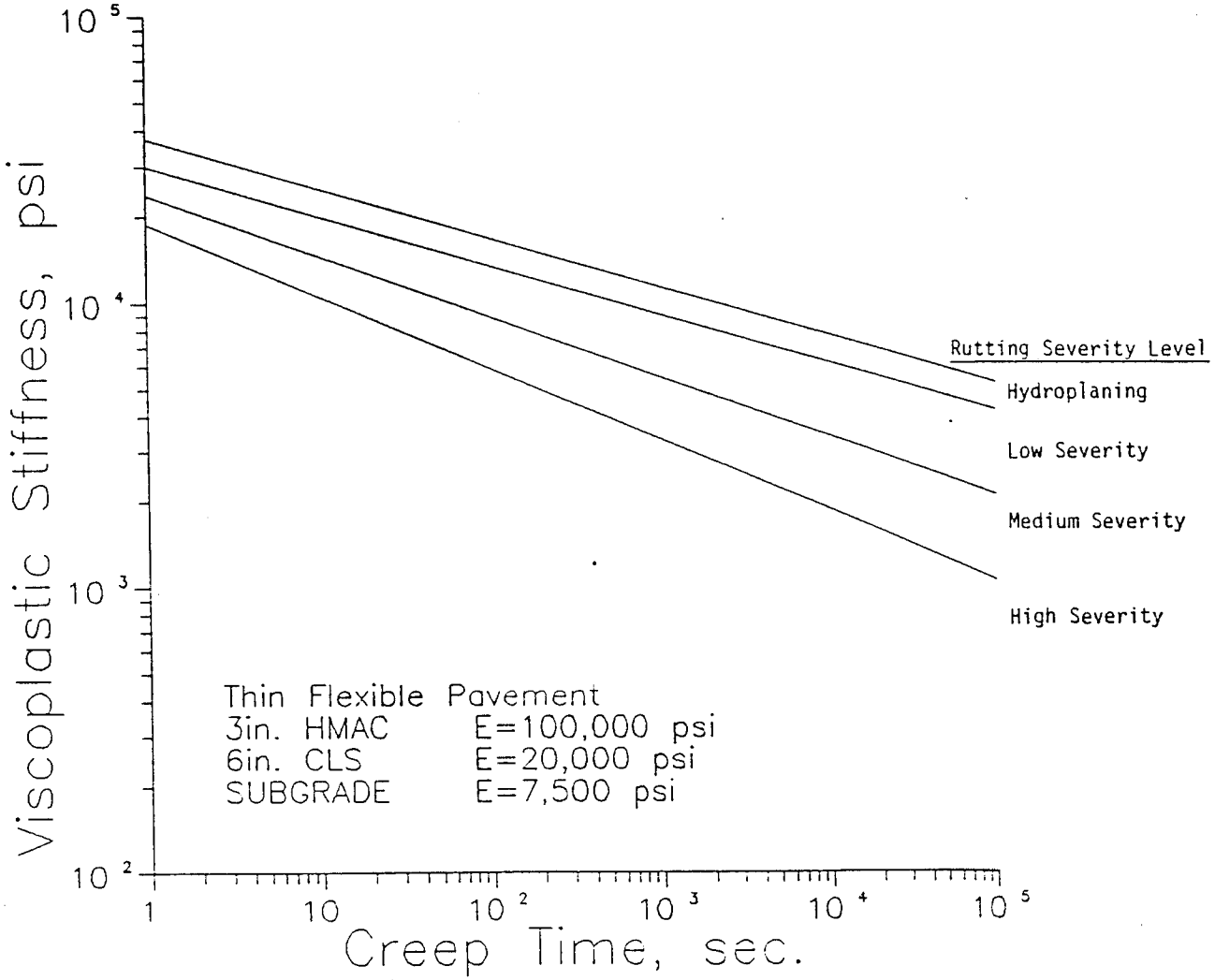
Viscoplastic Stiffness, psi
10 5
10 4
10 3
10 2
1
10
10 2
10 3
10 4
10 5
Creep Time, sec.
Rutting Severity Level
Hydroplaning
Low Severity
Medium Severity
High Severity
Thin Flexible Pavement
3in. HMAC E=100,000 psi
6in. CLS E=20,000 psi
SUBGRADE E=7,500 psi

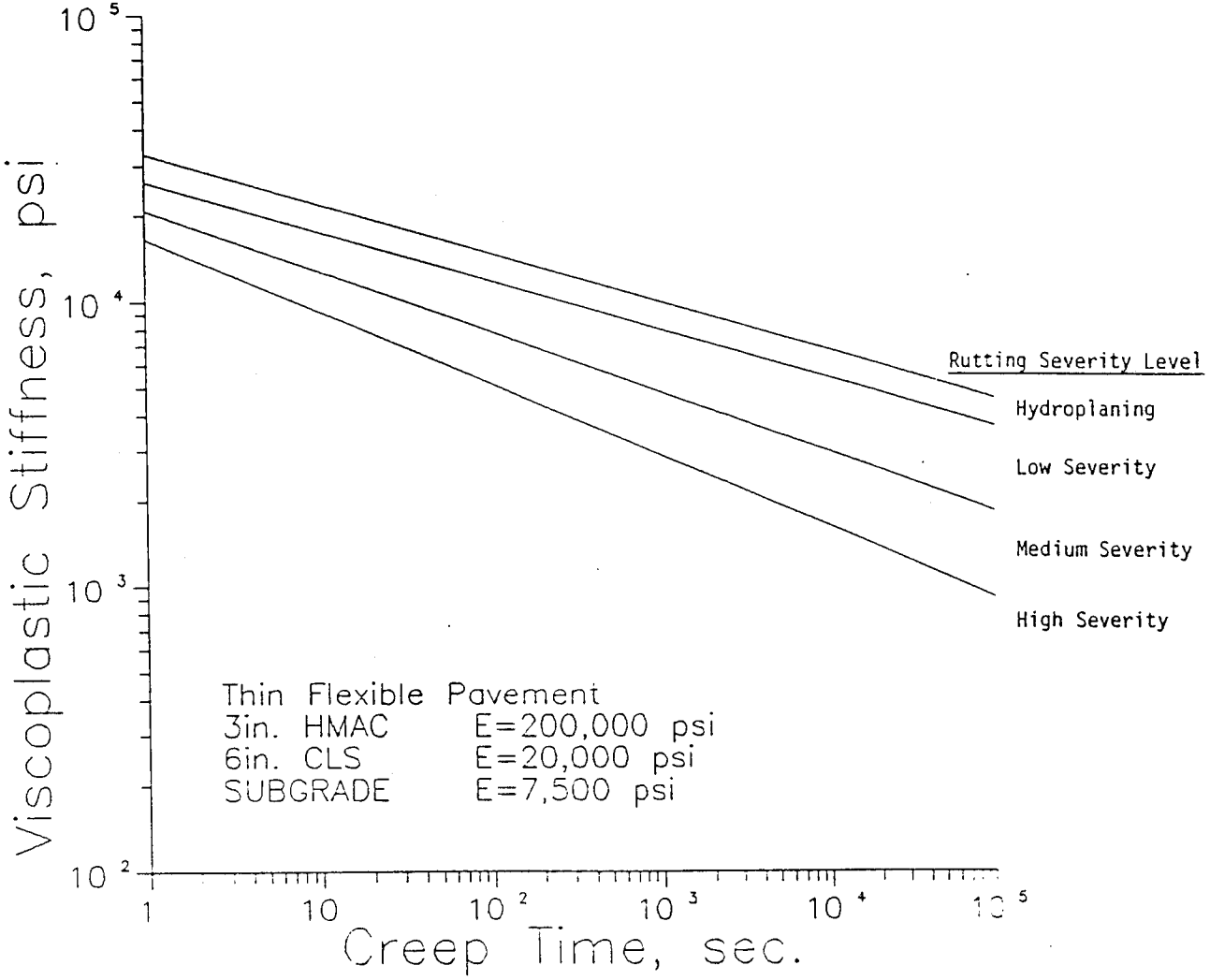
Viscoplastic Stiffness, psi
10^5
10^4
10^3
10^2
1
10
10^2
10^3
10^4
10^5
Creep Time, sec.
Rutting Severity Level
Hydroplaning
Low Severity
Medium Severity
High Severity
Thin Flexible Pavement
3in. HMAC E=200,000 psi
6in. CLS E=20,000 psi
SUBGRADE E=7,500 psi

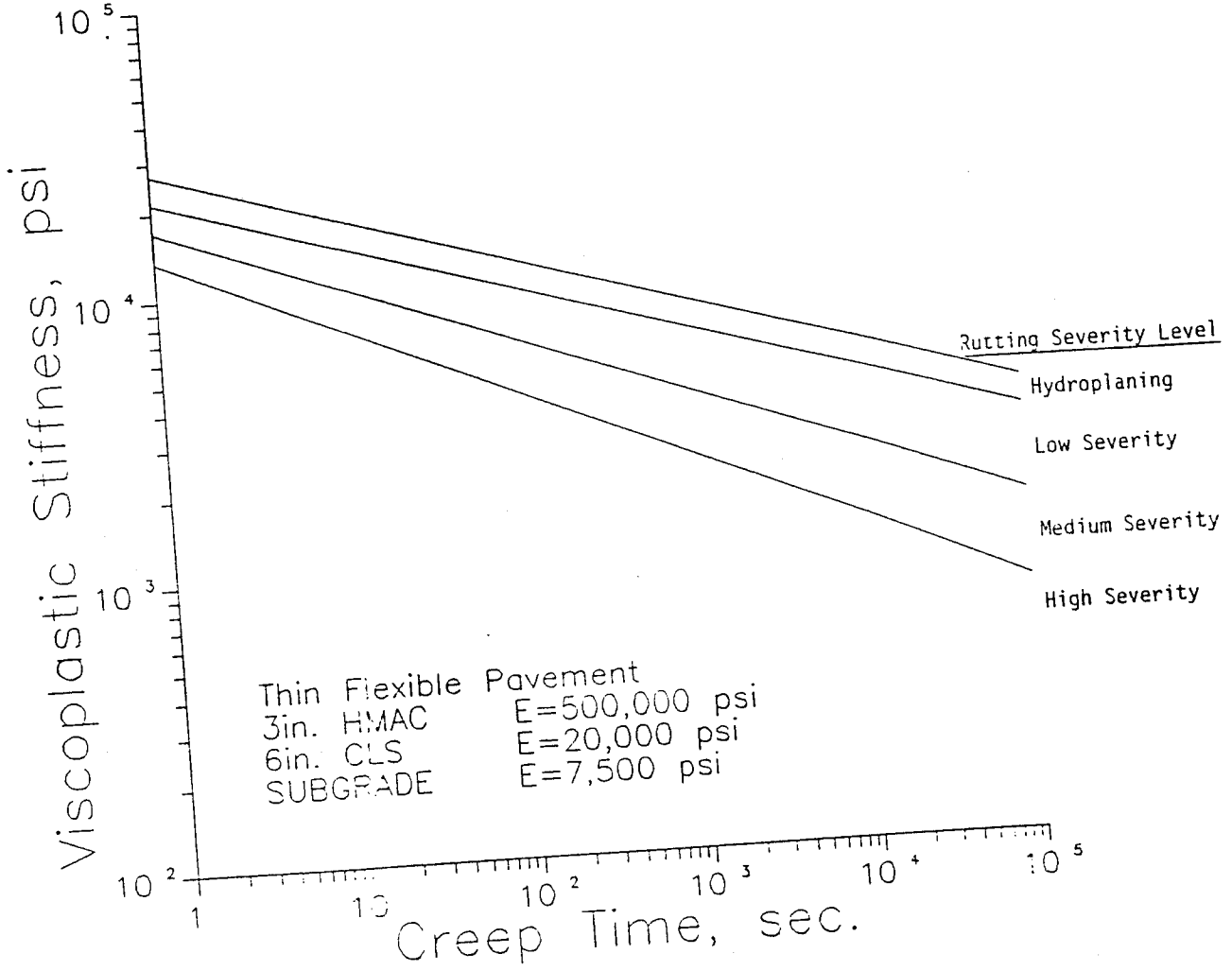
Viscoplastic Stiffness, psi
10^5
10^4
10^3
10^2
Rutting Severity Level
Hydroplaning
Low Severity
Medium Severity
High Severity
Thin Flexible Pavement
3in. HMAC E=500,000 psi
6in. CLS E=20,000 psi
SUBGRADE E=7,500 psi
1
10^2
10^3
10^4
10^5
Creep Time, sec.

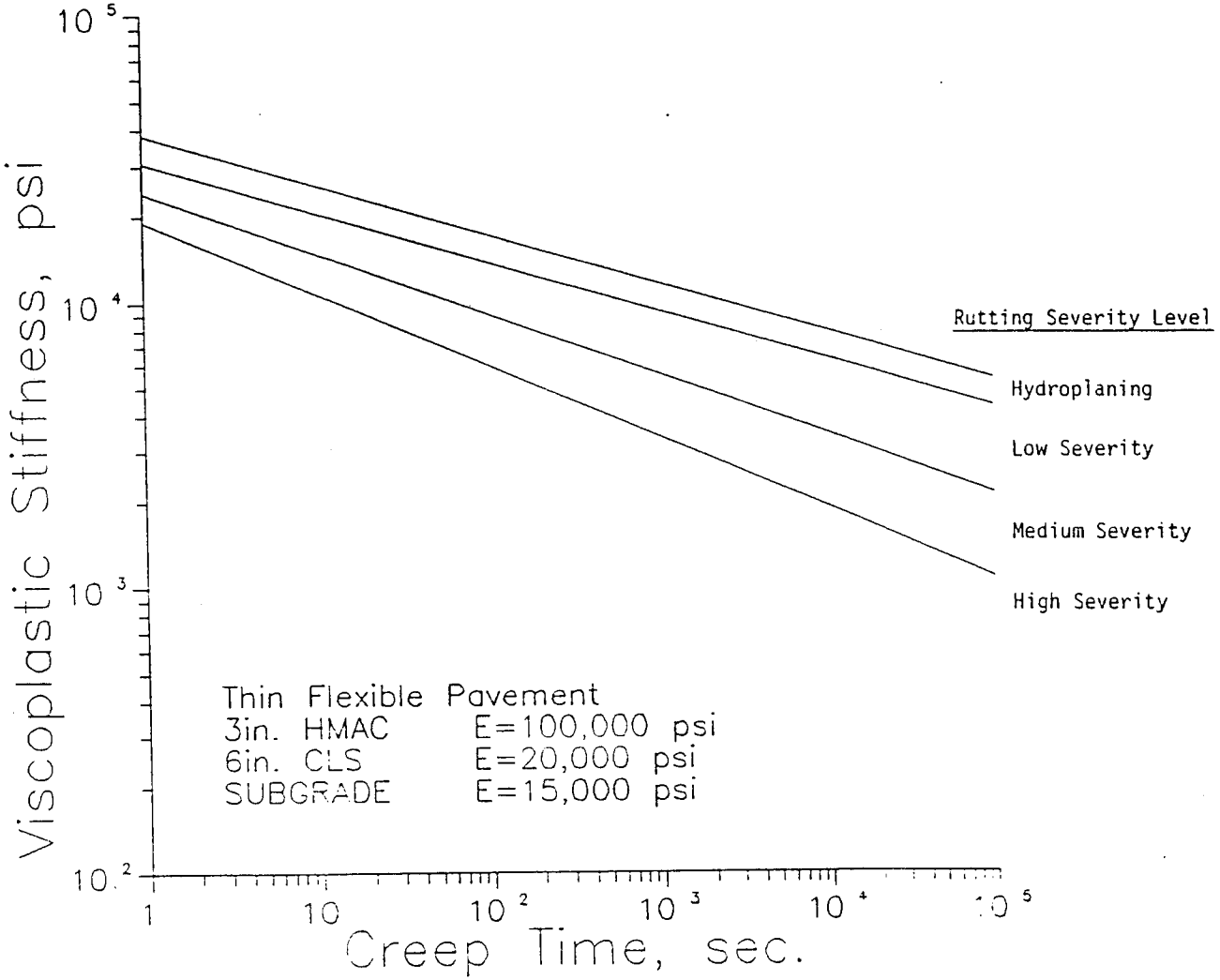
Viscoplastic Stiffness, psi
10^5
10^4
10^3
10^2
1
10
10^2
10^3
10^4
10^5
Creep Time, sec.
Rutting Severity Level
Hydroplaning
Low Severity
Medium Severity
High Severity
Thin Flexible Pavement
3in. HMAC E=100,000 psi
6in. CLS E=20,000 psi
SUBGRADE E=15,000 psi

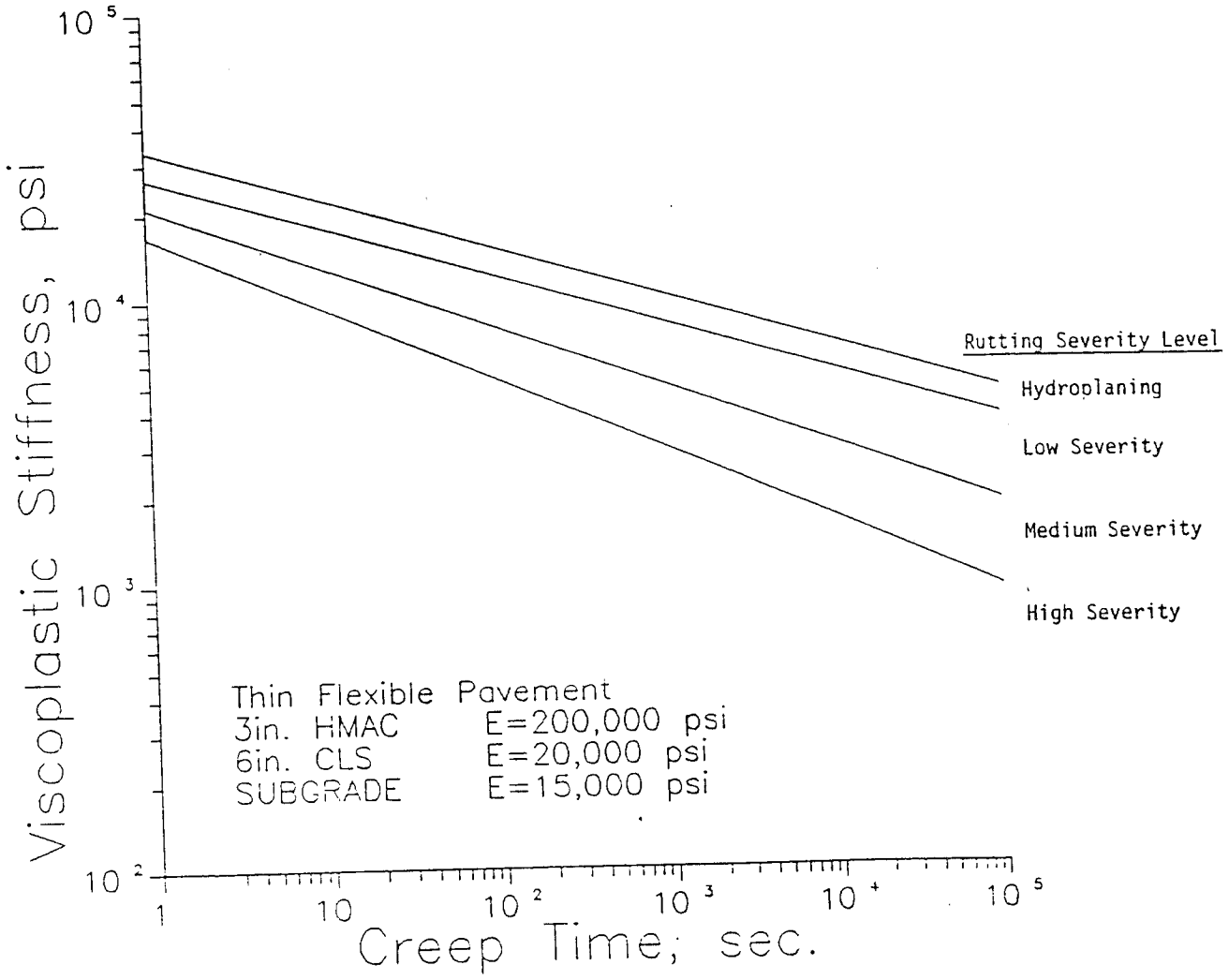
Viscoplastic Stiffness, psi
10 5
10 4
10 3
10 2
1
10
10 2
10 3
10 4
10 5
Creep Time, sec.
Rutting Severity Level
Hydroplaning
Low Severity
Medium Severity
High Severity
Thin Flexible Pavement
3in. HMAC E=200,000 psi
6in. CLS E=20,000 psi
SUBGRADE E=15,000 psi

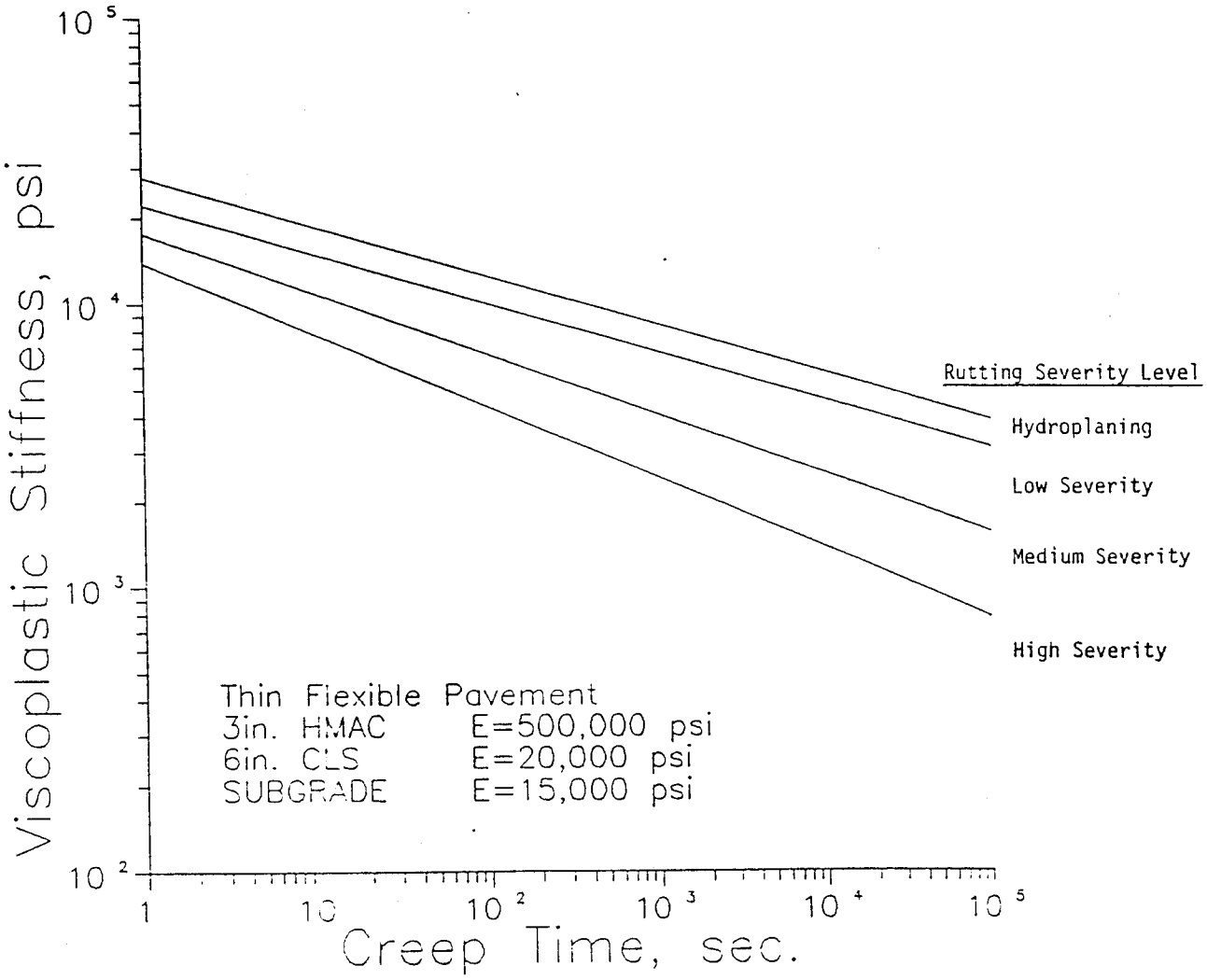
Viscoplastic Stiffness, psi
10^5
10^4
10^3
10^2
1
10
10^2
10^3
10^4
10^5
Creep Time, sec.
Rutting Severity Level
Hydroplaning
Low Severity
Medium Severity
High Severity
Thin Flexible Pavement
3in. HMAC E=500,000 psi
6in. CLS E=20,000 psi
SUBGRADE E=15,000 psi

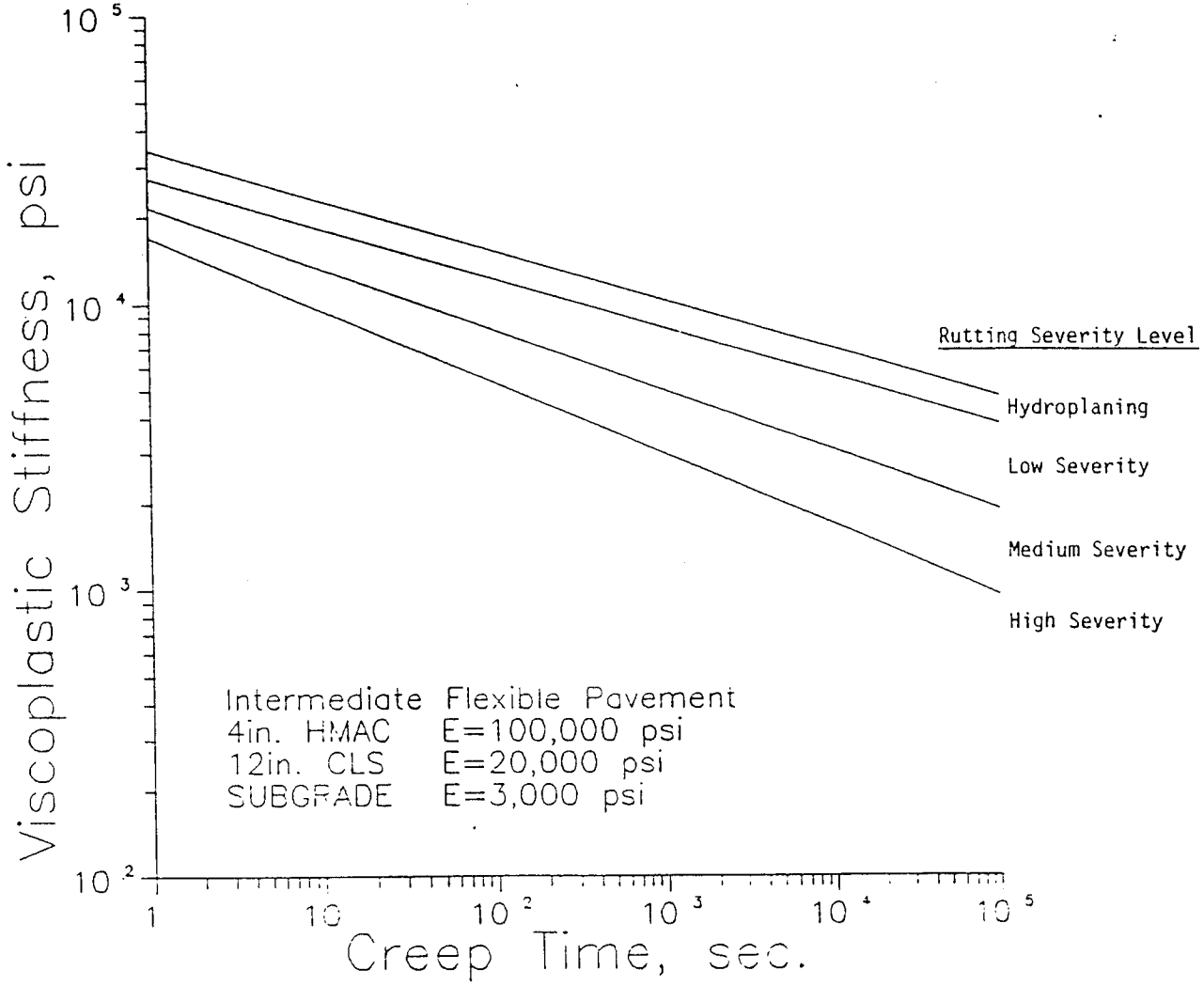
Viscoplastic Stiffness, psi
10 5
10 4
10 3
10 2
1
10
10 2
10 3
10 4
10 5
Creep Time, sec.
Rutting Severity Level
Hydroplaning
Low Severity
Medium Severity
High Severity
Intermediate Flexible Pavement
4in. HMAC E=100,000 psi
12in. CLS E=20,000 psi
SUBGRADE E=3,000 psi

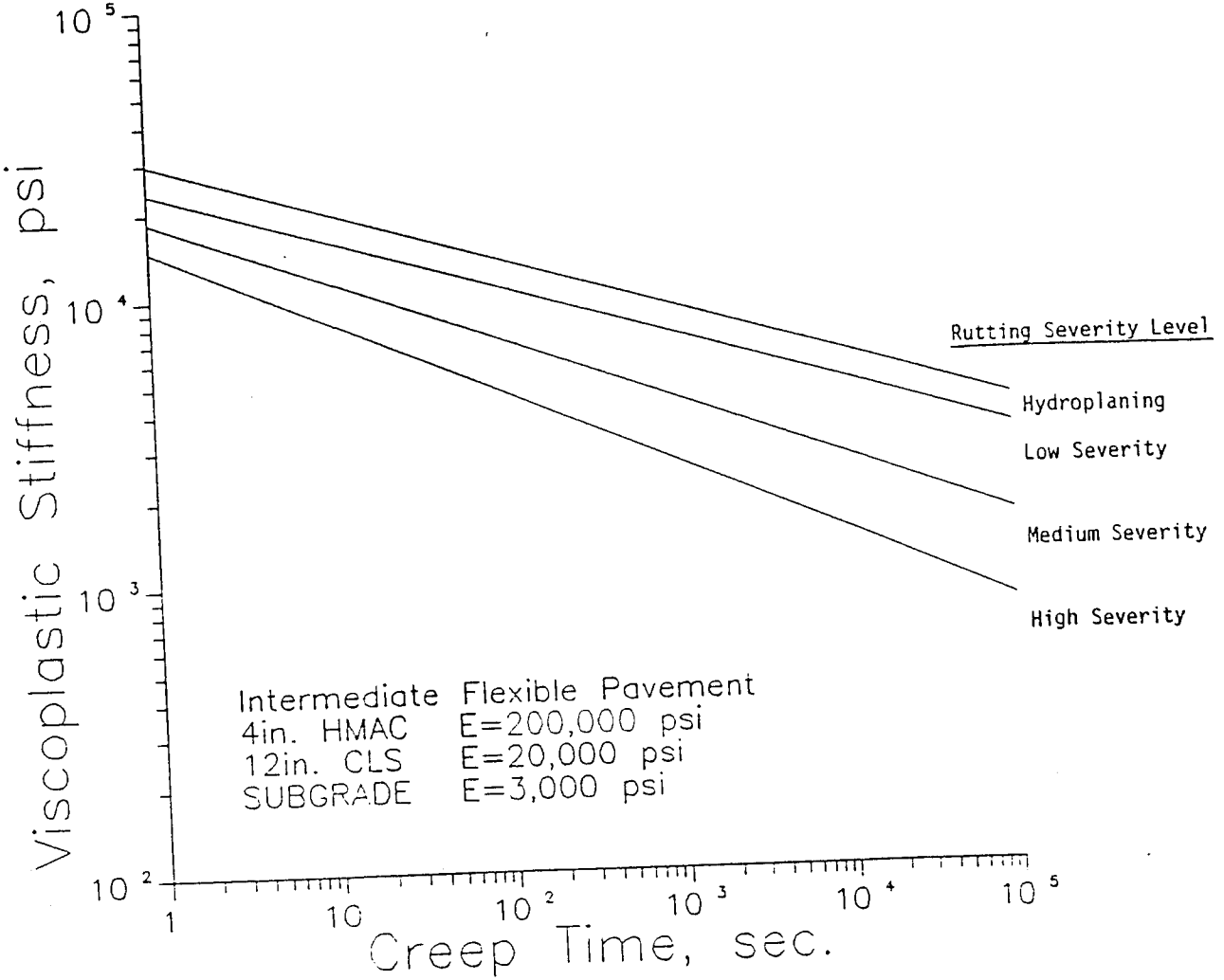
Viscoplastic Stiffness, psi
10^5
10^4
10^3
10^2
Creep Time, sec.
1
10
10^2
10^3
10^4
10^5
Rutting Severity Level
Hydroplaning
Low Severity
Medium Severity
High Severity
Intermediate Flexible Pavement
4in. HMAC E=200,000 psi
12in. CLS E=20,000 psi
SUBGRADE E=3,000 psi

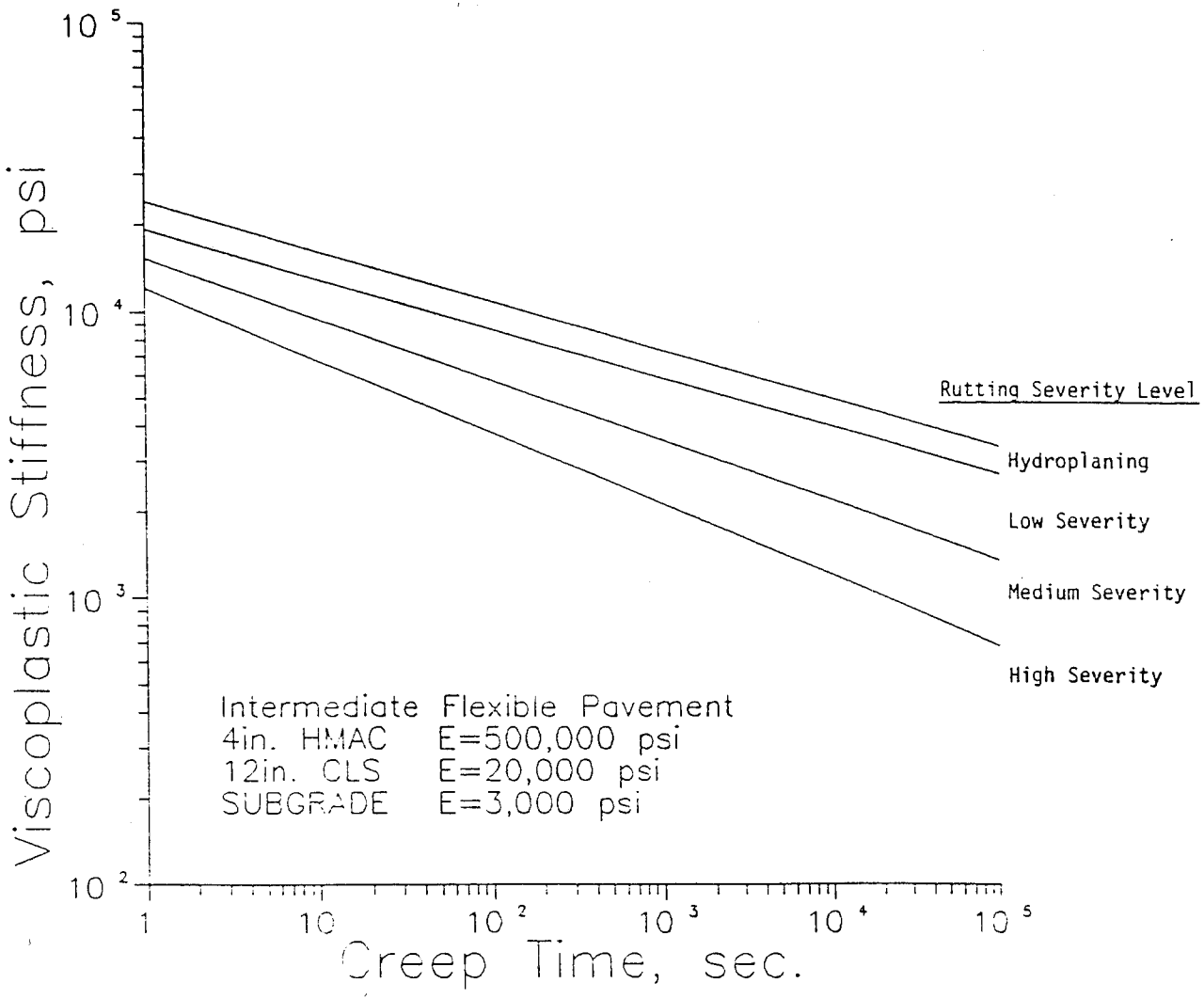
Viscoplastic Stiffness, psi
10^5
10^4
10^3
10^2
1
10
10^2
10^3
10^4
10^5
Creep Time, sec.
Rutting Severity Level
Hydroplaning
Low Severity
Medium Severity
High Severity
Intermediate Flexible Pavement
4in. HMAC E=500,000 psi
12in. CLS E=20,000 psi
SUBGRADE E=3,000 psi

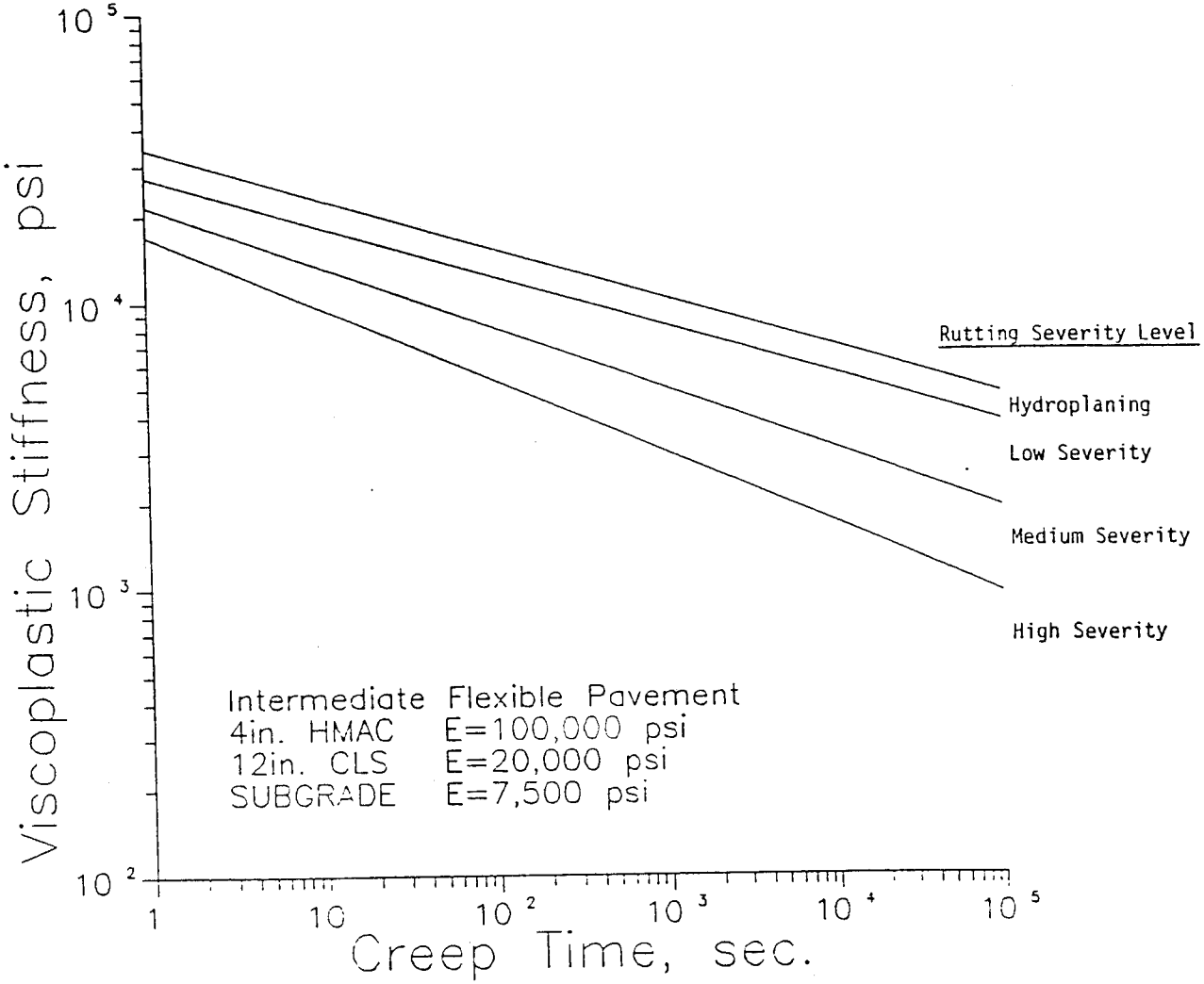
Viscoplastic Stiffness, psi
10 5
10 4
10 3
10 2
1
10
10 2
10 3
10 4
10 5
Creep Time, sec.
Rutting Severity Level
Hydroplaning
Low Severity
Medium Severity
High Severity
Intermediate Flexible Pavement
4in. HMAC E=100,000 psi
12in. CLS E=20,000 psi
SUBGRADE E=7,500 psi

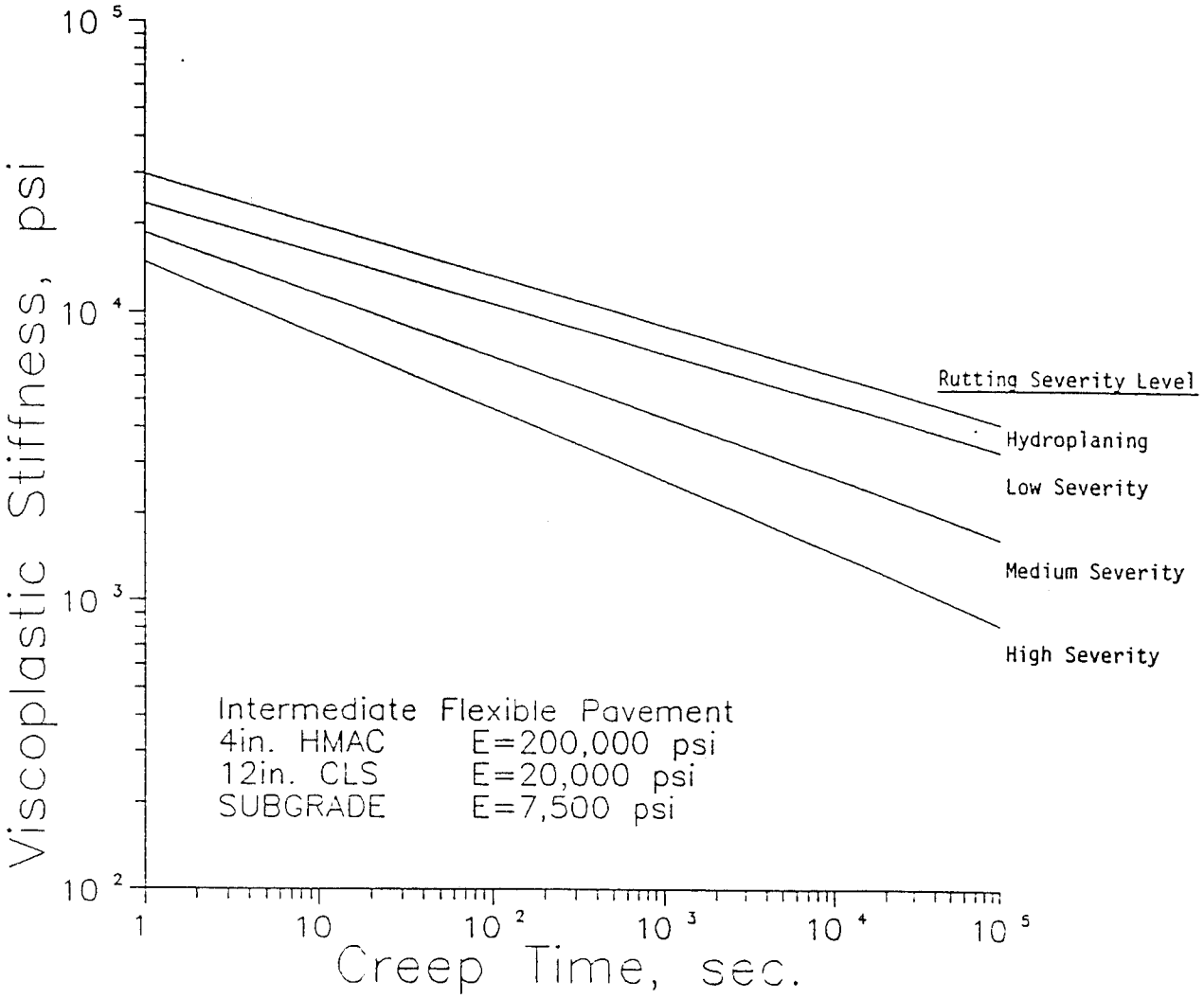
Viscoplastic Stiffness, psi
10 5
10 4
10 3
10 2
1
10
10 2
10 3
10 4
10 5
Creep Time, sec.
Rutting Severity Level
Hydroplaning
Low Severity
Medium Severity
High Severity
Intermediate Flexible Pavement
4in. HMAC E=200,000 psi
12in. CLS E=20,000 psi
SUBGRADE E=7,500 psi

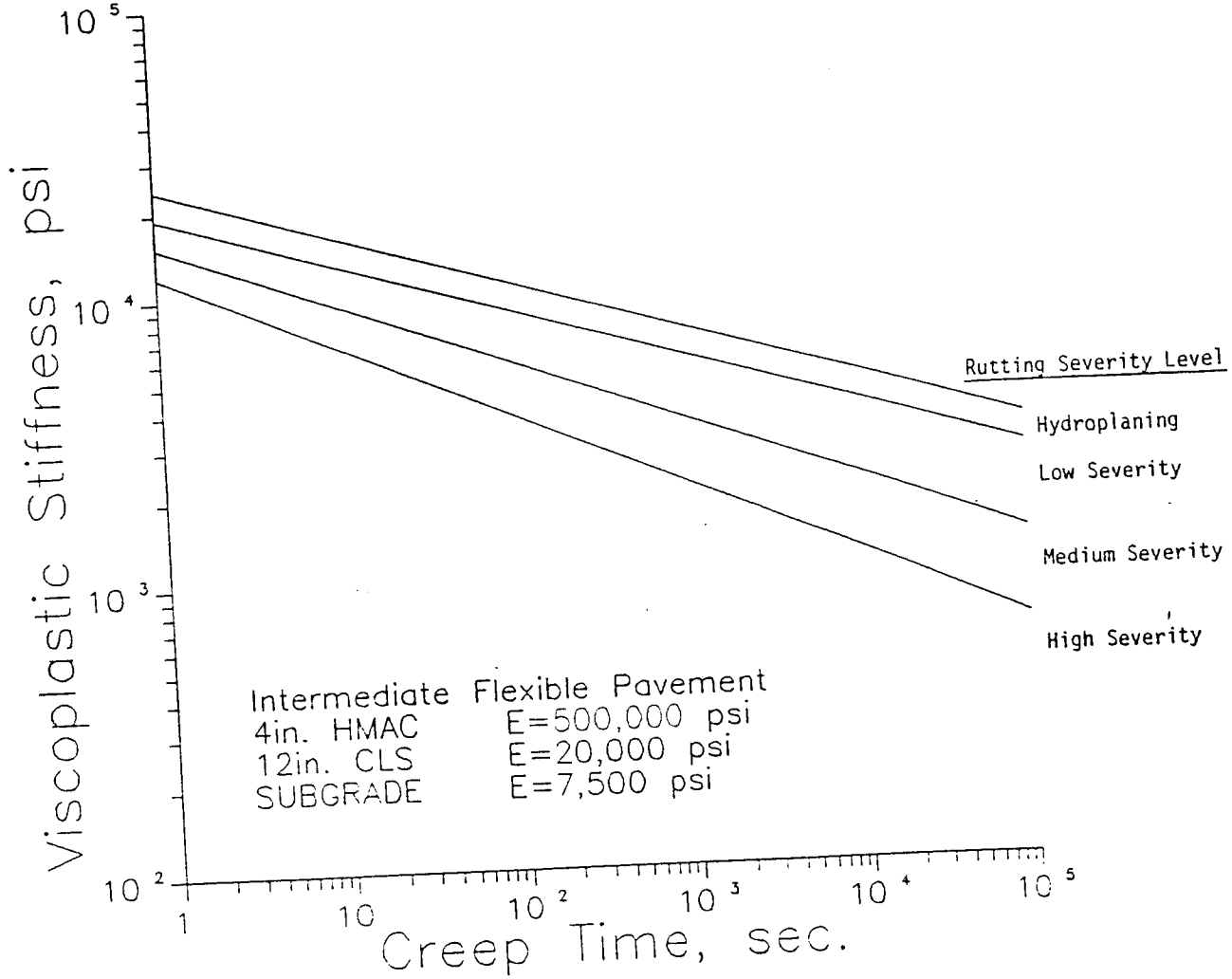
Viscoplastic Stiffness, psi
10 5
10 4
10 3
10 2
Creep Time, sec.
1
10
10 2
10 3
10 4
10 5
Rutting Severity Level
Hydroplaning
Low Severity
Medium Severity
High Severity
Intermediate Flexible Pavement
4in. HMAC E=500,000 psi
12in. CLS E=20,000 psi
SUBGRADE E=7,500 psi

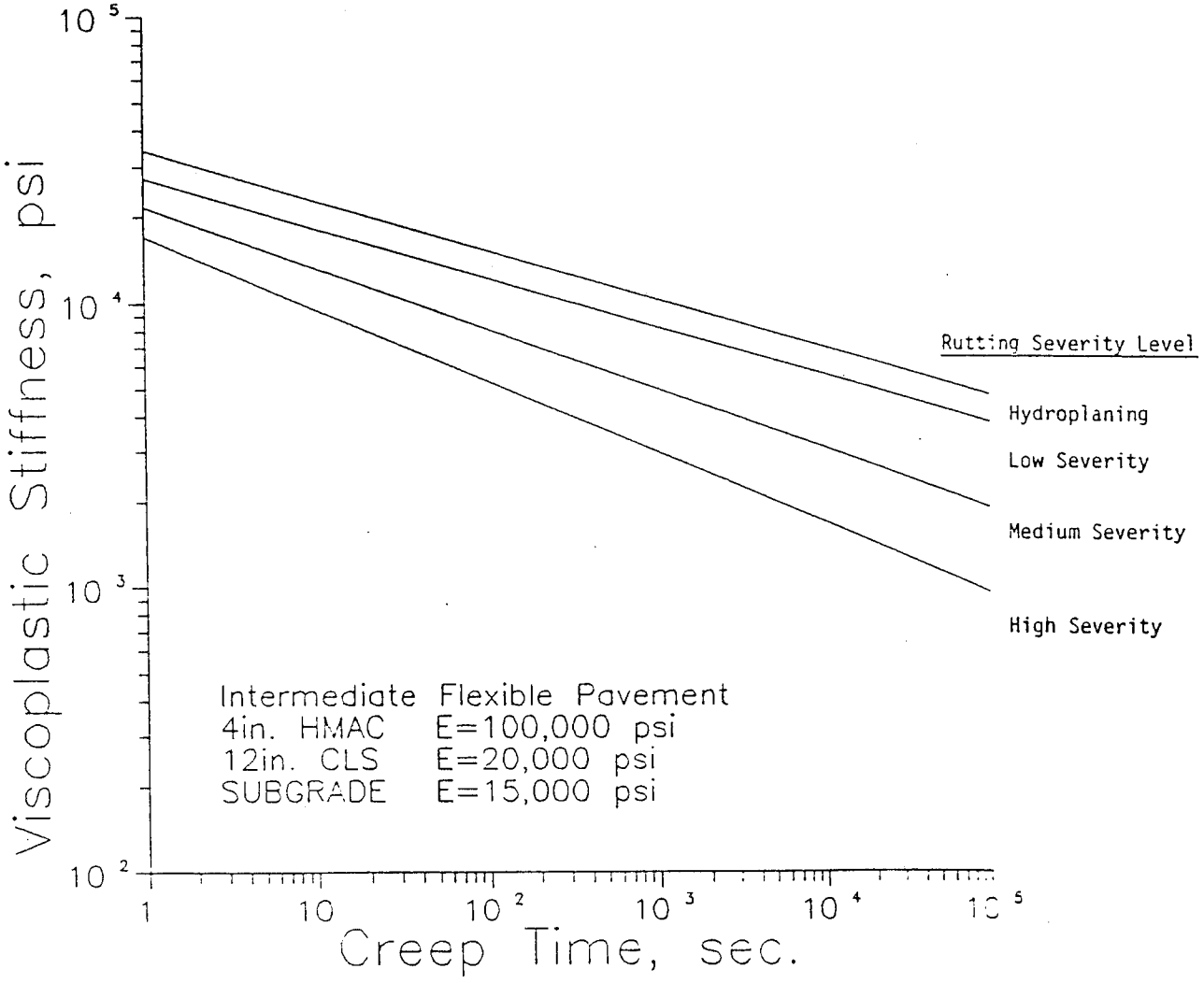
Viscoplastic Stiffness, psi
10^5
10^4
10^3
10^2
1
10
10^2
10^3
10^4
10^5
Creep Time, sec.
Rutting Severity Level
Hydroplaning
Low Severity
Medium Severity
High Severity
Intermediate Flexible Pavement
4in. HMAC E=100,000 psi
12in. CLS E=20,000 psi
SUBGRADE E=15,000 psi

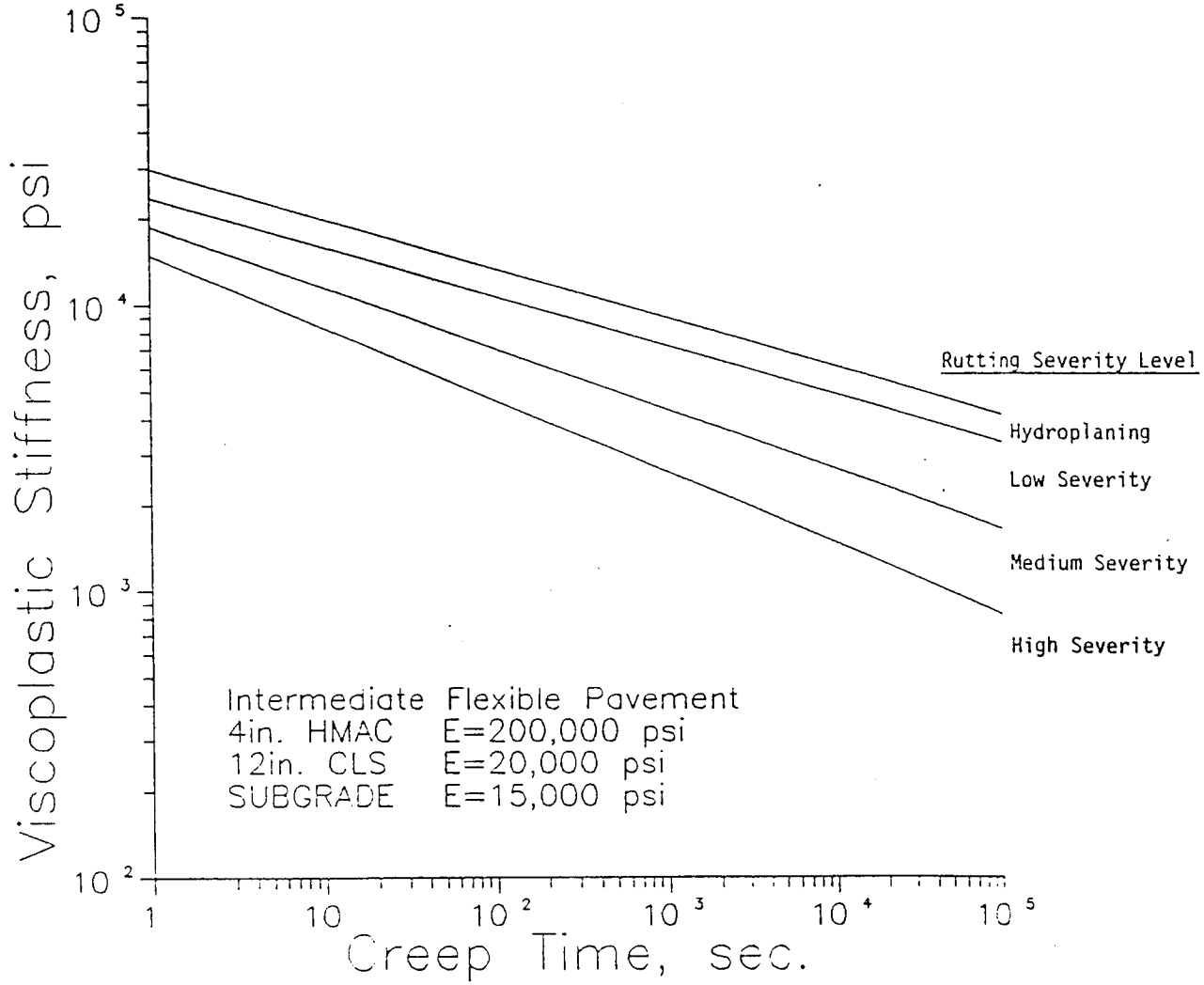
Viscoplastic Stiffness, psi
10^5
10^4
10^3
10^2
1
10
10^2
10^3
10^4
10^5
Creep Time, sec.
Rutting Severity Level
Hydroplaning
Low Severity
Medium Severity
High Severity
Intermediate Flexible Pavement
4in. HMAC E=200,000 psi
12in. CLS E=20,000 psi
SUBGRADE E=15,000 psi

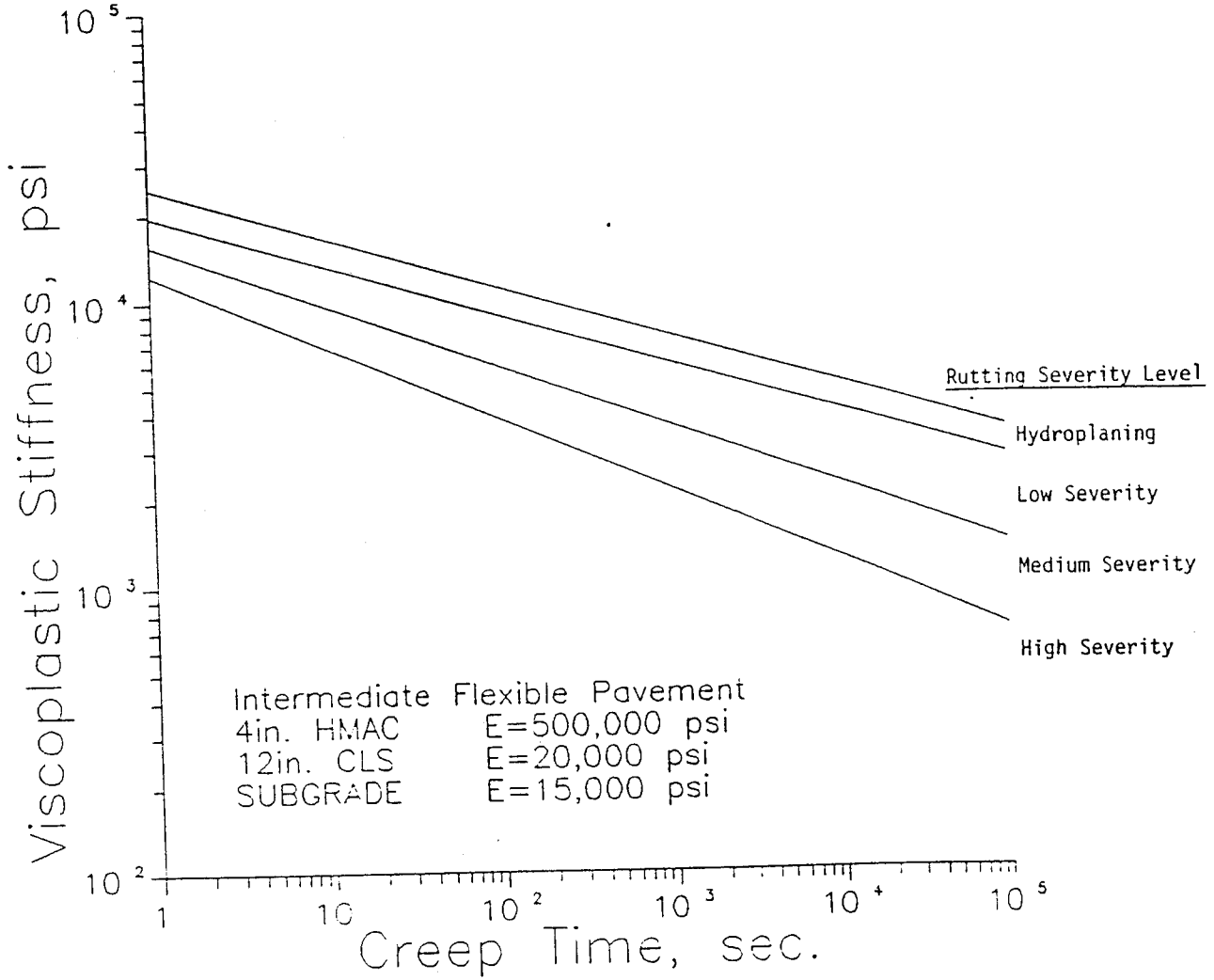
Viscoplastic Stiffness, psi
10^5
10^4
10^3
10^2
1
10
10^2
10^3
10^4
10^5
Creep Time, sec.
Rutting Severity Level
Hydroplaning
Low Severity
Medium Severity
High Severity
Intermediate Flexible Pavement
4in. HMAC E=500,000 psi
12in. CLS E=20,000 psi
SUBGRADE E=15,000 psi

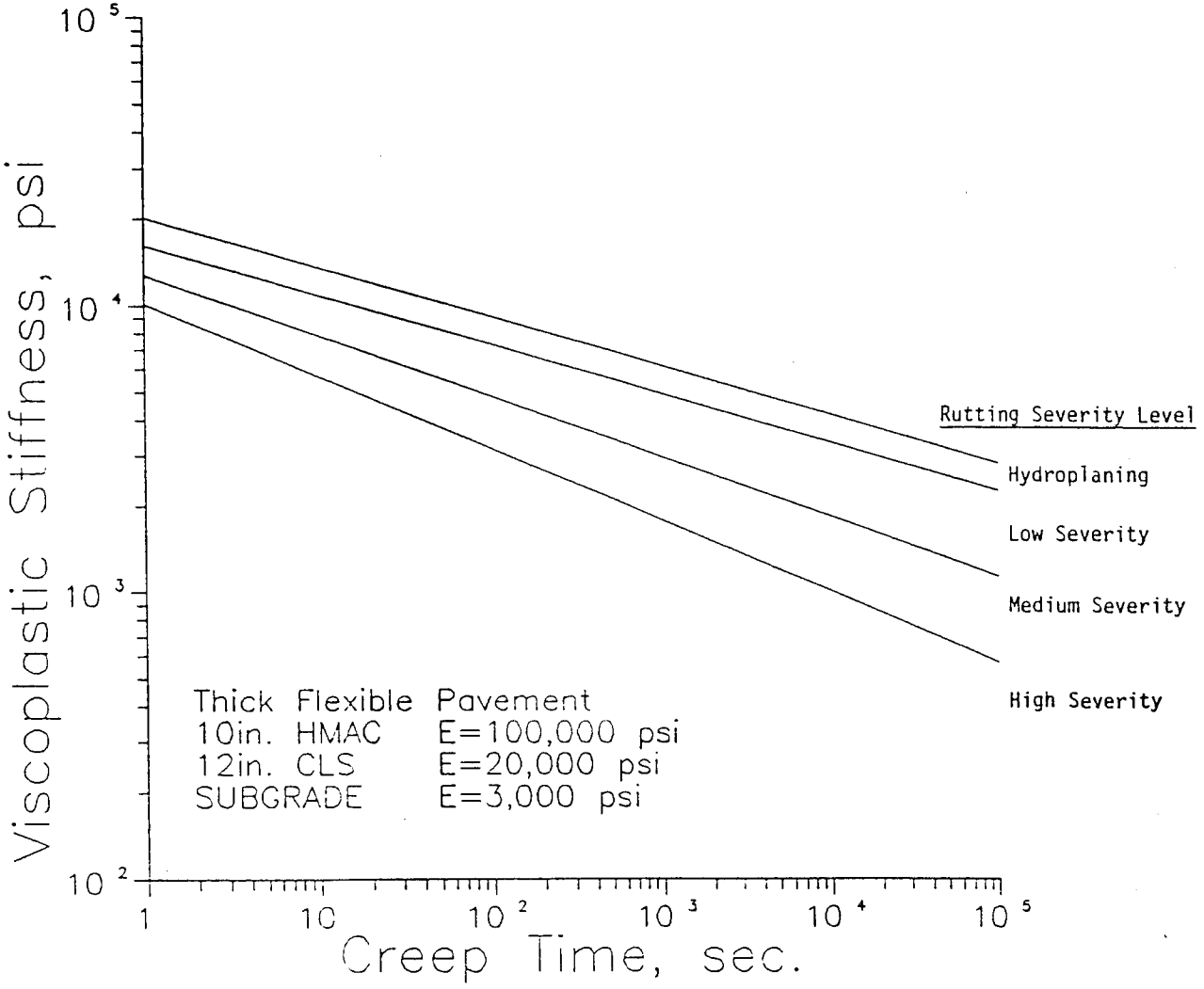
Viscoplastic Stiffness, psi
10 5
10 4
10 3
10 2
1
10
10 2
10 3
10 4
10 5
Creep Time, sec.
Rutting Severity Level
Hydroplaning
Low Severity
Medium Severity
High Severity
Thick Flexible Pavement
10in. HMAC E=100,000 psi
12in. CLS E=20,000 psi
SUBGRADE E=3,000 psi

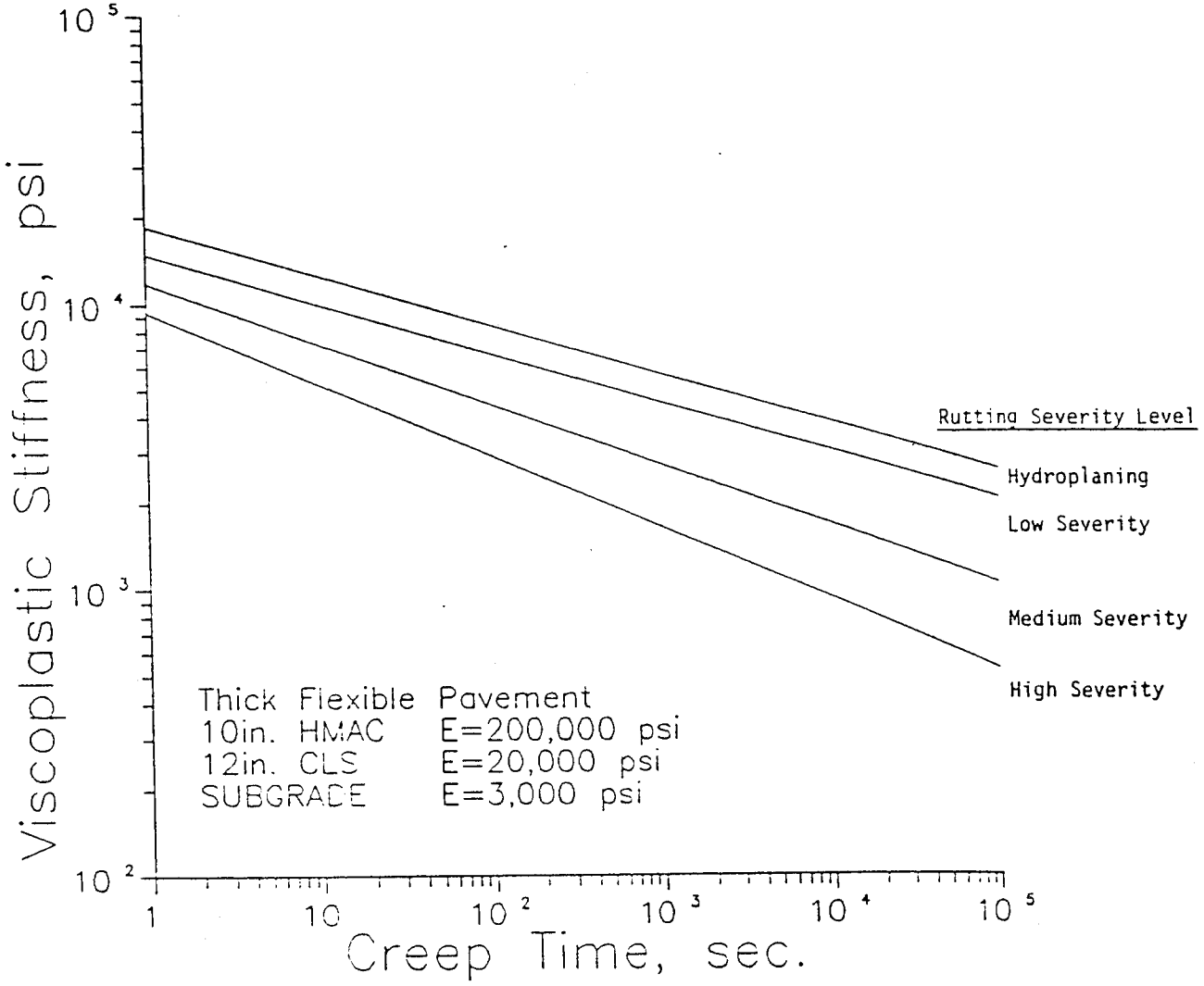
Viscoplastic Stiffness, psi
10^5
10^4
10^3
10^2
1
10
10^2
10^3
10^4
10^5
Creep Time, sec.
Rutting Severity Level
Hydroplaning
Low Severity
Medium Severity
High Severity
Thick Flexible Pavement
10in. HMAC E=200,000 psi
12in. CLS E=20,000 psi
SUBGRADE E=3,000 psi

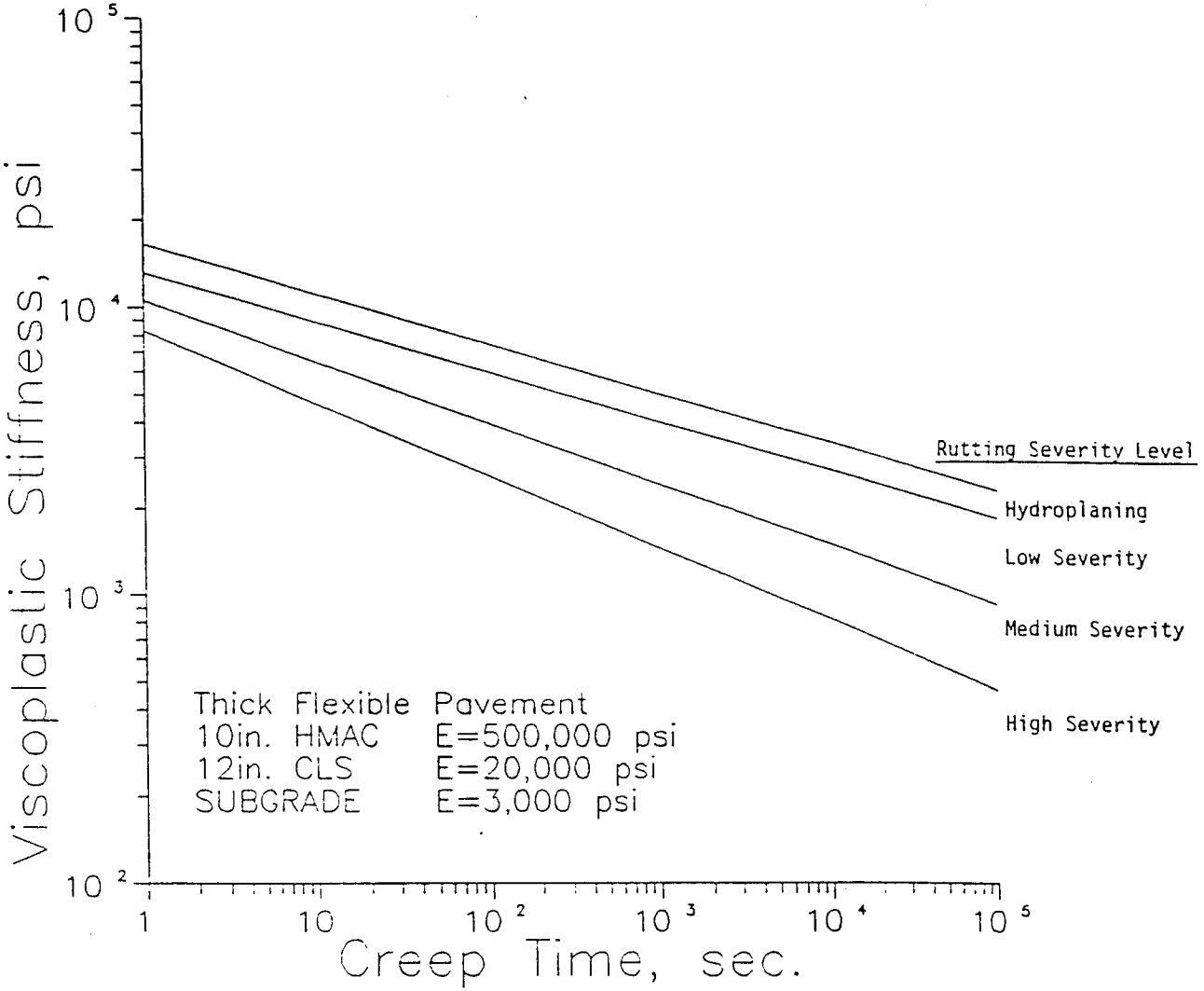
Viscoplastic Stiffness, psi
10^5
10^4
10^3
10^2
1
10
10^2
10^3
10^4
10^5
Creep Time, sec.
Rutting Severity Level
Hydroplaning
Low Severity
Medium Severity
High Severity
Thick Flexible Pavement
10in. HMAC E=500,000 psi
12in. CLS E=20,000 psi
SUBGRADE E=3,000 psi

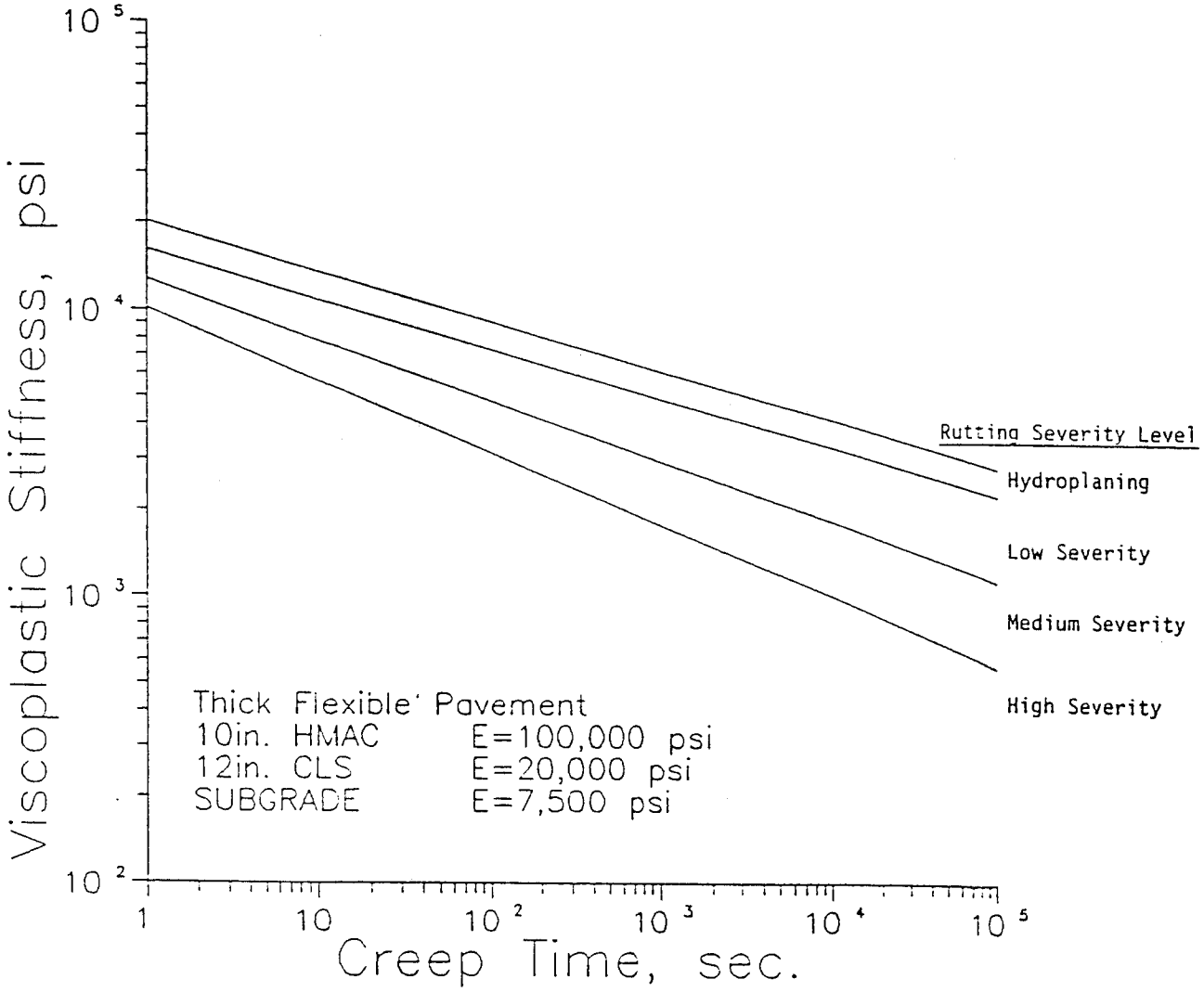
Viscoplastic Stiffness, psi
10 5
10 4
10 3
10 2
1
10
10 2
10 3
10 4
10 5
Creep Time, sec.
Rutting Severity Level
Hydroplaning
Low Severity
Medium Severity
High Severity
Thick Flexible Pavement
10in. HMAC E=100,000 psi
12in. CLS E=20,000 psi
SUBGRADE E=7,500 psi

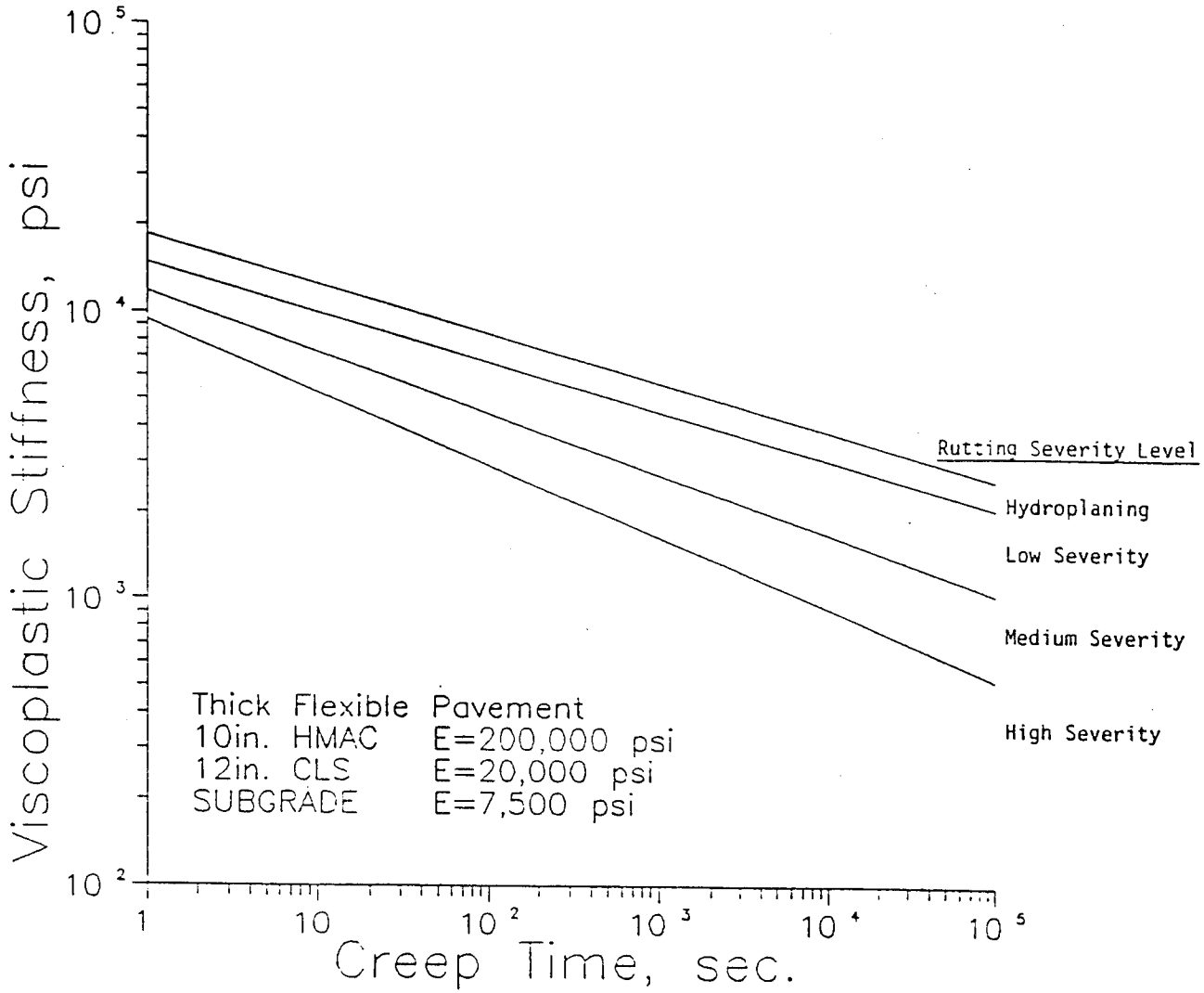
Viscoplastic Stiffness, psi
10 5
10 4
10 3
10 2
1
10
10 2
10 3
10 4
10 5
Creep Time, sec.
Rutting Severity Level
Hydroplaning
Low Severity
Medium Severity
High Severity
Thick Flexible Pavement
10in. HMAC E=200,000 psi
12in. CLS E=20,000 psi
SUBGRADE E=7,500 psi

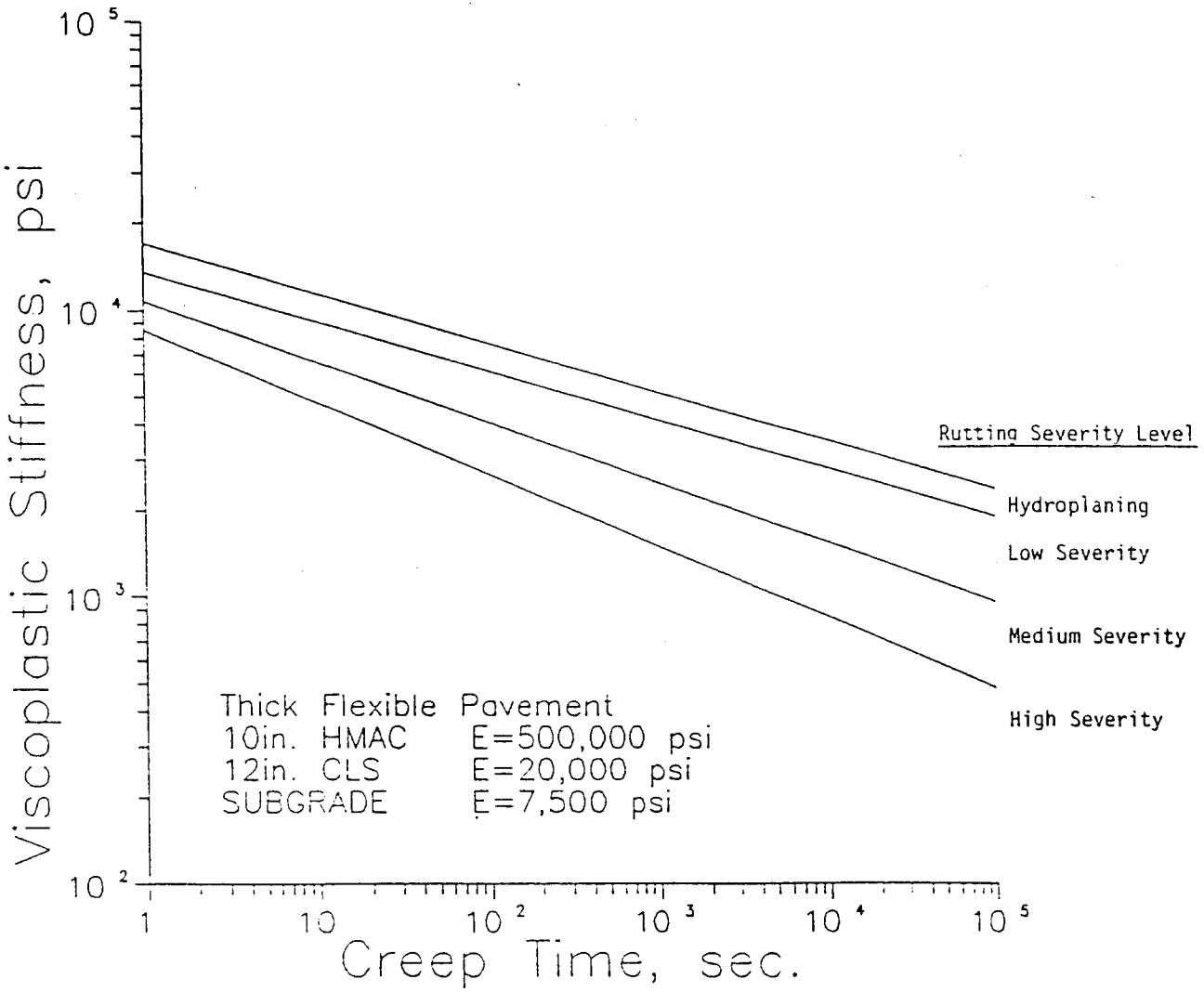
Viscoplastic Stiffness, psi
10 5
10 4
10 3
10 2
1
10
10 2
10 3
10 4
10 5
Creep Time, sec.
Rutting Severity Level
Hydroplaning
Low Severity
Medium Severity
High Severity
Thick Flexible Pavement
10in. HMAC E=500,000 psi
12in. CLS E=20,000 psi
SUBGRADE E=7,500 psi

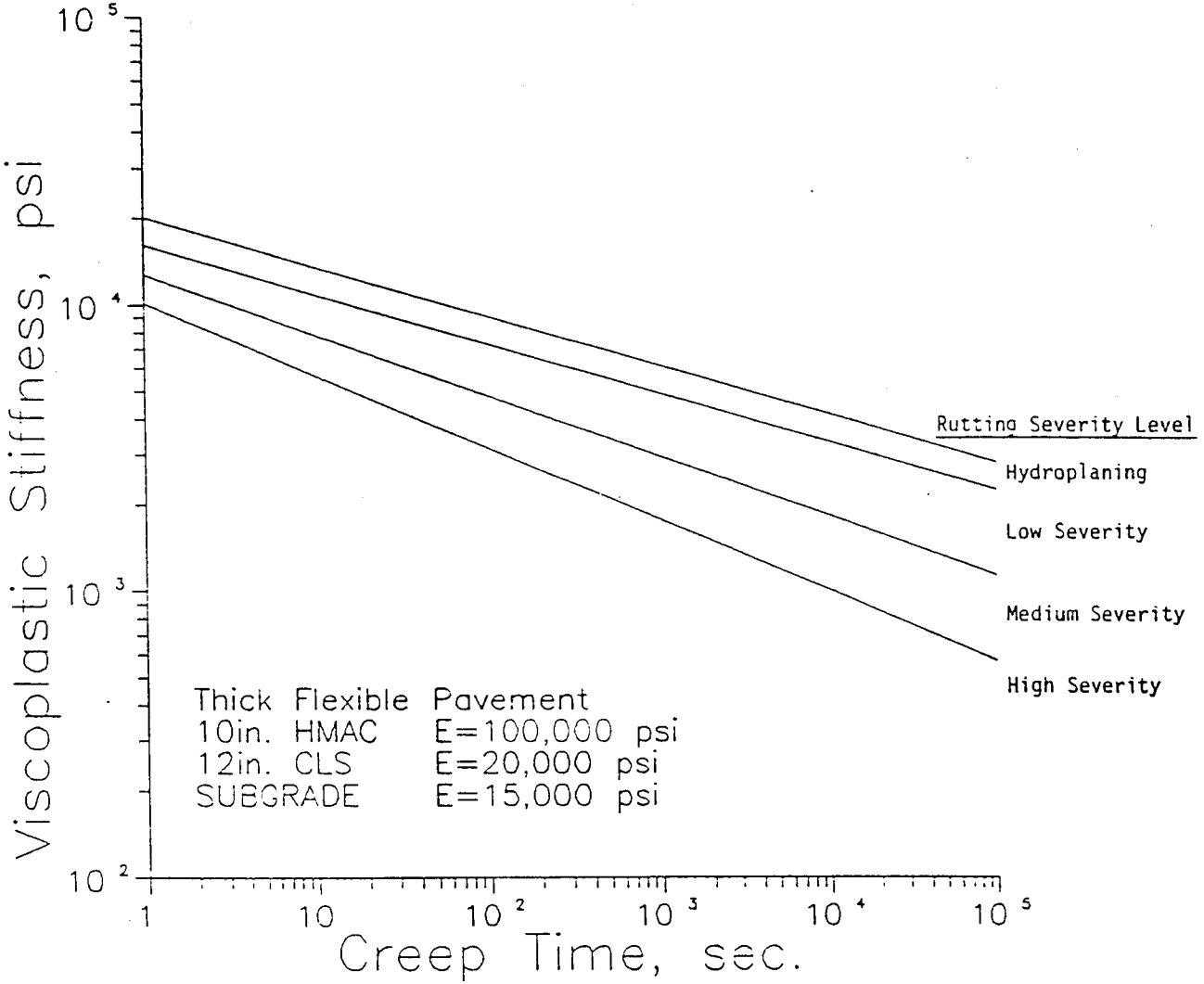
Viscoplastic Stiffness, psi
10^5
10^4
10^3
10^2
1
10
10^2
10^3
10^4
10^5
Creep Time, sec.
Rutting Severity Level
Hydroplaning
Low Severity
Medium Severity
High Severity
Thick Flexible Pavement
10in. HMAC E=100,000 psi
12in. CLS E=20,000 psi
SUBGRADE E=15,000 psi

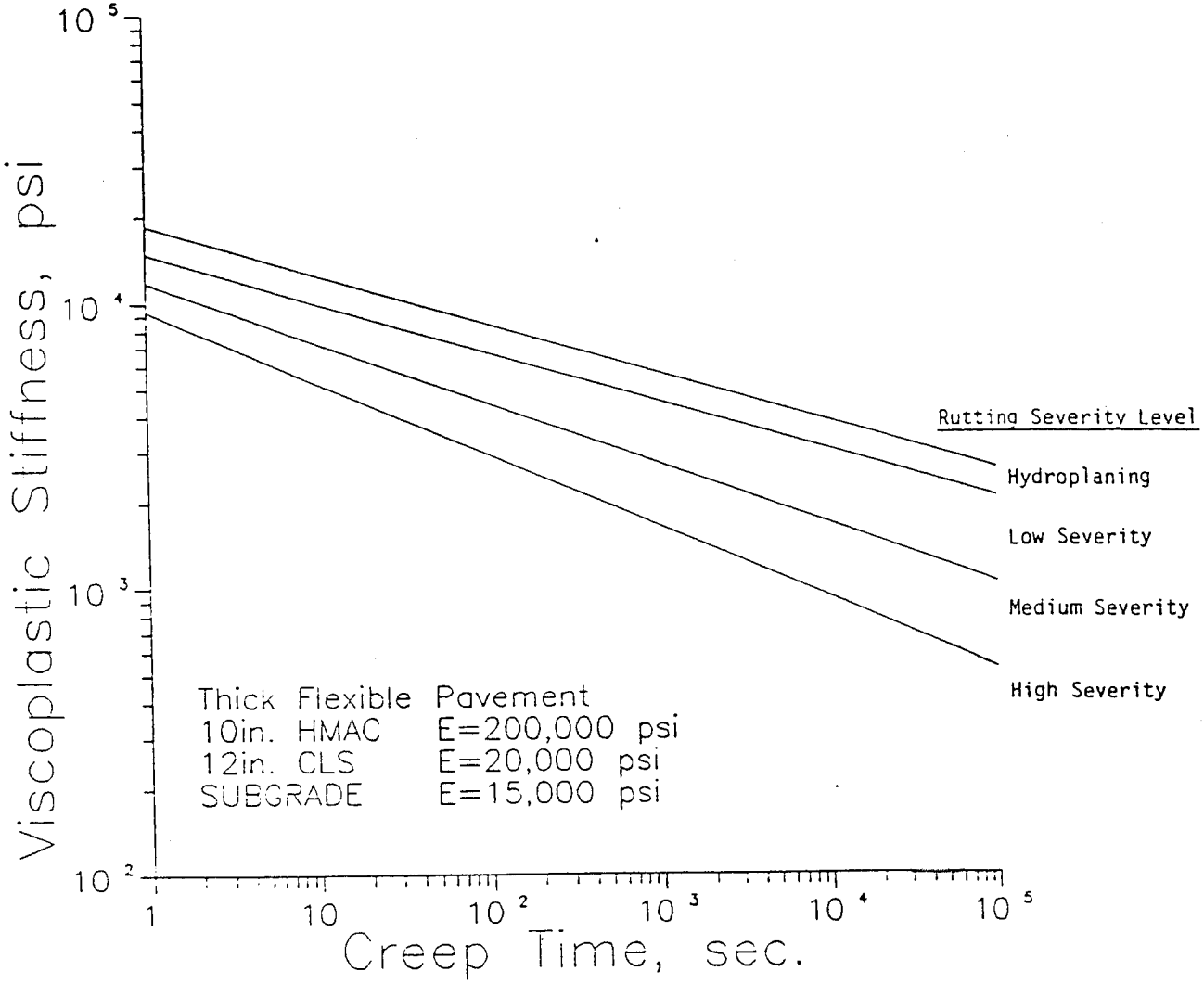
Viscoplastic Stiffness, psi
10^5
10^4
10^3
10^2
1
10
10^2
10^3
10^4
10^5
Creep Time, sec.
Rutting Severity Level
Hydroplaning
Low Severity
Medium Severity
High Severity
Thick Flexible Pavement
10in. HMAC E=200,000 psi
12in. CLS E=20,000 psi
SUBGRADE E=15,000 psi

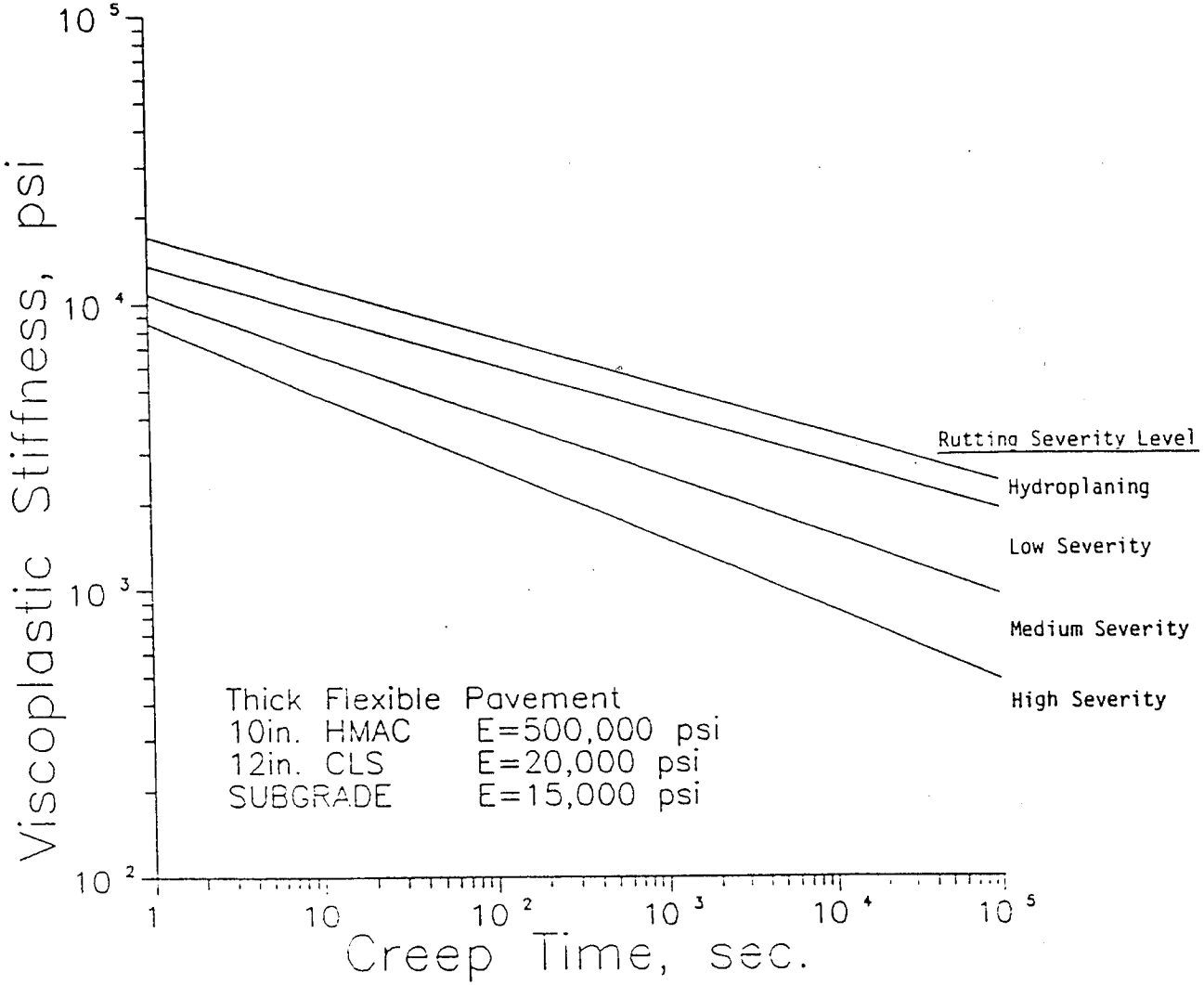
Viscoplastic Stiffness, psi
10^5
10^4
10^3
10^2
1
10
10^2
10^3
10^4
10^5
Creep Time, sec.
Rutting Severity Level
Hydroplaning
Low Severity
Medium Severity
High Severity
Thick Flexible Pavement
10in. HMAC E=500,000 psi
12in. CLS E=20,000 psi
SUBGRADE E=15,000 psi

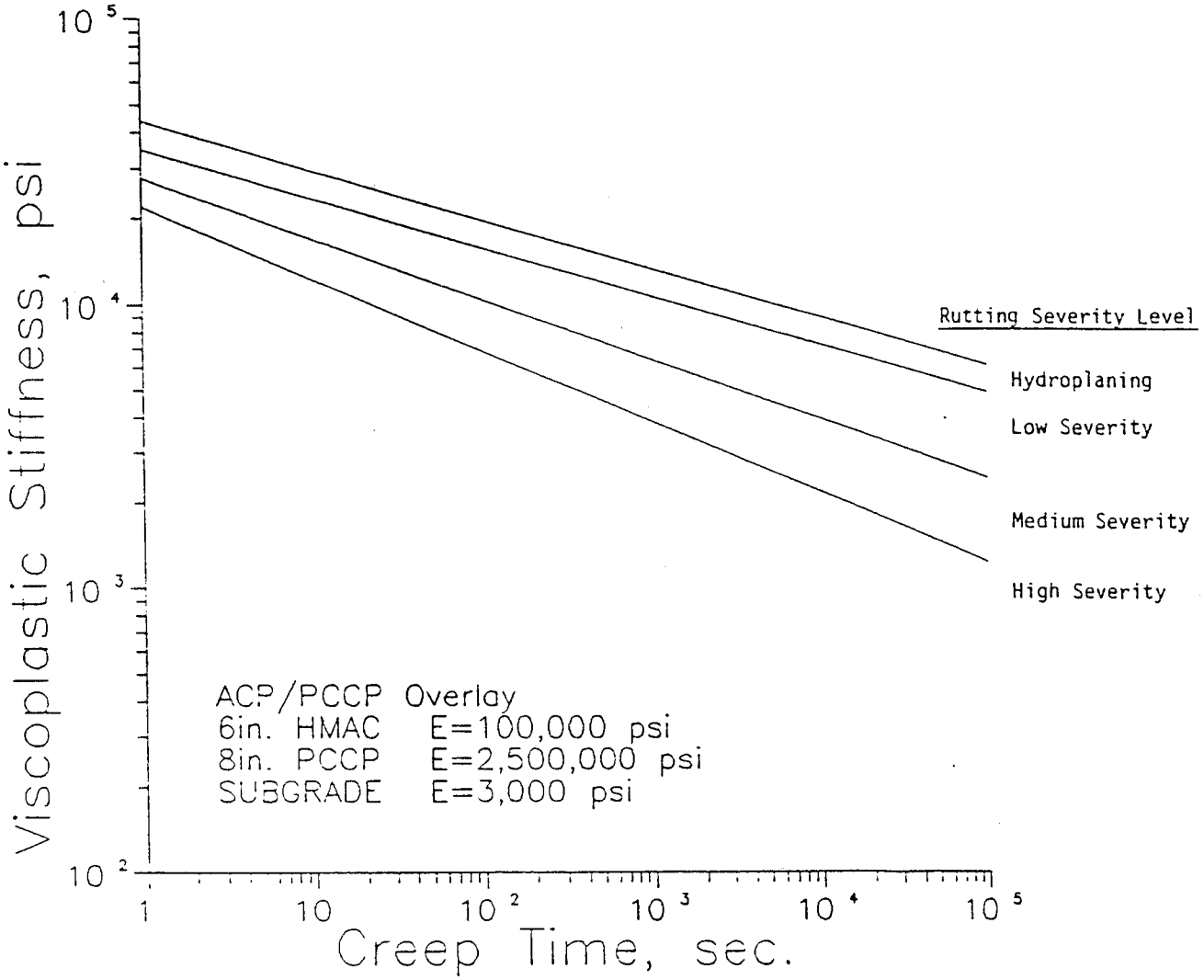
Viscoplastic Stiffness, psi
10^5
10^4
10^3
10^2
1
10
10^2
10^3
10^4
10^5
Creep Time, sec.
Rutting Severity Level
Hydroplaning
Low Severity
Medium Severity
High Severity
ACP/PCCP Overlay
6in. HMAC E=100,000 psi
8in. PCCP E=2,500,000 psi
SUBGRADE E=3,000 psi

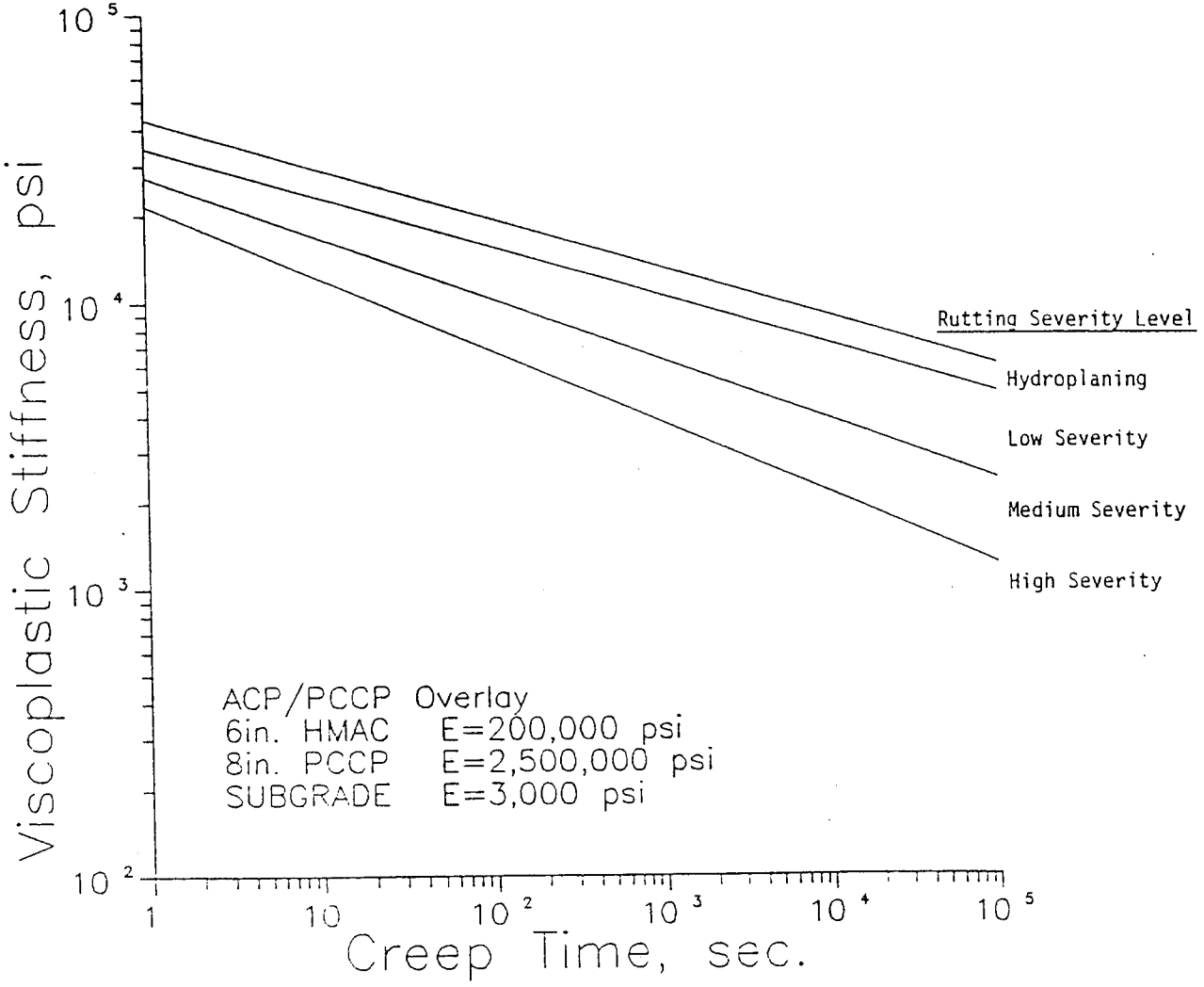
Viscoplastic Stiffness, psi
10^5
10^4
10^3
10^2
1
10
10^2
10^3
10^4
10^5
Creep Time, sec.
Rutting Severity Level
Hydroplaning
Low Severity
Medium Severity
High Severity
ACP/PCCP Overlay
6in. HMAC E=200,000 psi
8in. PCCP E=2,500,000 psi
SUBGRADE E=3,000 psi

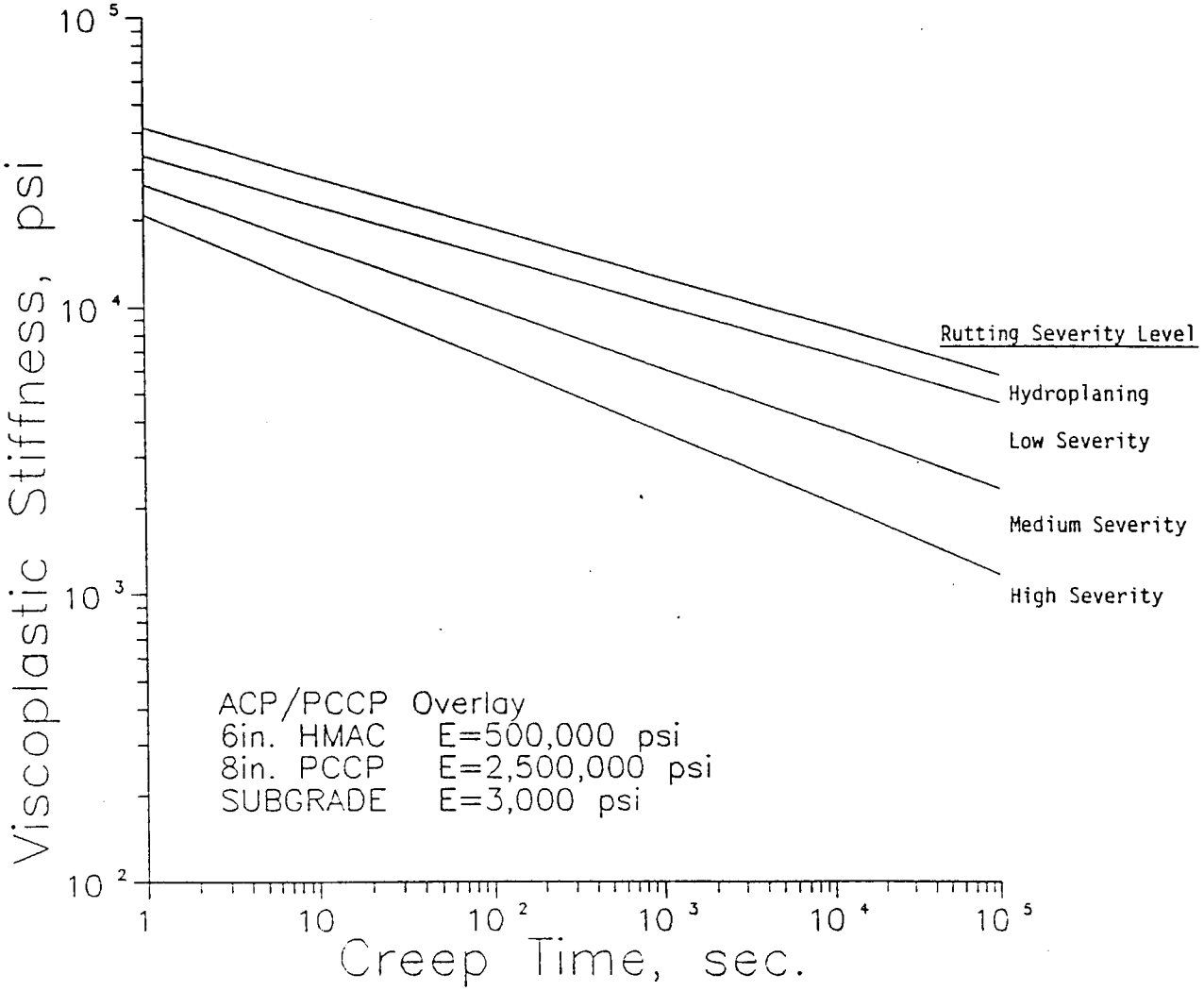
Viscoplastic Stiffness, psi
10^5
10^4
10^3
10^2
1
10
10^2
10^3
10^4
10^5
Creep Time, sec.
Rutting Severity Level
Hydroplaning
Low Severity
Medium Severity
High Severity
ACP/PCCP Overlay
6in. HMAC E=500,000 psi
8in. PCCP E=2,500,000 psi
SUBGRADE E=3,000 psi

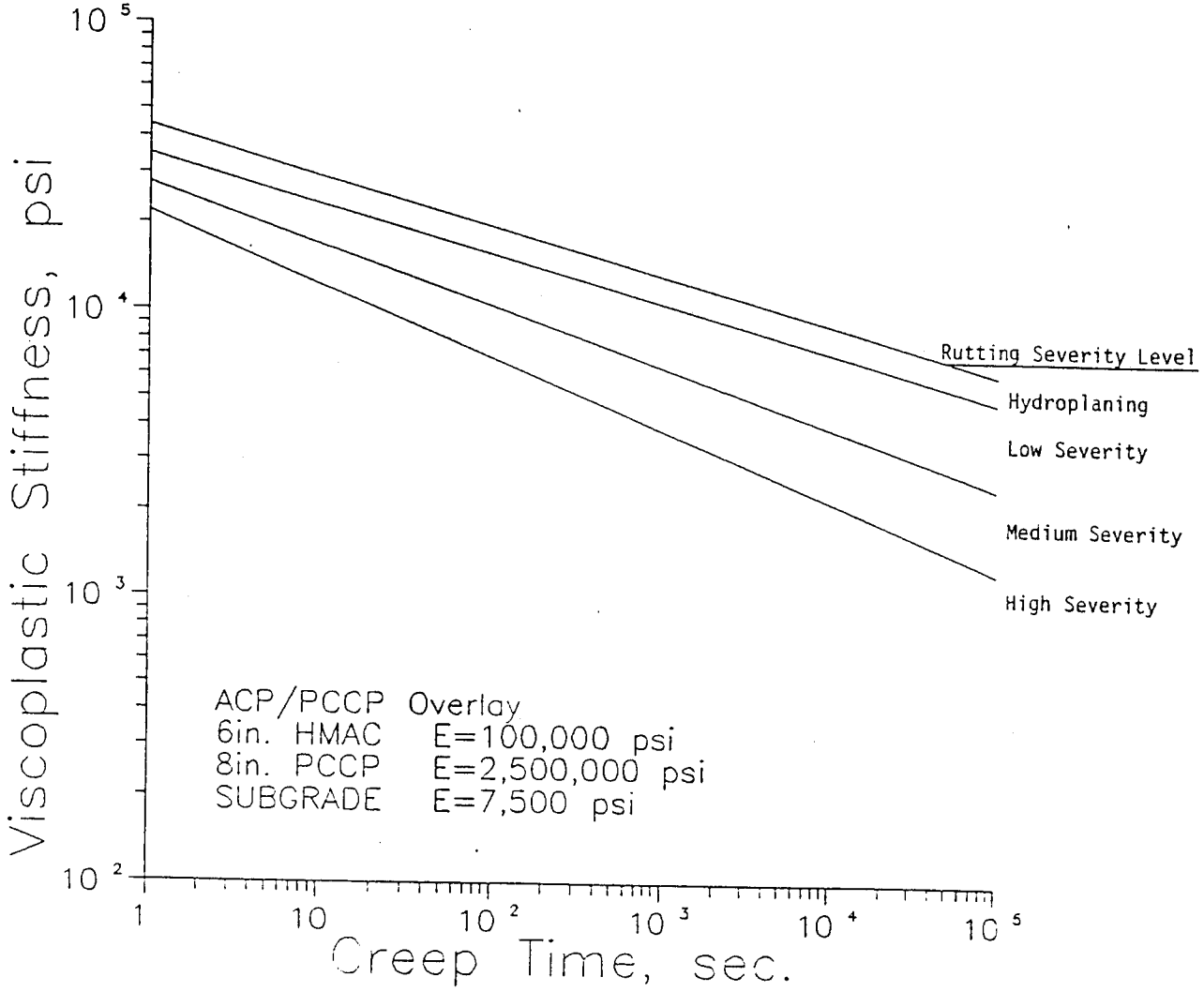
Viscoplastic Stiffness, psi
10 5
10 4
10 3
10 2
1
10
10 2
10 3
10 4
10 5
Creep Time, sec.
Rutting Severity Level
Hydroplaning
Low Severity
Medium Severity
High Severity
ACP/PCCP Overlay
6in. HMAC E=100,000 psi
8in. PCCP E=2,500,000 psi
SUBGRADE E=7,500 psi

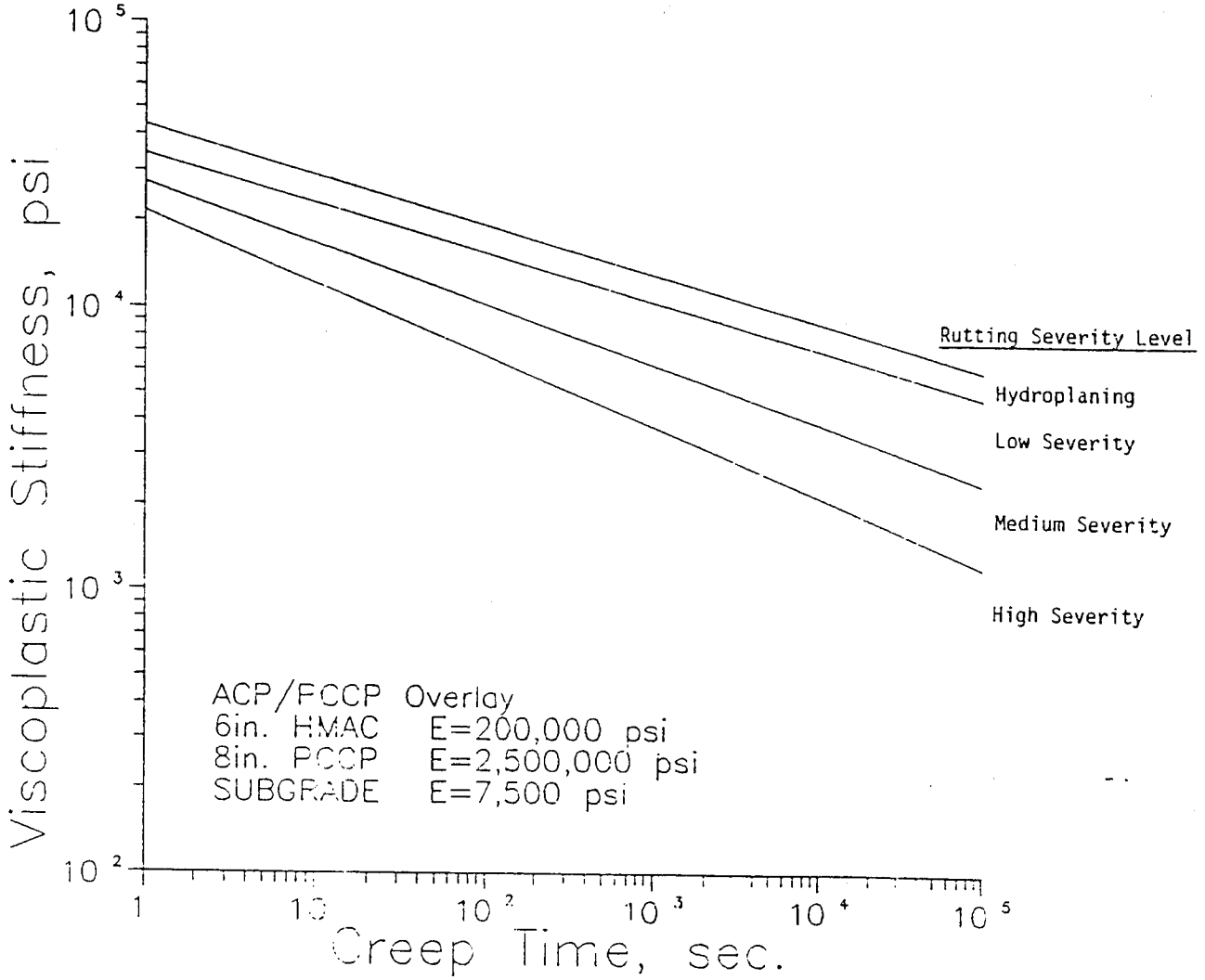
Viscoplastic Stiffness, psi
10^5
10^4
10^3
10^2
1
10
10^2
10^3
10^4
10^5
Creep Time, sec.
Rutting Severity Level
Hydroplaning
Low Severity
Medium Severity
High Severity
ACP/PCCP Overlay
6in. HMAC E=200,000 psi
8in. PCCP E=2,500,000 psi
SUBGRADE E=7,500 psi

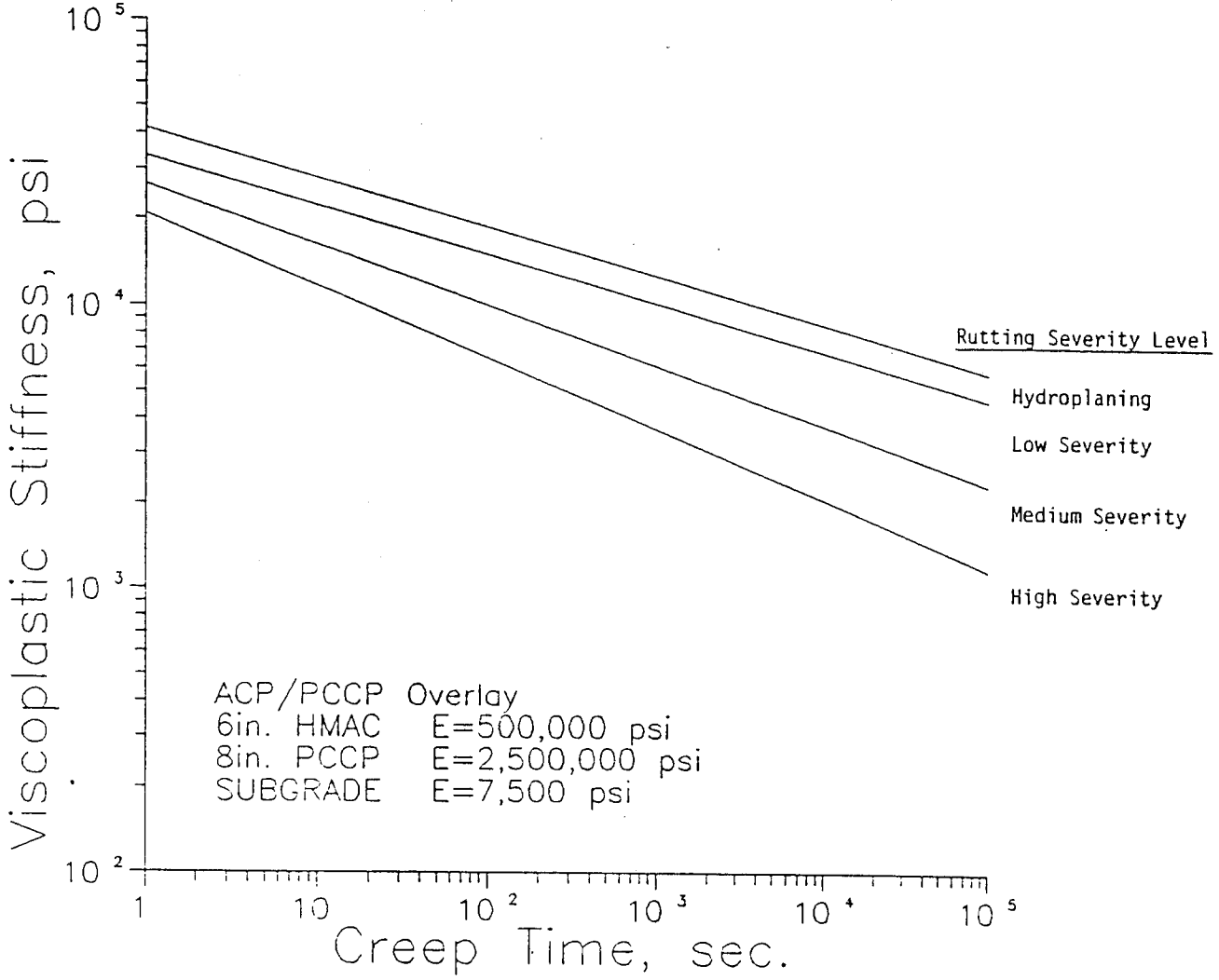
Viscoplastic Stiffness, psi
10 5
10 4
10 3
10 2
1
10
10 2
10 3
10 4
10 5
Creep Time, sec.
Rutting Severity Level
Hydroplaning
Low Severity
Medium Severity
High Severity
ACP/PCCP Overlay
6in. HMAC E=500,000 psi
8in. PCCP E=2,500,000 psi
SUBGRADE E=7,500 psi

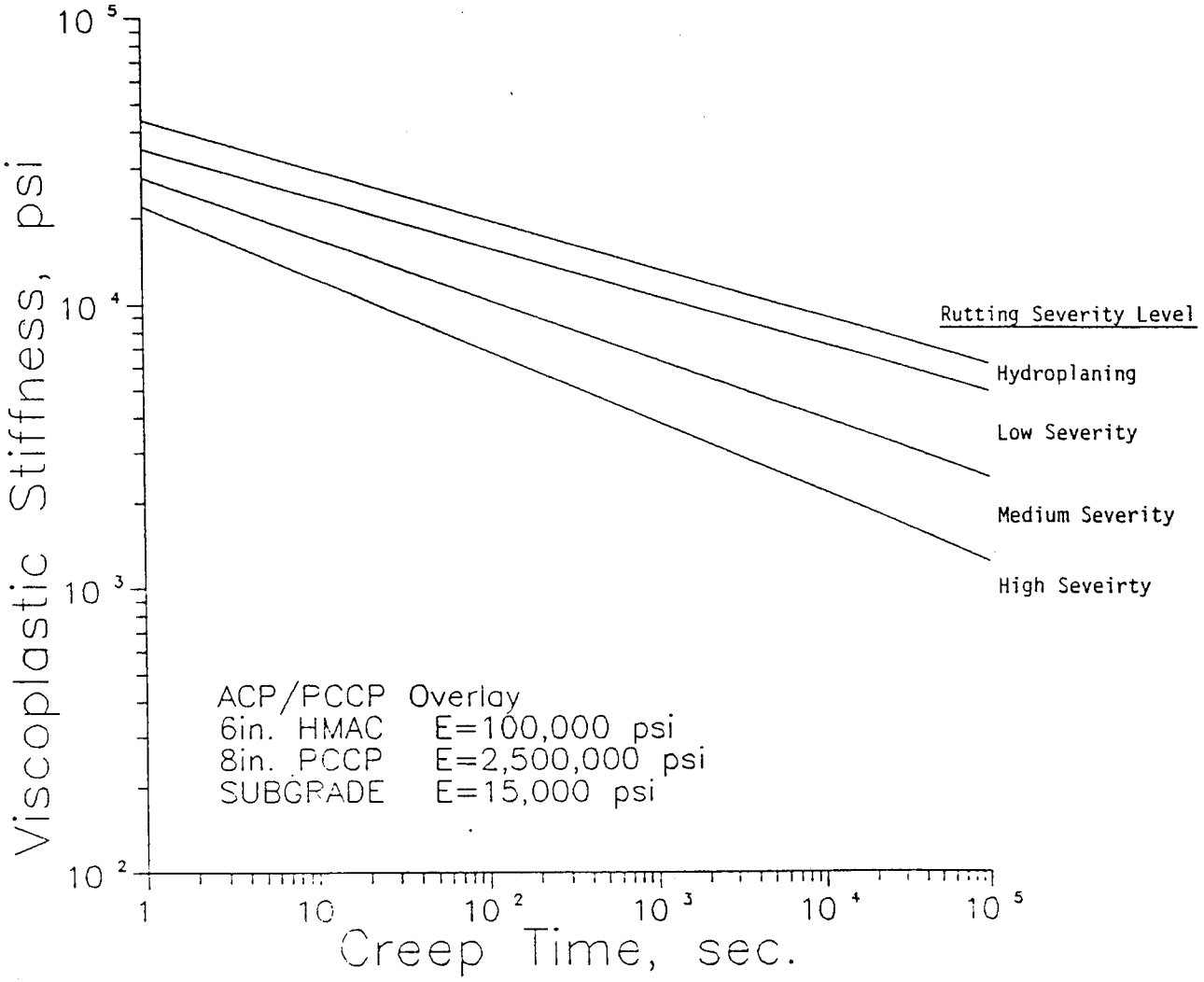
Viscoplastic Stiffness, psi
10^5
10^4
10^3
10^2
1
10
10^2
10^3
10^4
10^5
Creep Time, sec.
Rutting Severity Level
Hydroplaning
Low Severity
Medium Severity
High Seveirty
ACP/PCCP Overlay
6in. HMAC E=100,000 psi
8in. PCCP E=2,500,000 psi
SUBGRADE E=15,000 psi

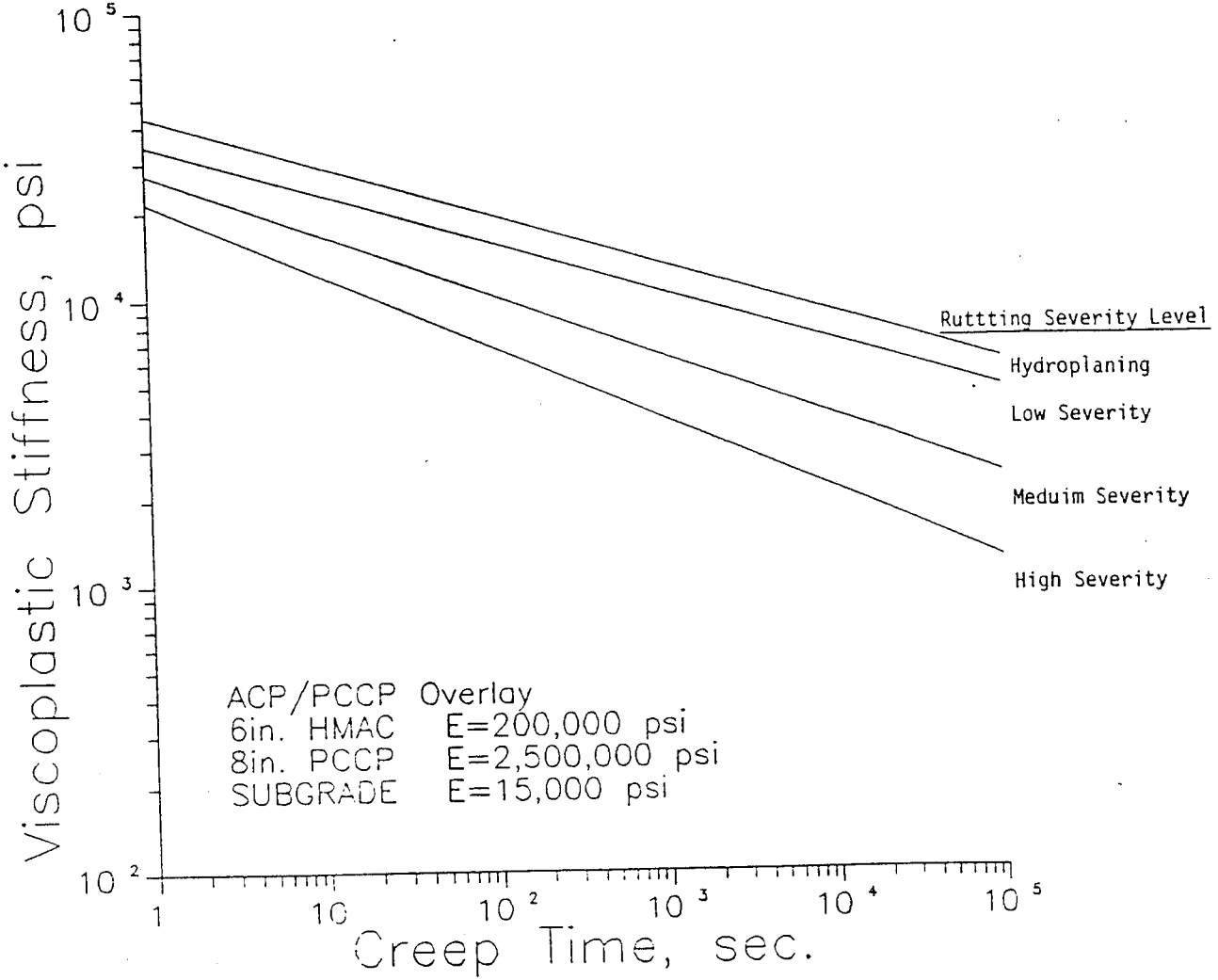
Viscoplastic Stiffness, psi
10^5
10^4
10^3
10^2
1
10
10^2
10^3
10^4
10^5
Creep Time, sec.
Ruttting Severity Level
Hydroplaning
Low Severity
Meduim Severity
High Severity
ACP/PCCP Overlay
6in. HMAC E=200,000 psi
8in. PCCP E=2,500,000 psi
SUBGRADE E=15,000 psi

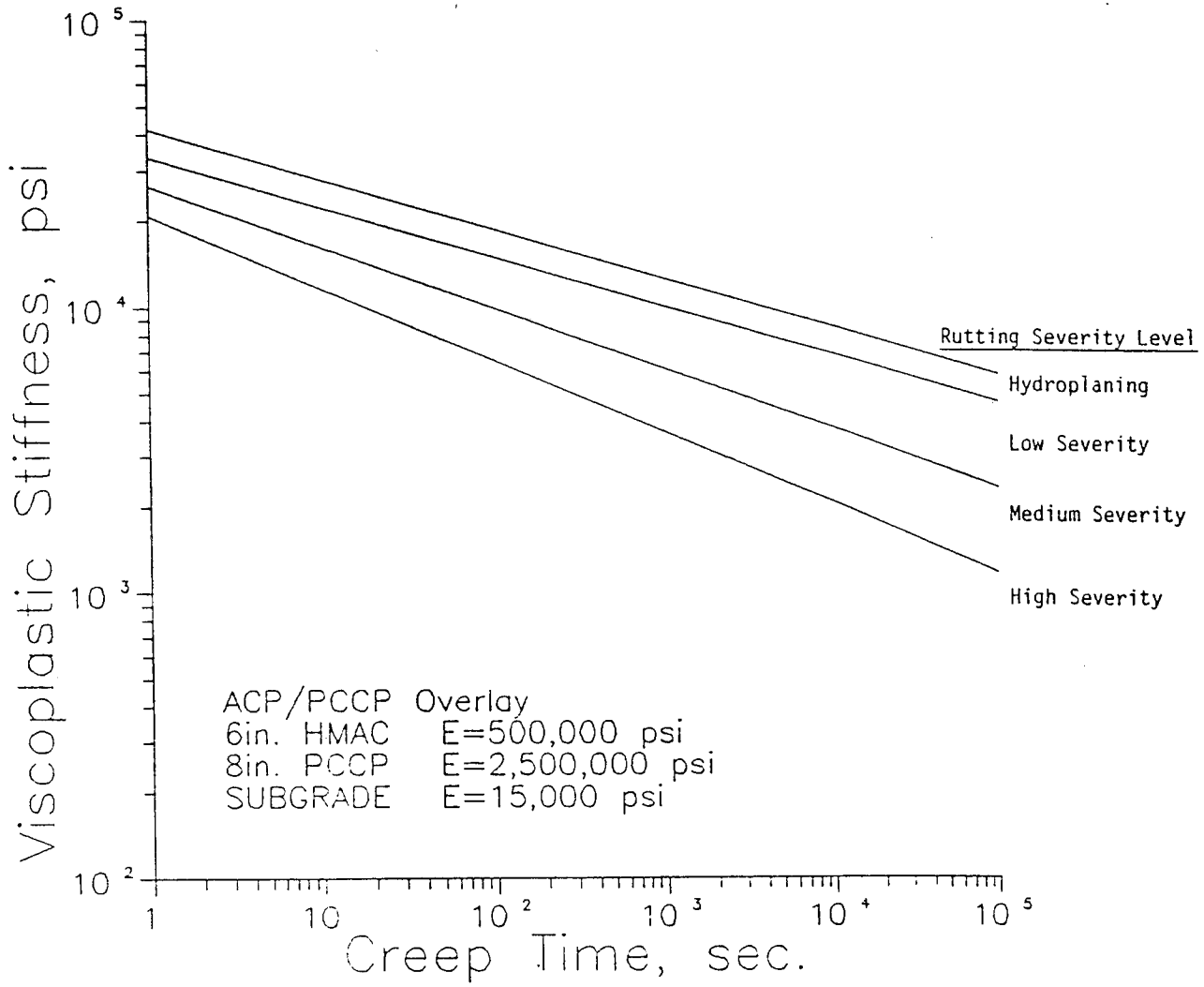
Viscoplastic Stiffness, psi
10^5
10^4
10^3
10^2
1
10
10^2
10^3
10^4
10^5
Creep Time, sec.
Rutting Severity Level
Hydroplaning
Low Severity
Medium Severity
High Severity
ACP/PCCP Overlay
6in. HMAC E=500,000 psi
8in. PCCP E=2,500,000 psi
SUBGRADE E=15,000 psi

APPENDIX C

RUTTING NOMOGRAPHS

APPENDIX C

RUTTING NOMOGRAPHS

General

As it was discussed in Chapter VI, a wide variety of variables in the rutting prediction model had to be accommodated through a series of nomographs. The rutting charts that are presented in Appendix B are for a very specific set of conditions that are stated on each chart. Improvements in three major areas were made to these charts in order to broaden their scope and application. These areas of improvements are:

a) A much broader range of layer moduli ratios was incorporated into the methodology (Tables C1 and C2). The effect of this on the distribution of vertical compressive stresses was summarized in the form of Z-Factor tables.
b) The limitation of a fixed traffic level, one million 18 kip equivalent single axle loads (ESAL), was removed through the direct use of creep/recovery data corresponding to any given level of traffic.
c) A rutting calculation example is provided which incorporates the effect of temperature and traffic distributions.

Procedure

The following is a stepwise procedure by which one can predict the rutting potential of an asphaltic concrete mixture. The procedure is based on a series of nomograph charts. The steps involved in each chart are given along with a hypothetical example. The example represents an HMAC which is identical to the mixture used in the Highway 21, Burleson County Project. Table C3 summarizes the temperature and traffic data. Total traffic is assumed to be 400 passes of 18 kip ESAL's per day. Tables C4 through C7 were reported by Li (24) for different climatic regions of Texas which was decribed in Figure 20, Page 33. Each table contains information regarding different temperature profiles and their durations. Table C3 was derived by Li (24) based on regression parameters that are presented in Table C4.

Table C1. Summary of flexible pavement layer moduli

Modular Replicates	Layer Moduli (Psi)		
	$E_{surface}$	E_{base}	$E_{subgrade}$
1	100,000	15,000	3,000
2	200,000	20,000	7,500
3	500,000	30,000	15,000

Table C2. Summary of HMAC/PCCP layer moduli

Modular Replicates	Layer Moduli (Psi)		
	$E_{surface}$	E_{PCC}	$E_{subgrade}$
1	100,000	2,500,000	3,000
2	200,000	2,500,000	7,500
3	500,000	2,500,000	15,000

Table C3. Temperature and traffic distributions of a 3-inch asphalt overlay structure constructed in Region II (Figure 20). (This table is from Reference 24 for typical temperature profiles for HMAC layers in each region of Texas.

Profile No.	Temperature (°F)	Sub-layer Temp. (°F) 1	2	3	% Time	% Traffic
1	< 75	68	70	72	25.69	18.24
2	75-85	79	81	82	25.69	19.97
3	86-95	90	89	88	14.93	18.70
4	96-105	100	97	94	14.70	17.72
5	105-115	110	105	101	12.15	17.87
6	115-125	118	112	107	6.82	7.50
		TOTAL			100	100

Table C4. Temperature profile of asphalt overlay structures constructed in Region I (Figure 20).

Profile No.	Temperature (°F)	Sublayer (°F) 1	2	3	4	5	% Time
1	< 75	64	67	69	70	72	45.25
2	75-85	80	80	80	80	80	16.67
3	85-95	90	87	84	82	80	12.62
4	95-105	100	95	91	88	85	13.77
5	105-115	110	104	99	95	91	11.69
			TOTAL				72

Table C5. Temperature profile of asphalt overlay structures constructed in Region II (Figure 20).

Profile No.	Temperature (°F)	Sublayer (°F) 1	2	3	4	5	% Time
1	< 75	68	70	72	74	75	25.58
2	75-85	79	81	82	84	85	25.81
3	85-95	90	89	88	87	86	15.05
4	95-105	100	97	94	91	88	14.58
5	105-115	110	105	101	97	94	12.15
6	115-125	118	112	107	103	99	6.83
			TOTAL				100

Table C6. Temperature profile of asphalt overlay structures constructed in Region III (Figure 20).

Profile No.	Temperature (°F)	Sublayer (°F) 1	2	3	4	5	% Time
1	< 75	67	70	72	74	75	36.00
2	75-85	80	81	82	83	84	18.98
3	85-95	90	88	87	86	84	12.96
4	95-105	100	96	93	90	87	12.73
5	105-115	110	105	100	96	92	14.58
6	115-125	117	111	105	100	96	4.75
			TOTAL				100

Table C7. Temperature profile of asphalt overlay structures constructed in Region IV (Figure 20).

Profile No.	Temperature (°F)	Sublayer (°F) 1	2	3	4	5	% Time
1	< 75	69	71	73	75	76	22.92
2	75-85	79	81	83	84	85	27.08
3	85-95	90	89	88	88	87	16.55
4	95-105	101	97	94	91	88	13.66
5	105-115	110	105	101	97	94	12.73
6	115-125	118	112	107	102	98	7.06
			TOTAL				100

Figure C1:

a) Select the appropriate Z-Factor from Tables C8 through C11.

b) Based on this selected Z-Factor, and the tire pressure (σ_o), one can arrive at the value of the $Z\sigma_o$-parameter (Figure C1).

Example:

- Nominal layer moduli

  $E_{surface}$ = 200,000 psi (replicate: 2)

  E_{PCC} = 2,500,000 psi (replicate: 1)

  $E_{subgrade}$ = 7,500 psi

  Structural classification = 212

  From left to right, each digit in structural classification number refers to the modular replicate numbers for surface, base, and subgrade, respectively (Tables C1 and C2).

  Z-factor = 0.96

- Average stress within the HMAC layer
- Tire pressure = 100 psi

  $Z\sigma_o$ = 96 psi (Figure C1)

Figure C2

a) The ratio of $Z\sigma_o$-parameter to the creep stress, σ_{lab}, is arrived at through Figure C2.

b) The effect of nonlinearities in the lab-to-field projections is accounted for by the 1.61 exponent (Figure C2).

Example:

$$\frac{Z\sigma_o}{\sigma_{lab}} = \frac{96 \text{ psi}}{14.5 \text{ psi}} = 6.62$$

$$\left[\frac{Z\sigma_o}{\sigma_{lab}}\right]^{1.61} = \left[6.62\right]^{1.61} = 20.97$$

Figure C3

a) From creep data (plot of ϵ_{vp} versus time of loading) determine the ϵ_{vp} values associated with a specific time interval. This is accomplished by multiplying the number of 18 kip ESAL's

Table C8. Z-Factors for Thick Flexible Pavements

Layer Modulus Designation (surface, base, subgrade)*	Z-Factor
111	0.58
211	0.56
311	0.53
121	0.60
221	0.57
321	0.53
131	0.19
231	0.58
331	0.55
112	0.59
212	0.56
312	0.53
122	0.60
222	0.57
322	0.54
132	0.62
232	0.59
332	0.55
113	0.59
213	0.56
313	0.53
123	0.60
223	0.57
323	0.54
133	0.62
233	0.59
333	0.55

* Numbers refer to modular replicates, Tables C1 and C2.

Table C9. Z-Factors for Thin Flexible Pavements

Layer Modulus Designation (surface, base, subgrade)*	Z-Factor
111	0.84
211	0.77
311	0.68
121	0.87
221	0.80
321	0.70
131	0.90
231	0.84
331	0.74
112	0.86
212	0.79
312	0.70
122	0.88
222	0.81
322	0.72
132	0.91
232	0.85
332	0.75
113	0.87
213	0.80
313	0.71
123	0.89
223	0.82
323	0.73
133	0.92
233	0.86
333	0.76

* Numbers refer to modular replicates, Tables C1 and C2.

Table C10. Z-Factors for Intermediate Flexible Pavements

Layer Modulus Designation (surface, base, subgrade)*	Z-Factor
111	0.80
211	0.73
311	0.65
121	0.83
221	0.76
321	0.67
131	0.86
231	0.80
331	0.70
112	0.80
212	0.73
312	0.65
122	0.83
222	0.76
322	0.67
132	0.87
232	0.80
332	0.71

* Numbers refer to modular replicates, Tables C1 and C2.

Table C11. Z-Factors for Overlay Pavements (ACCP/PCCP)

Layer Modulus Designation (surface, base, subgrade)	Z-Factor
111	0.97
211	0.96
311	0.94
112	0.97
212	0.96
312	0.94
113	0.97
213	0.96
313	0.94

* Numbers refer to modular replicates, Tables C1 and C2.

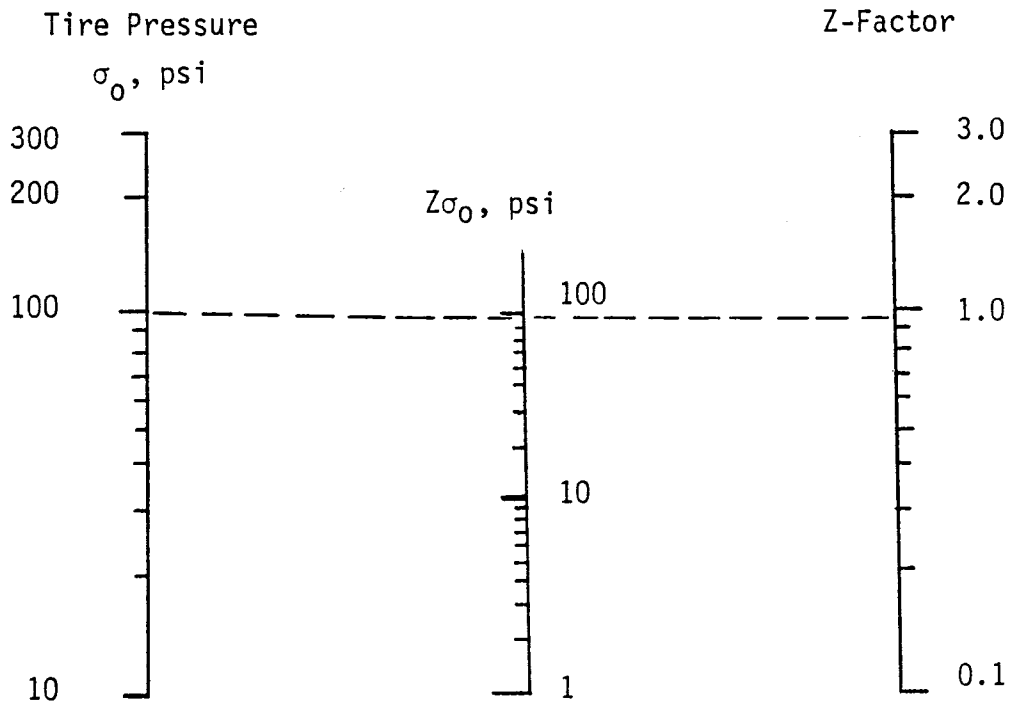

Figure C1: Nomographic solution for transformation of tire pressure into an average condition of compressive stress within the HMAC layer defined by the Z-factor.

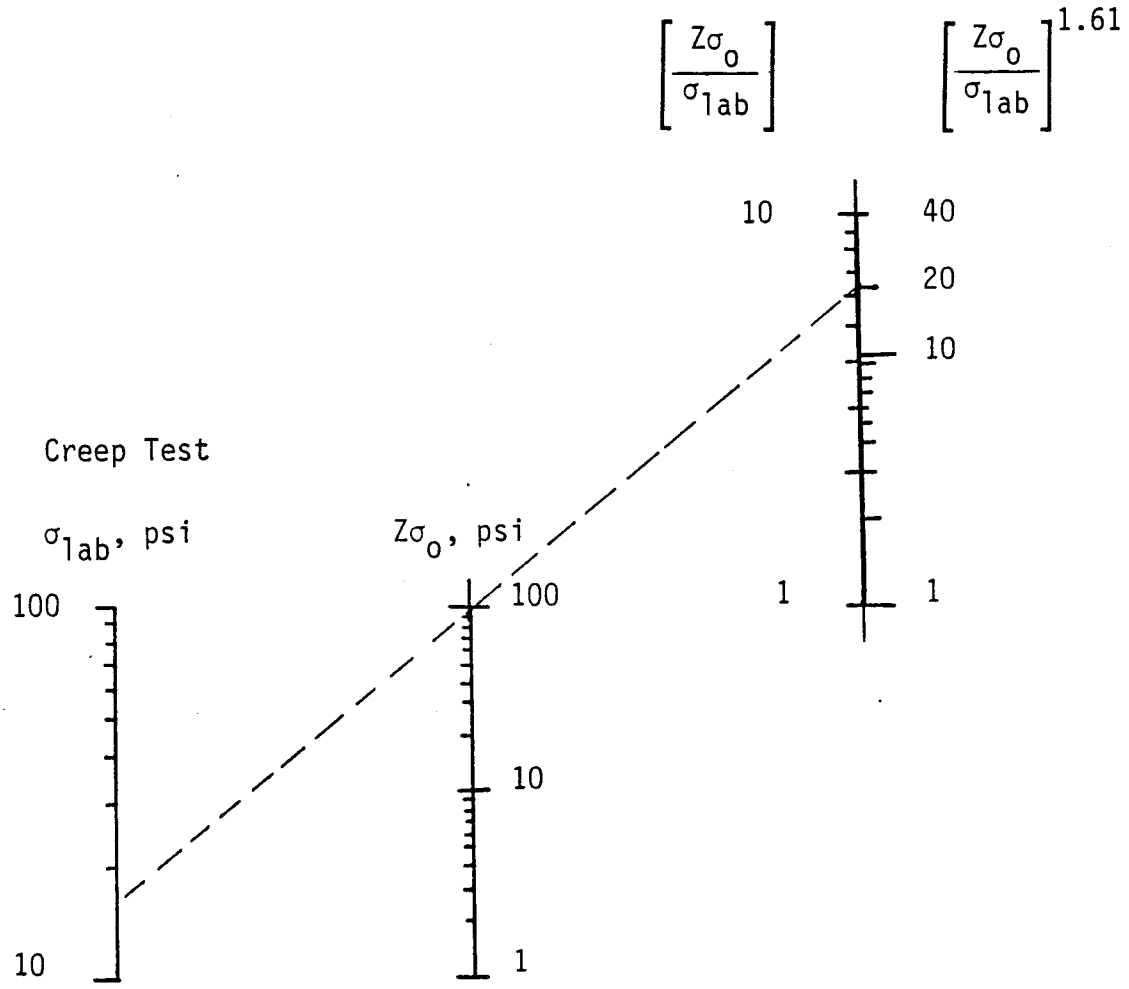

Figure C2: Nomographic solution for nonlinear transformation of creep-stress into the predicted pavement stresses.

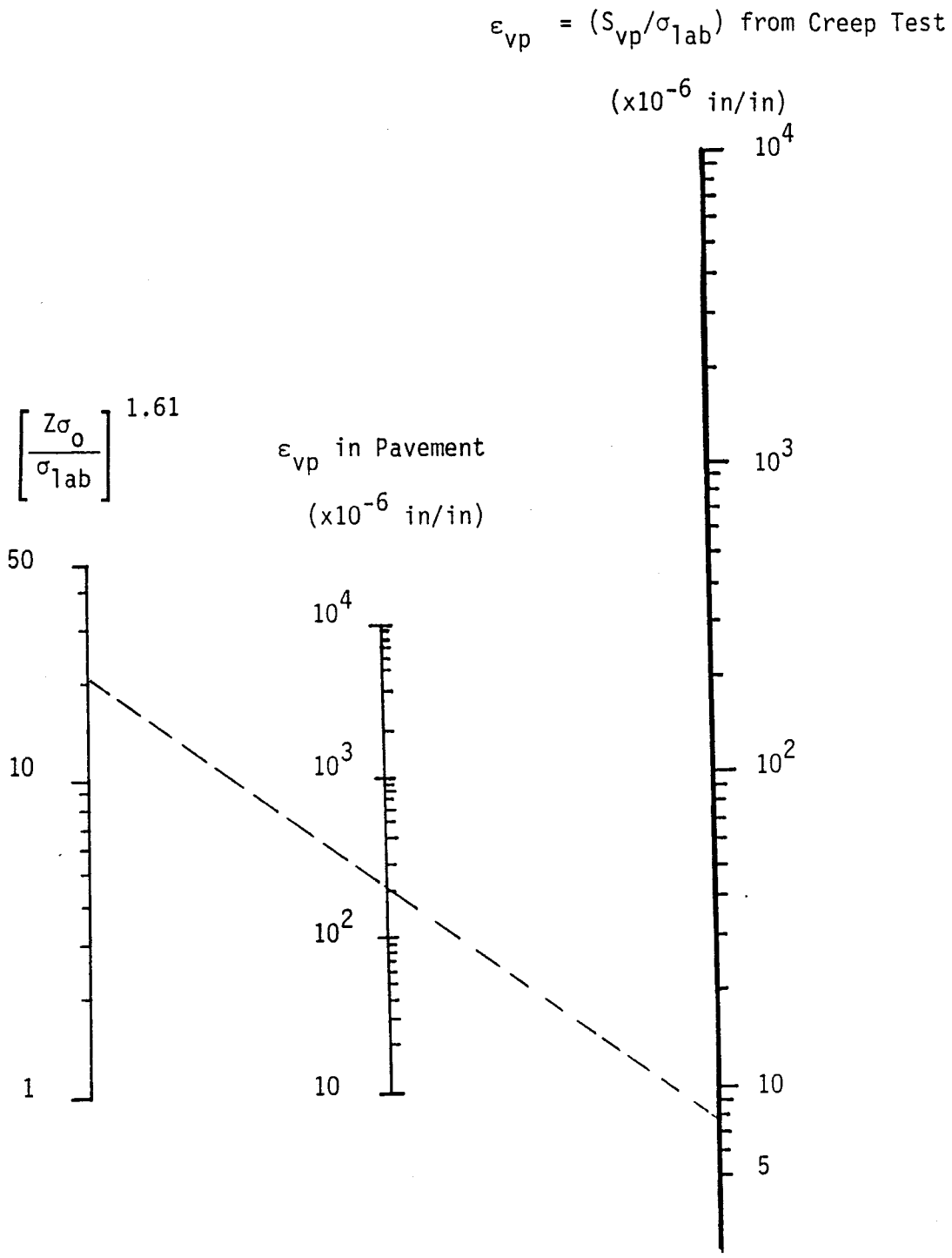

Figure C3: Nomographic solution for a nonlinear transformation of viscoplastic strains measured during the creep test into the predicted pavement deformations.

applied during the time interval by the dwell time for each load application. A dwell time of between 0.01 and 0.1 seconds is typically used in such analyses (43, 46). These results are recorded in column 5 of Tables C12 through C14.

b) Calculate the viscoplastic stiffness of HMAC corresponding to each temperature profile (profiles 1 through 6) by dividing the viscoplastic strains (column 5) by the laboratory creep stress and record the results in column 6 of Tables C12 through C14.

c) Based on the average pavement temperture for each sublayer, calculate the shift factor for the creep data from Figure 74, Page 119. In the example, the creep data were determined at 70°F. Thus, the shift factor for Profile 1, sublayer #3 (Table C12) is based on a $\Delta T = -2$. For this condition, log $a_T = +0.20$. These values are recorded in column 4 of Tables C12 through C14.

d) The shifted $S_{vp}(t)$ values are recorded in column 7 of Tables C12 through C14. Using Figure C3, one can arrive at numbers recorded in column 8 of Tables C12 through C14.

Figure C4

a) Calculate the rut depth in the pavement based on the thickness of HMAC and the information recorded in column 8 of Tables C12 through C14.

b) The summation of rut depths, recorded in the last column of tables C12 through C14, represents the daily rut depth predicted for the critical portion of each year (April through October).

Table C10. Rutting calculations for the bottom one inch portion of the 3 inch ACP/PCCP overlay example problem.

Profile No.	Pavement Temperature (°F)	Traffic (18 kip ESAL's)	Shift Factor log (a_T)	Creep/Recovery Data			Field Projections	
				$\epsilon_{vp}(t)$* (x10^{-6} in/in)	$S_{vp}(t)$ (x10^{6} psi)	Shifted $S_{vp}(t)$	$\left[\frac{S_{vp}}{\sigma_{lab}}\right] \cdot \left[\frac{Z\sigma_o}{\sigma_{lab}}\right]^{1.61}$ (x10^{-6} in/in)	Rut Depth (in.)
1	68	73	+0.20	7.75	1.871	2.9653	102.5416	1.03x10^{-4}
2	79	80	-0.35	7.83	1.852	0.6277	367.3590	3.70x10^{-4}
3	90	75	-0.40	7.77	1.866	0.7429	409.3123	4.10x10^{-4}
4	100	71	-0.50	7.73	1.876	0.5932	512.5468	5.12x10^{-4}
5	110	72	-0.55	7.74	1.873	0.5279	576.0080	5.76x10^{-4}
6	118	29	-0.65	7.01	2.0685	0.4631	656.6152	6.57x10^{-4}

ADT = 400 (equivalent to 1.46x10^5/year).

Daily rut depth in sublayer #1 = 2.63 x 10^{-3} in/day.

Annual rut depth, April through October, in sublayer #1 = 0.552 in.

* Numbers are determined from data presented in Appendix D for District 17 Project.

Table C11. Rutting calculations for the middle one inch portion of the 3 inch ACP/PCCP overlay example problem.

Profile No.	Pavement Temperature (°F)	Traffic (18 kip ESAL's)	Shift Factor log (a_T)	Creep/Recovery Data			Field Projections	
				$\epsilon_{vp}(t)$* (x10^{-6} in/in)	$S_{vp}(t)$ (x10^{6} psi)	Shifted $S_{vp}(t)$	$\left[\frac{S_{vp}}{\sigma_{lab}}\right] \cdot \left[\frac{Z\sigma_o}{\sigma_{lab}}\right]^{1.61}$ (x10^{-6} in/in)	Rut Depth (in.)
1	70	73	0	7.75	1.871	1.8710	102.5416	1.03x10^{-4}
2	81	80	7.83	7.83	1.852	1.4711	206.6923	2.07x10^{-4}
3	89	75	7.77	7.77	1.866	0.7429	409.2947	4.09x10^{-4}
4	97	71	7.73	7.73	1.876	0.6656	456.8284	4.57x10^{-4}
5	105	72	7.74	7.74	1.873	0.5256	537.5972	5.38x10^{-4}
6	112	29	7.01	7.01	2.0685	0.5697	533.7158	5.33x10^{-4}

ADT = 400 (equivalent to 1.46x10^5/year).

Daily rut depth in sublayer #2 = 2.25 x 10^{-3} in.

Annual rut depth, April through October, in sublayer #2 = 0.472 in.

* Numbers are determined from data presented in Appendix D for District 17 Project.

Table C12. Rutting calculations for the top one inch portion of the 3 inch ACP/PCCP overlay example problem.

Profile No.	Pavement Temperature (°F)	Traffic (18 kip ESAL's)	Shift Factor log (a_T)	Creep/Recovery Data $\epsilon_{vp}(t)$* (x10^{-6} in/in)	$S_{vp}(t)$ (x10^{6} psi)	Shifted $S_{vp}(t)$	Field Projections $\left[\frac{S_{vp}}{\sigma_{lab}}\right] \cdot \left[\frac{Z\sigma_o}{\sigma_{lab}}\right]^{1.61}$ (x10^{-6} in/in)	Rut Depth (in.)
1	72	73	-0.05	7.75	1.871	1.8710	102.5416	1.03x10^{-4}
2	82	80	-0.10	7.83	1.852	1.4711	206.6923	2.07x10^{-4}
3	88	75	-0.40	7.77	1.866	0.7429	409.2947	4.09x10^{-4}
4	94	71	-0.43	7.73	1.876	0.6970	436.2482	4.36x10^{-4}
5	101	72	-0.50	7.74	1.873	0.5923	513.3632	5.13x10^{-4}
6	107	29	-0.53	7.01	2.0685	0.6105	498.0590	4.98x10^{-4}

ADT = 400 (equivalent to 1.46x10^{5}/year).

Daily rut depth in sublayer #3 = 2.63 x 10^{-3} in/day.

Annual rut depth, April through October, in sublayer #3 = 0.552 in.

* Numbers are determined from data presented in Appendix D for District 17 Project.

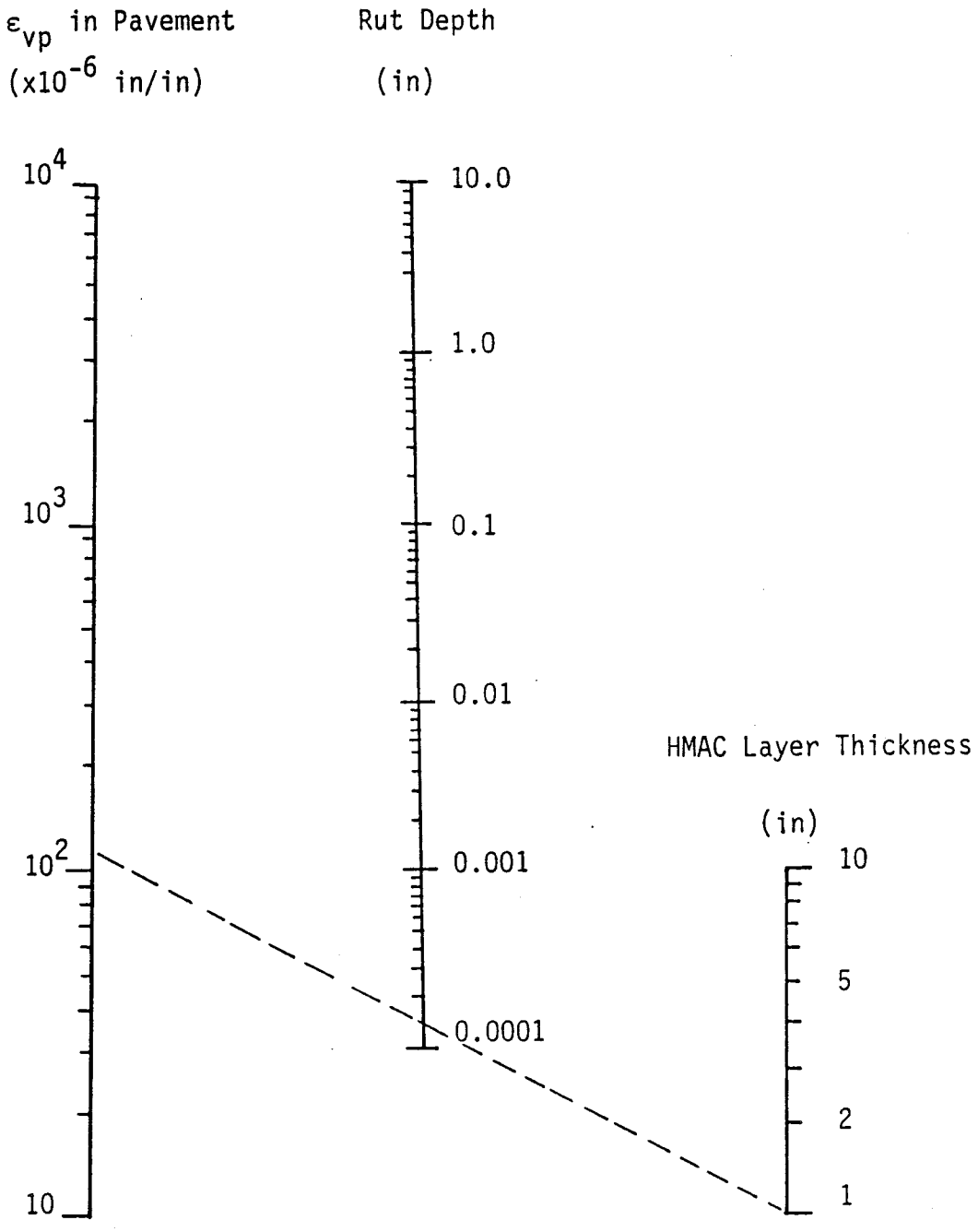

Figure C4: Nomographic solution for determination of the rut depth from creep/recovery data.

APPENDIX D

PROCEDURE OUTLINE AND DESIGN EXAMPLE

APPENDIX D

PROCEDURE OUTLINE AND DESIGN EXAMPLE

A hypothetical mix design example is presented in this section in order to demonstrate the procedures involved in a fully integrated fashion.

The design/analysis procedure presented in this study is considered to be complimentary to and will build on the existing Texas SDHPT method (3) which specifies an air void content of three percent and acceptable stability based on the Hveem procedure (1).

The procedure outlined below is illustrated using the following hypothetical example:

Pavement Identification:	U.S. Highway 21 in Burleson County, Texas (District 17).
Pavement Structural Category:	Intermediately thick, flexible pavement, new construction.
Climatic Region:	Region III, according to Figure 20, page 33.
Subgrade Properties:	Subgrade is a moderately plastic clay with a Texas Triaxial Classification of 5.0. From Figure D1, the approximate subgrade resilient modulus is 5,000 psi. However, subgrade stabilization with lime has improved the supporting value of the subgrade increasing the triaxial classification to 3.5 (approximate resilient modulus of 15,000 psi). Thus, the supporting value is considered to be relatively strong.

The following is a step-by-step procedure by which this hypothetical mixture is to be analyzed.

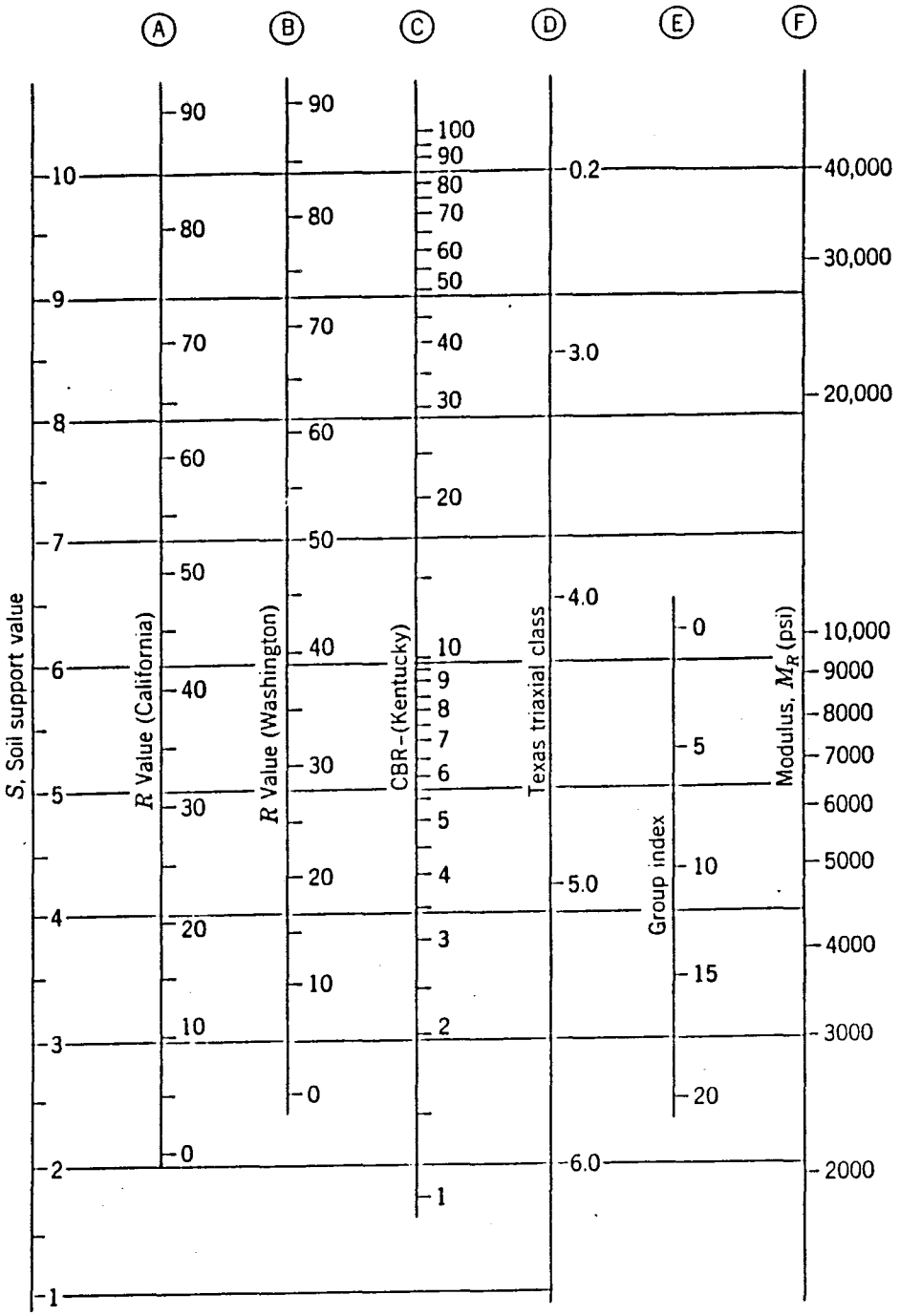

Figure D1. Soil support value correlations (after Reference 33).

Basic Design

1. Design the asphaltic mixture under investigation according to the Texas Test Method (3).

Field Conditions

2. Acquire the following information regarding the pavement structure in the field:
   - 2.1 Structural design (layer thickness, materials, subgrade strength, etc.).
   - 2.2 Climatic conditions: location within the state and mean annual air temperature, Figures 20, page 33, and 17, page 28, respectively. Select the proper climatic region and the associated critical design temperature for rutting evaluation (Table 1, page 32).
   - 2.3 Traffic level to which the pavement is subjected.

Structural Soundness

3. Investigate the structural soundness in terms of the HMAC layer stiffness.
   - 3.1 Measure the resilient modulus of the mixture under investigation at four temperatures (0°F, 32°F, 77°F, and 104°F). Figure D2 illustrates the typical data on the District 17 mixture.
   - 3.2 Determine the mean annual pavement temperature, representing the geographical location of District 17, from Figures 17, page 28, and 33, page 53.
   - 3.3 Evaluate the resilient modulus of the mixture in question at the mean annual pavement temperature from Figure D2.
   - 3.4 Verify the adequacy of this mixture resilient modulus for the structural requirements according to the following steps:
     - 3.4.1 Establish the resilient modulus threshold for subgrade protection.
       - 3.4.1.1 Select the proper chart based on pavement category (Figures 29 through 32, pages 49 through 52). Select Figure 31, page 51, for

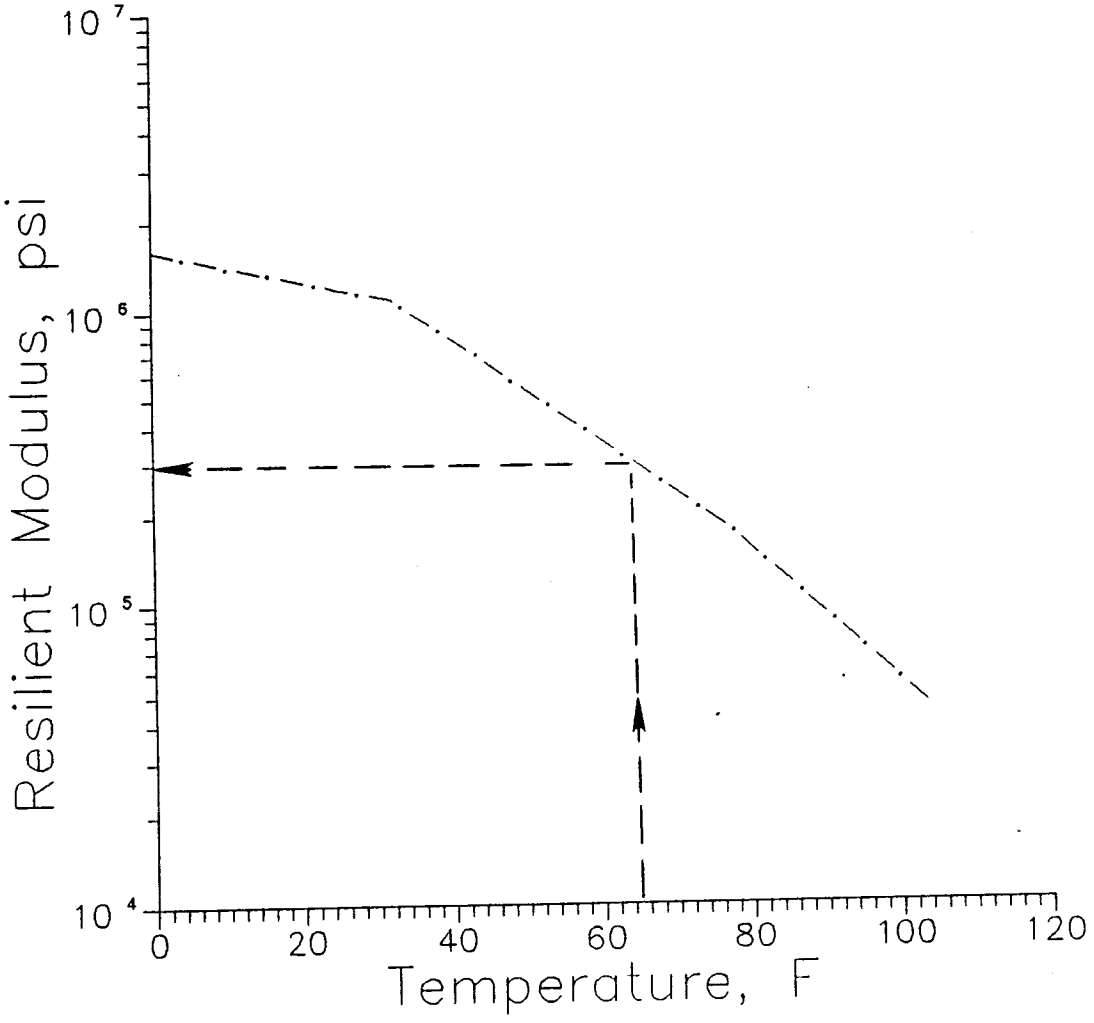

Figure D2. Resilient modulus versus temperature for the District 17 Project.

the District 17 project.

3.4.1.2 Evaluate the resilient modulus threshold based on the level of subgrade stiffness, and the design traffic level, for this example: 3 x 10^6 passes of 18 kip ESAL (using Figure 31, page 51). The resilient modulus of the mixture, determined in Step 3.3, should be equal to or greater than this threshold value or else mixture modifications will be necessary. The mixture for Highway 21 does satisfy this requirement (Figure D3), if lime stabilization of the subgrade is successfully accomplished and a subgrade modulus of 15,000 psi is achieved. It is later illustrated (Appendix E) that the HMAC used in this project does not offer adequate protection for a 7,500 psi subgrade.

Fatigue Analysis

4. Evaluate load-related fatigue performance.

4.1 Select the proper tensile strain chart based on the pavement structure in which the mixture is to be used, subgrade stiffness, and the resilient modulus threshold (Figures 34 through 36, pages 56 through 58). Figure 35, page 56, shall be used for the District 17 Project.

4.2 Enter into the proper chart selected from Step 4.1 with the resilient modulus of the mixture in question at the average annual pavement temperature, evaluated in Step 3.3, and determine the induced tensile strain in the asphalt layer. Figure D4 illustrates the data for District 17 as an example.

4.3 Enter into the fatigue criteria chart with the resilient modulus and the induced tensile strain; determine the fatigue performance potential of the mixture. Figure D5 depicts the fatigue performance of our example mixture which is relatively low (5 x 10^5 passes of 18 kip ESAL).

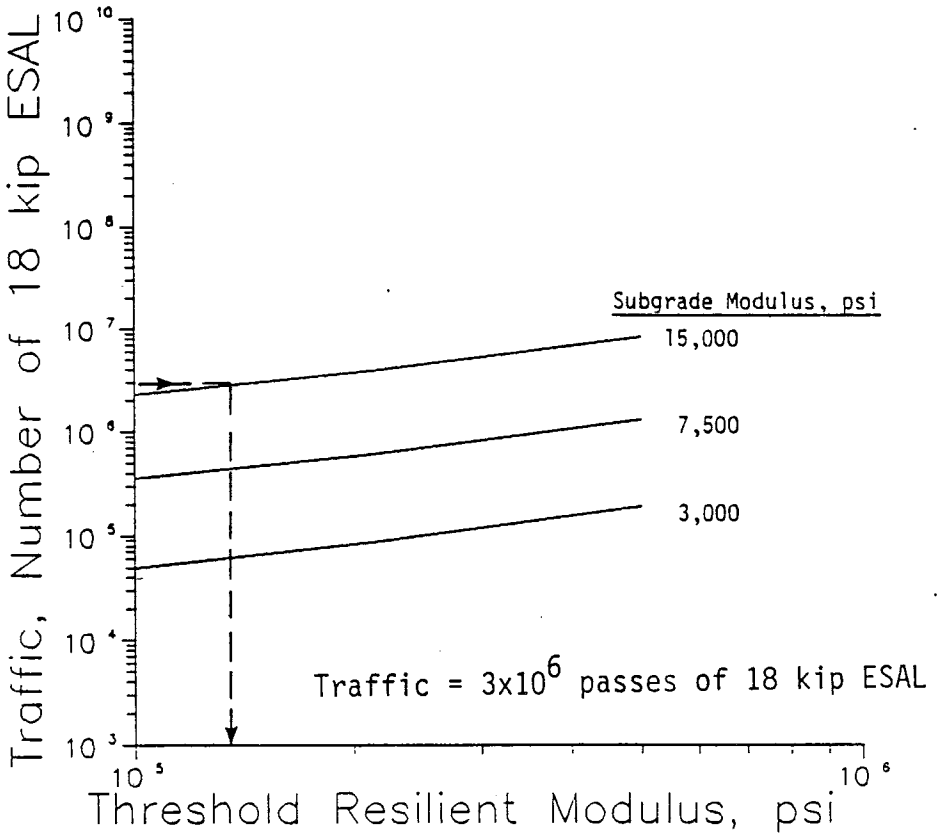

Figure D3. Threshold resilient modulus for District 17.

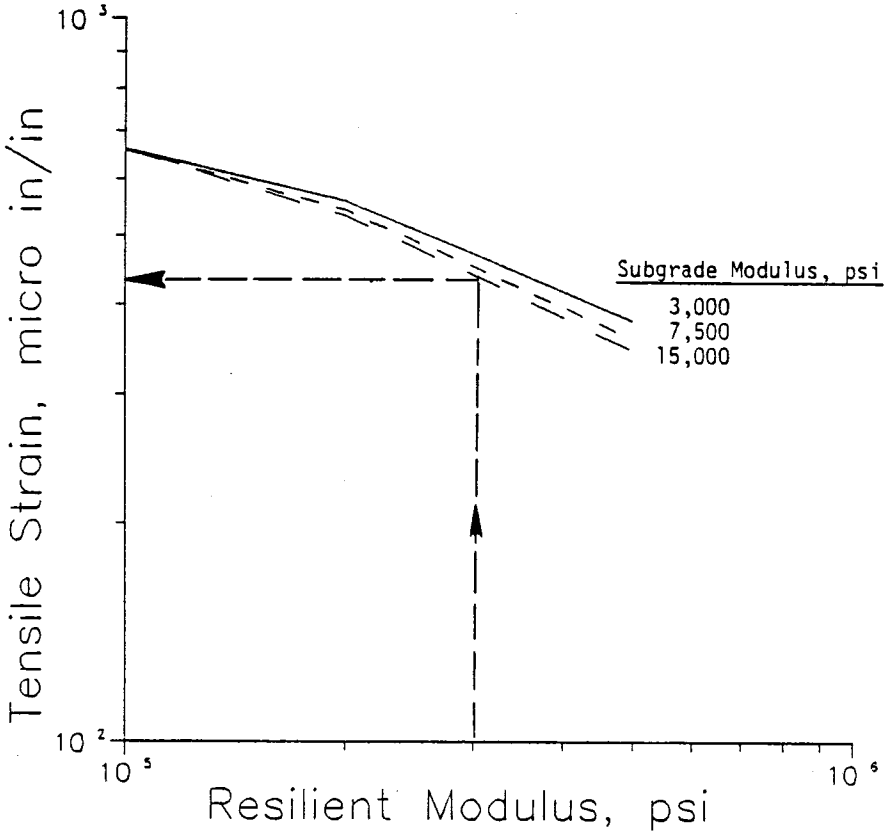

Figure D4. Induced tensile strain for District 17 Project.

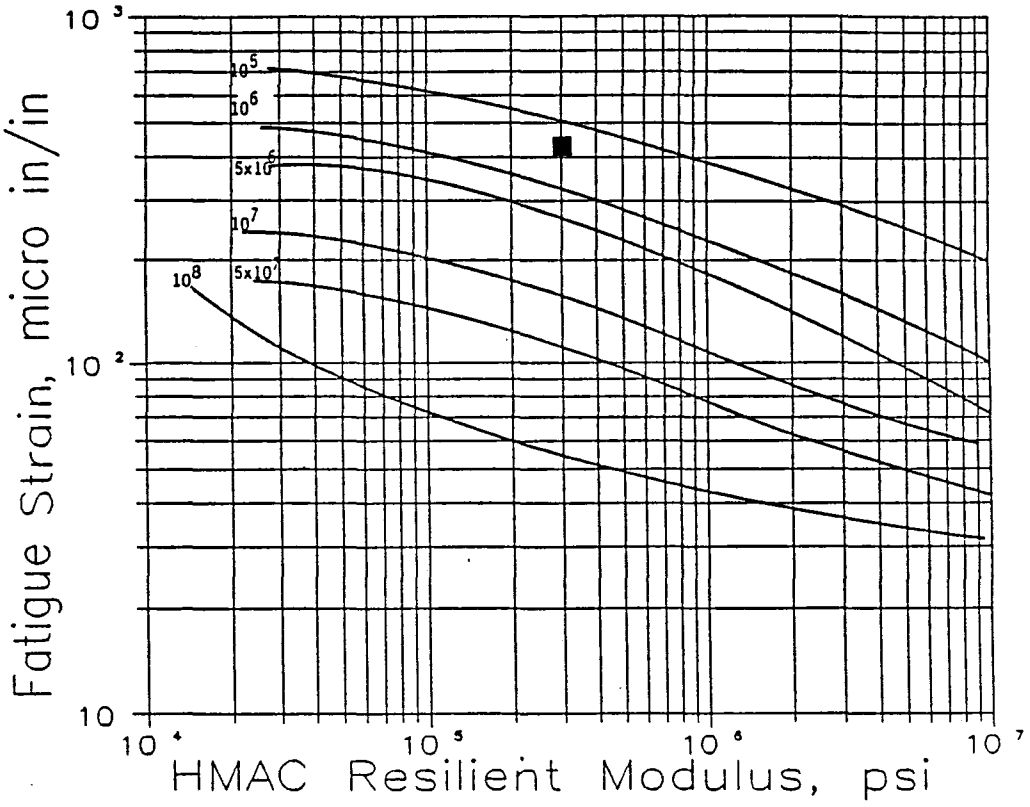

Figure D5. Predicted fatigue life of the mixture in the District 17 Project (5 x 10^5 passes of 18 kip ESAL).

4.4 Since, the predicted fatigue performance level is lower than the design value ($5 \times 10^5 < 3 \times 10^6$ passes of 18 kip ESAL's), alterations in the asphalt and/or aggregate and their proportions may be necessary.

Rutting Analysis

5. Establish the permanent deformation potential of the mixture under investigation.

5.1 Establish the plastic and viscoplastic deformation potential of the mixture in question through the creep test.

5.1.1 Conduct the creep/recovery test according to the procedure detailed in Appendix A. Figure D6 is an example for Highway 21 mixture.

5.1.2 Develop the viscoplastic stiffness parameter ($\sigma/\epsilon_{vp}(t)$), see Figure D7.

5.1.3 Laboratory creep tests are usually conducted at room temperature (77°F). The pavement temperature at which rutting becomes a potential problem is usually above 70°F. As a result, creep/-recovery properties, measured in the laboratory, must be measured at the proper temperature level or they must be transformed in order to represent the rutting potential at field temperatures.

5.1.3.1 Determine the design temperature for the permanent deformation analysis based on the pavement category and the climatic region within which the pavement will be placed or now exists (Table 1, page 32).

5.1.3.2 Based on the design temperature for deformation analysis determined in the previous step, the ring and ball softening point of bitumen, and the creep test temperature, obtain the shift factor (a_T) for the viscoplastic stiffness versus time plot using Figure D8.

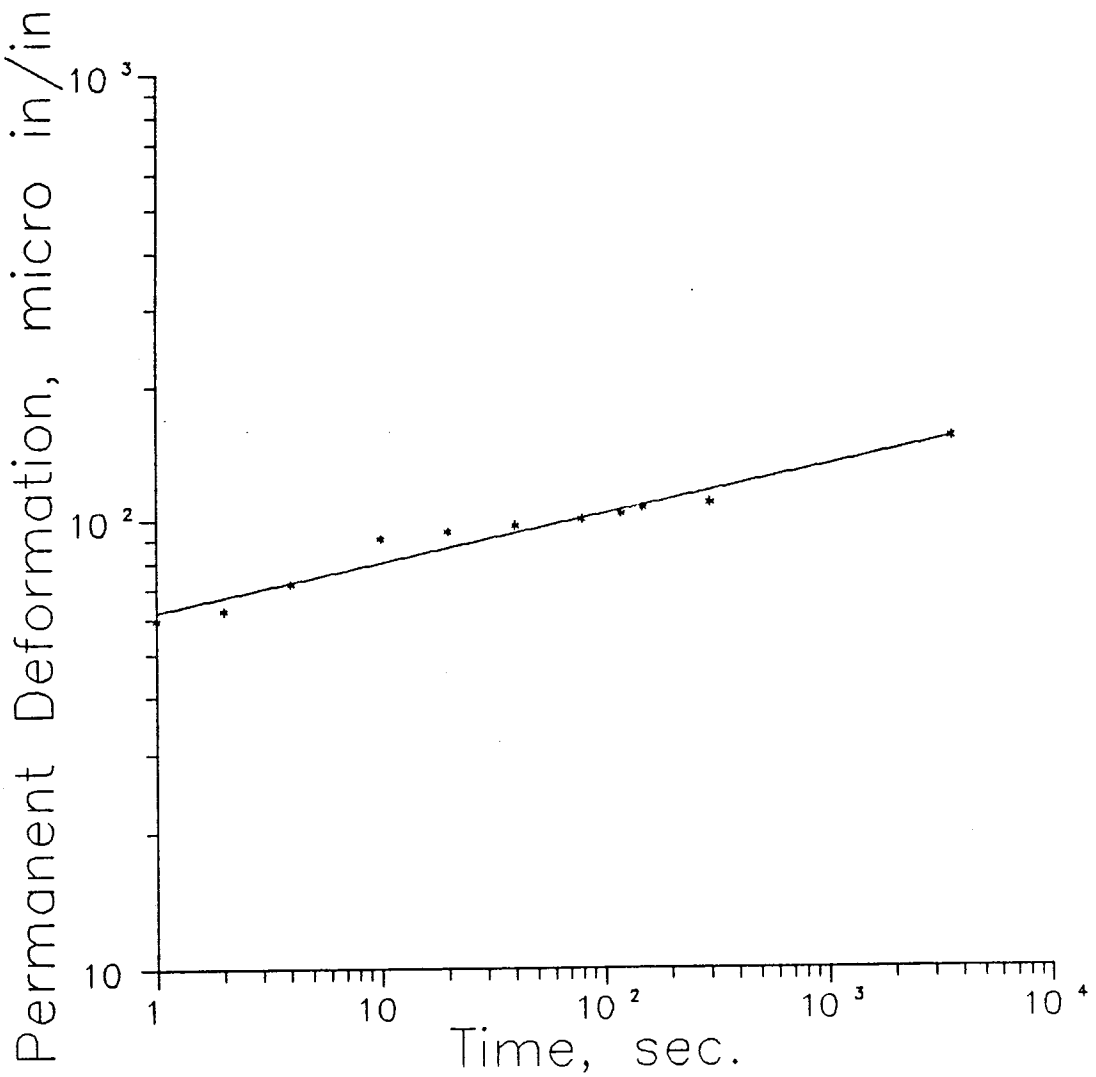

Figure D6. District 17 permanent deformation data measured from creep/recovery test.

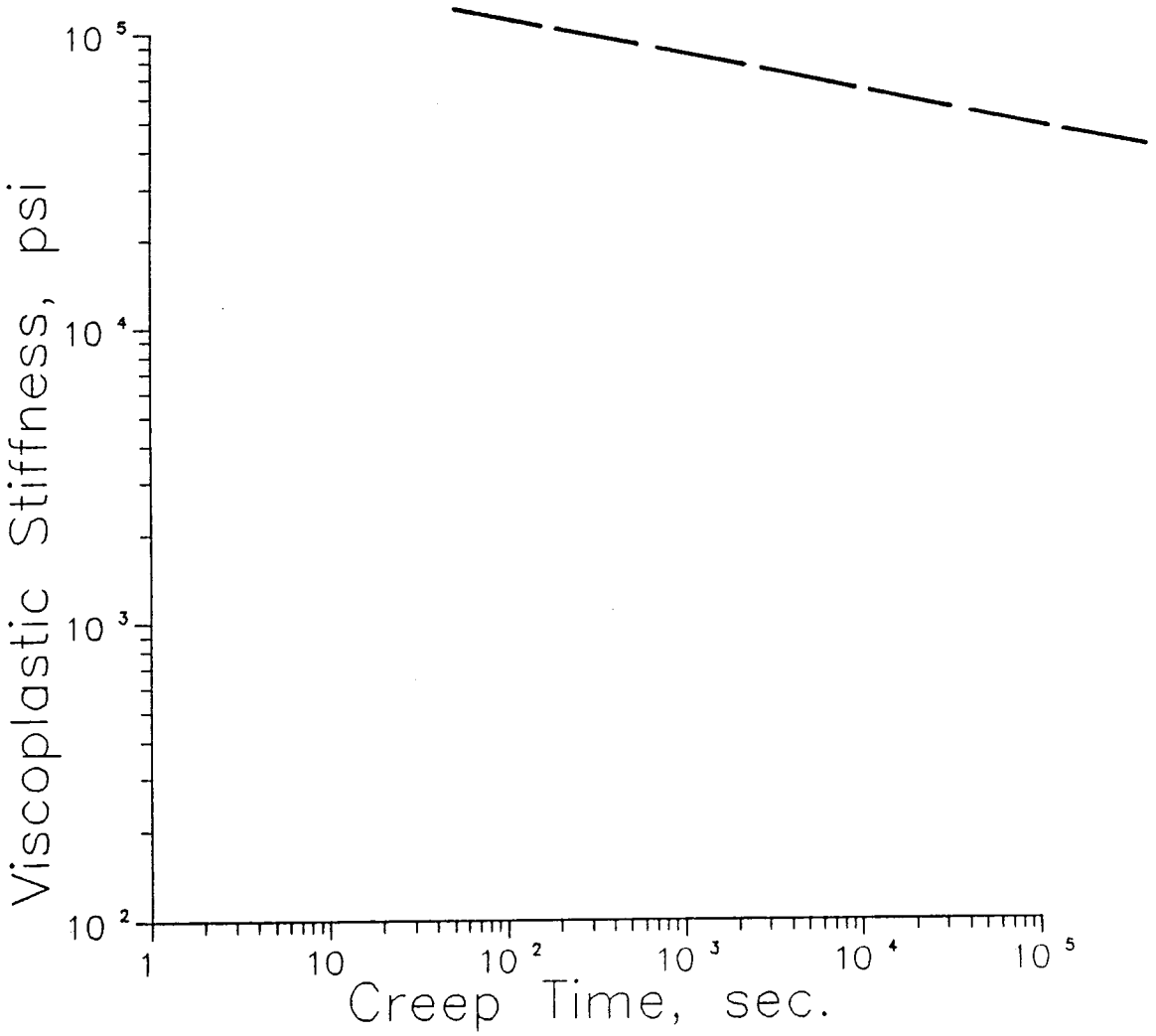

Figure D7. Viscoplastic stiffness trend for District 17 Project.

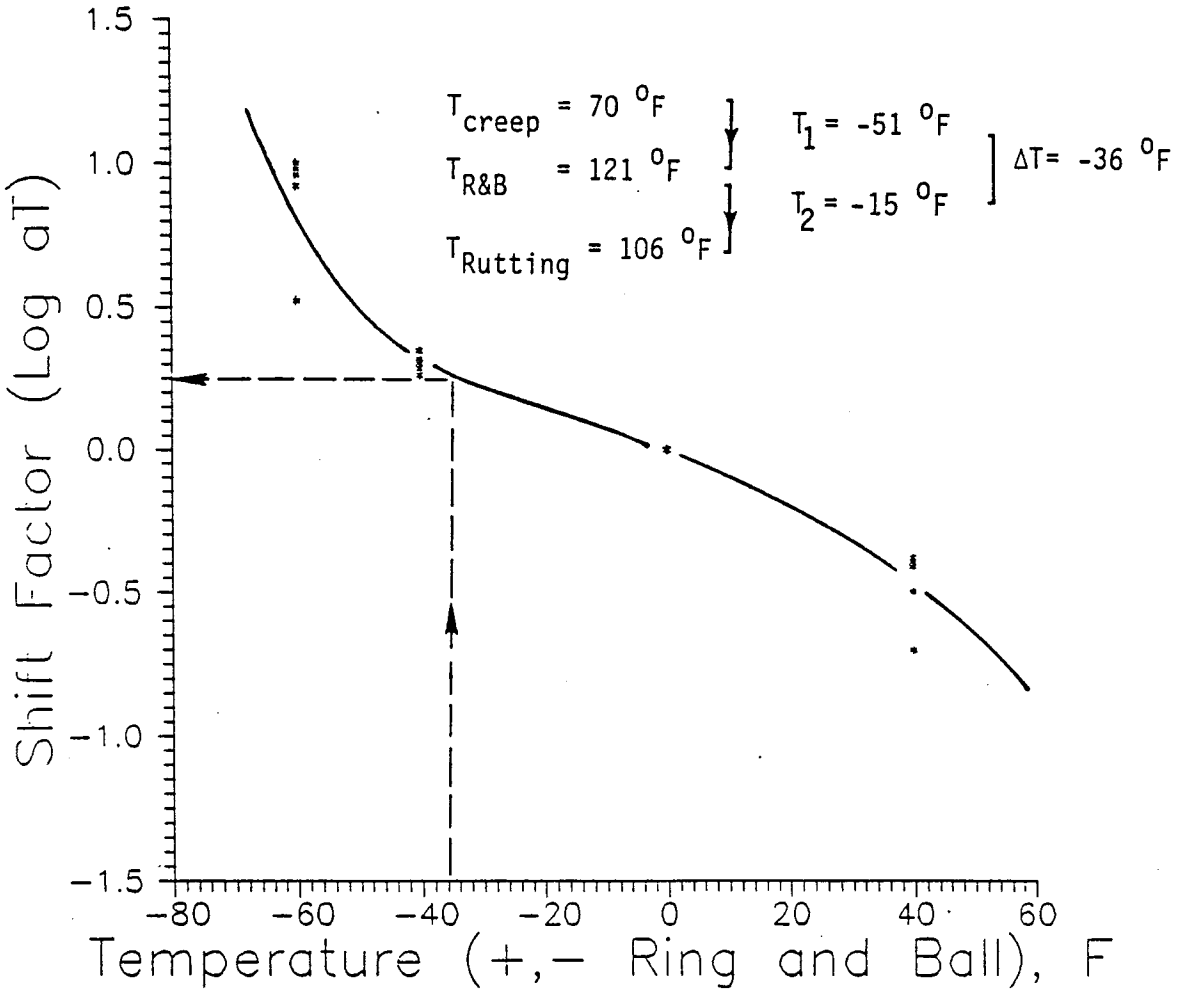

Figure D8. Viscoplastic shift which is required for the District 17 Project mix in order to transform laboratory-measured permanent deformation into actual pavement rutting predictions.

corresponding to the pavement structure and the mixture resilient modulus at the design temperature determined in Step 5.1.3.1.

5.2.1 Plot the viscoplastic stiffness trend, determined in Step 5.1.2, on the chart selected in Step 5.2, Figure D9.

5.2.2. Shift the curve plotted in Step 5.2.1 according to the shift factor (a_T) determined in Step 5.1.3.2. The curve is to be shifted to the left for field temperatures higher than the laboratory. Figure D9 illustrates the shifting process.

5.3 Determine the rutting potential of the mixture under investigation based on the position of the shifted viscoplastic stiffness curve with respect to the rutting criteria zones (Figure D9).

5.4 If the predicted rutting potential determined in the previous step is below the acceptable level, a combination of modifications may be necessary. One may have to modify asphalt cement content and/or grade, aggregate gradation, and aggregate surface texture characteristics.

Thermal Cracking Analysis

6. Evaluate low temperature cracking potential of the mixture.

6.1 Determine the region in which the mixture will be placed (Figure D10).

6.2 Based on the climatic region within which the pavement exists and the resilient modulus versus temperature category, the proper low temperature fracture boundary curve was selected (Figure 77, page 125) to fit the requirements of this example.

6.3 Determine the tensile strength failure envelope using the indirect tensile test (0.02 inches per minute) at 0°F, 32°F, and 77°F.

6.4 Superimpose the failure envelope on the appropriate boundary charts (Figure D11). The example mixture

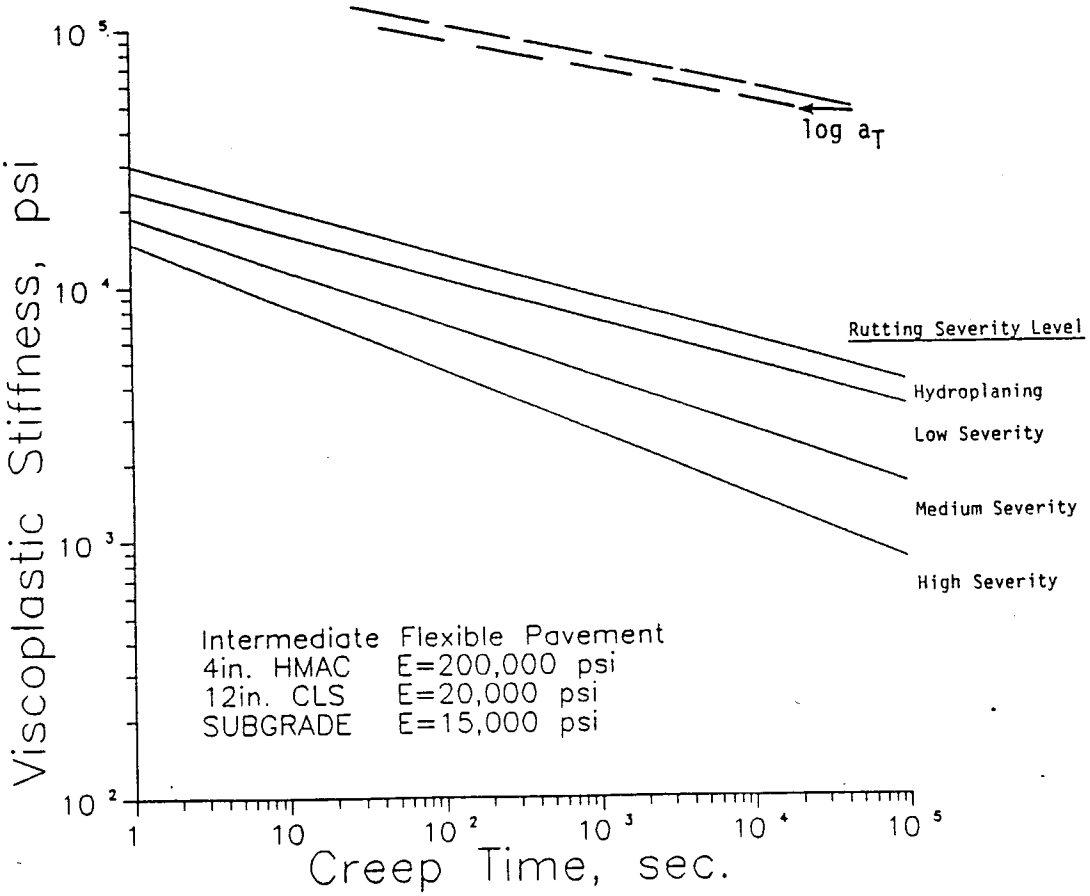

Figure D9. Characterization of rutting potential for District 17 HMAC.

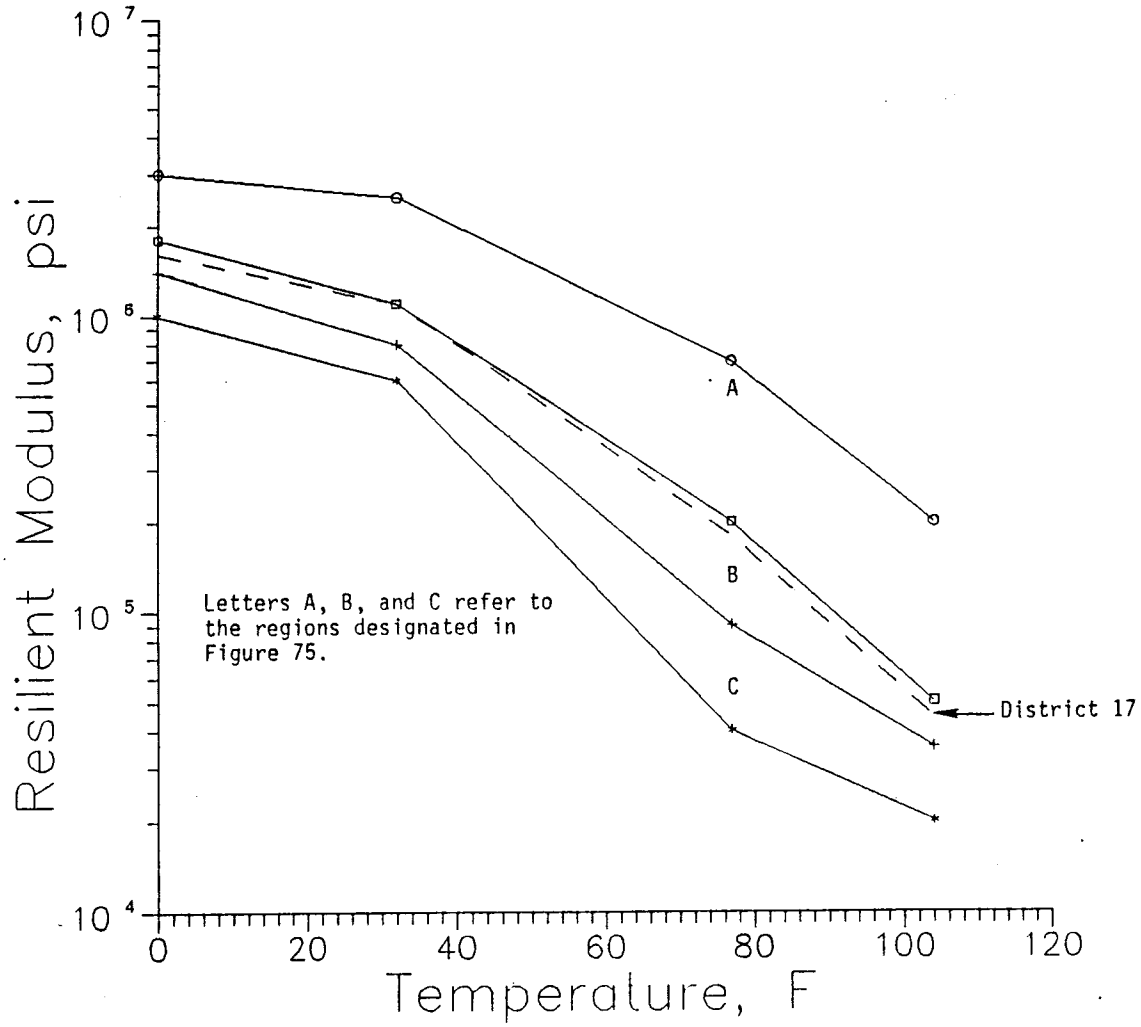

Figure D10. Resilient modulus versus temperature relationship for District 17 mix plotted on the resilient modulus classification chart.

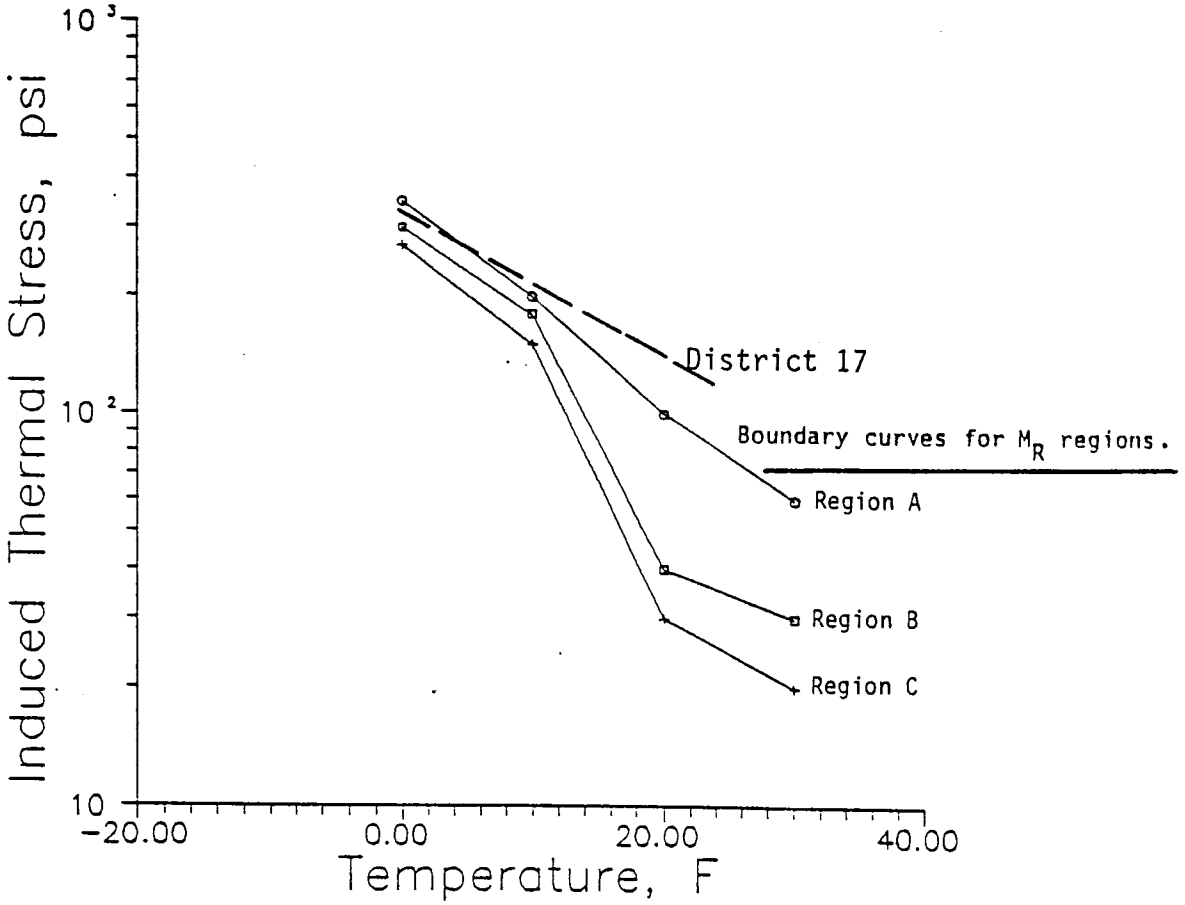

Figure D11. Low temperature cracking characterization of the mixture used in Highway 21 (District 17) Project.

demonstrated an acceptable level of resistance to low temperature cracking.

6.5 If the superimposed failure envelope transgresses the boundary curves corresponding to the mixture stiffness, mixture modifications may be needed. These modifications should be aimed towards increasing tensile strength while maintaining enough flexibility (i.e. relatively low stiffness).

APPENDIX E

FIELD VERIFICATION

APPENDIX E

FIELD VERIFICATIONS

This section deals with the results of a series of mix designs and analyses conducted using raw asphalt cements and aggregates collected from the four project locations described in Chapter VIII. Since procedural details of the proposed methodology are given in Appendix D, the results in this section are presented in a brief and comparative format.

1. Excessive Subgrade Deformation

A threshold resilient modulus had to be established for each individual mixture in order to verify the structural soundness of the pavements to which the mixtures were applied. The term "structural soundness" in this section refers to the ability of the asphaltic layer to distribute the vertical compressive stresses in a fashion by which the vulnerable subgrade is protected from excessive deformation.

Figure E1 depicts the plot of diametral resilient modulus over a range of temperatures (0°, 32°, 77°, and 104°F) for the four mixtures identified in Chapter VIII. All mixtures, with the exception of the high stiffness AC-40 mix which was used at the San Antonio's Loop 410 frontage road (District 15) Project, fall in the same cluster of resilient moduli. The AC-40 mix, expectedly, showed higher resilient moduli over the range of temperatures because of the higher viscosity asphalt cement.

Figure E2 demonstrates that a resilient modulus of 7.2×10^5 psi is required by the subgrade protection criteria for the U.S. Highway 60, Carson County (District 4) Project a traffic level of 10^5. Referring to Figure E1, at the mean annual pavement temperature which is 58°F for the U.S. Highway 60 (District 4) Project, the mixture shows 4×10^5 psi which is lower than the threshold resilient modulus level (7.2×10^5 psi). Plans are underway to overlay the U.S. Highway 60 pavement during the summer of 1988 and this will remedy the potential overstressing of the subgrade.

Figure E3 indicates that a threshold resilient modulus of 3.8×10^5 psi is required for the remaining three projects. It was assumed that these projects would be exposed to 10^6 passes of 18 kip

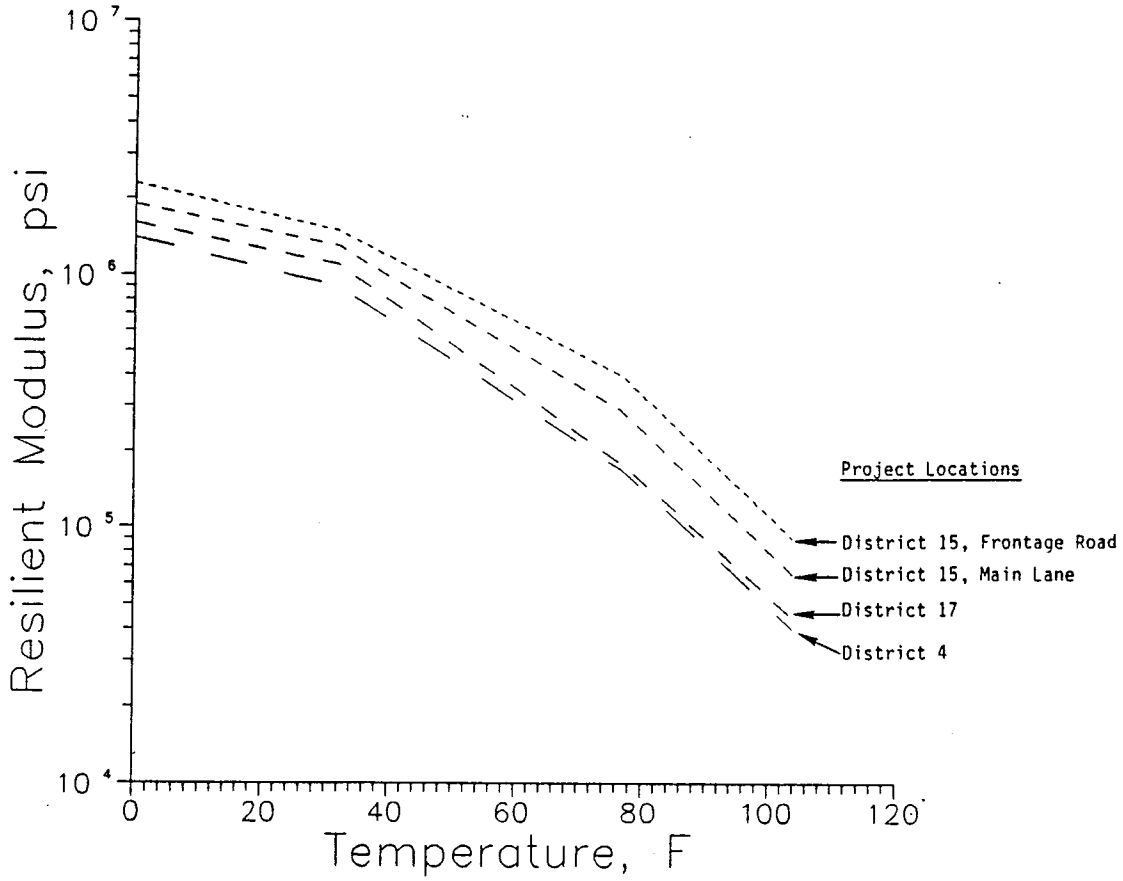

Figure E1. Diametrial resilient modulus versus temperature relationship for the four mixtures that were included in the verification phase.

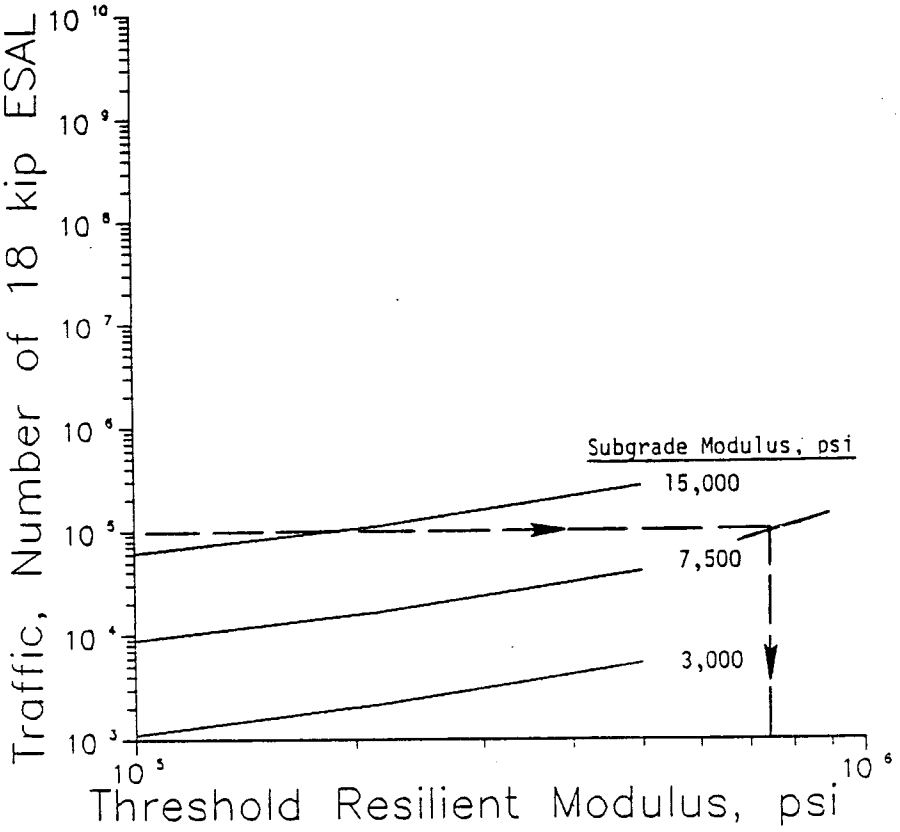

Figure E2. Subgrade protection criteria for the District 4 Project.

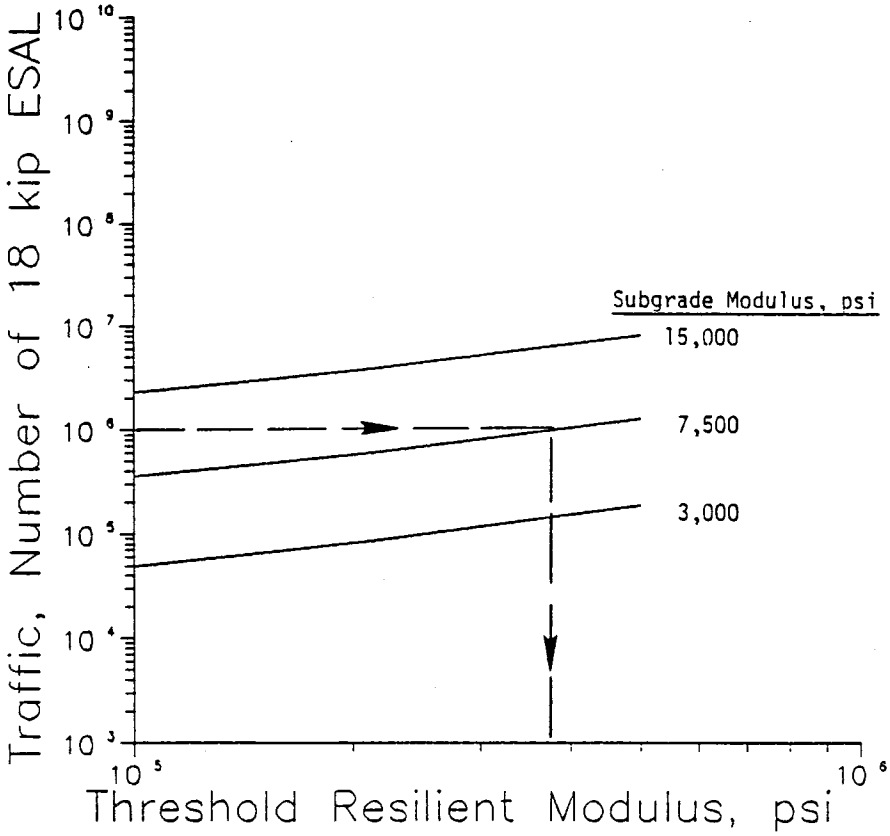

Figure E3. Subgrade protection criteria for Districts 15 and 17 Projects.

ESAL's over the period of analysis. The "high stiffness" AC-40 mix and the "light-weight" AC-20 mix constructed at Loop 410, San Antonio (District 15), showed the resilient moduli of 3.7 x 10^5 psi and 3.2 x 10^5 psi, respectively, at the mean annual pavement temperature of 70°F. This is slightly below the threshold level (3.8 x 10^5 psi), and therefore some subgrade overstressing may occur.

The mixture constructed at the Highway 21 (District 17) Project showed a resilient modulus of 3 x 10^5 psi, at the mean annual pavement temperature of 68°F. Again, this level of mixture stiffness is below the specified threshold (3.8 x 10^5 psi) and subgrade overstressing can potentially cause some rutting.

2. Load-Induced Fatigue Cracking

Figure E4 shows that the load-induced repeated tensile strain at the bottom of the asphalt layer constructed at the U.S. Highway 60 (District 4) Project is 5.1 x 10^2 micro in/in. In a similar format, Figure E5 demonstrates that the Loop 410 main lane (District 15), the Loop 410 frontage road (District 15), and the Highway 21 (District 17) Project have asphalt surface layers which exhibit the following tensile strains: 4.3 x 10^2 micro in/in, 4.2 x 10^2 micro in/in, and 4.5 x 10^2 micro in/in, respectively.

Figure E6 depicts the predicted fatigue performance of the four mixtures under review. The U.S. Highway 60 (District 4) was the only project with a relatively low level of fatigue life (8 x 10^4 passes of 18 kips ESAL). The remaining three projects all demonstrated mediocre fatigue resistance (about half a million passes of 18 kip ESAL).

3. Rutting

The results from creep/recovery tests were plotted on the appropriate rutting criteria charts. Figure E7 illustrates that the mixture used in U.S. Highway 60 (District 4) Project, a thin flexible structure, demonstrated a potential for low severity rutting after a time corresponding to one million passes of 18 kip ESAL. The remaining three pavements were classified under the "intermediate flexible" category. Mixture performance with respect to rutting on these three projects was revealed to be satisfactory (Figure E8).

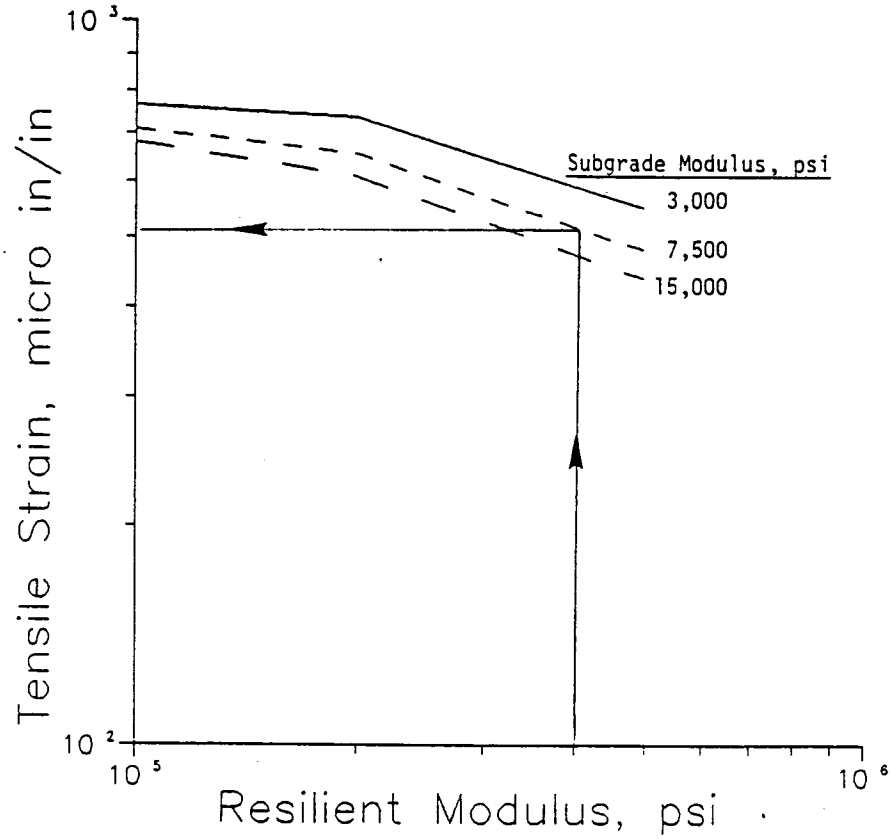

Figure E4. Induced repeated tensile stain at the bottom of the HMAC layer for the District 4 Project.

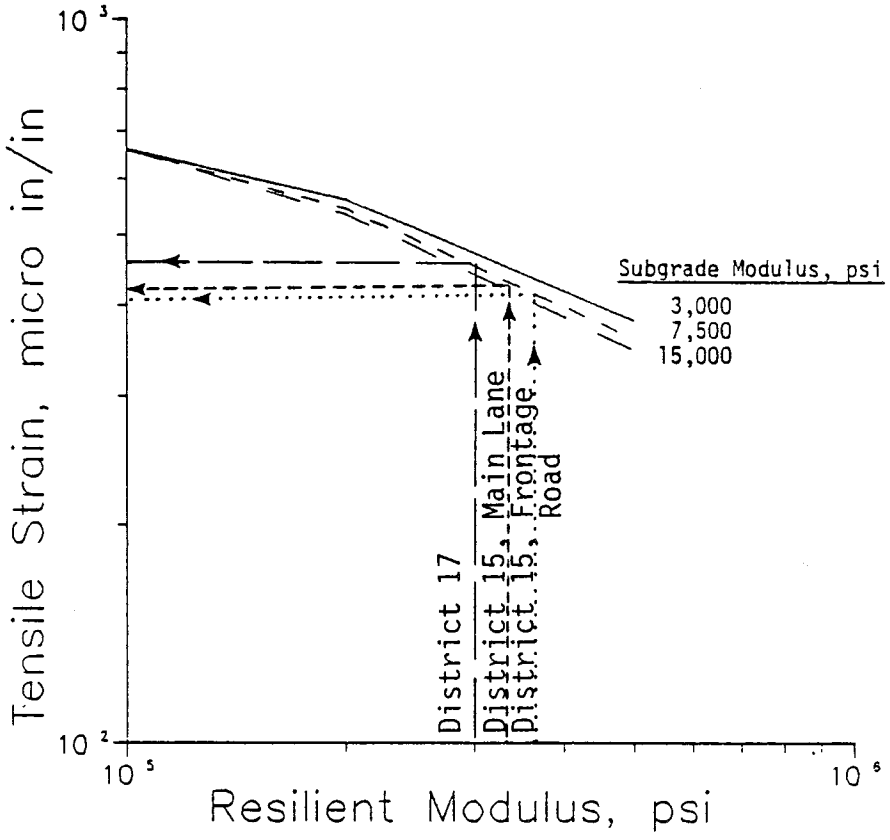

Figure E5. Induced repeated tensile strain at the bottom the HMAC layer for the Districts 15 and 17 Projects.

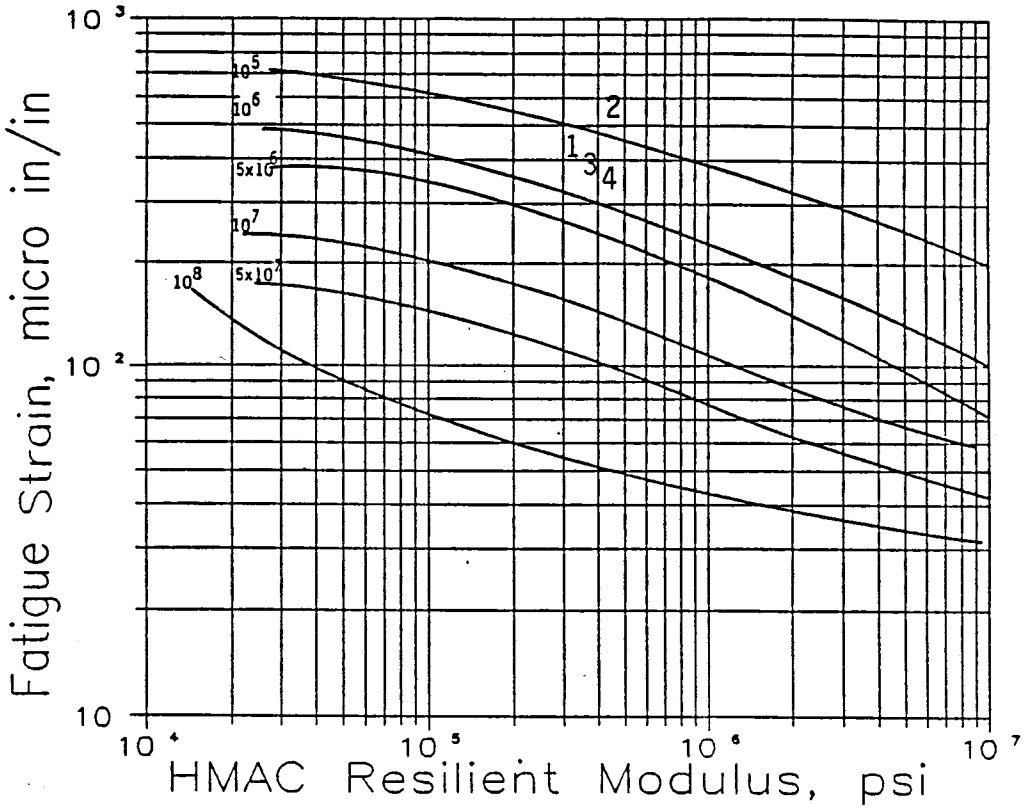

Figure E6. Predicted fatigue performance for all four mixtures that were included in the verification phase: #1 - District 17, #2 - District 4, #3 - District 15, main lane, and #4 - District 15, frontage road.

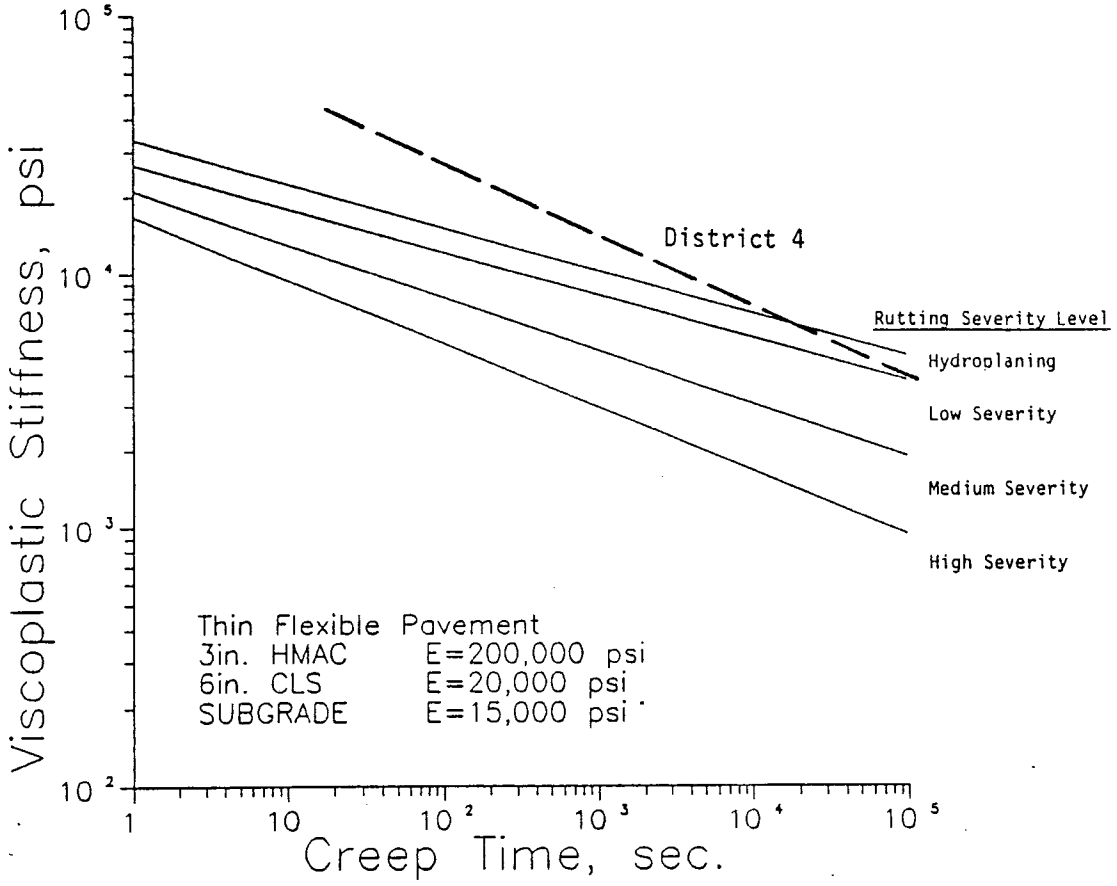

Figure E7. Rutting potential characterization for the District 4 Project.

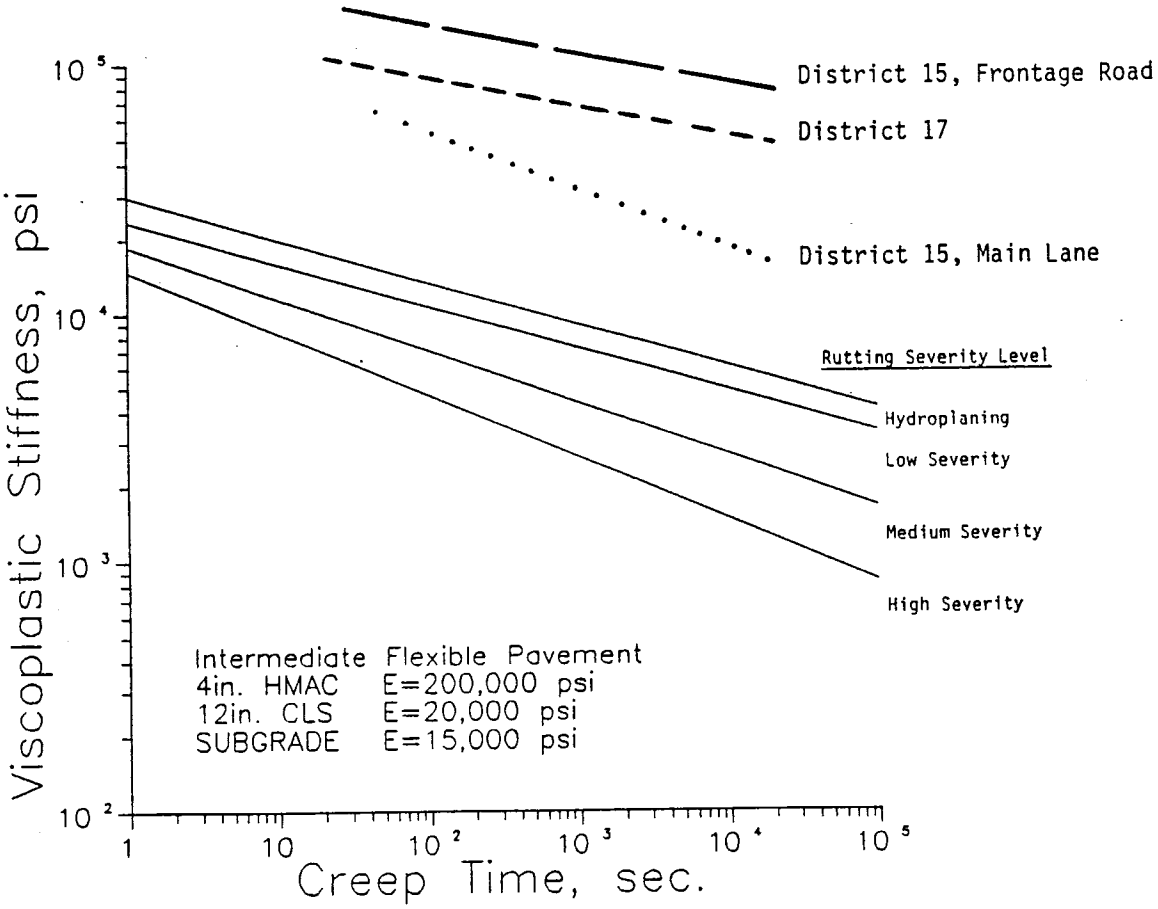

Figure E8. Rutting potential characterization for the Districts 15 and 17 Projects.

The level of traffic for the rutting analysis was set at one million passes of 18 kips ESAL. The effect of critical rutting temperatures, which are expected in the field at each project location and are higher than the laboratory temperature (70°F) used during the creep test, was accounted for using the shift factors that were developed in Chapter VI.

4. Thermal Cracking

Tensile stresses induced by sudden drops in temperature are assumed to be responsible for this mode of pavement distress. Figure E9 is used to determine the zone under which the resilient modulus versus temperature data are classified. In borderline resilient modulus classification cases, more weight was given to the data at lower temperatures.

Figure E9 illustrates that both mixtures used in San Antonio's Loop 410 (District 15) Project were classified in Region A of the resilient modulus versus temperature relationship. Mixtures used in U.S. Highway 60 (District 4) Project and Highway 21 (District 17) Project fell in Region B.

Figure E10 demonstrates a superposition of the indirect tension failure envelope for the U.S. Highway 60 (District 4) HMAC on the induced tensile stress boundary curves representing the conditions for the geographical location of the project. The failure envelope does not transgress over the boundary curve corresponding to the Region B resilient modulus, and therefore, an acceptable resistance to low temperature cracking is expected for the mixture. If the resilient modulus classification for this mixture were a Region A class, i.e. a stiffer mix, the resistance of the mix to thermal cracking would have been declared as unacceptable.

Figure E11 depicts that both San Antonio's Loop 410 (District 15) Projects may incur thermal cracking. This is due to the low tensile strengths exhibited by these mixtures at low temperatures along with higher moduli which resulted in the transgression of boundary curves corresponding to Region A. The mixtures used in the Highway 21 (District 17) Project, however, do not transgress the Region B boundary curve which translates into an acceptable level of resistance to thermal cracking for that mixture.

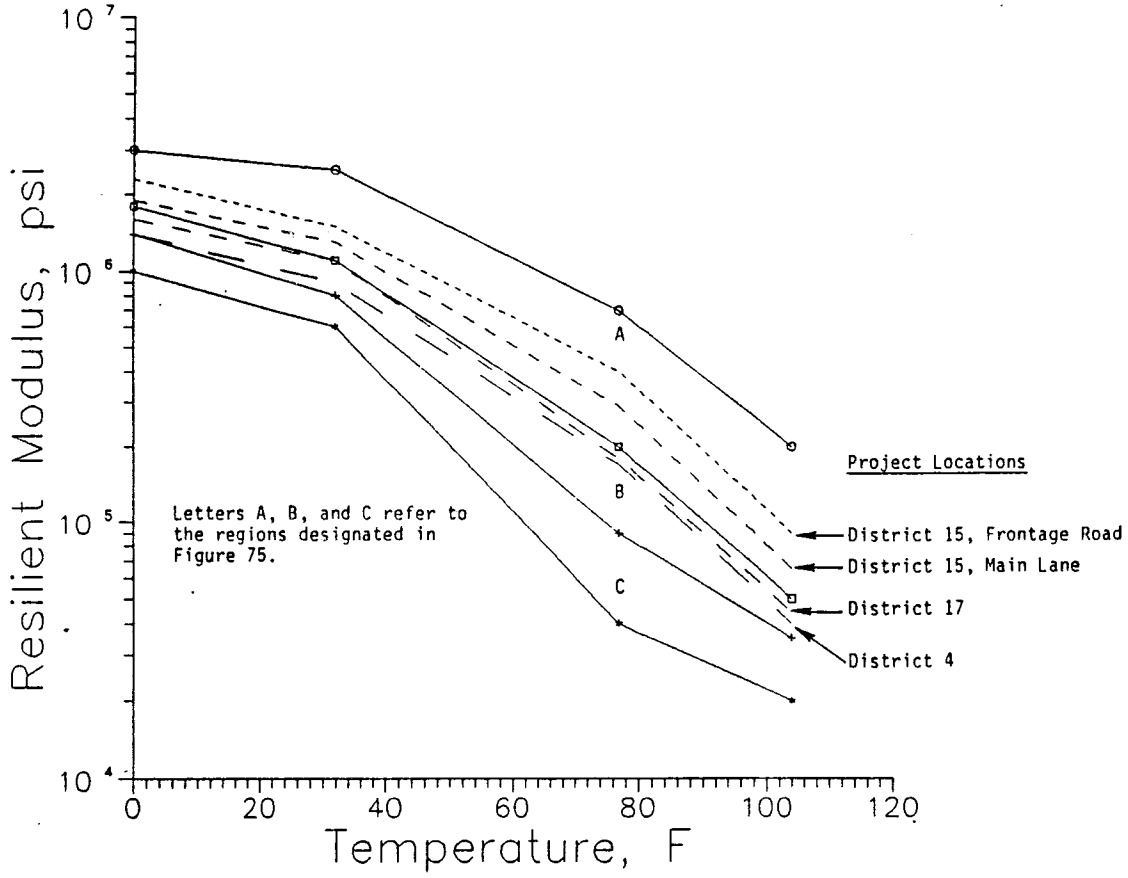

Figure E9. Resilient modulus versus temperature classification chart.

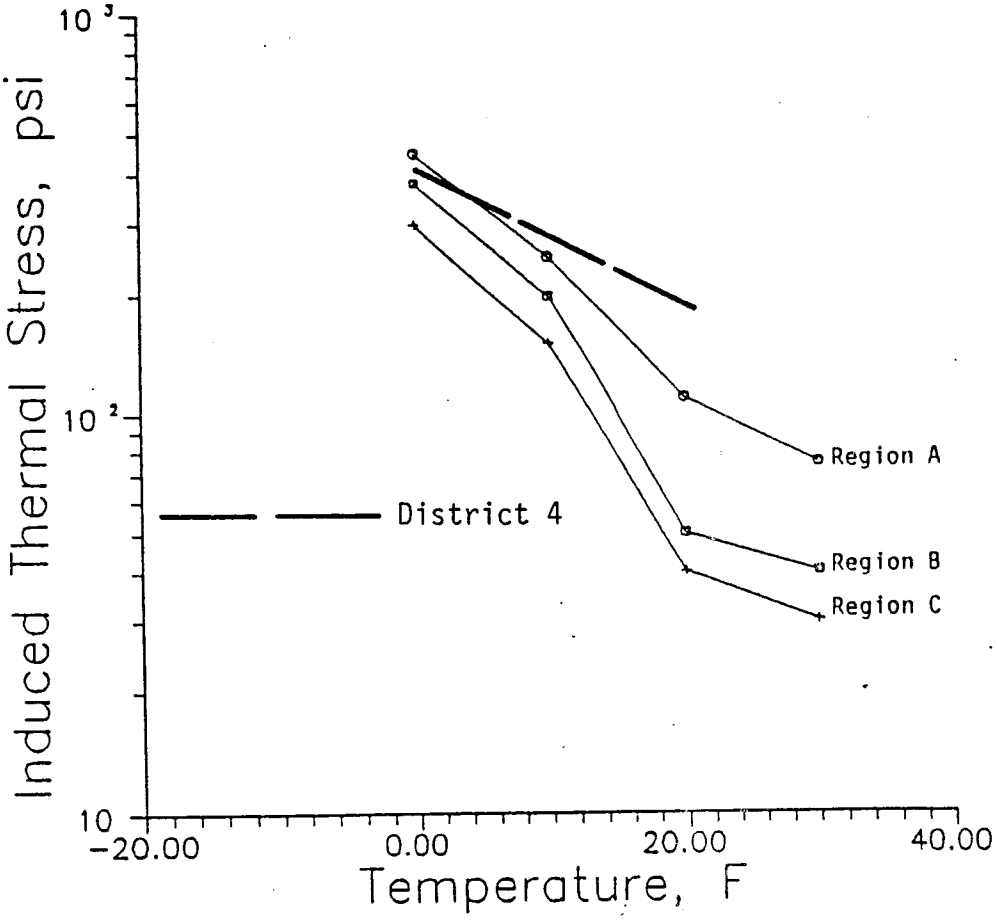

Figure E10. Indirect tensile failure envelope for District 4 mixture, superimposed on induced thermal stress versus temperature relationship for climatic regions I and III.

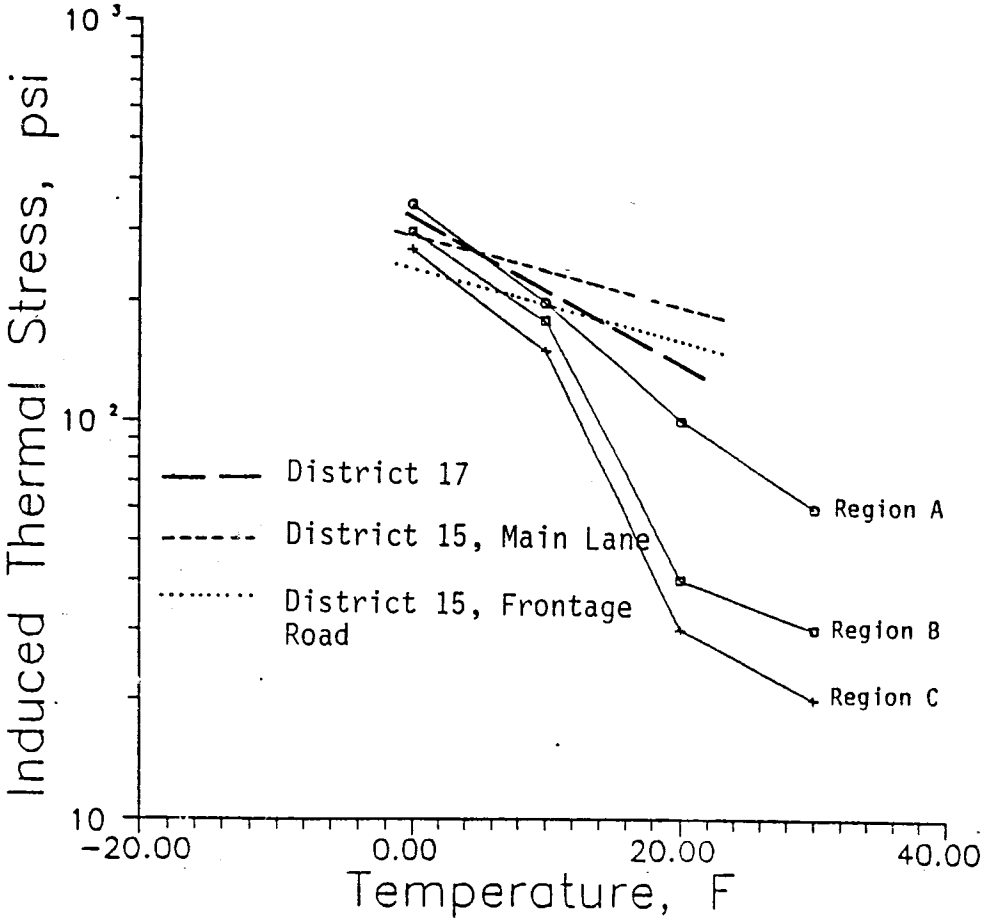

Figure E11. Indirect tensile failure envelopes for Districts 15 and 17 mixtures, superimposed on induced thermal stress versus temperature relationship for climatic regions II and IV.